University of Southampton

Rare Earth Element Systematics in Ancient and Modern Hydrothermal Systems

Deborah Mary Wells

A dissertation submitted for the Degree of Doctor of Philosophy

School of Ocean and Earth Science
November 1998

Declaration

This dissertation describes my own original work except where acknowledgement is made in the text. It does not exceed the page limit and is not substantially the same as any work that has been, or is being submitted to any other university for any degree, diploma or other qualification.

UNIVERSTIY OF SOUTHAMPTON

ABSTRACT

FACULTY OF SCIENCE

SCHOOL OF OCEAN AND EARTH SCIENCE

Doctor of Philosophy

Rare earth element systematics in ancient and modern hydrothermal systems

Deborah Mary Wells

The geochemical significance of on-axis diffuse fluids, in addition to those formed during the waning phases of hydrothermal systems and off-axis crustal ageing processes, has been investigated through a comparison of the rare earth element (REE) systematics of hydrothermal materials from the ore-forming hydrothermal systems of the TAG vent field, 26° N Mid-Atlantic Ridge, and 90 Myr Troodos Ophiolite, Cyprus.

Ophiolites integrate a long (*c.* 20 Myr) history of seafloor alteration, which reflects both axial and off-axis hydrothermal processes. Spatially-resolved laser ablation inductively coupled plasma-mass spectrometric (LA ICP-MS) REE analyses of individual alteration phases within stockwork-mineralised Troodos lavas have been used to deconvolve the complex alteration processes associated with crustal generation at an oceanic spreading ridge. REE mobility was associated with the development of both high- (~200 to 350° C) and low-temperature (<100° C) secondary phases which precipitated within contrasting alteration regimes (discharge- and recharge-dominated respectively). Low-temperature alteration phases are the major repository for the REEs in lavas which are depleted in the light REE ± Eu relative to pristine volcanic glass compositions. These data indicate that much of the REE signature of the alteration pipe is a post-mineralisation overprint acquired in the waning stages of hydrothermal activity and during the protracted alteration of the oceanic basement, rather than on-axis greenschist facies hydrothermal alteration.

Submersible and drilling studies of the TAG mound have led to the development of models of mound growth and fluid evolution within an actively-forming seafloor sulphide deposit. The REEs have been used to test the applicability of these models to processes of sulphide mound and metalliferous sediment formation which occurred within the Troodos ophiolite. The REE patterns of umber, ochre and sulphide sampled from a section through the top of the Skouriotissa ore body clearly demonstrate extensive seawater ingress and circulation throughout the upper ore body during waning hydrothermalism and cooling of the mound, which has resulted in the overprinting of any original hydrothermal signatures in both mound sediments and sulphides. This study has demonstrated that the geochemistry of the sulphide mound deposits continues to evolve following the peak of hydrothermal activity, and that the seawater overprinting of the Skouriotissa deposit is the end product of a process which we only see the initiation of on the modern seafloor.

At TAG, the origin of far-field Mn and Fe-rich oxide crusts has remained controversial over 25 years of investigations of the vent field. The REE and Nd isotope data presented in this thesis indicate these ferromanganese deposits are forming by a combination of sedimentation of Mn-rich particulates from the TAG hydrothermal plume, and direct precipitation from diffuse hydrothermal fluids seeping from the rift valley wall. The REE data reveal that the separation of manganese from other hydrothermally-derived metals at TAG is due to both plume processes and the spatial distribution of diffuse flow within the vent field.

The studies presented in this dissertation have demonstrated the use of REEs as tracers of chemical processes in ancient and modern hydrothermal systems on a wide range of temporal and spatial scales.

Contents

1 Introduction 1
1.1 Hydrothermal circulation at mid-ocean ridges 3
1.2 Subsurface structure of seafloor hydrothermal systems 5
1.3 Temporal variability of seafloor hydrothermal systems 6
1.4 Tectonic ridge crest processes 8
1.5 Magmatic and volcanic ridge crest processes 10
1.6 Tectonic, magmatic and volcanic controls on hydrothermal activity 12
1.7 Hydrothermal fluids 13
1.7.1 High-temperature fluids 14
1.7.2 Diffuse flow 14
1.8 Sulphide mineralisation 15
1.8.1 Black smoker chimneys 16
1.8.2 Seafloor sulphide mounds 17
1.9 Hydrothermal plumes 18
1.10 Metalliferous sediments 21
1.11 Aims of the present study 22
1.12 Dissertation outline 23

2 Rare Earth Elements and Neodymium isotopes 24
2.1 Introduction 24
2.2 Fundamental properties 25
2.3 REEs in seawater 26
2.4 REEs in oceanic basalts 27
2.5 REEs in hydrothermal fluids 29
2.6 REEs in hydrothermal sulphides 31
2.7 REEs in hydrothermal sulphate 35
2.8 REEs in hydrothermal plumes 36
2.9 REEs in metalliferous sediments 38
2.10 Neodymium isotopes 39
2.11 Cretaceous seawater 41

3 Sampling and Materials 42
3.1 Introduction 42
3.2 TAG vent field, 26°N Mid-Atlantic Ridge 43
3.2.1 Low-temperature field 45
3.2.2 Relict sulphide mounds 46
3.2.3 TAG sulphide mound and stockwork 47
3.2.3.1 Fluid compositions 48
3.2.3.2 ODP drilling results 49
3.2.3.3 Sulphide mineralogy 52
3.2.4 TAG models of mound growth and sediment formation 53
3.2.4.1 The role of anhydrite formation 53
3.2.4.2 Dynamic mound processes 55
3.2.4.3 Mound ochres 58

3.2.4.4 Metalliferous sediments 59
3.3 The Troodos ophiolite complex , Cyprus 60
3.3.1 Overview of the geological history of Cyprus 61
3.3.2 Structure of the Troodos ophiolite 63
3.3.2.1 Mantle sequence 64
3.3.2.2 Plutonic sequence 64
3.3.2.3 Sheeted dyke complex 67
3.3.2.4 Volcanic sequence 68
3.3.2.5 Massive sulphide ore bodies 69
3.3.2.6 Ore deposit morphology and mineralogy 70
3.3.2.7 Metalliferous sediments 73
3.4 Summary 74

4 Hydrothermal alteration of the oceanic crust 75
4.1 Introduction 75
4.2 Thermal and alteration history of ODP Hole 504B 76
4.3 Thermal and alteration history of Troodos crustal rocks 79
4.4 Chemical and mineralogical transformations during crustal alteration 81
4.4.1 Alteration of the volcanic section 81
4.4.2 Alteration of the sheeted dykes 83
4.4.3 Reaction zones 84
4.4.4 Discharge zones 85
4.5 Water/rock ratios in axial hydrothermal systems 88
4.6 Differences in the style of alteration between Troodos and *in situ* oceanic crust 89
4.7 Summary 91

5 Analytical Methods
5.1 Laboratory Materials 93
5.1.1 Laboratory Conditions 93
5.1.2 Reagents 93
5.1.3 Apparatus 95
5.2 Sample digestions 95
5.2.1 Metalliferous oxides 95
5.2.2 Metalliferous sediments, sulphides and altered basalts 96
5.3 REE analysis 96
5.3.1 Ion-exchange separations 97
5.3.2 Mass spectrometry 98
5.3.3 Accuracy and precision of solution REE data 101
5.3.4 Laser Ablation ICP-MS 106
5.4 Nd isotope ratio analysis 111
5.5 Major and trace element analysis 111
5.6 X-ray diffraction 113
5.7 Transmission electron microscopy 113

6 Rare earth element mobility in a mineralised alteration pipe within the Troodos ophiolite, Cyprus 115
6.1 Introduction 115
6.2 Oceanic hydrothermal upflow zones 118
6.2.1 Seafloor basalts 118

6.2.2 ODP Hole 504B 118
6.2.3 TAG sulphide mound, 26°N MAR 117
6.3 Troodos mineralised stockworks & alteration pipes 121
6.4 The Pitharokhoma alteration pipe 123
6.4.1 Wall rock alteration 126
6.5 Sampling & Methods 126
6.6 Results 128
6.6.1 Pitharokhoma dykes 132
6.6.2 Pitharokhoma lava 135
6.6.3 Interstitial sediments 140
6.6.4 Massive pyritic mineralisation 143
6.7 Discussion 143
6.7.1 Leached facies 144
6.7.2 Chlorite-smectite mixed layer facies 144
6.7.3 Smectitic facies 146
6.7.4 REE composition of the mineralising fluid 146
6.7.5 Axial alteration *versus* crustal ageing processes 147
6.7.6 REE mobility in hydrothermal systems 148
6.7.7 REE mobility in the TAG stockwork 150
6.8 Conclusions 152

7 The rare earth element geochemistry of an ophiolitic hydrothermal sulphide mound and associated metalliferous sediments 154
7.1 Introduction 154
7.2 Geochemical proxies of hydrothermal processes at TAG 156
7.3 Troodos sulphide mound and metalliferous sediment deposits 158
7.3.1 Umbers 158
7.3.2 Ochres 160
7.4 Sampling 161
7.5 Analytical methods 165
7.6 Results 166
7.6.1 Major and trace elements 166
7.6.2 Rare earth elements 170
7.7 Discussion 181
7.7.1 Skouriotissa & Kinousa sulphides 181
7.7.2 Metalliferous sediments 182
7.7.3 Ce anomalies 193
7.7.4 Ochre formation 195
7.7.5 Origin of the Margi sediment 195
7.5.6 Trace metal contents 196
7.8 Conclusions 198

8 The origin of low-temperature hydrothermal deposits from the TAG vent field, 26°N Mid-Atlantic Ridge 201
8.1 Introduction 201
8.2 Hydrothermal ferromanganese deposits 202
8.3 Low-temperature hydrothermal deposits in the TAG vent field 204
8.4 Physical and chemical properties of the TAG hydrothermal plume .. 205

8.5 Sampling & Methods 208
8.5.1 Rare earth elements 208
8.5.2 Neodymium isotopes 211
8.5.3 XRD analysis 214
8.5.4 TEM analysis 214
8.6 Results 214
8.6.1 XRD & TEM results 214
8.6.2 Rare earth elements 215
8.6.3 Nd-isotopes 221
8.7 Discussion 221
8.7.1 Seawater scavenging of REEs 221
8.7.2 Cerium fractionation 223
8.7.3 REE evidence for diffuse venting in the low-temperature field 225
8.7.4 Radiogenic isotope systematics 230
8.8 Conclusions 239

9 Summary and Conclusions 241

Appendix 246

References 248

List of Figures

2.1 REE patterns for N-MORB, seawater and vent fluid 28
2.2 REE patterns for TAG vent fluids 32
2.3 REE patterns for TAG mound sulphides 34
2.4 REE patterns for TAG and EPR metalliferous sediments 37
3.1 Map of the TAG vent field 44
3.2 Cross section through the active TAG mound 51
3.3 Sub-surface mineralisation processes within the TAG mound 56
3.4 Tectonostratigraphic terrains within the island of Cyprus 62
3.5 Lithologic units of the Troodos ophiolite, Cyprus 65
3.6 Simplified geological map of the Troodos ophiolite, Cyprus 66
4.1 Chemical processes occurring during hydrothermal alteration 82
5.1 Elution curves for small REE cation exchange columns 99
5.2 ICP-MS REE values for standards compared with recommended values 107
5.3 Comparison of REE values obtained by solution and LA ICP-MS 110
6.1 REE patterns for REE patterns for N-MORB, seawater and vent fluid 116
6.2 Geological map of the northern flank of the Troodos ophiolite, Cyprus 124
6.3 Alteration map of the Pitharokhoma open pit 127
6.4 Whole rock REE patterns for Pitharokhoma dykes 134
6.5 REE data for Pitharokhoma lavas 136
6.6 REE data for Pitharokhoma sediments and massive pyrite 141
6.7 REE data for TAG mound stockwork-altered basalts 151
7.1 Sampling localities for Troodos sulphides, umbers and ochres 162
7.2 Geological map of the Skouriotissa Mine 164
7.3 Published REE data for Troodos ochres and umbers 174
7.4 REE patterns for Troodos sulphides 175
7.5 REE patterns for Skouriotissa ochres and umbers 177
7.6 REE patterns for Mathiati, Margi and Kambia metalliferous sediments 178
7.7 LA ICP-MS REE data for the Margi metalliferous sediment 180
7.8 Relationship between TiO_2, Al_2O_3 and SiO_2 content in Troodos umbers and ochres 183
7.9 Relationship between Nd_n/Yb_n ratio and SiO_2 and TiO_2 content in Troodos umbers and ochres 186
7.10 Relationship between TiO_2 and Nd content in Troodos umbers and ochres 187
7.11 Relationship between Fe_2O_3 and Nd content in Troodos umbers and ochres 189
7.12 Relationship between the Ce anomaly and Fe_2O_3 and TiO_2 content in Troodos umbers and ochres 190
7.13 Relationship between Fe_2O_3 and SiO_2 content in Troodos umbers and ochres 192
7.14 Relationship between MnO and Fe_2O_3 content in Troodos umbers and ochres 192
7.15 Relationship between Nd content and Nd_n/Yb_n ratio in Troodos umbers and ochres 194

8.1 Sampling localities for the TAG ferromanganese crusts 209
8.2 REE patterns for TAG ferromanganese crusts 217
8.3 REE patterns for BRAVEX samples 219
8.4 REE patterns for *WHOI* samples 220
8.5 Histogram of $\varepsilon_{Nd}(0)$ values of TAG ferromanganese crusts 222
8.6 Seawater normalised REE patterns for TAG ferromanganese crusts 226
8.7 REE patterns for some mixtures of TAG black smoker fluids and seawater 228
8.8 Relationship between $\varepsilon_{Nd}(0)$ value and Yb_n /Nd_n ratio in TAG samples 233
8.9 Relationship between $^{187}Os/^{186}Os$ and $\varepsilon_{Nd}(0)$ value in TAG samples 236
8.10 Relationship between $^{187}Os/^{186}Os$ and Eu anomaly in TAG samples 238

List of Tables

1.1 Timescales of observations of seafloor hydrothermal systems 9
4.1 Alteration zones in the Troodos ophiolite and ODP Hole 504B 77
4.2 Mineralogical and chemical characteristics of the alteration zones 78
4.3 Water/rock ratios in seafloor hydrothermal systems 87
5.1 REE concentrations in the in-house 10 x chondrite standard 94
5.2 Ion-exchange column specifications 94
5.3 ICP-MS instrument operating conditions 100
5.4 Isotopes monitered for analysis by ICP-MS 102
5.5 Precision & accuracy of REE solution data (BHVO-1 basalt standard) 103
5.6 Precision & accuracy of REE solution data (in-house REE standard) 104
5.7 Precision & accuracy of REE solution data (AMKG-1895) 105
5.8 Quantitation limits for REEs in solution 108
5.9 Reproducibility of Nd standard JMC 321 112
5.10 Precision of XRF major element data 114
6.1 Alteration facies in the Pitharokhoma alteration pipe 125
6.2 Description of Pitharokhoma samples 129
6.3 Major and trace element data for Pitharokhoma samples 131
6.4 REE data for Pitharokhoma samples 133
7.1 Major and trace element data for Troodos sulphide and metalliferous sediment samples 167
7.2 A comparison with some published major and trace element data 168
7.3 REE data for Troodos sulphide and metalliferous sediment samples 171
7.4 Comparison of the trace element compositions of some Troodos and modern metalliferous sediments 197
8.1 Description of TAG ferromanganese crusts 210
8.2 Comparison of REE content of picked and unpicked TAG samples 212
8.3 Nd isotope composition of TAG samples 213
8.4 REE data for TAG samples 215

Acknowledgements

I would like to thank Rachel Mills and Steve Roberts for their help and guidance throughout my postgraduate studies, least of all the driving lessons in Cyprus. Damon Teagle, Joe Cann, Pietro Coletta, Graham Penwright, Costas Xenophontos of the Cyprus Geological Survey, Stuart Swiny and the staff of the Cyprus American Archaeological Research Institute in Nicosia are thanked for their contributions towards a successful field season in 1996. In Southampton, Posy Boella provided constant help in the laboratory, and happily tackled many difficult sample digestions. Andy Milton and Rex Taylor provided invaluable help with ICP-MS and TIMS analyses. Bob Jones, John Ford, Barbara Cressey, Barry Marsh, Phil Warwick, Ian Croudace and Daphne Woods helped me overcome many of the problems I encountered undertaking this research. Gordon Cressey at the Natural History Museum kindly performed XRD analyses. Geoff Thompson at the Woods Hole Oceanographic Institute is thanked for supplying the archived *Alvin* material analysed in this study. Mervyn Greaves provided invaluable advice on column separation techniques.

Over the last four years I have enjoyed activities ranging from spore collecting in the New Forest to surfing in Cornwall with Michael, Barbara, Cathy, Emily, Jim, Matt, Helen, Eta, Mikee, Paul, Katie, Mia, Ruth, Jon, Cathy, Tricky, Russell, Moss, George, Crooksy, John and Ant. I have particularly enjoyed the time I have spent back at home with Chris and Michelle, and more recently Taylor. Finally I would like to thank my family for their support throughout the entire time I have spent studying in Southampton.

Chapter 1

Introduction

The discovery of 'Black Smoker' sulphide chimneys venting copious amounts of metal-rich hydrothermal fluids at ~350 °C surrounded by unique ecosystems, is perhaps the most surprising and important result of research in the deep oceans over the last 20 years. The black smoker structures are one of the most spectacular seafloor expressions of kilometre-scale sub-seafloor hydrothermal systems formed where cold seawater penetrates into hot, recently-emplaced volcanic crust at oceanic spreading ridges, which are the principal site of exchange between the deep and surface geochemical systems of the Earth. Metal sulphide deposits accumulate around seafloor hydrothermal vents where hot, acidic hydrothermal fluids mix with cold, oxic seawater [reviews by Hannington *et al.* 1995; Tivey 1995]. Realistic modelling of the magnitude of geochemical and thermal fluxes caused by oceanic hydrothermal circulation is essential in balancing global chemical and heat budgets, but problematic, as the structure of these systems and the magnitude of the hydrothermal water flux is still poorly constrained [review by Elderfield & Schultz 1996].

While studies of modern vent sites can characterise the spatial distribution of hydrothermal activity on the seafloor, insights into the temporal evolution of mineralising hydrothermal systems are more readily obtained from studies of ophiolites, that represent land-bound fragments of oceanic lithosphere accreted at ancient spreading centres [Gass 1968]. Compared with oceanic studies, ophiolites offer the advantage of three-dimensional on-land exposure of entire oceanic crustal sections to stratigraphic depths that remain unsampled in the ocean basins. Ophiolitic massive sulphide ore bodies are widely distributed throughout the geological record, and constitute a major world resource of base metals (copper, lead and zinc) [Franklin *et al.* 1981]. The size, sulphide mineralogy and textures, and metalliferous sediment associations of some of the largest seafloor sulphide structures are similar to ophiolite-hosted sulphide deposits [Oudin *et al.* 1981; Oudin & Constantinou 1984; Herzig *et al.* 1991; Hannington *et al.* 1998], despite the greater diversity in the tectonic settings of ophiolite formation compared with ocean crust generation at mid-ocean ridges [e.g. Miyashiro 1973; Pearce 1975; Pearce 1980; Pearce

1982; Pearce *et al.* 1984]. Early studies of hydrothermal alteration and mineralisation in ophiolites gave rise to genetic models for seafloor sulphide deposits, that have remained largely unchanged over 20 years of research into active vent systems [e.g. Spooner & Fyfe 1973; Spooner & Bray 1977; Spooner *et al.* 1977]. Ophiolite-based studies of seafloor hydrothermal systems complement the modern oceanic database by placing important constraints on processes occurring in the subsurface of hydrothermal systems, that are often inferred from limited seafloor measurements of the physical and chemical characteristics of vent fluids and their associated deposits [e.g. Richardson *et al.* 1987; Kelley & Robinson 1990; Bickle & Teagle 1992; Kelley *et al.* 1992; Bickle *et al.* 1998]. In this respect, the Troodos ophiolite complex of Cyprus has been of great importance. The Troodos ophiolite was generated at a Tethyan ridge associated with Late Cretaceous seafloor spreading [Gass 1968]. It is one of the few ophiolites with an undisrupted stratigraphy, and although formed in a supra-subduction zone rather than typical mid-oceanic setting [Pearce 1975; Robinson *et al.* 1983; Rautenschlein *et al.* 1985] shows an oceanic crustal section and alteration similar to that predicted for normal mid-oceanic crust. Numerous studies have demonstrated that the Troodos massive sulphides, metalliferous sediments and hydrothermally-altered crustal rocks are the products of seafloor hydrothermal processes comparable with those occurring on the mid-ocean ridge system [e.g. Constantinou & Govett 1972; Constantinou & Govett 1973; Spooner & Fyfe 1973; Spooner & Bray 1977; Spooner *et al.* 1977; Constantinou 1980; Adamides 1990; Boyle 1990; Gillis & Robinson 1990*a,b*].

The rare earth elements (REEs) can be used as tracers of hydrothermal processes in both the modern setting and the geological record. An important part of the investigation into modern vent sites has involved the use of the REEs to constrain the geochemical evolution of the mineralising systems [Michard *et al.* 1983; Michard & Albarède 1986; Campbell *et al.* 1988*b*; Michard 1989; German *et al.* 1990; Gillis *et al.* 1990; Klinkhammer *et al.* 1994; Mitra *et al.* 1994; Mills & Elderfield 1995*a*; James & Elderfield 1996; Humphris 1998]. The chemical coherence of the group, coupled with a predictable range in solubility and complexation chemistry with increasing atomic number and decreasing ionic radius, make the REEs ideal tracers in hydrothermal systems, which are characterised by sharp gradients in physical conditions. Investigations of modern seafloor hydrothermal systems by dredging, submersible operations and limited drilling at ridge crests have led to the creation of a comprehensive REE data set encompassing vent fluids and plumes, hydrothermal sulphides and sulphates, and near- and far-field metalliferous sediments [e.g. Bender *et al.*

1971; Bence 1983; Michard *et al.* 1983; Michard & Albarède 1986; Barrett & Jarvis 1988; Campbell *et al.* 1988*b*; Owen & Olivarez 1988; Michard 1989; Barrett *et al.* 1990; German *et al.* 1990; Gillis *et al.* 1990; German *et al.* 1993; Mills *et al.* 1993; Klinkhammer *et al.* 1994; Mitra *et al.* 1994; Mills & Elderfield 1995*a*; Klinkhammer *et al.* 1995; James & Elderfield 1996].

This dissertation addresses some important problems relating to the structure and temporal evolution of ocean ridge hydrothermal systems. This has been achieved through an evaluation and comparison of the REE systematics of hydrothermal materials recovered from the Trans-Atlantic Geotraverse (TAG) vent field, 26° N, Mid-Atlantic Ridge with similar materials from the 90 Myr mineralising hydrothermal systems preserved within the Troodos Ophiolite, Cyprus. Both the TAG vent field and Troodos ophiolite have been the subject of numerous (and sometimes comparative) studies of submarine hydrothermal systems. Additionally, recent drilling in the TAG vent field by the Ocean Drilling Program (ODP) in 1994 revealed for the first time the internal structure of an actively forming oceanic sulphide deposit, that previously was limited to inferences made from on-land analogues [Humphris *et al.* 1995]. Consequently, the REE data obtained in this study can be interpreted within well-established frameworks of the physical, chemical and structural controls on hydrothermal processes in both the modern and ancient settings.

This chapter provides an overview of the nature, controls and consequences of hydrothermal circulation at oceanic spreading centres. Observations and measurements of modern vent systems are integrated with descriptions of ophiolite-hosted hydrothermal mineralisation and crustal alteration, in addition to the results of some experimental and theoretical studies of ridge crest hydrothermal activity.

1.1 Hydrothermal circulation at mid-ocean ridges

Although deep-sea hydrothermal vents were only relatively recently discovered [Corliss *et al.* 1979], they are now known to be a relatively common phenomenon on the 55 000 km global ridge-crest system in a range of tectonic settings, encompassing fast- and slow-spreading centres, fracture zones, seamounts and back-arc spreading centres associated with subduction zones [review by German *et al.* 1995*a*]. Convective hydrothermal circulation is initiated at spreading centres as a direct consequence of the accretion of new oceanic lithosphere at the ridge axis. Cold seawater percolating into highly fissured crust at the ridge crest becomes heated by conduction from an underlying axial heat source,

consisting of either hot rock or magma. Seawater is transformed into an acidic, reduced, metal- and sulphide-bearing fluid during a sequence of reactions with the basaltic crust at elevated temperature and pressure beneath the ridge crest [review by Alt 1995]. The hydrothermal fluid rises to vent at the seafloor as a black smoker fluid [e.g. Speiss 1980*a*], or mixes with seawater in the shallow subsurface of the system [e.g. Edmond *et al.* 1979*a*].

Prior to any observations of deep sea hydrothermal vents, the large-scale convective circulation of seawater through the global ridge crest and flanks had been inferred from the discrepancy between measured and predicted conductive heat losses for crust less than 60 Myr on the fast-spreading East Pacific Rise (EPR) [Lister 1972]. This hydrothermal circulation carries a significant fraction (~24%) of global heat loss [Sclater *et al.* 1980] and cycles the entire ocean volume through the seafloor every 10 to 50 Myr, constituting a major pathway for chemical exchange between the earth, the ocean and atmosphere [Edmond *et al.* 1979*a*]. Estimates of the total hydrothermal heat flux derived from geophysical methods are *c.* $9 \pm 2 \times 10^{12}$ W [e.g. Morton & Sleep 1985; Sleep 1991; Stein & Stein 1994]. The volume of seawater (hydrothermal mass flux) affected by the hydrothermal heat flux depends critically on the temperature of the circulating fluids. The heat anomaly extends to a crustal age of 65 ± 10 Myr, where the observed and predicted conductive heat flow coincide [Stein *et al.* 1995].

Derivations of hydrothermal mass fluxes are frustrated by uncertainties in the values of off-axis *versus* axial fluxes, and the partitioning of the axial heat flow between ~350°C black smoker and lower-temperature diffuse flow. Thermal modelling of hydrothermal circulation indicates that the axial heat flux is between 10 and 20% of the total heat loss at the ridge axis, requiring extensive low-temperature circulation on the ridge flanks [Wolery & Sleep 1976; Morton & Sleep 1985]. For a given heat flux, the hydrothermal water flux is inversely related to the temperature of the venting fluids. Advective heat loss on the ridge flanks occurs at lower temperatures than in the axial zone, because ~350°C fluids can only be produced by heating in close proximity to a magmatic heat source [Kadko *et al.* 1995]. Consequently, the seawater flux through the ridge flanks is substantially greater than at the axis [Kadko *et al.* 1995]. Considerable uncertainties still exist in deriving estimates of the off-axis water flux, as the fraction of magmatic heat not removed in the axial region and the average temperature of the flow are not known [Elderfield & Schultz 1996]. Additionally, within the axial zone the partitioning of the heat flow between high-

temperature black smoker and lower-temperature diffuse flow is not yet well established on a global scale [Elderfield & Schultz 1996], but individual vent field measurements indicate that diffuse fluids may transport an order of magnitude more heat than discrete venting [Schultz *et al.* 1992; Schultz *et al.* 1996].

1.2 Subsurface structure of seafloor hydrothermal systems

Newly-accreted basaltic lithosphere is cooled by extensive seawater circulation through the ridge crest and flanks. Most black smoker fluids sampled at active vents have exit temperatures close to 350° C [review by Von Damm 1990]. Although the subsurface structure of hydrothermal systems is poorly constrained, this observation requires that for much of their evolution, recharge fluids (seawater) penetrate to depths close to the level of crystallising magmatic intrusions (~2 km) [Cann & Strens 1982; Cann *et al.* 1985]. Heat is rapidly extracted either across a thin static boundary layer in the crystalline roof of a convecting magma chamber (time constant of 1000's of years) [Cann & Strens 1982], or in a dynamic 'cracking front' where fluid penetrates hot, recently crystallised plutons (time constant 10's to 100's of years) [Lister 1982; Lowell & Germanovich 1994]. The 20 year period over which observations are available is far too short to reveal the critical temporal variations which would enable a choice to be made between these two models. However, it has been argued that the necessary heat to produce a large massive sulphide deposit can be more efficiently derived from a magma chamber than hot rock, and additionally that there is no evidence of large degrees of alteration that would be associated with cracking fronts in the gabbros of ophiolite complexes [Cann & Strens 1982; Cann et al. 1985]. This phase of hydrothermal circulation is characterised by rapid heat extraction, high water temperatures and high flow rates [Lister 1982]. The high-temperature fluids rise essentially adiabatically from the reaction zone to vent at the seafloor, or mix with cooler fluids in the near sub-surface [Sleep 1991]. Fluid residence times of only ~3 to 10 years in the upflow zone of the hydrothermal system have been inferred from radioisotope measurements of Juan de Fuca Ridge (JdFR) black smoker fluids [Kadko & Moore 1988; Kim & McMurtry 1991]. Fault-controlled discharge of hydrothermal fluids has been inferred for the Troodos ophiolite [Varga & Moores 1985], and the TAG vent field [Kleinrock & Humphris 1996].

Cann *et al.* [1985] have proposed that both fluid recharge and discharge in subseafloor hydrothermal systems are channelled by faults, although Bickle & Teagle [1992] have

argued for diffuse recharge zones, because channelling of downwelling seawater is not apparent in the Sr-isotope composition of altered basalts in the sheeted dyke complex of the Troodos ophiolite, Cyprus [Bickle & Teagle 1992; Bickle *et al.* 1998].

1.3 Temporal variability of seafloor hydrothermal systems

Seafloor hydrothermal activity is necessarily transient in nature, as the rate of heat extraction by hydrothermal circulation exceeds the heat supplied from the mantle to the crust *via* episodic magma injection [e.g. Cann & Strens 1982; Lowell & Germanovich 1994]. Even disregarding large hydrothermal emissions termed 'megaplumes' [e.g. Cann & Strens 1989; Baker *et al.* 1987; Baker *et al.* 1989], black smokers have rates of thermal discharge greater than can be sustained by seafloor spreading. As the typical heat flux from a black smoker system is ~50 to 500 MW [Schultz *et al.* 1992], the heat available on a steady state basis from the cooling oceanic crust could only maintain venting for <10% of the time [Cann & Strens 1982]. Similarly, the heat loss from a single black smoker chimney (~3 x 10^5 kW) at 21°N EPR is equivalent to the expected conductive heat loss for a segment of spreading centre 4 to 7 km long and extending out to 1 Myr crust either side of the ridge crest [Macdonald *et al.* 1980]. The predicted temporal instability of the hydrothermal flux is consistent with the view that ocean ridge crests undergo cycles of tectonic and magmatic activity [Lowell & Germanovich 1994], which have also been recognised from the constructional morphology of parts of the Troodos extrusive sequence [Schmincke & Bednarz 1990].

The initiation of hydrothermal venting within the tectonic-magmatic cycles of oceanic ridges is not yet well understood. However, observations of sudden changes in the chemical and/or thermal output of vent fields at 9-10°N EPR on the Southern JdFR associated with dyke intrusion and subsequent seafloor volcanic eruptions provides evidence that seafloor spreading episodes may be punctuated by extreme perturbations in hydrothermal activity [Baker *et al.* 1989; Von Damm *et al.* 1995]. 'Megaplumes' are extremely large hydrothermal plumes resulting from catastrophic emissions from black smoker systems that may represent sudden emptying of an entire crustal hydrothermal reservoir [Baker *et al.* 1987; Baker *et al.* 1989; Nojiri *et al.* 1989; Cathles 1993; Cann & Strens 1989]. A megaplume on the Cleft segment of the Southern JdFR was associated with a heat output equivalent to the normal output from the underlying vent field (*c.* 30 000 MW), and 10-1000 times that of a single black smoker [Baker *et al.* 1989].

Importantly, megaplume fluids are compositionally distinct, indicating that chemical budgets extrapolated on the basis of stable vent chemistries may be unreliable, depending on the frequency and duration of megaplume events [Baker 1995]. Additionally, an active vent at 9°N EPR was recently observed to evolve from vapour-rich to brine-rich fluid compositions in the three years following a volcanic eruption within the vent field [Von Damm *et al.* 1995; Von Damm *et al.* 1997].

Following these initial perturbations, vent fluid compositions appear to enter a steady-state phase of evolution, that is typical of most systems that have been sampled on the mid-ocean ridge system. The longest existing time series of vent fluid compositions are for the TAG vent field, MAR [Campbell *et al.* 1988*b*; Edmond et al. 1995; Edmonds *et al.* 1996; Gamo *et al.* 1996], 21°N on the EPR [Speiss *et al.* 1980; Edmond *et al.* 1982; Von Damm *et al.* 1985*a*; Campbell *et al.* 1988*a*] and the Guaymas Basin in the Gulf of California [Von Damm *et al.* 1985*b*; Campbell *et al.* 1988*a*]. The hydrothermal vents sampled in these studies have shown stable fluid and exit temperatures over the decadal timescales of observation. The lack of any critical temporal variability in these systems is consistent with vent fluid compositions that are buffered to observed compositions by water-rock interactions at depth, and also that the mixing-cooling history of the fluids has been relatively stable over these time periods [e.g. Campbell *et al.* 1988*a*].

While many seafloor hydrothermal systems are observed to approach steady-state conditions, it is difficult to ascertain if true chemical equilibrium is achieved [Von Damm 1995]. Early thermodynamic modelling of vent fluids at 21° N, EPR and the Guaymas Basin indicated that chemical composition of the fluids did not correspond to equilibrium control except for quartz [Bowers *et al.* 1985]. Subsequent modelling with an improved thermodynamic database for 21°N and 13-11°N, EPR suggested the fluid chemistry is rock-buffered by equilibrium reactions between the hydrothermal fluid and a greenschist facies mineral assemblage at depth [Bowers *et al.* 1988]. Laboratory experiments have shown that full equilibrium between all the mineralogical rock components is unlikely to occur, and that there are likely to be only a limited number of equilibrium reactions, such as plagioclase alteration to epidote [Berndt *et al.* 1989]. Although low whole-system water/rock ratios indicate that the total extent of subsurface alteration of the oceanic crust is low [review by Von Damm 1995], geochemical exchange in hydrothermal systems is predicted to be dominated by reactions at locally higher ratios along the shallow recharge paths of hydrothermal fluids [Bickle & Teagle 1992].

The relative duration of the perturbed and steady-state venting episodes, and the characteristics of the waning phases of these systems are poorly constrained from only 20 years of observations of active seafloor vents [Von Damm 1995]. However, seafloor observations can be integrated with the results of ODP Hole 504B that has sampled a ~2 km section of 5.9 Myr mineralised ocean crust, and studies of hydrothermal alteration in ophiolites to gain insights into the temporal evolution of hydrothermal systems, from their inception to lower-temperature evolution following the peak of hydrothermal activity and alteration (Table 1.1). While ODP drilling has sampled the volcanic basement at numerous locations on the ocean floor, Hole 504B is the best modern counterpart of the crustal sections exposed in ophiolites as it is the only basement hole to penetrate through the volcanic section into the underlying sheeted dyke complex. [e.g. Alt *et al.* 1996]. Hydrothermal alteration in Hole 504B and the Troodos ophiolite are discussed in Chapter 4 of this dissertation.

1.4 Tectonic ridge crest processes

New oceanic lithosphere is created by intrusive and extrusive activity at the crest of the mid-ocean ridge system, which is a complex and dynamic environment. The topography of the axial rift valley depends on the balance between structural extension and magmatic accretion, and changes approximately continuously with spreading rate [Searle 1992]. However, slow-spreading ridges near areas of high mantle heat flow (e.g. hot spots) have a morphology more characteristic of fast-spreading ridges, while intermediate spreading ridges develop a median valley where they are juxtaposed against cold lithosphere at ridge-transform intersections [Searle 1992].

At slow- and intermediate-spreading rates (e.g. MAR; ~25 mm yr^{-1} full rate) inward-dipping normal faults dominate the ridge-parallel fault population, and account for most of the topography of the median valley, which is maintained by rotation of pre-existing fault blocks at the edge of the median valley [Searle 1992]. The rift axis of slow-spreading centres is dominated by an axial rift valley 30 to 45 km wide and 1 to 2 km deep [Smith & Cann 1993]. Consequently, hydrothermal plumes are entirely trapped and transported within the axial valley, which has important implications for models of formation of metalliferous sediment and distal low-temperature hydrothermal precipitates at slow-spreading ridges. At fast-spreading ridges (e.g. EPR; 180 mm yr^{-1} full rate), extension at the ridge crest by normal faulting is much less significant. Outward dipping faults with

Table 1.1: Timescales of observations of the seafloor hydrothermal systems discussed in this thesis: Vent initiation to crustal ageing processes

Examples of:	Timescales of observation/alteration:	Observations:	References:
***A.* Seafloor vent sites**			
Vent initiation:			
9°N EPR	1991, 1994	Volcanic eruption in 1991	1,2
JdFR	1986, 1987	'Megaplume' events in 1986 and 1987	3,4
Steady-state time series:			
21°N, EPR	1979, 1981, 1985	Small, multiple sulphide accumulations at ridge axis	5,6,7
Guaymas Basin	1982, 1985	Sedimented ridge	8,9
TAG vent field, 26°N MAR	1986, 1990, 1993, 1994, 1995	Off-axis fault-controlled deposit	10,11,12,13,14
***B.* ODP drilling:**			
Hole 504B, Costa Rica Rift	0 to 5.9 Myr	Low-T & 'stockwork-type' mineralisation	e.g. 15,16,17,18
***C.* Geological record:**			
Troodos ophiolite, Cyprus	0 to 15-20 Myr	*c.* 20 Myr of low-T crustal ageing processes superimposed on high-T axial alteration	e.g. 19,20,21,22,23,24,25,26,27

[1]Von Damm *et al.* [1995]; [2]Von Damm *et al.* [1997]; [3]Baker *et al.* [1987]; [4]Baker *et al.* [1989]; [5]Edmond *et al.* [1982]; [6]Von Damm *et al.* [1985*a*]; [7]Campbell *et al.* [1988*a*]; [8]Von Damm *et al.* [1985*b*]; [9]Campbell *et al.* [1988*b*]; [10]Mitra *et al.* [1994]; [11]Edmond *et al.* [1995]; [12]James & Elderfield [1996]; [13]Edmonds *et al.* [1996]; [14]Gamo *et al.* [1996]; [15]Honnorez *et al.* [1985]; [16]Alt *et al.* [1985]; [17]Alt *et al.* [1986]; [18]Alt *et al.* [1996]; [19]Staudigel *et al.* [1986]; [20]Gillis & Robinson [1988]; [21]Richardson *et al.* [1987]; [22]Gillis & Robinson [1990*a*]; [23]Gillis & Robinson [1990*b*]; [24]Staudigel & Gillis [1990]; [25]Bickle & Teagle [1992]; [26]Bickle *et al.* [1998]; [27]Wells *et al.* [1998]

similar displacements form a few kilometres from the axis, giving rise to a horst-and-graben tectonic fabric, which has no topographic median valley but a narrow topographic high [Searle 1992; Smith & Cann 1993].

Mid-ocean ridges are ordered into segments that are separated by transform and non-transform offsets, typically with offsets of ≥100 km and a few 10's of km respectively. The scale and style of ridge segmentation varies between fast- and slow-spreading centres. While overlapping spreading centres are common at fast-spreading centres, slow-spreading ridges are more regularly segmented by transform fault zones with large offsets. At slow-spreading ridges rock types from all crustal levels to the upper mantle are exposed in fracture zones; at intermediate and fast spreading ridges only volcanics are exposed [Karson 1990].

Following the recognition of ophiolites as on-land fragments of ridge-generated oceanic crust [Gass 1968], many petrogenic and structural models for deep portions of the oceanic crust have utilised the unique three-dimensional exposure of oceanic crustal sections in ophiolites [e.g. Moores & Vine 1971]. However, the use of ophiolite complexes to understand those processes occurring in the upper oceanic crust was slow until the realisation that many of the low-temperature, brittle deformation structures preserved within ophiolites reflect crustal accretion, rather than obduction processes [e.g. Varga & Moores 1985; Nicolas 1989]. Subsequent mapping of three-dimensional Troodos ridge tectonic structures has lead to the recognition of fossil axial grabens, an oceanic transform fault and apparent propagating rift margin [Varga & Moores 1985; Moores *et al.* 1990].

1.5 Magmatic and volcanic ridge crest processes

Marine geophysical studies of mid-ocean ridges have constrained the structure of the crust at mid-ocean ridges [e.g. Raitt 1963; McConnell *et al.* 1966; Christensen & Salisbury 1975; White 1984; Detrick 1991]. The seismic structure of the oceanic crust is controlled by petrological differences modified by hydrothermal circulation, metamorphic alteration and by the presence of cracks and fissures [White 1984]. The seismicity of fast and slow spreading ridges is distinctive [e.g. Toomey *et al.* 1985; Detrick 1991; Kong *et al.* 1992]. Seismic studies along the fast-spreading EPR (9° N to 13° N) have detected semi-continuous low-velocity zones at ~2 km depth, corresponding to sill-like axial magma chambers (2 km wide and less than 1 km thick), surrounded by partially molten crystal mush or hot solidified rocks [Detrick 1991]. A crustal model of a fast-spreading centre has

a volcanic layer of fissure fed sheet and pillowed flows, a homogenous sheeted dyke complex and a plutonic section with a long-lived magma chamber [review by Searle 1992]. The structure of ocean crust at the MAR is more complex and spatially variable than the EPR [Smith & Cann 1993]. Seismic imaging beneath the along-axis high of the MAR at 26°N ridge has revealed zones of hot rock at the sites of most recent magma injection [e.g. Kong *et al.* 1992], but the steady-state melt lens characteristic of the EPR ridge crest are absent. Microearthquakes on the MAR to depths exceeding 8km indicate that the entire crustal section is cooled to within the field of brittle deformation behaviour [Toomey *et al.* 1985; Toomey *et al.* 1988]. Crustal construction at slow-spreading centres is inferred to occur *via* discrete magma bodies that rise through the crust to feed axial volcanoes on the valley floor [Smith & Cann 1993]. Consequently, the crustal models for slow-spreading centres have pillow volcanoes overlying a heterogeneous sheeted dyke complex with some high-level intrusions, and a plutonic section comprising many small plutons [Smith & Cann 1993]. There is a lesser degree of volcanic continuity than at fast-spreading ridges, with periods of 10^4 years between major volcano-forming episodes, during which the ridge crest evolves by amagmatic, tectonic extension [Smith & Cann 1993].

The crustal section of the Troodos ophiolite is recognised as having been constructed during episodic volcano-tectonic-hydrothermal cycles, similar to those occurring at modern mid-oceanic ridges [Schmincke & Bednarz 1990]. Normal faults and dykes dip towards the axes of structural grabens preserved on the northern flank of the ophiolite, which preserve the relationships between structural, magmatic and hydrothermal processes operating during Troodos seafloor spreading [Varga & Moores 1985]. On Troodos, periods of crustal accretion are inferred to have been punctuated by episodes of amagmatic extensional faulting [Varga & Moores 1990]. Various spreading rates have been proposed for the Troodos ophiolite. Similarities in the dimensions of Troodos axial grabens and the MAR rift valley [Boyle & Robertson 1984] and the episodic nature of axial magmatism (representing multiple magma chambers rather than a steady-state melt lens) [Varga & Moores 1985] are suggestive of intermediate- to slow-spreading rates, while the generally subdued topography of the lava/sediment contact is a characteristic feature of faster-spreading ridges [Allerton & Vine 1987]. These contrasting observations may reflect the episodic nature of magma supply to the spreading centre, with grabens produced during amagmatic tectonic extension, at a time-integrated spreading rate considerably higher than found along current slow-spreading ridges [Varga & Moores 1990].

1.6 Magmatic, tectonic and volcanic controls on hydrothermal activity

The location of active hydrothermal vents must be controlled by the local ridge crest tectonic-magmatic regime, although this relationship is poorly understood due to limited surveying of the mid-ocean ridge system at sufficiently high resolution [review by Fornari & Embley 1995]. However, differences in magma supply and tectonic styles at fast- and slow-spreading centres affects the stability of the permeability structure of the upper crust [e.g. Karson 1990; Karson 1991] and is therefore predicted to influence the nature, depth and longevity of hydrothermal circulation and crustal alteration [e.g. Karson & Rona 1991]. This may account for the observed differences between long-lived hydrothermal sites such as TAG vent field on the slow-spreading MAR and the generally smaller sulphide deposits formed from transient systems on faster spreading ridges [Fornari & Embley 1995].

Ballard *et al.* [1982] proposed a volcano-tectonic cycle for the Galapagos Spreading Centre (GSC) where hydrothermal circulation is initiated by volcanic eruptions. The most intense hydrothermal activity is predicted to occur near the along-strike topographic high of the ridge crest which occurs approximately mid-way between two transform faults [Francheteau & Ballard 1983]. However, tectonic features are clearly important in controlling venting at other sites. Many large deposits at a range of spreading rates (TAG, Endeavour and Explorer Ridges and 13° N EPR) are associated with normal faulting at the edges of the axial rift valley. In the case of the TAG vent field, axis-transverse structures are also inferred to be important in maintaining the high permeability discharge zones [Kleinrock & Humphris 1996]. A deep-tow survey of hydrothermal plumes between 36°N and 38°N on the MAR also found tectonic parameters to be the dominant control on the location of focused hydrothermal discharge [German *et al.* 1996]. On this section of the MAR, the majority of hydrothermal sites are located on highly tectonised crust near to non-transform offsets, rather than at the centre of individual ridge segments, and on areas of the seafloor characterised by the absence of any freshly erupted basalts [German *et al.* 1996].

While the large-scale structure and longevity of hydrothermal systems is controlled by the major structural elements of the ridge crest such as rift boundary faults, on a vent field scale hydrothermal discharge is dependant on near-surface permeability [Hannington *et al.* 1995]. Newly generated oceanic lithosphere is pervasively cut by fissures that form very close to the ridge axis [Searle 1992]. These structures, as well as local variations in lava

morphology and volcanic features such as ponded flows, lava tubes and collapsed talus can influence the permeability structure of the shallow crust (upper 300 m), and impart a permeability stratigraphy that can favour localised hydrothermal circulation [Fornari & Embley 1995].

Ophiolitic lavas have a somewhat different morphology compared with mid-ocean ridge basalts (MORB), that may have had implications for near-surface permeability and fluid flow through the upper Troodos crust. Troodos basalts were produced by partial melting of depleted mantle peridotites of a mantle wedge under hydrous conditions, in the presence of fluids emanating from a subducted slab [Pearce 1975], compared with MORB that is produced by prolific (*c.* 15-30 %) partial melting of the mantle at shallow levels (<30 km) under essentially anhydrous conditions [e.g. Green & Ringwood 1967; Jaques & Green 1980]. The high vesicularity of Troodos lavas and the broader spectrum of extrusive processes compared to MORB volcanoes is attributed to enhanced viscosities and volatile exsolution at similar inferred extrusion depths [Schmincke & Bednarz 1990]. Within the ophiolite, major sulphide ore bodies occur within axial seafloor grabens, and appear to be related to hydrothermal circulation along graben faults, driven by the late intrusion of plutons into highly deformed and tectonically thinned oceanic crust [Varga & Moores 1985].

1.7 Hydrothermal fluids

Studies of deep sea hydrothermal vents began with the discovery of diffuse fluids and low-temperature hydrothermal oxide and silicate deposits at the GSC as part of a joint French-American submersible investigation of the ridge crest [Klinkhammer *et al.* 1977; Lupton *et al.* 1977; Corliss *et al.* 1979; Edmond *et al.* 1979*a,b*; Speiss *et al.* 1980*a,b*; Klinkhammer 1980; Fehn *et al.* 1983]. The metal-poor fluids were recognised to have been diluted with cold seawater in the shallow subsurface of the hydrothermal system [Edmond *et al.* 1979*a*]. The first ~380° C 'black smoker' fluid was sampled 2 years later at 21°N on the EPR [Speiss *et al.* 1980*a,b*] and had a composition similar to the predicted end-member high temperature fluid at Galapagos [Edmond *et al.* 1982; Von Damm *et al.* 1985*a*]. Every vent field subsequently sampled has extended the range of known vent fluid compositions [review by Von Damm 1995]. Most research efforts have been towards characterising black smoker chemistries, as these fluids are easier to sample without dilution by local seawater than lower-temperature diffuse flow [but see Schultz *et al.*

1992; James & Elderfield 1996; Schultz *et al.* 1996].

1.7.1 High-temperature fluids

Seawater is transformed into hydrothermal fluid by a series of incremental reactions between seawater and basalt (and more rarely sediment) at elevated temperatures and pressures during circulation through the ocean ridge system. The observed changes in water chemistry are a function of variables including temperature, pressure, basalt composition (that shows limited variation along the mid-ocean ridge), the composition of any sediment cover (that where present, can be highly variable), whether the basalts have been previously altered, whether fluid-rock equilibrium is achieved at depth, and whether the fluids have undergone phase separation or mixed with cooler fluids in the subsurface of the system during their ascent to the seafloor [e.g. Hajash 1975; Bischoff & Dickson 1975; Van Damm *et al.* 1985*b*; Berndt *et al.* 1988; Palmer & Edmond 1989*a*; Berndt *et al.* 1989; Von Damm 1990; Seyfried *et al.* 1991; Von Damm 1995; James *et al.* 1995; German *et al.* 1995*b*].

The critical changes in fluid chemistry that occur during hydrothermal circulation are a reduction in pH, the complete loss of Mg and SO_4, and increases in Si and H_2S, the trace alkali elements (K, Li, Rb, Cs), volatile elements (He, H_2, CH_4, H_2S and CO_2) and in Fe, Mn and the other ore-forming elements (Cu, Zn, As, Se, Cd, Co Ag and Pb) [Von Damm 1990]. The observed variations in chloride content of vent fluids (*c.* 30 to 200% of seawater values) necessitates phase separation and brine/vapour segregation in the subsurface of the system [review by Von Damm 1995]. These processes have also been invoked to account for the range of compositions of fluid inclusions in the upper plutonics of the Troodos ophiolite [Cowan & Can 1988]. Phase separation has a profound effect on the distribution of metals at hydrothermal vents, that are stabilised in solution by chloride-complexation [Von Damm 1990]. Metals are partitioned into the chloride-rich, high salinity phase while the concentration of gases is greater in the vapour-rich phase [Von Damm *et al.* 1995; Von Damm *et al.* 1997].

Studies of ophiolites have not generally been able to constrain the hydrothermal fluid chemistry because they integrate a long history of alteration, which may or may not be dominantly related to axial venting processes [Gillis & Robinson 1990*a,b*; Gillis & Robinson 1988; Wells *et al.* 1998].

1.7.2 Diffuse flow

Thermal considerations indicate that the low-temperature circulation of low-temperature pore fluids through the flanks of the ocean ridge system is responsible for advection of ~80% of the hydrothermal heat flux associated with crustal accretion [Morton & Sleep 1985]. The chemical fluxes associated with the off-axis hydrothermal flux are not well known, as the flank flow is too diffuse to be readily sampled [review by Elderfield & Schultz 1996]. Diffuse fluids with temperatures ranging from <10 to ~100°C are also ubiquitous in axial hydrothermal systems, where the partitioning of the heat transport between black smoker and diffuse fluids is not well constrained. However, numerous observations of extensive areas of diffuse flow at many vent sites, and the results of the few experimental studies indicate that the heat and mass flux associated with diffuse flow may be up to an order of magnitude greater than that of focused high-temperature flow [Schultz *et al.* 1992].

Diffuse flow may represent the earliest form of discharge at vent fields, prior to the development of insulating chimneys that inhibit seawater mixing. Diffuse fluids are also typically present at the margins of high temperature upflow where hydrothermal fluids mix with seawater, and additionally dominate the waning stages of hydrothermal activity as the magmatic intrusion beneath the ridge solidifies [review by Hannington *et al.* 1995]. Diffuse fluids are frequently associated with deposits of Fe- and Mn-oxides, authigenic clays and silica [e.g. Edmond *et al.* 1979*b*; Thompson *et al.* 1985; Alt *et al.* 1987], and are often surrounded by biological communities, as they represent a significant nutrient source [review by Jannasch 1995].

Diffuse flow is not only more important than black smoker fluids in terms of mass and heat transport, but also in defining the high-temperature end product of hydrothermal mineralisation [e.g. Edmond *et al.* 1995; Tivey *et al.* 1995]. Diffuse fluids formed by seawater ingress into sulphide mounds act to 'zone refine' the sulphide ore, by dissolving lower-temperature (Zn-rich) sulphides within the mound and re-depositing them at the cooler margins of the deposit [Mitra *et al.* 1994; Edmond *et al.* 1995; Tivey *et al.* 1995; *James et al.* 1996]. A similar origin has been implied for the zonation that has been frequently recognised in on-land sulphide ore bodies [Franklin *et al.* 1981; Edmond *et al.* 1995].

1.8 Sulphide mineralisation

By definition a 'massive sulphide' deposit contains sulphide minerals in excess of ~50%, in addition to any disseminated sulphide mineralisation [Graf 1977]. Massive sulphide deposits located around black smoker sulphide chimneys were first described at 21°N, EPR [Speiss *et al.* 1980*b*], and have subsequently been located along much of the explored mid-ocean ridge system [Rona 1984]. The massive sulphide deposits of the Troodos ophiolite complex are among the best known ancient analogues of seafloor sulphide mineralisation at mid-ocean ridges [Constantinou & Govett 1973; Constantinou 1980; Adamides 1980; Adamides 1990]. They are spatially and genetically associated with structural grabens produced during Tethyan seafloor spreading [Varga & Moores 1985], and exhibit a style of mineralisation and bulk compositions similar to modern vent sulphides [e.g. Haymon & Kastner 1981; Oudin *et al.* 1981; Rona *et al.* 1986; Fouquet *et al.* 1988; Hannington *et al.* 1991; Hannington *et al.* 1995; Hannington *et al.* 1988].

1.8.1 Black smoker chimneys

The hydrothermal flux of dissolved metals, sulphide and silica are released into the oceans at deep sea vents. Seafloor sulphide deposits and particle-rich hydrothermal plumes form as the hydrothermal fluid comes into contact with cold, oxic seawater. Turbulent mixing in natural systems results in a considerable variety of vent morphologies, with flanges, beehive diffusers, flanges, mounds, and steep sided edifices forming vent deposits, in addition to chimney orifices [Tivey 1995]. In spite of this diversity, early descriptive, numerical and chemical models for the sequence of mineral precipitation at hydrothermal vents were based on the spectacular black smoker chimneys, that differ from other vent structures by having a central chalcopyrite-lined conduit and anhydrite-rich outer wall [Haymon 1983; Janecky & Seyfried 1984; Bowers *et al.* 1985; Bowers *et al.* 1988; Tivey & McDuff 1990]. Iron sulphides (pyrite and pyrrhotite) are the most commonly observed minerals in black smoker chimneys , followed by zinc sulphides (sphalerite and wurtzite) and variable amounts of copper sulphides (primarily isocubanite, bornite and chalcopyrite) with occasional lead sulphide (galena) [review by Hannington *et al.* 1995]

The principal physical and chemical parameters that influence the morphology and style of mineralisation in seafloor hydrothermal systems are pH and redox conditions (fugacity of oxygen and sulphur, fO_2 and fS_2), temperature (mixing-cooling history), water depth (stockwork mineralisation can be induced by subcritical boiling of upwelling fluids), source rock composition and near-surface permeability [reviews by Hannington *et al.*

1995; Tivey *et al.* 1995]. Many of these parameters do not vary significantly along the mid-ocean ridge system [Tivey 1995], and most black smoker fluids have compositions buffered close to equilibrium with pyrite-pyrrhotite-magnetite [Hannington *et al.* 1995].

Determinations of chimney growth rates and ages in vent fields on the EPR, JdFR and MAR using U-series isotope geochronology studies indicate that vent chimneys form rapidly, with active and inactive chimneys having ages from ~0.5 to 2.5 years, while larger sulphide edifices have ages up to ~20 years [Lalou & Brichet 1982; Kadko *et al.* 1985; Moore & Stakes 1990; Lalou *et al.* 1990; Stakes & Moore 1991]. Off-axis structures at 12°N, EPR have sulphide ages between ~2000 and 20,000 yrs [Lalou *et al.* 1985], while samples from the TAG field, 26°N, MAR indicate sulphide precipitation in the same locality over the last ~40,000 years [Lalou *et al.* 1993; You & Bickle 1998].

Inactive chimneys collapse due to sulphide mass wasting and dissolution of the anhydrite cement at ambient seafloor temperatures [Hannington *et al.* 1995]. Collapsed chimneys may form a part of the rubbly surface of seafloor sulphide deposits, or are completely oxidised and may form inputs to near-field metalliferous sediments [Metz *et al.* 1998; German *et al.* 1993; Mills *et al.* 1993]. Sulphide chimneys are not well preserved in older vent complexes, and only rarely recognised in ophiolitic sulphide bodies [Oudin *et al.* 1981; Oudin & Constantinou 1984].

1.8.2 Seafloor sulphide mounds

Dissolved metals, sulphide and silica are dispersed within the oceanic environment when hydrothermal fluids vent through seafloor sulphide structures. A more efficient mineralisation process is the deposition of metals, sulphide and silica within seafloor sulphide mounds [e.g. Edmond *et al.* 1995; Tivey *et al.* 1995]. The ore-forming elements are deposited subsurface due to cooling and mixing with entrained seawater [Tivey *et al.* 1995]. While black smokers may be present, the fluid flow from the mound surface frequently includes a range of lower-temperature diffuse fluids [e.g. Mitra *et al.* 1994; James *et al.* 1996].

Cyprus-type massive sulphide bodies are also assumed to have formed by a combination of sub-surface mineralisation and accumulating chimney talus [Constantinou & Govett 1973; Constantinou 1980; Oudin *et al.* 1981; Oudin & Constantinou 1984]. Sulphide debris at the surface of sulphide mounds becomes cemented and reworked by later sulphide mineralisation [Constantinou & Govett 1973]. Consequently, seafloor sulphide

mounds and Cyprus-type ore bodies are dominated by recrystallised pyrite [Constantinou & Govett 1973; Humphris *et al.* 1995], compared with young chimney deposits which show a range of morphologies, compositions and sulphide textures [e.g. Haymon & Kastner 1981].

1.9 Hydrothermal plumes

Hydrothermal plumes form as vent fluids entrain large quantities of seawater before reaching density equilibrium with the surrounding seawater, tens to hundreds of metres above the vent source. Hydrothermal plumes integrate and disperse the thermal and chemical output from seafloor vent systems, and their anomalous properties can be used to estimate chemical and thermal hydrothermal fluxes from the underlying vent field [review by Lupton 1995]. Additionally, because they have a broad lateral extent in the water column that far exceeds the point sources of seafloor venting, they have been used as an oceanic exploration tool to locate new hydrothermal vent fields on the mid-ocean ridge system [review by Baker *et al.* 1995]. Hydrothermal plumes are identified by their anomalous physical properties (temperature, salinity and density), elevated concentrations of dissolved elements (Mn, Fe, Al, Si, methane, hydrogen and radon) and suspended particles [review by Lupton 1995]. To date, *c.*10% of the mid-ocean ridge system has been examined for chemical or physical evidence of hydrothermal plumes [e.g. Klinkhammer *et al.* 1977; Lupton *et al.* 1977; Weiss *et al.* 1977; Jenkins *et al.* 1978; Baker *et al.* 1985; Klinkhammer *et al.* 1985; Klinkhammer *et al.* 1986; German *et al.* 1994; German *et al.* 1996; Wilson *et al.* 1996].

The buoyant plume is that portion of the plume having positive buoyancy and finite vertical velocity. The plume is diluted during ascent from the seafloor by seawater entrainment caused by shear flow between the buoyant hydrothermal fluid and ambient seawater [Lupton 1995]. The plume is diluted 10^2 to 10^3 in the first 5 to 10 m of rise, then another order of magnitude before reaching density equilibrium with surrounding seawater and spreading as a neutrally buoyant layer [Lupton 1995]. The neutrally buoyant plume comprises diluted vent fluid (including entrained diffuse fluids), ambient seawater at the same level, and seawater from deeper in the water column that has been entrained during plume ascent [e.g. Rudnicki & Elderfield 1992]. The height of plume rise is dependent upon the entrainment coefficient, the density gradient of the local water column, and less critically on the discharge buoyancy (heat) flux, and for most vent fields is ~150 to 300 m

above the seafloor [Speer & Rona 1989]. Plume studies at TAG, 26°N MAR, suggest that the total heat entering the overlying water column from hydrothermal activity is in the range 500 to 1000 MW [Rudnicki & Elderfield 1992]. However a megaplume mapped in 1986 on the JdFR was associated with a much larger heat flux (*c.* 30 000 MW) than plumes formed by steady-state venting [Baker *et al.* 1989]. The megaplume was 20 km in diameter, almost 600 m thick, and was centred 800 m above the ridge crest. [Baker *et al.* 1989].

In the Pacific Ocean, hydrothermal plumes are widely dispersed and oxidised in the regional mid-depth circulation, and can be detected by their anomalous properties several thousands of kilometres from their ridge crest sources [Lupton & Craig 1981; Edmond *et al.* 1982; Klinkhammer & Hudson 1986]. In the Atlantic, the height of buoyant plume rise is considerably less than the height of the bounding walls of the axial rift valley (*c.* 2 km), and MAR plumes are trapped and transported entirely within the axial rift valley [Klinkhammer *et al.* 1985; Klinkhammer *et al.* 1986].

The chemical evolution of vent fluids continues within hydrothermal plumes [e.g. Feely *et al.* 1987; Dymond & Roth 1988; Trocine & Trefry 1988; Mottl & McConachy 1990; German *et al.* 1990 Kadko *et al.* 1990; German *et al.* 1991*a,b*; Feely *et al.* 1992; German & Sparks 1993; Rudnicki & Elderfield 1993; Mitra *et al.* 1994]. Rapid mixing between high-temperature vent fluids and seawater within a few seconds to a few minutes of venting causes the precipitation of around 50% of the Fe in the vent fluid in a non-equilibrium assemblage of sulphide, sulphate and oxide particles above the throat of the chimney and in the buoyant plume [Rudnicki & Elderfield 1993; Lilley *et al.* 1995]. Larger sulphide and sulphate particles quickly settle from the buoyant plume and begin to dissolve in ambient seawater [Feely *et al.* 1987; Dymond & Roth 1988; Trocine & Trefry 1988]. The remaining dissolved Fe is oxidised over a longer time-scale to fine grained oxyhydroxide particles in the buoyant plume [Mottl & McConachy 1990; Rudnicki & Elderfield 1993]. Manganese displays a near-conservative behaviour in the buoyant- and neutrally buoyant plume, and is a sensitive tracer of plume dispersion as it resists oxidation for some time after discharge, in contrast to iron and many other metals [Klinkhammer *et al.* 1983]. The precipitation of Mn in the neutrally buoyant plume occurs by microbially-mediated oxidative scavenging processes [Cowen *et al.* 1990]. Microbial activity related to the oxidation of methane and H_2 has also been demonstrated to be important in hydrothermal plumes [Kadko *et al.* 1990; Cowen *et al.* 1986]. Particulate Mn

concentrations in the neutrally buoyant plume increase away from the vent field to distances of ~80-150 km, where they start to decrease by dilution with ambient suspended matter [Dymond & Roth 1988; Feely *et al.* 1992].

The impact of hydrothermal venting on seawater chemistry depends on subsequent chemical reactions, mixing and dispersal within hydrothermal plumes [e.g. Mitra *et al.* 1994; German *et al.* 1990; German *et al.* 1991*a,b*; Kadko 1993]. Plumes contains hydrothermal tracers derived from the vent fluid (e.g. ^{3}He, Mn, Fe, hydrogen and suspended particles) and tracers that have entirely or in part been introduced by seawater entrainment (e.g. salinity, silica and radon) [review by Kadko *et al.* 1995]. Conservative tracers are those elements or species whose concentration is sensitive only to dilution. The only true conservative tracers in hydrothermal plumes are temperature, salinity and inert gases such as ^{3}He. Dissolved manganese is not a true conservative tracer because its concentration is sensitive to slow microbially-mediated oxidation [Cowen *et al.* 1986; Cowen *et al.* 1990]. Because Fe- and Mn-oxyhydroxide particles provide extensive sites for chemical reaction and exchange, most tracers exhibit non-conservative properties because their concentrations are affected by chemically or microbially-mediated uptake processes [Kadko *et al.* 1995]. Chalcophile elements such as Cu, Zn, Cd and Pb that precipitate as sulphide phases exhibit non-conservative behaviour as they are removed from the neutrally buoyant plume due to differential sedimentation and/or oxidative dissolution [German *et al.* 1991*a*]. Some trace elements coprecipitate with Fe-oxyhydroxides in the buoyant plume, without any further uptake during plume rise and dilution. This behaviour is characteristic of the oxyanions (P, U, V, Mo, Cr and As), which are largely derived from seawater entrained during buoyant plume rise [Trocine & Trefry 1988; Trefry & Metz 1989; Feely *et al.* 1990; German 1991a; Rudnicki & Elderfield 1993]. In contrast, particle-reactive elements like the REE and Th are continually scavenged from seawater onto plume particle surfaces in the buoyant and neutrally buoyant plume. The REE/Fe and Th/REE ratios of these particles increase with distance from the vent source [Klinkhammer *et al.* 1983; German *et al.* 1990, 1991*a*; Rudnicki & Elderfield 1993]. Particle scavenging during lateral transport of the plume away from the vent affects the chemistry of ambient water [e.g. Klinkhammer *et al.* 1983], and impacts the ocean on a scale exceeding the local ridge crest as seawater is focused through the plume *via* horizontal transport processes [Kadko *et al.* 1995]. Co-precipitation and/or scavenging plays an important role in the geochemical cycles of several elements in seawater, balancing the global budget for the REEs and playing an important role in the

removal of oxyanions (~70% of the riverine flux) [Rudnicki & Elderfield 1993; Kadko 1993].

The ultimate fate of the plume particle load is to contribute to the formation of metalliferous sediments on the seafloor. In the Pacific Ocean, metalliferous sediments extend off-axis for several thousands of kilometres from their ridge-crest sources [Lupton & Craig 1981; Klinkhammer & Hudson 1986]. In the Atlantic, both near- and far-field hydrothermal deposits are confined to the axial rift valley [Metz *et al.* 1988; Mills *et al.* 1993].

1.10 Metalliferous sediments

The association of metalliferous sediments with active mid-ocean ridges has been observed since the 1960's concurrent with the development of models of seafloor spreading [Böstrom & Peterson 1966; Böstrom & Peterson 1969]. Metalliferous sediments were first studied on the EPR, but were subsequently found to delineate the entire mid-ocean ridge system [Arrhenius & Bonatti 1965; Skornyakova 1965; Bostrom & Peterson 1966; Bostrom & Peterson 1969; Bender *et al.* 1971; Piper 1973; Dymond & Veeh 1975], and occur as the basal facies of sediments that overlie the oceanic basement [Dymond *et al.* 1973; Barrett *et al.* 1987].

With the recognition of ophiolites as fragments of ancient seafloor [Gass 1968], many of the metalliferous sediments in the geological record could also be attributed to hydrothermal processes occurring at ancient oceanic spreading centres [e.g. Robertson & Hudson 1973; Robertson 1976; Robertson & Fleet 1986; Boyle 1990; Robertson & Boyle 1993]. Metalliferous sediments have been studied from ancient seafloor settings including the Pindos ophiolite, Greece [Robertson & Varnavas 1993], the Semail ophiolite, Oman [Fleet & Robertson 1980; Robertson & Fleet 1986; Karpoff *et al.* 1988] and the Troodos ophiolite, Cyprus [Wilson 1959; Constantinou & Govett 1972; Robertson 1976; Boyle 1990].

Metalliferous sediments associated with submarine hydrothermal systems form in three ways; from plume input [Bender *et al.* 1971; Dymond *et al.* 1973; Dymond & Veeh 1975; Ruhlin & Owen 1986; Barrett & Jarvis 1988; Olivarez & Owen 1989, Olivarez & Owen 1991], by the alteration of hydrothermal sulphides [Shearme *et al.* 1983; Metz *et al.* 1988; German *et al.* 1993; Mills *et al.* 1993] and by the direct precipitation of oxides from low temperature fluids [Toth 1980; McMurtry & Yeh 1981; McMurtry *et al.* 1983; Alt 1988;

Mills & Elderfield 1995*a*; Mills *et al.* 1996].

While hydrothermal effluents on the EPR are dispersed laterally by the mid-depth oceanic circulation [Lupton & Craig 1981; Edmond *et al.* 1982], the depth of the median rift valley on the MAR (1-2 km deep) confines the products of hydrothermal venting to the axial rift valley, and their dispersal to only 10's of kilometres from the hydrothermal vents [Klinkhammer *et al.* 1986]. Studies of MAR sediments have generated models for the formation of near-field metalliferous sediments, that are complex mixtures of material from multiple sources [e.g. Mills *et al.* 1993]. Near-field metalliferous sediments in the TAG vent field, MAR are formed by settling through the water column of particles from laterally dispersed hydrothermal plumes, by the mass wasting and oxidative degradation of hydrothermal sulphide structures, and precipitation from, or alteration by low-temperature fluids, with additional detrital and biogenic inputs [Metz & Trefry 1985; Metz *et al.* 1988; Mills *et al.* 1993; German *et al.* 1993; Mills *et al.*1996]. Ochreous sediments comprising oxidised and partially oxidised sulphides, goethite, minor smectite amorphous oxides have been described from the EPR [Alt 1988] and the TAG vent field [Mills & Elderfield 1995*a*]. These sediments are similar to those occurring in the seafloor-weathered upper zones of Troodos massive sulphide deposits [Robertson 1976].

Studies of metalliferous sediments have allowed assessment of the fluxes associated with hydrothermal activity over time [review by Mills & Elderfield 1995*b*]. The formation of metalliferous sediments has the greatest impact on the global budgets of those elements that are scavenged from seawater by hydrothermal plume particulates [Kadko 1993]. Metalliferous sediment formation affects the global budgets of many elements, but represents a major sink for the REE, V and P [Mills & Elderfield 1995*b*].

1.11 Aims of the present study

This dissertation presents a comparison of the REE systematics of hydrothermal materials from the Trans-Atlantic Geotraverse (TAG) vent field, 26° N Mid-Atlantic Ridge and the Troodos Ophiolite, Cyprus. Previous investigations of both areas have been instrumental in the recognition of the significance of hydrothermal circulation at mid-ocean ridges, and in developing models of the mineralising systems. The aims of the present study are to:

- compare the REE systematics of hydrothermal deposits in both settings
- establish the relative REE mobility in a Troodos stockwork-type massive sulphide deposit during axial hydrothermal alteration and subsequent ageing of the oceanic

basement

- use the REEs as geochemical proxies of hydrothermal processes to determine if the current TAG model of sulphide mineralisation and metalliferous sediment formation is applicable to Troodos sulphide mound deposits
- use the REEs and Nd-isotopes to investigate the mode of formation of low-temperature Mn- and Fe-rich oxide deposits from the TAG vent field

1.12 Dissertation outline

Chapter 2 describes some applications of REE geochemistry to investigations of the processes operating within seafloor hydrothermal systems. Chapter 3 compares the spectrum of metalliferous deposits associated with ridge crest hydrothermal activity within the TAG vent field, and the Troodos ophiolite, Cyprus. The current TAG models of sulphide mineralisation and metalliferous sediment formation are also described. Chapter 4 provides an overview of the processes of hydrothermal alteration of the oceanic crust, as deduced from studies of *in situ* ocean crust and the altered crustal rocks of the Troodos ophiolite. Chapter 5 describes the analytical techniques employed in this study to measure the REE, major and trace element compositions of the hydrothermal materials investigated in this dissertation.

The results of this study are presented in Chapters 6, 7 and 8. Chapter 6 describes the distribution of REEs between high- and low-temperature secondary minerals within the lavas of a stockwork-mineralised alteration pipe within the Troodos ophiolite. REE data are presented for whole-rock samples, in addition to high- and low-temperature secondary alteration phases. These data have been used to infer fluid compositions and mixing in a hydrothermal upflow zone, and to establish relative REE mobility during axial hydrothermal alteration and subsequent ageing of the oceanic basement. Chapter 7 of this dissertation presents REE and other geochemical data for a suite of samples collected from the Skouriotissa ore body and other sites of hydrothermalism within the Troodos ophiolite. Sampling of Skouriotissa sulphides and associated metalliferous sediments was undertaken on a similar scale to on the seafloor at TAG, to allow interpretation of the results within the framework of the TAG model, and to better assess the effects of post-ore alteration. In chapter 8, the REEs have been used to investigate the mode of formation of low temperature Mn-oxide deposits from the TAG hydrothermal vent field, in light of previously suggested models. Chapter 9 provides a synthesis of these investigations. The appendix provides a glossary of terms used throughout the dissertation.

Chapter 2

Rare Earth Elements and Neodymium isotopes

2.1 Introduction

The unique chemical characteristics of the rare earth elements make them useful indicators of material sources, and subsequent mixing and fractionation processes in complex geological systems. They have been extensively utilised in petrological investigations [review by Haskin 1984], sediment provenance studies [e.g. Piper 1974; McLennan 1989] and to better understand the processes controlling the chemistry of the oceans [Elderfield 1988]. More recently the REEs have been applied to investigations of hydrothermal circulation and mineralisation at oceanic ridge crests [Michard *et al.* 1983; Michard & Albarède 1986; Campbell *et al.* 1988*b*; Michard 1989; German *et al.* 1990; Gillis *et al.* 1990; Klinkhammer *et al.* 1994; Mitra *et al.* 1994; Mills & Elderfield 1995*a*; James & Elderfield 1996].

The properties of the REEs as tracers of source and/or mixing are ideally suited to studies of hydrothermal systems. The mechanisms controlling their concentration and mass fractionation can be elucidated, because their fundamental chemical properties are similar, but vary in a systematic and predictable manner with increasing atomic number (and decreasing atomic radius). Additionally, two of the REEs (Ce and Eu) can exist in two different valence states within the range of redox conditions observed within seafloor hydrothermal systems. It is therefore possible to separate the role of oxidation from that of all other processes affecting the behaviour of these two elements, by comparing their concentrations with those of the adjacent REEs.

In this chapter, the fundamental properties of the REE are discussed, and some applications of REE geochemistry and Nd-isotopes systematics to studies of ore-forming hydrothermal systems are reviewed.

2.2 Fundamental properties

The REEs (La through to Lu) typically exist as trivalent cations of a similar size in natural systems. The REEs exhibit very similar chemical properties due to their electronic structure, that permits only limited geochemical fractionation within the group. Electrons are progressively added to the inner 4*f* sub-shell with increasing atomic number. These electrons are sufficiently shielded by outer 5*s* electrons that their addition does not lead to major differences in chemical reactivity. The small observed differences in chemical behaviour are a consequence of the small but steady decrease in atomic volume of the REE with increasing atomic number. This is due to an increase in effective nuclear charge across the group, that causes a reduction in the size of the 4*f* sub-shell referred to as the lanthanide contraction. For example, in eight-fold co-ordination the ionic radius of La is 1.160 Å compared with 0.977 Å for Lu [Shannon 1976]. These variations can lead to enrichments or depletions of the light REEs (LREEs: La to Eu) relative to the heavy REEs (HREEs: Gd to Lu) by affecting complexation and surface-adsorption constants through the group [e.g. Cantrell & Byrne 1987; Wood 1990*a,b*; Haas *et al.* 1996]. These effects lead to predictable differences in the way the REEs partition into mineral phases and are transported in solution [e.g. Onuma *et al.* 1968; Morgan & Wandless 1980; Klinkhammer *et al.* 1994].

Mass fractionation of Ce and Eu from the other REEs occurs because they display a redox chemistry. While the trivalent REE exhibit a high degree of chemical coherence, redox conditions in geochemical systems may promote the formation of Ce^{4+} and Eu^{2+}, which can then fractionate from the trivalent REEs. The existence of these states can be partly explained on the basis of the enhanced stability of a half-filled 4*f* sub-shell (Eu^{2+}), while Ce^{4+} has the electronic configuration of the noble gas xenon. Ce exists in this higher oxidation state in oxic seawater as a highly insoluble solid phase (refer to section 2.3). The Eu^{3+}/Eu^{2+} redox boundary is below the lower limit of the stability field of water at earth surface conditions, although Eu^{2+} exists in submarine hydrothermal fluids formed under conditions of elevated temperature and low pH (section 2.5) [Sverjensky 1984].

Because nuclides with even atomic numbers have a greater natural abundance, REE data are normalised to a reference material with a similar saw-tooth pattern of absolute REE concentrations. This produces smooth patterns of relative abundances, in which subtle fractionation of the LREE from the HREE, and any anomalous behaviour of Ce and Eu can be discerned. Chondrite or shale composites are common compositions to which REE

data are normalised. It is instructive to normalise to a source component within the system under consideration, to better discern and interpret the mass fractionation trends. The REE data presented in this dissertation are normalised to a composite chondrite composition [Evensen *et al.* 1978].

The Ce anomaly, Eu anomaly, and the fractionation between the LREE and the HREE are often quantified to facilitate comparison of sample data. The REE data presented in this dissertation were obtained by inductively coupled plasma-mass spectrometry (ICP-MS), that allows concentration determinations of all fourteen naturally-occurring REEs. However, many of the published REE data discussed in this thesis were obtained by thermal ionisation-mass spectrometric isotope dilution (TI-MS ID). This is a highly accurate technique, the basis of which is the determination of the isotopic composition of each REE by mass spectrometry. Consequently, this method is not applicable to the four mono-isotopic REEs (Pr, Tb, Ho and Tm). In order to facilitate comparison of the ICP-MS data with published TI-MS ID data, the Ce anomaly has been calculated using La and Nd (rather than La and Pr) data. The deviation of Ce and Eu from the other REE can be expressed as:

$$\text{Eu anomaly} = \frac{\text{Eu}}{\text{Eu}^*} = \frac{2\text{Eu}_n}{\text{Sm}_n + \text{Gd}_n}$$

and

$$\text{Ce anomaly} = \frac{\text{Ce}}{\text{Ce}^*} = \frac{3\text{Ce}_n}{2\text{La}_n + \text{Nd}_n}$$

where the subscript n refers to the normalised values and the superscript * refers to the value obtained by linear interpolation between adjacent elements. In chapters 6, 7 and 8 of this dissertation the Nd_n/Yb_n and La_n/Sm_n ratios are used to quantify the fractionation of the LREE from the HREE and the relative degree of LREE depletion respectively. In the absence of Gd data for every sample, the chondrite normalised Eu/Sm (Eu_n/Sm_n) ratio has occasionally been used to approximate the Eu anomaly.

2.3 REE in seawater

The REEs are transported to the oceans chiefly transported as a particulate load, with a

REE pattern that is primarily a function of provenance [Piper 1974; McLennan 1989]. Because the oceanic residence times of the REEs (e.g. ~270 yr for Nd [Goldberg *et al.* 1963]) are less than the mixing time of the ocean (~10^3 yr), they have a heterogeneous distribution in seawater [Elderfield 1988]. REE concentrations in the oceans generally increase with depth, showing a nutrient-like cycle of assimilation into settling particles and deep regeneration, although in detail their behaviour is decoupled from that of silica and nutrients [Elderfield 1988; Piepgras & Jacobsen 1992].

The chondrite-normalised REE compositions of North Atlantic and Pacific seawater are shown in Fig. 2.1. Seawater is characterised by low REE abundances (pmol kg^{-1}), and a pronounced negative Ce anomaly. Seawater is HREE-enriched compared with detrital continental inputs, although this enrichment is not particularly apparent in Fig. 2.1, in which the REE data are normalised to a chondrite (rather than shale) composition. The anomalously low concentration of Ce in seawater is due to its autocatalytic oxidative removal as highly insoluble CeO_2, that is rapidly scavenged onto Mn-oxide phases [Goldberg 1961]. Speciation of the trivalent REEs in seawater is dominated by carbonate complexation [Cantrell & Byrne 1987]. The degree of complexation with seawater carbonate ligands increases with atomic number, rendering the HREE more soluble in seawater (accounting for the relative HREE-enrichment), and hence less prone to particle-reactive uptake than the LREE [Elderfield 1988]. The seawater distribution pattern and concentration of the trivalent REEs is a function of the degree of modification of the REE input signal from the continental weathering by biogeochemical cycling of the vertical particle flux (preferential removal of LREEs onto Mn- and Fe-oxides and organic matter-coated particulates that are recycled at depth) and lateral advection in the deep ocean circulation [Elderfield 1988].

2.4 REEs in oceanic basalts

Mid-ocean ridge basalts (MORB) are compositionally heterogeneous, reflecting fundamental variations in mantle source trace element compositions [review by Saunders 1984]. The most abundant type of ocean ridge basalt erupted at oceanic ridges is "normal" MORB (N-MORB) [Saunders 1984]. A typical N-MORB composition is shown in Fig. 2.1. N-MORB is characteristically depleted in LREEs, as well as other incompatible elements, and has low $^{87}Sr/^{86}Sr$ and high $^{143}Nd/^{144}Nd$ ratios, indicating derivation from a mantle source which has undergone a previous melt extraction [e.g. White & Hofmann

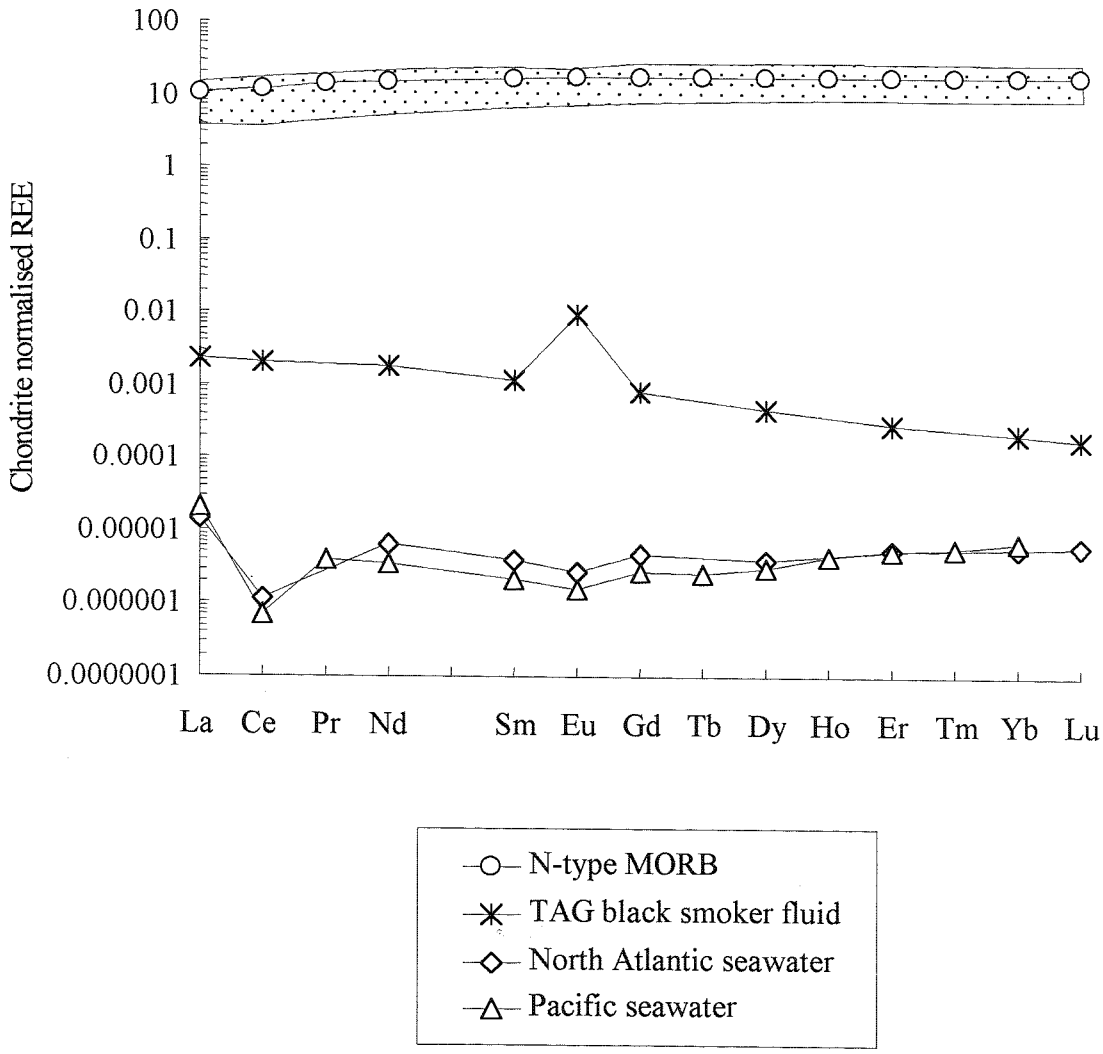

Figure 2.1: Chondrite normalised REE data for N-MORB, North Atlantic and Pacific seawater and a TAG black smoker fluid. Data are from Sun & McDonough [1989], Mitra *et al.* [1994] and Bau *et al.* [1996]. The shaded area shows the range in REE content of Troodos volcanic glasses, which are presumed to be free of the effects of any secondary alteration. Data are from Rautenschlein *et al.* [1985].

1982; Sun & McDonough 1989].

N-MORB is erupted exclusively along the MAR from 22°N (immediately south of the Kane Transform) to 33°40'N, south of the Hayes Transform [review by Smith & Humphris 1998]. Basalts erupted on the TAG segment of the MAR represent a maximum of ~11 % to 25 % partial melting of the upper mantle based on major-, trace- and rare earth element modelling, and have evolved from multiple primary magmas by olivine and plagioclase fractionation at 4 to 6 Kb pressure with limited degrees of crystallisation in shallow magma chambers [Meyer & Bryan 1996; Smith & Humphris 1998]. Also shown in Fig. 2.1 is a field representing the range of REE compositions of Troodos volcanic glasses analysed by Rautenschlein *et al.* [1985]. These glasses are presumed to be free from the effects of secondary alteration and have a REE composition similar to N-MORB.

Basalt partition co-efficient data show that the constituent mineral phases of MORB fractionate the REEs to different extents, depending critically on the similarity between REE cation size and lattice space, and also on factors such as the temperature, pressure and oxygen fugacity of the magmatic system [e.g. Onuma *et al.* 1968; Henderson 1982]. Average distribution co-efficients for the REE, excluding Eu, are commonly <1 for many rock forming minerals [review by Henderson 1982]. Plagioclase has higher distribution coefficients for the LREE (and particularly Eu^{2+}) than the HREE, in contrast to olivine and pyroxene that preferentially incorporate the HREEs [Henderson 1982]. This observation has implications for interpretations of the REE distribution patterns of high-temperature vent fluids (section 2.5) [e.g. Klinkhammer *et al.* 1994].

2.5 REEs in hydrothermal fluids

Seawater is chemically modified during low-temperature reactions with basalt within zones of hydrothermal recharge [e.g. Hellman & Henderson, 1977; Humphris *et al.* 1978; Ludden & Thompson 1978; Ludden & Thompson 1979; Juteau *et al.* 1979; Alt *et al.* 1986; Staudigal & Hart 1983; Gillis & Robinson 1990*a,b*; Minai *et al.* 1990; Gillis *et al.* 1992]. However, experimental and theoretical studies have shown that black smoker fluids acquire their chemical signature at depths of 2 to 3 km within the crust, where plagioclase alteration in a reaction zone above an axial heat source generates fluids in partial equilibrium with greenschist facies mineral assemblages [Bischoff & Dickson 1975; Bowers *et al.* 1985, Bowers *et al.* 1988; Berndt *et al.* 1988, Berndt *et al.* 1989]. Axial

hydrothermal alteration of the oceanic crust gives rise to ~350° C black smoker fluids with a REE composition that exhibit little variability between vent fields, and that exhibits a distinct REE pattern compared with either basalt or seawater (Fig. 2.1) [Michard *et al.* 1983; Campbell *et al.* 1988*b*; Klinkhammer *et al.* 1994; Mitra *et al.* 1994]. Black smoker fluids are enriched in REEs (one to four orders of magnitude) over seawater concentrations and display a large positive Eu anomaly, an enrichment in LREEs relative to the HREEs and no Ce anomaly [Michard *et al.* 1983; Michard & Albarède 1986; Campbell *et al.* 1988; Michard 1989; Mitra *et al* 1994; Klinkhammer *et al.* 1995; Edmond *et al.* 1995]. This pattern is common to all known high-temperature fluids from sediment-free ridges, although there is a some variation in the degree of Eu and LREE enrichment between different vent sites [Klinkhammer *et al.* 1994; Mitra *et al.* 1994].

Patterns of high-temperature axial alteration preserved in ophiolites are the record of reactions between wall rock and black smoker fluids ascending from the reaction zone, that may modify their REE composition prior to venting [e.g. Regba *et al.* 1991; Gillis *et al.* 1992; Valsami & Cann 1992]. However, the striking similarities in the chondrite normalised REE patterns of black smoker fluids sampled from contrasting oceanic settings suggests that they are fixed in the reaction zone of the system during the alteration of MORB (anorthitic) plagioclase surfaces to hydrothermal (albitic) plagioclase [Klinkhammer *et al.* 1994], while complexation in solution may play a role in subsequent REE fractionation [e.g. Bau 1991; Haas *et al.* 1995]. The concentration the trivalent REEs in the end-member fluid is inferred to be controlled by dissolution-precipitation of MORB plagioclase, in which they occupy Ca lattice sites [Klinkhammer *et al.* 1994]. The striking Eu anomaly of vent fluids is a function of both the crystallisation history of the basalt (Eu^{2+} substitutes for Sr in plagioclase during magma crystallisation) and subsequent alteration processes, as Eu preferentially substitutes for Sr in hydrothermal plagioclase [Klinkhammer *et al.* 1995]. The enhanced stability of divalent over trivalent Eu at elevated temperatures (>250°C) and low pH has also been invoked to explain the striking Eu enrichments of vent fluids [Sverjensky 1984; Wood 1990*b*; Bau 1991]. Divalent Eu dominates at temperatures in excess of 250° C, while at lower temperatures the relative stability of divalent and trivalent Eu will also depend on pH and complexing ligands in solution [Sverjensky 1984]. Hydrothermal activity is not expected to affect the REE content of oceanic rocks, because the REE content of hydrothermal fluids is *c.* 10^2 to 10^6 lower than MORB values [Michard *et al.* 1983, Michard 1989].

Because REE concentrations in seawater are 1-4 orders of magnitude lower than hydrothermal fluid, solutions that are mixtures of seawater and hydrothermal fluid have to be highly seawater dominated (*c.* >90%) before the seawater influence (negative Ce anomaly, HREE enrichment) becomes apparent in the REE pattern. In this respect, tracers such Sr-isotope ratios are better than the REEs for indicating the degree of mixing between hydrothermal fluid and seawater prior to hydrothermal mineral precipitation. However, the REEs have proved extremely useful in investigating the *evolution* of fluid compositions by the precipitation and dissolution of various mineral phases in the shallow subsurface of hydrothermal systems, and within seafloor sulphide mounds [e.g. Gillis *et al.* 1990; Mills & Elderfield 1995*a*; James & Elderfield 1996; Humphris 1998; Goulding *et al.* 1998]. For example, within the active TAG sulphide mound, black smoker fluid compositions are modified by the simultaneous precipitation of anhydrite and sulphides in different parts of the mound, as a consequence of mixing with entrained seawater [Tivey *et al.* 1995]. These diffuse fluids vent from the mound surface with modified REE compositions [Mitra *et al.* 1994; James and Elderfield 1996]. The chondrite normalised REE patterns for white smoker fluid and diffuse flow sampled from the surface of the TAG sulphide mound are shown in Fig. 2.2. The diffuse fluids have REE concentrations predicted by mixing of a black smoker fluid with seawater, except for Eu which is enriched above TAG end-member fluids [Mitra *et al.* 1994; James & Elderfield 1996]. The elevated Eu concentrations of the white smoker fluids are inferred to reflect extensive subsurface precipitation of anhydrite within the mound, that has a low partition coefficient for Eu [Mills & Elderfield 1995*a*]. Similarly, the Eu anomaly of diffuse flow can be modelled by mixing white smoker fluid and seawater, with the simultaneous dissolution of some mound anhydrite [James & Elderfield 1996].

2.6 REEs in hydrothermal sulphides

In most rock-forming minerals, the REEs fill lattice sites in eight-fold coordination [Shannon 1976], although a combination of charge and size imbalance restricts their entry into many minerals [McLennan 1989]. REE partitioning into sulphides and sulphates occurs *via* crystal lattice substitution, according to the degree of match or mis-match of the REE cations with the size of existing lattice sites. This approach was first adopted in an investigation of REE partitioning between pyroxenes and their host lavas [Onuma *et al.* 1968]. REEs do not fit easily in small sulphide lattices, as the ionic radius of Fe^{2+} is 0.780

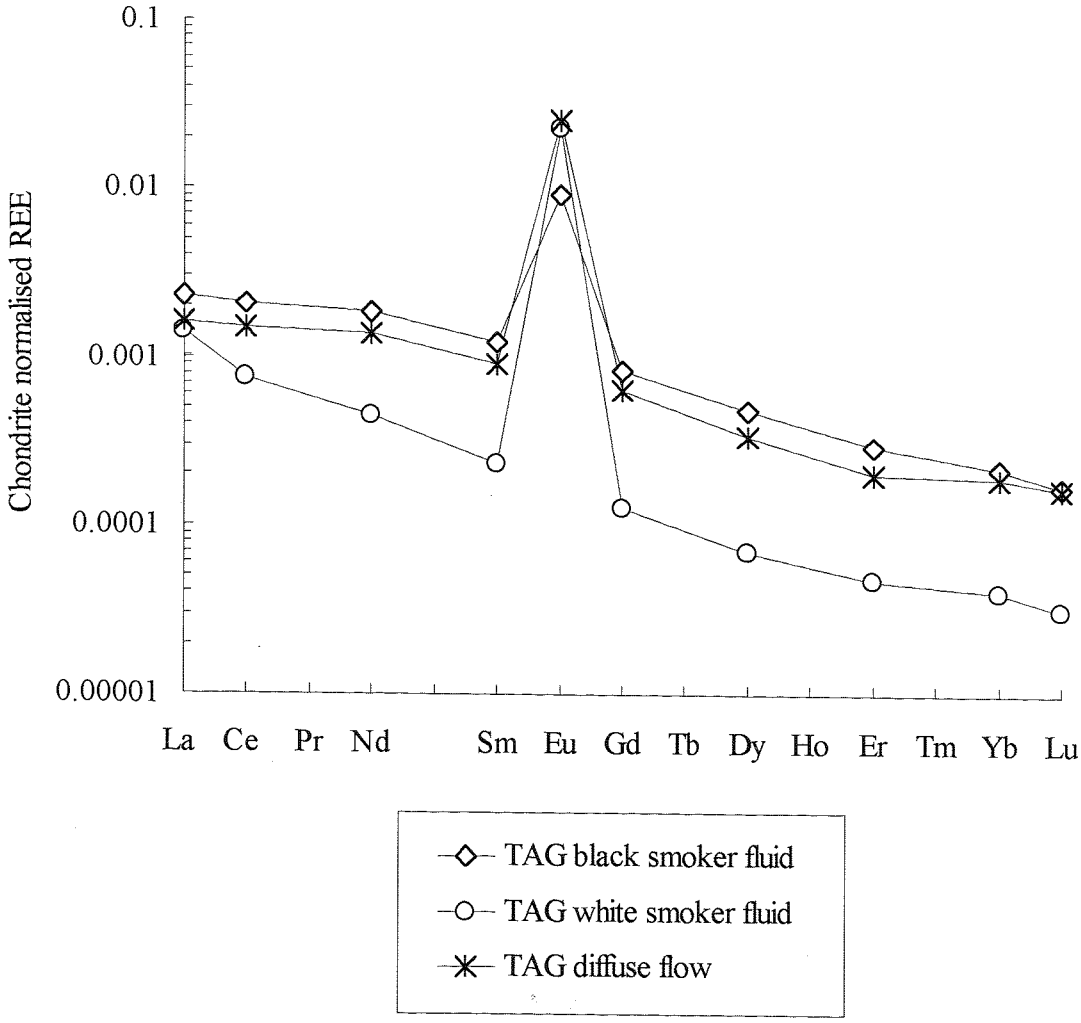

Figure 2.2: Chondrite normalised REE patterns for a TAG black smoker, white smoker and diffuse fluids sampled from the surface of the active TAG mound. Fluid data are from Mitra *et al.* [1994] and James & Elderfield [1996]. The elevated Eu concentration of the white smoker fluids is inferred to reflect subsurface precipitation of anhydrite within the mound, which has a low partition coefficient for Eu. The REE pattern of diffuse flow can be explained as a mixture of black smoker fluid and seawater, with simultaneous anhydrite dissolution [James & Elderfield 1996].

Å in eight-fold co-ordination, compared with 0.977 Å for Lu, the smallest trivalent REE cation [Shannon 1976]. This disparity in ionic radius is reflected by very low REE abundances in hydrothermal sulphides [Morgan & Wandless 1980].

Some REE patterns for TAG black smoker chimney and mound sulphides are shown in Fig. 2.3. The TAG sulphides have extremely low REE concentrations (0.006-0.008 ppm Nd), and patterns that resemble vent fluids, though with a reduced Eu anomaly and a relative HREE enrichment [Mills & Elderfield 1995*a*]. The REE distribution patterns of white smoker chimney sulphides are similarly HREE enriched and Eu-depleted in comparison to white smoker fluid compositions [Mills & Elderfield 1995*a*]. The fractionation of REEs that occurs during sulphide precipitation from hydrothermal fluids is strongly influenced by crystallographic control, whereby there is preferential uptake of smaller HREEs into the sulphide lattice [e.g. Morgan & Wandless 1980]. TAG mound sulphides show variable Eu-enrichments, that is inferred to reflect precipitation from fluids that have compositions intermediate between those of black and white smoker fluids [Mills & Elderfield 1995*a*].

Vent fluid-like REE patterns have been noted in seafloor sulphides from 21°N EPR [Bence 1983], and also in Ordovician massive sulphides [Graf 1977]. However, the REE composition of some seafloor sulphides do not resemble those of nearby venting black smoker fluids. Sulphides from Green Seamount off the EPR show the preferential incorporation of HREE relative to parental fluid compositions but lack the striking Eu enrichment that characterises vent fluids [Alt 1988]. This must reflect mass fractionation during precipitation besides that which can be attributed to crystallographic control [Alt 1988]. Similarly, unconsolidated hydrothermal sulphides from the Snake Pit vent field, 23° N MAR [Detrick *et al.* 1986*a,b*] show lesser LREE-enrichments than the high-temperature fluids, and do not display any anomalous Eu-enrichment [Gillis *et al.* 1990]. These sulphides are inferred to either precipitate from fluids isolated from the main discharge zone, that are less Eu-enriched than black smoker fluids venting at the seafloor, or from fluids which have cooled and/or mixed with seawater in the shallow subsurface of hydrothermal system, thus affecting the speciation and transport of divalent Eu (section 2.5) [Gillis *et al.* 1990].

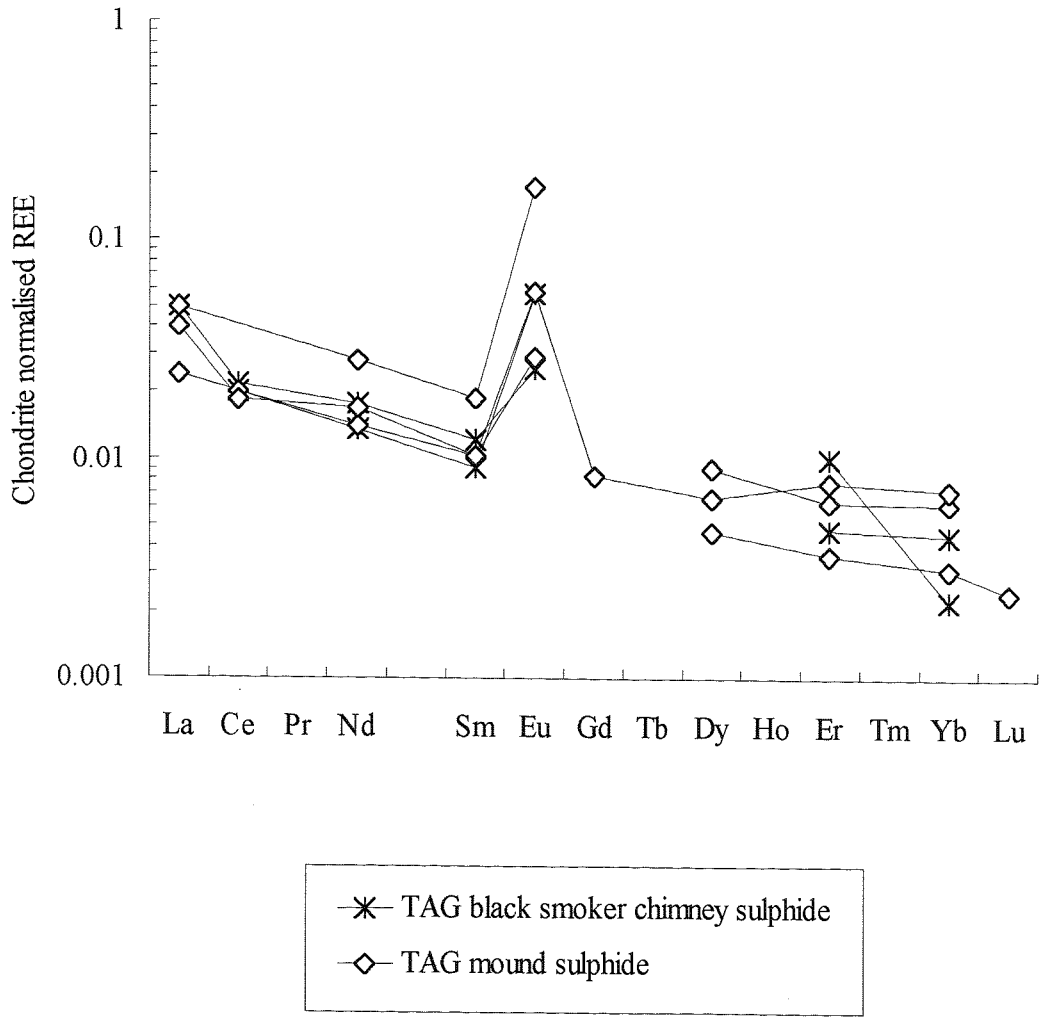

Figure 2.3: Chondrite normalised REE patterns for TAG chimney and mound sulphides. The REE patterns of the chimney sulphides resemble the fluid patterns in form, but with a reduced Eu anomaly, due to crystallographic constraints on the incorporation of the large Eu^{2+} cation. The range of Eu anomalies observed for the mound sulphides may indicate their precipitation from fluids with compositions intermediate between black and white smoker compositions. Data are from Mills & Elderfield [1995*a*].

2.7 REEs in hydrothermal sulphate

The precipitation of anhydrite containing high levels of REEs (Nd = 0.607 to 6.15 ppm) is the main mechanism for the removal of REEs from hydrothermal fluids circulating within the TAG sulphide mound [Mills & Elderfield 1995*a*; Humphris *et al.* 1998]. The trivalent REEs have a similar ionic radius to Ca^{2+}, hence will readily substitute into the anhydrite lattice [Shannon 1976; Morgan & Wandless 1980]. TAG anhydrites have REE patterns that resemble vent fluids, although with reduced Eu anomalies because of the mis-match in size of the large divalent Eu cation (1.25 Å ionic radius) and Ca lattice site (Ca^{2+} = 1.12 Å) [Shannon 1976].

Studies of the REE composition of TAG anhydrite have been instructive in revealing the nature and consequences of seawater entrainment, and fluid mixing and evolution during circulation within the mound [Mills & Elderfield 1995*a*; Humphris 1998]. Ongoing anhydrite precipitation within the TAG mound enhances the positive Eu anomaly in the residual fluid, causing evolution from black smoker compositions [Mills & Elderfield 1995*a*; Humphris 1998]. Humphris [1998] measured the REE content of 39 anhydrite samples from different areas within the mound that were sampled by ODP drilling. All TAG anhydrite samples display positive Eu anomalies and varying degrees of LREE enrichment, which do not show any systematic variation with either depth or textural setting [Humphris 1998]. Uptake of the trivalent REEs is inferred to be controlled by complexation in solution [Humphris 1998]. REEs in hydrothermal fluids may form weak chloride complexes, in the absence of other complexing ligands (e.g. carbonate or fluoride anions) [Wood 1990*b*]. The enhanced stability of LREE chloride complexes at high temperatures and low pH is inferred to cause mass fractionation of the trivalent REEs during anhydrite precipitation, by a process continual discrimination against the more soluble LREEs [Humphris 1998]. This leads to a concomitant increase in the La_n/Yb_n and decrease in the trivalent REE content of the residual fluid [Humphris 1998]. The incorporation of Eu depends on the proportion of trivalent and divalent Eu in the hydrothermal fluid, as the Eu^{3+} cation will not be discriminated against during anhydrite precipitation [Humphris 1998]. Mixing between hydrothermal fluid and cooler seawater within the TAG mound may promote the formation of Eu^{3+} by decreasing the temperature and increasing the oxygen fugacity of the fluid [Humphris 1998].

These processes are evident not only in the REE patterns of anhydrite, but also in the fractionated REE patterns of TAG diffuse fluids, white smoker and mound sulphides, and

Fe-oxide sediments that precipitate from diffuse fluids over a large proportion of the mound surface [Mills & Elderfield 1995*a*; James & Elderfield 1996; Mills *et al.* 1996; Humphris 1998; Goulding *et al.* 1998]. The REE signatures of these hydrothermal materials therefore provides evidence for fluid evolution by processes related to mound growth. The current model TAG models of mound growth and fluid evolution are discussed in Chapter 3 of this dissertation.

2.8 REEs in hydrothermal plumes

Vent fluids are enriched in REEs 10 to 10,000 times over seawater levels. However, deep-sea hydrothermal vents do not affect the REE pattern of seawater, as the hydrothermal REEs are rapidly scavenged onto Fe- and Mn-oxyhydroxide particles that form during plume rise and dispersal [Olivarez & Owen 1989; German *et al.* 1990; Olivarez & Owen 1991]. These processes result in a net removal of REEs from seawater, to the extent that dissolved REEs reach sub-ambient levels in seawater in the vicinity of hydrothermal vents [Klinkhammer *et al.* 1983]. The REEs behave conservatively during early mixing with seawater (to dilutions of ~10%) because they are not removed appreciably from seawater during sulphide formation, while in the buoyant plume they show a high particle reactivity [Mitra *et al.* 1994]. The rate of REE removal in the TAG plume is similar in magnitude to the riverine input flux of these elements [Rudnicki & Elderfield 1993].

At TAG, the majority of fine-grained Fe-oxyhydroxides form within the 40 minutes of buoyant plume rise. Metal uptake is a function of instantaneous co-precipitation, and kinetically-controlled scavenging [Rudnicki & Elderfield 1993]. Near-vent oxyhydroxide particles from the TAG neutrally buoyant plume have REE patterns that are both Ce-depleted and Eu-enriched, reflecting REE uptake from vent fluid and seawater sources [German *et al.* 1990]. The vent fluid REE signature is rapidly overprinted as the particles are dispersed from the near-field to the distal plume. Chondrite normalised REE patterns for some plume particulates and underlying metalliferous sediments are shown in Fig. 2.4. TAG far-field plume particulates and TAG and EPR plume-derived sediments display distinctive seawater-like REE patterns [Barrett & Jarvis 1988].

Mass fractionation of seawater-derived REEs occurs *via* the preferential scavenging of the MREEs in near-field plume particulates and metalliferous sediments [Rudnicki &

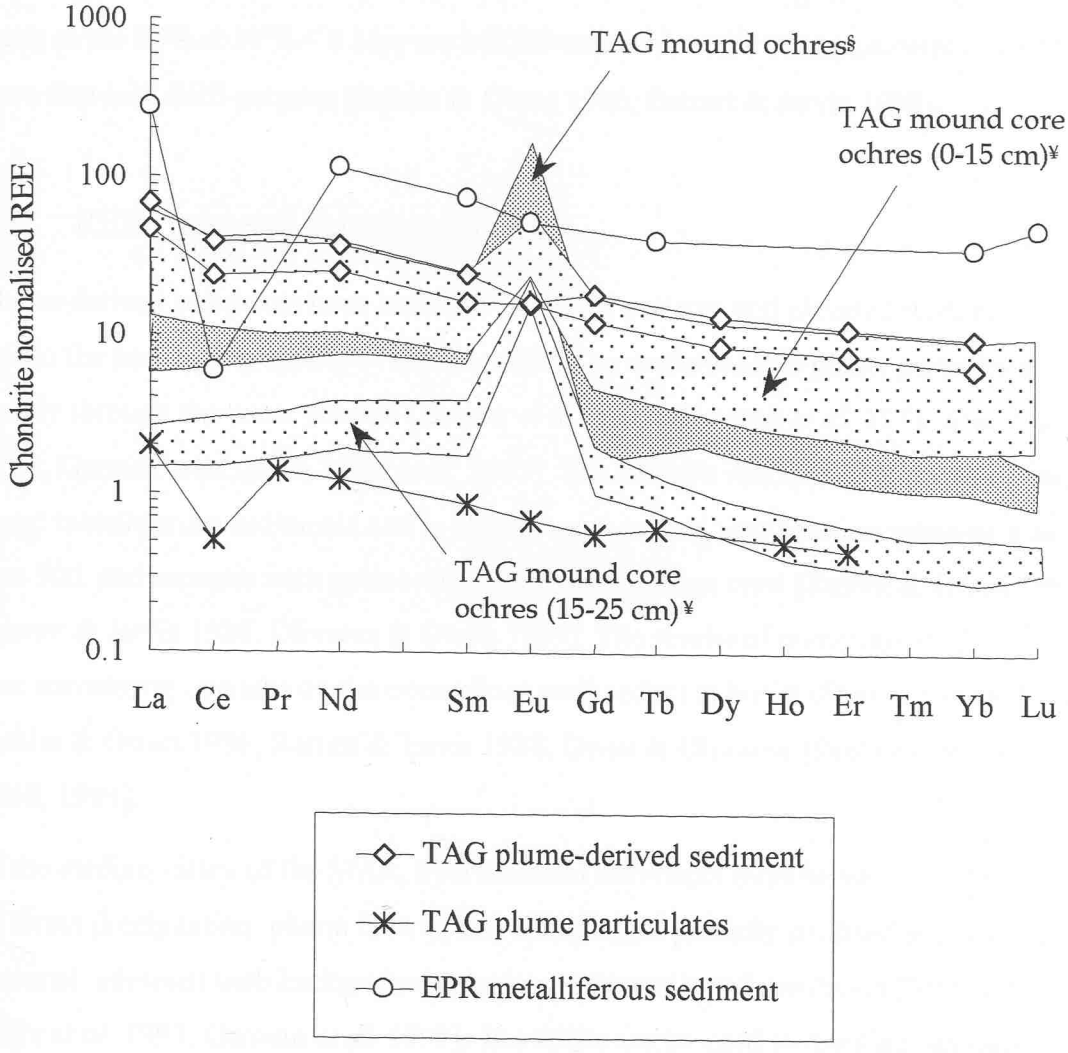

Figure 2.4: Chondrite normalised REE data for some TAG and EPR metalliferous sediments and Fe-oxyhydroxide particulates from the TAG neutrally buoyant plume. TAG plume-derived sediment data are from Mills [1992] and Mills *et al.* [1993]. Plume particulate data are from German *et al.* [1990] (REE concentrations have been multiplied by 10^6 to plot on this graph). REE data for TAG mound ochres are from §Mills & Elderfield [1995*a*] and ¥Goulding *et al.* [1998]. The EPR sample (598-5-6, 58-60 cm) is a 15.9 Myr sediment sampled 9 km from the palaeo-rise crest at 19°S by Deep Sea Drilling Project (DSDP) Leg 92. Data are from Ruhlin & Owen [1986].

Elderfield 1993]. These MREE-enriched REE patterns are inferred to flatten over time due to continued scavenging uptake of the less soluble LREE from seawater [Cantrell & Byrne 1987; Koeppenkastrop & De Carlo 1992]. Sediments from DSDP cores along the western flank of the EPR at 19°S < 8 Myr are MREE-enriched, while those sediments >10 Myr have flattened REE patterns [Ruhlin & Owen 1986; Barrett & Jarvis 1988].

2.9 REEs in metalliferous sediments

Plume-derived sediments have seawater-like REE patterns and elevated REE/Fe ratios, due to the scavenging uptake of seawater REEs as oxyhydroxide plume particles settle slowly through the water column [Bender *et al.* 1971; Dymond *et al.* 1973; Marchig *et al.* 1982; German *et al.* 1993; Mills *et al.* 1993]. The REE/Fe ratios of EPR proximal and distal metalliferous sediments and in DSDP cores exceed vent solution ratios by a factor of 2 to 500, and increase with palaeo-distance from the ridge crest [Ruhlin & Owen 1986; Barrett & Jarvis 1988; Olivarez & Owen 1989]. The results of numerous studies indicate that scavenging operates on the ocean floor until sediment burial [Dymond *et al.* 1973; Ruhlin & Owen 1986; Barrett & Jarvis 1988; Owen & Olivarez 1988; Olivarez & Owen 1989, 1991].

In the median valley of the MAR, hydrothermal sediments form by various combinations of direct precipitation, plume fall-out and slumping of partially oxidised sulphidic material, admixed with background pelagic and biogenic sedimentation [Metz *et al.* 1988; Mills *et al.* 1993; German *et al.* 1993]. The REEs can be used to discriminate between these modes of sedimentation, because the resulting REE patterns are characterised by varying degrees of seawater influence. Slumped and oxidised sulphides are rapidly redeposited in the near-field environment without contact with large volumes of seawater. Even after partial oxidation, this material is characterised by vent fluid-like REE patterns [German *et al.* 1993; Mills *et al.* 1993]. Near field ochreous sediments from Green Seamount in the East Pacific that contain oxidised and partially oxidised sulphides have similar vent-fluid like REE patterns [Alt 1988].

Iron-oxide sediments form *in situ* by direct precipitation from upwelling diffuse fluids in a zone of low-temperature deposition at the southern periphery of the active TAG mound [Tivey *et al.* 1995; Mills *et al.* 1996; Goulding *et al.* 1998]. These sediments consist of hematite, goethite with amorphous silica and quartz [Tivey *et al.* 1995]. Texturally these sediments are similar to those forming on the seafloor by fallout from the TAG plume.

However, they have fractionated vent fluid-like REE patterns with a large Eu anomaly, no Ce anomaly and low La_n/Nd_n compared with the TAG high-temperature fluid (Fig. 2.4) This is inferred to indicate precipitation from fluids whose composition has been modified by anhydrite precipitation within the mound and changes in REE complexation during fluid mixing [Mills & Elderfield 1995*a*; Mills *et al.* 1996; Goulding *et al.* 1998]. In the upper part of one core from the southern periphery of the TAG mound, ochres display both positive Eu and small negative Ce anomalies (Fig. 2.4). This provides evidence for seawater ingress and REE overprinting of vent-fluid derived REEs in this core [Goulding *et al.* 1998].

Fe- and Mn-oxyhydroxide phases react with biogenic opal to form smectite during the diagenetic recrystallisation of plume-derived sediments [Dymond & Eklund 1978; Barrett & Jarvis 1988]. With increasing sediment age, progressively more REE are transferred to poorly crystalline smectite and/or are scavenged from pore waters by these phases [Barrett & Jarvis 1988]. Although there is some redistribution of the REEs during diagenesis, bulk REE patterns stay seawater-like [Barrett & Jarvis 1988], or become more seawater-like [Goulding *et al.* 1998].

2.10 Neodymium isotopes

Isotopic fractionation of Nd occurs as ^{147}Sm decays to ^{143}Nd by alpha particle emission, with a half-life of 1.06×10^{11} years. Different geochemical reservoirs within the earth (chiefly oceanic and crustal rocks) have evolved with different Sm/Nd ratios and therefore have distinctive $^{143}Nd/^{144}Nd$ ratios [Zindler & Hart 1986]. The $^{143}Nd/^{144}Nd$ ratio is commonly expressed as in terms of the symbol ε_{Nd} (0) as parts per 10^4 (by mass) deviations from the chondritic uniform reservoir CHUR(0) bulk earth value of ε_{Nd} (0) = 0.512638, where:

$$\varepsilon_{Nd}(0) = \left[\left(\frac{(^{143}Nd/^{144}Nd)_{measured}}{(^{143}Nd/^{144}Nd)_{CHUR(0)}} \right) - 1 \right] \times 10^4$$

Because REE residence times are less than the oceanic mixing time, Nd-isotopes can used to identify sources of Nd in addition to mixing, transport and depositional processes within the ocean [Elderfield 1988; Piepgras & Wasserburg 1980; Piepgras & Jacobsen

1992]. The Nd isotope composition of seawater is sensitive to the age, and the proportions of crustal- and mantle-derived REE inputs (i.e. $^{147}Sm/^{144}Nd$ ratio of input materials). Because REEs in the ocean are dominated by continental rather than mantle sources, the observed range in ε_{Nd} (0) values of seawater chiefly reflects the influence of continental drainage to the ocean basins [Piepgras & Wasserburg 1980; Goldstein & Jacobsen 1987]. The continental crust has $\varepsilon_{Nd}(0)$ values that vary from -10 to -30, while MORB values are typically around +10. The ε_{Nd} (0) values of Atlantic seawater are low (*c.*-13.5 $\pm$ 0.5) because of large river and aeolian input rates of the products of continental weathering , compared with the Pacific Ocean (average ε_{Nd} (0) = *c.*-3). Intermediate values are found in the Indian Ocean (average ε_{Nd} (0) = *c.*-9) [Piepgras *et al.* 1979; Piepgras & Wasserburg 1980; Goldstein & Jacobsen 1987; Piepgras & Wasserburg 1987].

The Nd-isotopic composition of vent fluids is variable. Fluids venting from the active TAG mound, 26°N MAR have ε_{Nd} (0) = +11.9 [T. Masuzerawa pers. comm.]. There are no published Nd-isotope data for TAG basalts. At 13° N, EPR, vent fluids have ε_{Nd} (0) = +6.2 and +4.7 [Michard & Albarède 1986], while at 21°N they range from ε_{Nd} (0) = -3.6 (similar to Pacific seawater) to +7.9, compared with a local MORB value of +9.7 [Piepgras & Wasserburg 1985]. Only a few of the samples lie on a mixing curve between Pacific seawater and MORB Nd isotopic compositions, and reactions with sediment or anomalous oceanic crust are invoked to account for those ε_{Nd} (0) values which are below local MORB [Piepgras & Wasserburg 1985].

Nd isotopes can be used in a comparable manner to normalised REE distribution patterns to identify different hydrothermal inputs into metalliferous sediments [e.g. Mills *et al.* 1993]. In the near field, the Nd isotopic compositions of sediments reflects inputs from sulphidic mound-derived, seawater and detrital sources [Mills *et al.* 1993]. In the hydrothermal plume, the mantle-derived Nd signature of plume particulates is rapidly overprinted by seawater-scavenged Nd. The isotopic composition of Nd is uniform in metalliferous sediments formed at distances varying from >1000 km to within 10 km of the EPR (ε_{Nd} (0) = -5.2 to -4.4) with no evidence of a greater MORB contribution in those sediments deposited closer to the ridge [Halliday *et al.* 1992]. The results of these studies indicate that hydrothermal Nd does not mix with seawater except on a very local scale close to vents and does not become entrained into the ocean circulation [Halliday *et al.* 1992; Mills *et al.* 1993].

2.11 Cretaceous seawater

It is difficult to predict what the REE composition of the Tethys ocean would have been, complicated by a 'greenhouse warming' event during the early and middle Cretaceous which lead to a dramatic decrease in the intensity of the oceanic thermo-haline circulation [Hays & Pitman 1973; Berner & Lasaga 1989]. Additionally, the Tethys ocean did not have a direct connection to any high latitude water masses [de Boer 1986]. The subsequent decrease in the oxygen supply to deep water masses led to the widespread accumulation of organic-rich black shales in a variety of palaeotectonic and palaeogeographic settings [e.g. de Boer 1986; Jenkyns 1980; Roth 1986].

The distribution of REEs in the Cretaceous ocean can be predicted to have been more heterogeneous than today, because of the reduced exchange of water masses between the ocean basins [e.g. de Boer 1986]. The distribution of Ce in anoxic basins is controlled by the oxidative-precipitation/reductive dissolution cycle of Ce, directly analogous to that of Mn [German *et al.* 1991*c*], while the distribution of the trivalent REEs is coupled to the precipitation/dissolution cycle of ferromanganese oxyhydroxides [Elderfield & Sholkovitz 1987]. In the sub-oxic and oxic waters of the Black Sea, there is little or no fractionation of Ce from the other REEs, indicative of reductive dissolution of Ce^{4+} to Ce^{3+} [German *et al.* 1991*c*]. Similar controls on Ce distribution may have been relevant for the Cretaceous Ocean. However, in common with plume-derived metalliferous sediments from the flanks of the EPR and the median valley of the MAR [e.g. Bender *et al.* 1971; Dymond *et al.* 1973; Marchig *et al.* 1982; German *et al.* 1993; Mills *et al.* 1993; Barrett *et al.* 1987; Olivarez & Owen 1989], the REE patterns of ophiolite-hosted sediments display modern seawater-like REE patterns with negative Ce anomalies and no positive Eu anomaly [e.g. Robertson & Fleet 1976; Goulding 1998]. The similarity in REE patterns of modern and ancient ridge crest sediments suggests that the REE pattern of Cretaceous seawater was not significantly different from that of the modern ocean. In light of this observation, the Ce anomalies of the hydrothermal materials analysed in this dissertation can be interpreted as occurring in response to evolving redox conditions in the hydrothermal system, related to seawater entrainment and mixing processes.

Chapter 3

The TAG vent field, 26°N MAR & Troodos ophiolite, Cyprus

3.1 Introduction

The TAG hydrothermal vent field has been comprehensively studied over the over the last 25 years. These studies have provided important insights into the inter-relationships between the tectonic-magmatic setting of hydrothermal activity and the formation of a range of metalliferous deposits at 26°N, MAR that includes one of the largest bare-ridge seafloor sulphide deposits, the active TAG mound [e.g. Rona 1973; M. Scott *et al.* 1974; Scott *et al.* 1974; Rona 1978; Scott *et al.* 1978; Rona 1980; Shearme *et al.* 1983; Rona *et al.* 1984; Thompson *et al.* 1985; Lalou *et al.* 1986; Rona *et al.* 1986; Campbell *et al.* 1988*b*; Metz *et al.* 1988; Karson & Rona 1990; German *et al.* 1990; Lalou *et al.* 1990; German *et al.* 1991*a,b*; Rudnicki & Elderfield 1992; Kong *et al.* 1992; German & Sparks 1993; Rudnicki & Elderfield 1993; German *et al.* 1993; Lalou *et al.* 1993; Mills *et al.* 1993; Elderfield *et al.* 1993; Rona *et al.* 1993*a,b*; Mitra *et al.* 1994; Humphris & Kleinrock 1996; Kleinrock & Humphris 1996]. Recent ODP drilling of the TAG deposit has extended the sampling to three dimensions, and has led to the development of a model of mound growth and fluid evolution [Humphris *et al.* 1995]. The current TAG model combines drilling observations with inferences made from the compositions of hydrothermal fluids and a range of hydrothermal precipitates sampled from the mound surface during previous submersible studies [e.g. Mills & Elderfield 1995*a*; Edmond *et al.* 1995; Humphris *et al.* 1995; Tivey *et al.* 1995; James & Elderfield 1996; Edmonds *et al.* 1996; Mills *et al.* 1996; Goulding *et al.* 1998; Mills *et al.* 1998; Teagle *et al.* 1998; Tivey *et al.* 1998].

This chapter provides an introduction to the TAG vent field and the Troodos ophiolite, Cyprus. The results of the TAG studies are reviewed, and compared with studies of

hydrothermal mineralisation within the Troodos ophiolite. This discussion will provide the framework within which the REEs will be used to test the applicability of the TAG model to processes of sulphide mound formation within the Troodos ophiolite in Chapter 7 of this dissertation.

3.2 The TAG vent field, 26° N Mid-Atlantic Ridge

The TAG vent field was discovered during the 1972 Trans-Atlantic Geotraverse (TAG) program of the National Oceanic and Atmospheric Association (NOAA) upon the dredging of very pure birnessite and todorokite crusts from the median valley of the MAR at 26°N [e.g. Rona 1973; Scott *et al.* 1974; M. Scott *et al.* 1974]. These deposits provided the first strong evidence of localised hydrothermal discharge on the mid-ocean ridge system [Rona 1973; Scott *et al.* 1974]. On a regional scale, the TAG vent field is situated between 2 and 8 km east of the axial neovolcanic ridge, on a 10 km segment of the east valley wall that is bounded by non-transform discontinuities exhibiting dextral offsets of less than 15 km [Rona *et al.* 1993*a*]. There is no evidence of active seafloor hydrothermal activity to the west of the axial rift [Rona 1980; Nelson & Forde 1991]. The spreading half-rates on this segment of the MAR are asymmetric (1.3 cm yr^{-1} to the east and 1.1 cm yr^{-1} to the west), and the east wall of the rift valley is higher and smoother in profile than the opposing west wall [Eberhart *et al.*1988]. The eastern wall is constructed from large blocks bounded by normal faults that create a step-like profile of fault scarps and terraces which vary from metres to 10's of metres in width and relief [McGregor & Rona 1975; Temple *et al.* 1979; Rona 1980].

Following its discovery, the TAG vent field was subsequently found to be one of the largest known seafloor hydrothermal areas. It contains a range of hydrothermal deposits between ~2400 and 3650 m water depth, in a 5 x 5 km zone that extends from high on the eastern wall down to the junction with the valley floor (Fig. 3.1) [Scott *et al.* 1974; Thompson *et al.* 1985; Rona *et al.* 1986; Rona *et al.* 1993*a,b*]. The deposits within the TAG field are the products of present-day and former seafloor hydrothermal activity, and provide a record of varied and episodic hydrothermalism at this locality over the last *c.*125,000 years [Lalou *et al.* 1993; Rona *et al.* 1993*a,b*]. The vent field comprises a presently active zone (TAG sulphide mound, 3650 m depth), the *Alvin* (3550 to 3450 m depth) and *Mir* (3450 m depth) relict high-temperature zones, and a low-temperature zone

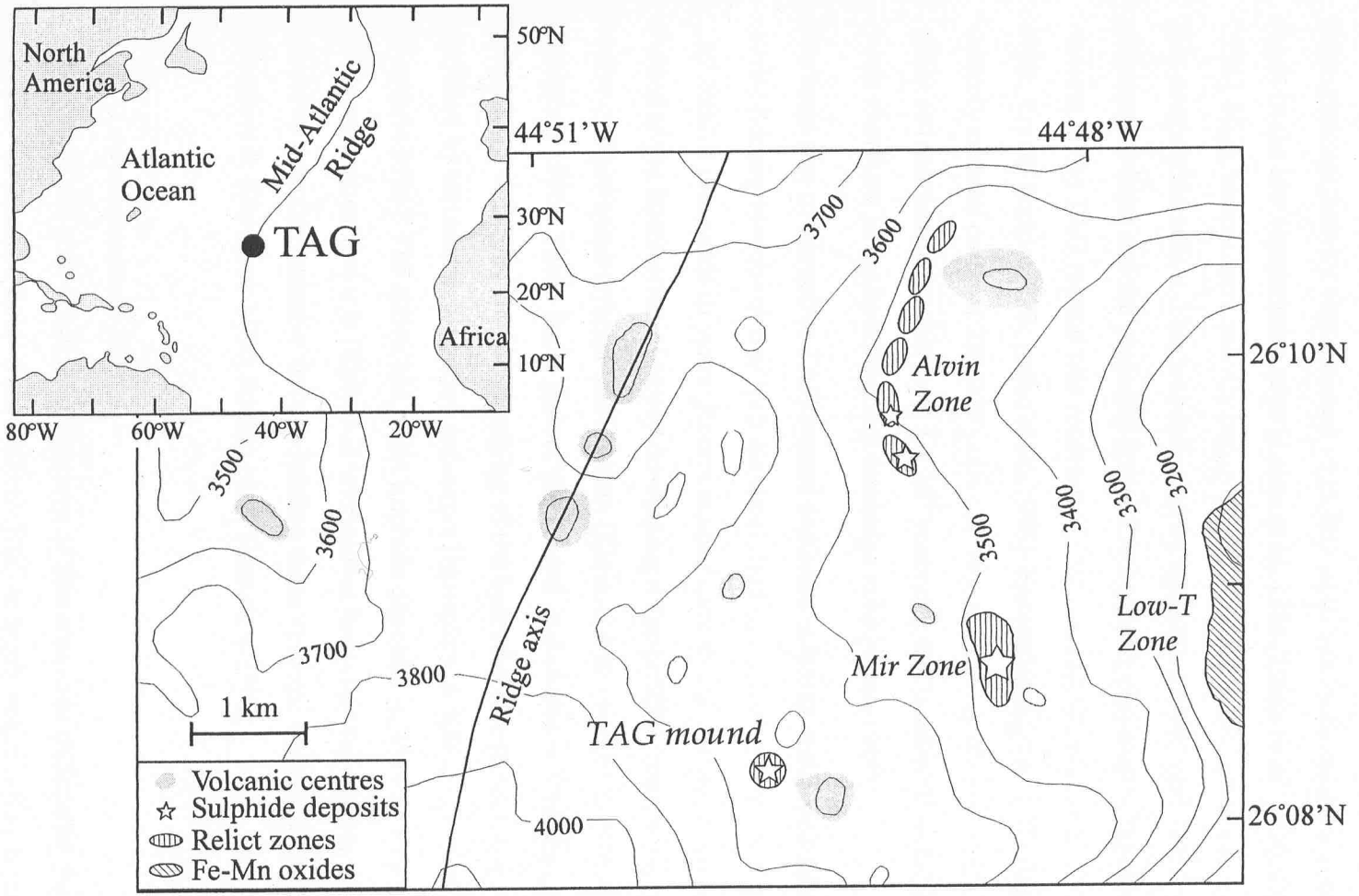

Figure 3.1: Bathymetric map of the TAG vent field showing the locations of volcanic domes, the active TAG sulphide mound, the *Alvin* and *Mir* relict hydrothermal zones and the low-temperature field on the eastern rift valley wall. Isobaths are at 100 m intervals. Adapted from Tivey *et al.* [1995].

(2400 to 3200 m depth). A chronology of hydrothermal activity in the four zones has been inferred from radiochemical dating of hydrothermal oxides and sulphides [Lalou *et al.* 1986; Lalou *et al.* 1990; Lalou *et al.* 1993; You & Bickle 1998; Lalou *et al.* 1998]. Hydrothermal activity was initiated ~125,000 years ago, with episodic venting of diffuse fluids in the low temperature zone [Lalou *et al.* 1986; Lalou *et al.* 1990; Lalou *et al.* 1998]. High-temperature activity began at ~100 kyr in the Mir zone, and by ~50 kyr all four zones were active. This was followed by sporadic activity until 4 kyr within the low-temperature zone and the presently active TAG mound, and until ~2 kyr for the *Mir* zone. Venting at the TAG mound was reactivated ~50 years ago [Lalou *et al.* 1990; Lalou *et al.* 1993; You & Bickle 1998; Lalou *et al.* 1998]. Encompassing the TAG field is a magnetic anomaly centred on crust 230,000 years old, that extends up the east wall of the axial valley to incorporate crust at least 1 x 10^6 years old; this is inferred to delineate a zone of basalt alteration in the hydrothermal discharge zone [Rona 1980].

The large size of the active TAG mound and relict sulphide mounds in relation to other seafloor deposits requires that hydrothermal fluid upflow has been localised at this site over tens of thousands of years. Recent studies have found that the TAG mound has formed at the intersection of newly developing ridge-parallel fissures and faults and an earlier oblique east-northeast fault system [Kleinrock & Humphris 1996; Humphris & Kleinrock 1996]. These faults dissect the mound, and evidence from the upper mound morphology indicates that the plumbing of the hydrothermal system is being continually modified by tectonic deformation processes [Humphris & Kleinrock 1996; Kleinrock & Humphris 1996]. The active and relict sulphide deposits occur in an area of numerous pillow volcanoes, and it is likely that intermittent hydrothermal activity at TAG has been related to episodic intrusive activity feeding these volcanic centres [Smith & Cann 1993; Humphris & Kleinrock 1996; Kleinrock & Humphris 1996].

3.2.1 Low-temperature field

Submersible and ship-board investigations of this area have delineated the vertical extent of a 'low-temperature field' from 2400 to 3200 m depth within which a range of fault-controlled ferromanganese and Fe-rich silicate deposits has been identified [Rona 1973; M. Scott *et al.* 1974; Scott *et al.* 1974; McGregor & Rona 1975; Temple *et al.* 1979; Thompson *et al.* 1985; Lalou *et al.* 1986]. Radiochemical analyses indicate that these deposits have ages ranging from 4000 to 125,000 years [Lalou *et al.* 1986; Lalou *et al.*

1990; Lalou *et al.* 1993], and are accumulating two orders of magnitude faster (100 to 200 mm Myr^{-1}) than typical open ocean hydrogenous ferromanganese deposits, due to enhanced metal inputs from seafloor hydrothermal activity [Scott *et al.* 1974]. These Mn and Fe-rich deposits have been interpreted as the products of deposition from diffuse fluids discharging from faults or seeping through the thin (<1 m) sedimentary cover within the low temperature field [Rona *et al.* 1984]. The discovery of active black smokers at the TAG mound on the floor of the rift valley in 1985 led to the reinterpretation of the low-temperature deposits as a distal, plume-derived manifestation of the high-temperature hydrothermal system [Klinkhammer *et al.* 1985; Klinkhammer *et al.* 1986; Rona *et al.* 1986]. The origin of these low-temperature deposits is re-examined in Chapter 8 of this dissertation based on an evaluation of their REE geochemistry.

3.2.2 Relict sulphide mounds

The *Alvin* and *Mir* zones are areas of discontinuous sulphide outcrop that occur 2 to 3 km north and northeast of the active TAG mound respectively, between water depths of ~3400 and 3500 m (Fig. 3.1). The *Mir* relict zone comprises a number of coalesced, sulphide mounds that form a large area of semi-continuous massive sulphide outcrop, up to 600 m in length [Rona *et al.* 1993*a,b*]. The sulphides have coarse-grained, recrystallised textures that are typical of hydrothermally-reworked sulphides in ophiolites [review by Hannington *et al.* 1998]. Sulphides at the mound surfaces are variably oxidised and silicified, with inactive standing and toppled sulphide chimneys and red metalliferous sediments on their upper surfaces [Rona *et al.* 1993*a*]. Iron and manganese oxides occur as dark stains on semi-consolidated tan carbonate sediment, and as coatings on fractured pillow lavas and basalt talus [Lalou *et al.* 1993]. The *Alvin* zone comprises several discontinuous, inactive sulphide deposits in an elongate array >2 km in extent [Rona *et al.* 1993*a,b*]. Several of these inactive mounds are similar in size to the TAG active mound (~200 m in diameter) [Rona *et al.* 1993*a,b*].

The relict sulphide mounds of the *Mir* and *Alvin* zones have been dissected by fault blocks of the adjacent lower east wall of the rift valley, rendering them susceptible to degradation by oxidation and mass-wasting [Rona *et al.* 1993*a,b*]. The mounds provide a source of oxide and sulphide material to sediments accumulating at the base of the east valley wall [Metz *et al.* 1988; Mills *et al.* 1993]. Where the sulphide mounds are not dissected by faults, a layer of oxidised sulphides preserves the mound interiors from

further seawater alteration [Hannington *et al.* 1998].

3.2.3 Active TAG mound

Active high temperature venting and sulphide precipitation within the TAG field are presently confined to the TAG hydrothermal mound. This was discovered following the detection of temperature, helium and manganese anomalies in the axial rift valley of the MAR over the TAG field, that were indicative of an large, high-temperature venting source at the base of the eastern valley wall [Rona 1978; Jenkins *et al.* 1980; Klinkhammer *et al.* 1985; Klinkhammer *et al.* 1986]. Subsequently, vent biota, black smokers and massive sulphides were observed on the TAG mound, located at 26°08'N 44°49'W at the junction of the east wall of the rift valley and the valley floor at water depths of 3620 m [Rona *et al.* 1986]. The TAG mound is a single large deposit located on crust at least 100,000 years old on the northwest side of a small volcanic dome, 2.4 km east of the axis of the rift valley (Fig. 3.1). The mound is a large constructional feature of altered and unaltered blocky sulphides and anhydrite that is 200 m in diameter, and displays 50 m of relief (Fig. 3.2) [Tivey *et al.* 1995]. Because of the tectonic controls on hydrothermal discharge within the vent field (section 3.2.1) the TAG mound is circular in plan view, in contrast to most other active seafloor vent sites where multiple small deposits are aligned parallel to the ridge axis, and the size of individual sulphide mounds is considerably smaller (<10 to 30 m) [review by Hannington *et al.* 1995]. Even at the vent sites that are similar in size to the TAG mound, for example on the Endeavour Segment of the JdFR (up to 200 m length), the Snakepit site on the MAR (up to 100 m length) and the Galapagos sulphide mounds on the Galapagos Ridge (up to 100 m length), smaller sulphide structures in linear arrays coalesce to form larger sulphide accumulations [Embley *et al.* 1988; Thompson *et al.* 1988; Delaney *et al.* 1992]. The Magic Mountain deposit on the Explorer Ridge is the most similar bare-ridge seafloor sulphide deposit to the TAG mound, measuring 300 m in diameter [Scott *et al.* 1990].

The TAG mound has grown episodically as two asymmetrically superposed sulphide/anhydrite terraces, which may reflect different phases of active growth [Lalou *et al.* 1998]. Mineral accumulation rates derived from heat flux density and diffuse fluid chemistry data suggest that mound sulphides and silica represent only 300 to 3000 years of active accumulation [James & Elderfield 1996]. This reflects episodic mound growth and sulphide input into surrounding sediments by mass wasting [Metz *et al.* 1988; Mills *et al.*

1993].

Prior to ODP drilling a decade of submersible, dredging and photographic studies of the TAG mound had characterised the near-surface of the deposit to a greater extent than other oceanic sulphide bodies. These studies had documented the mound morphology [Thompson *et al.* 1985; Rona *et al.* 1986; Tivey *et al.* 1995; Humphris & Kleinrock 1996], the geochemistry of venting hydrothermal fluids [Campbell *et al.* 1998*b*; Mitra *et al.* 1994; Edmond *et al.* 1995; Edmonds *et al.* 1996] and mineral precipitates [Mills & Elderfield 1995*a*; Tivey *et al.* 1995]. Differences in venting fluid and hydrothermal precipitate compositions had been used to infer dynamic mineralisation processes occurring in the subsurface of the mound [Mills & Elderfield 1995; James & Elderfield 1996]. Additional studies identified inputs of mound material to the apron of near-field metalliferous sediments that surround the mound [German *et al.* 1993], and characterised the impact of hydrothermal venting from mound on water column chemistry, metalliferous sediment formation and the degree of modification of the hydrothermal flux by chemical reactions occurring within the TAG hydrothermal plume [German *et al.* 1990; German *et al.* 1991*a,b*; Mills 1992; Rudnicki & Elderfield 1992; Rudnicki & Elderfield 1993; German & Sparks 1993; Mitra *et al.* 1994].

3.2.3.1 Fluid compositions

Extensive fluid flow occurs through the TAG mound surface at a variety of temperatures. Hydrothermal fluid is diffuse (~25° C) over much of mound surface, and focused in two areas of black (>360° C) and white smoker (260 to 300° C) fluid venting from discrete sulphide edifices. Black smoker fluids currently vent from 10 m-high chalcopyrite-pyrite-anhydrite chimneys clustered at the apex of a steep-sided 10-20 m high conical edifice constructed from blocks of massive anhydrite, interspersed with platy massive chalcopyrite and marcasite. This 'Black Smoker Complex' (BSC) comprises the upper terrace of the mound and is located to the northwest of the mound centre. Mass wasting of the west, north and east sides of the BSC has exposed material rich in quartz, amorphous silica ± pyrite ± Fe-oxyhydroxides [Tivey *et al.* 1995]. There is an area of low heat flow to the west of the BSC, suggesting an area of shallow recharge. Lower-temperature white smoker fluids emanate from small (1-2 m) sphalerite spires that occur in the 'Kremlin' area in the southeast region of the lower mound terrace [Tivey *et al.* 1995].

Time series data for TAG fluids exist from 1986, 1990, 1993, 1994 and 1995 [Campbell *et*

al. 1988*b*; Edmond *et al.* 1995; Edmonds *et al.* 1996; Gamo *et al.* 1996]. The major element compositions and exit temperatures of the black smoker fluids are similar to solutions from Pacific vents, despite the slower spreading rate and greater hydrostatic pressure of the MAR [Campbell *et al.* 1988*b*]. However, the trace element composition of TAG and other MAR vent fluids indicate that down-welling recharge fluids have reacted with basalt previously altered at low temperatures [Campbell *et al.* 1988*b*; James *et al.* 1995] that may limit the supply of metals to new seafloor vents at these sites [Klinkhammer *et al.* 1995].

The major ion chemistry of TAG black smoker fluids appeared to be stable following ODP drilling, which can be inferred not to have penetrated the mound sufficiently to affect the circulation and mixing processes that control the fluid compositions [Edmonds *et al.* 1996]. Prior to drilling in 1994, the Kremlin area was observed to have changed from a site of white smoker to vigorous black smoker venting [Edmonds *et al.* 1996]. Dynamic changes in the sub-surface mound plumbing are inferred to have caused the white smoker system to heat up to temperatures of ~350°C [Edmonds *et al.* 1996].

Low temperature fluids percolate through hydrothermal precipitates on the mound surface and through talus that occurs on the sides of, and surrounds the mound. The heat flux associated with diffuse flow at the surface of the TAG mound is *c.*2000 MW, an order of magnitude greater than the high-temperature heat flux [Schultz *et al.* 1996]. The chemical composition of TAG diffuse fluids indicates they are important in creating and modifying the ore deposit [James & Elderfield 1996; Mills *et al.* 1996]. These processes are discussed further in section 3.2.6.

3.2.3.2 ODP drilling results

ODP drilling of seventeen holes at five locations on the mound to a maximum depth of 125 metres below seafloor (mbsf) in 1994 revealed for the first time the internal structure of an actively forming oceanic sulphide deposit, that previously was limited to inferences made from on-land analogues [Humphris *et al.* 1995]. Striking features of drilling were the abundance of anhydrite and the highly brecciated nature of the mound interior [Humphris *et al.* 1995]. The mound comprises a complex assemblage of sulphide-anhydrite-silicate breccias and has grown during successive high temperature episodes as an *in situ* breccia pile on the seafloor [Humphris *et al.* 1995; Knott *et al.* 1998]. A laterally and vertically zoned mineralised stockwork, ~100 m in diameter underlies the mound and

extends to at least 125 mbsf [Humphris *et al.* 1995]. The stratigraphy of the holes drilled in the five areas has been combined to produce a composite section through the mound (Fig. 3.2) [Humphris *et al.* 1995].

The upper 5-10 m of the deposit comprises a carapace of massive sulphide debris and Fe-gossans, which is partially cemented by colloform pyrite and cherty silica (Si-Fe-oxyhydroxides), and onlaps relatively unaltered, and partially hematised basalts at the mound margins [Hannington *et al.* 1998]. The sulphide debris encompasses porous and colloform pyrite, and recrystallised massive pyrite ± chalcopyrite. The delicate textures of collapsed sulphide chimneys are only occasionally preserved within the upper part of the mound, being largely destroyed by hydrothermal recrystallisation and replacement with coarser grained pyrite. Veins of pyrite and sphalerite are found cutting recrystallised pyrite [Hannington *et al.* 1998], as in the relict Mir zone [Rona *et al.* 1993*a*]. These textures, as throughout the whole mound, indicate a complex paragenesis, with multiple generations of vein-filling, recrystallisation, annealing and cementation [Knott *et al.* 1998].

Beneath this carapace, several breccia units have been identified, all of which may or may not be present in any given vertical section [Humphris *et al.* 1995]. The upper 10-20 m of the mound is characterised by massive pyrite breccias, comprising clasts of pyrite in a pyrite matrix with minor quartz and/or anhydrite [Humphris *et al.* 1995]. These breccias display a range of morphologies, from sulphide talus in a matrix of sulphide sand, to recrystallised pyrite cemented by colloform pyrite and occasionally sphalerite [Hannington *et al.* 1998]. Sandy pyrite in the uppermost breccias closely resembles the detrital pyrite being weathered out of large anhydrite blocks at the base of the BSC [Hannington *et al.* 1998]. Within the massive pyrite breccias, original chimney structures and textures are severely modified by sequential sulphide overgrowth, recrystallisation and partial dissolution [Knott *et al.* 1998].

In the high-temperature upflow zone beneath the BSC, massive pyrite breccias are underlain to 45 mbsf by an anhydrite-rich zone, which occurs above a vertically extensive quartz-pyrite stockwork. To 30 mbsf this zone consists of matrix-supported pyrite-anhydrite breccias comprising clasts of pyrite in a pyrite matrix with >10% volume anhydrite. These are underlain to 45 mbsf by pyrite-silica-anhydrite breccias, that are composed of pyrite, quartz + pyrite and silicified basalt clasts in a matrix of >10% volume anhydrite + quartz [Humphris *et al.* 1995]. Composite anhydrite veins up to 45 cm wide occur throughout this zone [Humphris *et al.* 1995].

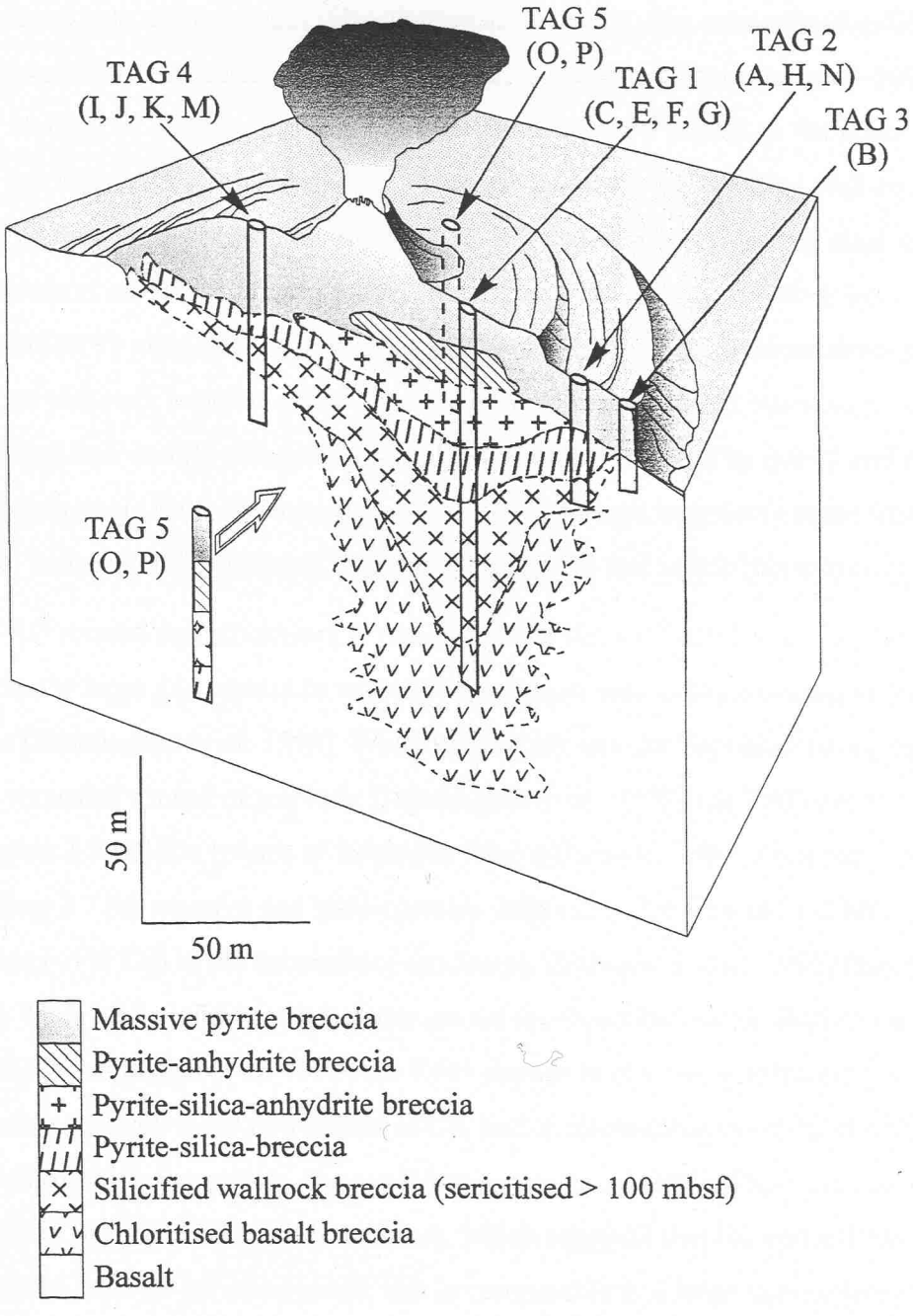

Figure 3.2: A schematic representation of the active TAG mound showing the surface morphology, the locations of 17 holes drilled in 5 areas of the sulphide mound during ODP Leg 158, and the simplified internal structure based on the drilling results. Recovery of rock core ranged from <1 to 63% with an average of ~12%. The mound comprises a complex assemblage of sulphide-anhydrite-silicate breccias and has grown during successive high temperature episodes as an *in situ* breccia pile on the seafloor over the last ~50,000 yrs. Figure adapted from Humphris *et al.* [1995].

The base of the anhydrite-rich zone marks the transition between the pyrite-dominated mound and the underlying stockwork. The stockwork is absent beneath the eastern half of the mound, consistent with a fault control that presently focuses hydrothermal upflow to the western side of the mound [Hannington *et al.* 1998]. The mineralised upflow zone comprises silicified, paragonitised and chloritised basalts [Honnorez *et al.* 1998]. The upper stockwork contains pyrite-silica breccias which are similar to the upper breccia units, but with >10% volume quartz. These are underlain by silicified wall-rock breccias, which contain significantly less pyrite (<50 vol.%) and are dominantly clast-supported [Humphris *et al.* 1998]. Quartz-pyrite veins extend throughout the stockwork zone from ~40 mbsf to 95 mbsf. Below 110 mbsf, and at the margins of the mineralised zone, the silicified wallrock breccias grade abruptly into chloritised basalt breccias, which contain chloritised and weakly mineralised basalt fragments cemented by quartz and pyrite [Humphris *et al.* 1995; Honnorez *et al.* 1998]. The basalt fragments range from 1 to 5 cm in size, and are totally replaced by quartz, paragonite and pyrite [Honnorez *et al.* 1998].

The TAG mound and stockwork is one of the few known deposits on the seafloor that is sufficiently large and mature to warrant comparison with ophiolite-hosted Cyprus-type ore bodies [Hannington *et al.* 1998]. While most black smoker deposits contain no more than a few thousand tonnes of sulphide [Hannington *et al.* 1998], the TAG deposit is estimated to contain 3.9 million tonnes of sulphides [Humphris *et al.* 1995; Humphris 1998] including 2.7 Mt massive and semi-massive sulphide (~2% Cu) and 1.2 Mt of mineralised breccias (~1% Cu) in the subseafloor stockwork [Humphris *et al.* 1995; Hannington *et al.* 1998]. Thus while land-based deposits are on average much larger than modern seafloor deposits [Hannington *et al.* 1995] the TAG deposit is of a comparable size. It is estimated to contain ~30,000 to 60,000 tonnes of Cu, and is comparable in size to the top 30% of massive sulphide deposits in Cyprus [Hannington *et al.* 1998]. There are four TAG-sized mounds in the relict *Mir* and *Alvin* zones, which suggests that the entire TAG field contains at least 20 Mt of sulphide; this is comparable to a large mining lease in Cyprus [Hannington *et al.* 1998].

3.2.3.4 Sulphide mineralogy

Numerous sulphide samples were collected from the surface of the mound prior to ODP drilling, during dredging operations and 25 submersible dives. Primary TAG sulphides comprise marcasite, pyrite, sphalerite, chalcopyrite and minor bornite, with abundant

anhydrite, amorphous silica and aragonite [Rona *et al.* 1986; Thompson *et al.* 1988; Hannington *et al.* 1988; Hannington *et al.* 1991; Tivey *et al.* 1995]. Pyrrhotite is absent, and quartz (which is the principal gangue material in the mound interior) is largely absent in surface samples [Hannington *et al.* 1998]. Chalcopyrite is most abundant in the vicinity of the high-temperature upflow zone, where it is intergrown with, and locally replaces pyrite in black smoker chimneys and sulphide crusts forming at the mound surface from black smoker fluids pooled beneath the BSC [Tivey *et al.* 1995]. White smoker chimneys, and blocks of sulphide exposed on the remainder of the lower platform are characterised by a primary pyrite-sphalerite-marcasite assemblage [Tivey *et al.* 1995]. The white smoker chimneys are porous, fine-grained structures composed of dendritic and colloform sphalerite with minor marcasite and late-stage amorphous silica [Hannington *et al.* 1991]. Fe-poor sphalerite occurs only in the uppermost part of the TAG deposit, filling open spaces and locally occupying late veins in the pyrite breccias [Hannington *et al.* 1998]. Mound breccias recovered during ODP drilling are shown to comprise mainly pyrite, anhydrite and quartz, lesser chalcopyrite (0 to 50 vol.%) and sphalerite (<5 vol.%) with galena in trace amounts (<<1 vol.%). These minerals replace and cement altered basalt fragments in the stockwork zone of the deposit [Hannington *et al.* 1998]. Total sulphur contents of mound breccias is close to 42%, similar to many Cyprus-type massive sulphides [Hannington *et al.* 1998].

3.2.4 TAG models of mound growth and metalliferous sediment formation

3.2.4.1 The role of anhydrite formation

ODP Drilling revealed the presence of unexpected amounts of anhydrite within the mound and capping the upflow zone at the mound surface (~3 x 10^8 kg), that had nonetheless been predicted on the basis of vent fluid chemistries and complex mineral assemblages (section 2.7) [Edmonds *et al.* 1995; Mills & Elderfield 1995*a*; Tivey *et al.* 1995]. The focused venting of black smoker fluids from the apex of the mound causes the entrainment of large volumes of seawater into the mound beneath the BSC. Mathematical models predict that seawater ingress and fluid flow within hydrothermal sulphide mounds is strongly influenced by changes in permeability structure and endmember fluid mass flux into the base of the structure, that will change as the system evolves [e.g. Dickson *et al.* 1995]. Anhydrite precipitates when seawater that has mixed to a greater or lesser extent with black smoker fluid is conductively heated to >150° C. The presence of anhydrite

within the mound implies the maintenance of high temperatures within the upflow zone, coupled with the entrainment and heating of substantial amounts of seawater. The anhydrite-rich zone (to ~40 mbsf) coincides with the palaeo-seafloor, which may represent a tectonically weak area where seawater can penetrate into the deposit [Brügmann *et al.* 1998]. Below ~40 mbsf, anhydrite occurs in vugs and coatings on breccia clasts. The elevated $^{87}Sr/^{86}Sr$ ratios of TAG anhydrites indicates that the mound is permeable to seawater to ~120 m depth, with the most seawater-like Sr ratios occurring at 120 mbsf directly below the BSC [Mills *et al.* 1998]. Seawater ingress and mixing within the mound is complex and chaotic at all scales, with no systematic variations either laterally or vertically within the mound, or within individual veins [Humphris 1998].

The discovery of large amounts of anhydrite within the TAG mound has enhanced our understanding of the formation of sulphide structures at the seafloor [Humphris *et al.* 1995]. Anhydrite precipitation and dissolution has clearly played a critical role in the development of the internal structure of the TAG mound, in addition to modifying the composition of hydrothermal precipitates and diffuse fluids venting from the mound surface [Mitra *et al.* 1994; Mills & Elderfield 1995*a*; James & Elderfield 1996]. During periods of high-temperature activity, pyrite breccias are inferred to be cemented by anhydrite precipitating in the upflow zone from conductively heated seawater [Hannington *et al.* 1998]. Because anhydrite has retrograde solubility, these breccias remain anhydrite-supported only for as long as high-temperatures are maintained in the upflow zone. Because high-temperature venting has been episodic over the lifetime of the TAG deposit [e.g. You & Bickle 1998], the breccias in the central portions of the mound have episodically collapsed during less vigorous hydrothermal activity or periods of hydrothermal quiescence. However, $^{230}Th/^{234}U$ anhydrite ages from TAG drill core up to ~10,000 years have been recorded indicating that not all the anhydrite within the mound is contemporary [You & Bickle 1998]. The repeated collapse of the anhydrite-supported portions of the mound during periods of hydrothermal quiescence is inferred to have caused *in situ* brecciation of the mound [Humphris *et al.* 1995]. The complex assemblage of breccia ores that comprise the TAG deposit are the result of repeated fragmentation, cementation and hydrothermal recrystallisation of earlier anhydrite and pyrite [Hannington *et al.* 1998]. The recognition of the importance of anhydrite precipitation and dissolution in the structure and evolution of the TAG mound has implications for on-land analogues such as Cyprus-type ore bodies, with similar brecciated textures which have previously been attributed to seafloor weathering and erosion [Hannington *et al.* 1998].

3.2.4.2 Dynamic mound processes

In addition to the abundance of anhydrite, other striking results of ODP drilling were the highly re-cemented nature of the sulphide body and the occurrence of altered basaltic fragments at stratigraphically shallow depths within the mound [e.g. Humphris *et al.* 1995; Brown & McClay 1998; Knott *et al.* 1998; Honnorez *et al.* 1998]. These observations confirmed the hypothesis developed from vent fluid, sulphide and Fe-oxide compositions that the system is highly dynamic and mineralisation episodic in nature [Mitra *et al.* 1994; Mills & Elderfield 1995*a*; James & Elderfield 1996; Edmond *et al.* 1995; Edmonds *et al.* 1996].

The sub-surface fluid flow and mineralisation processes inferred to be occurring within the active TAG mound are summarised in Fig. 3.3. Mound growth occurs by pyrite precipitation, both within the mound and as surficial chimney structures, and additionally by subsurface anhydrite precipitation in the upper 30-40 m of the deposit [Humphris *et al.* 1995]. In addition to anhydrite precipitation, seawater circulation and mixing within the mound causes significant dissolution and re-precipitation (reworking) of mound sulphides, through the formation of diffuse hydrothermal fluids [Tivey *et al.* 1995; Edmond *et al.* 1995]. The mixing/cooling processes that lead to the formation of diffuse fluids greatly increase the efficiency of the ore-forming process compared with individual chimney venting, as they induce ongoing sulphide precipitation within the mound beneath the cap of older sulphides, reducing the loss of sulphur and metals to the hydrothermal plume [Edmond *et al.* 1995; Tivey *et al.* 1995]. Diffuse flow is also important in stripping metals soluble at lower temperatures from the interior of the mound and concentrating them at the top of the mound. This 'zone-refining' of the TAG deposit occurs as a consequence of the differing solubilities of Cu and Zn sulphides at different temperatures and pH, and creates mineral zonation on a deposit scale [Tivey *et al.* 1995; Edmond *et al.* 1995]. The pH of fluids circulating within the mound is lowered as pyrite precipitates due to conductive cooling and mixing with cool, ingressing seawater. Low-temperature sulphides such as sphalerite are more readily dissolved that by these low pH fluids, causing redistribution of Zn and other trace metals to the cooler outer margins of the deposit. This zonation is particularly apparent in the Kremlin area of the mound, where sphalerite-pyrite assemblages precipitate from white smoker fluids containing ~15 % seawater and ~85% of the high-temperature hydrothermal end-member [Edmond *et al.* 1995]. Compared with black smokers, these white smoker fluids are more acidic, enriched in Zn and depleted in Cu, Fe and H_2S [Edmond *et al.* 1995]. Comparison of the compositions of a range of

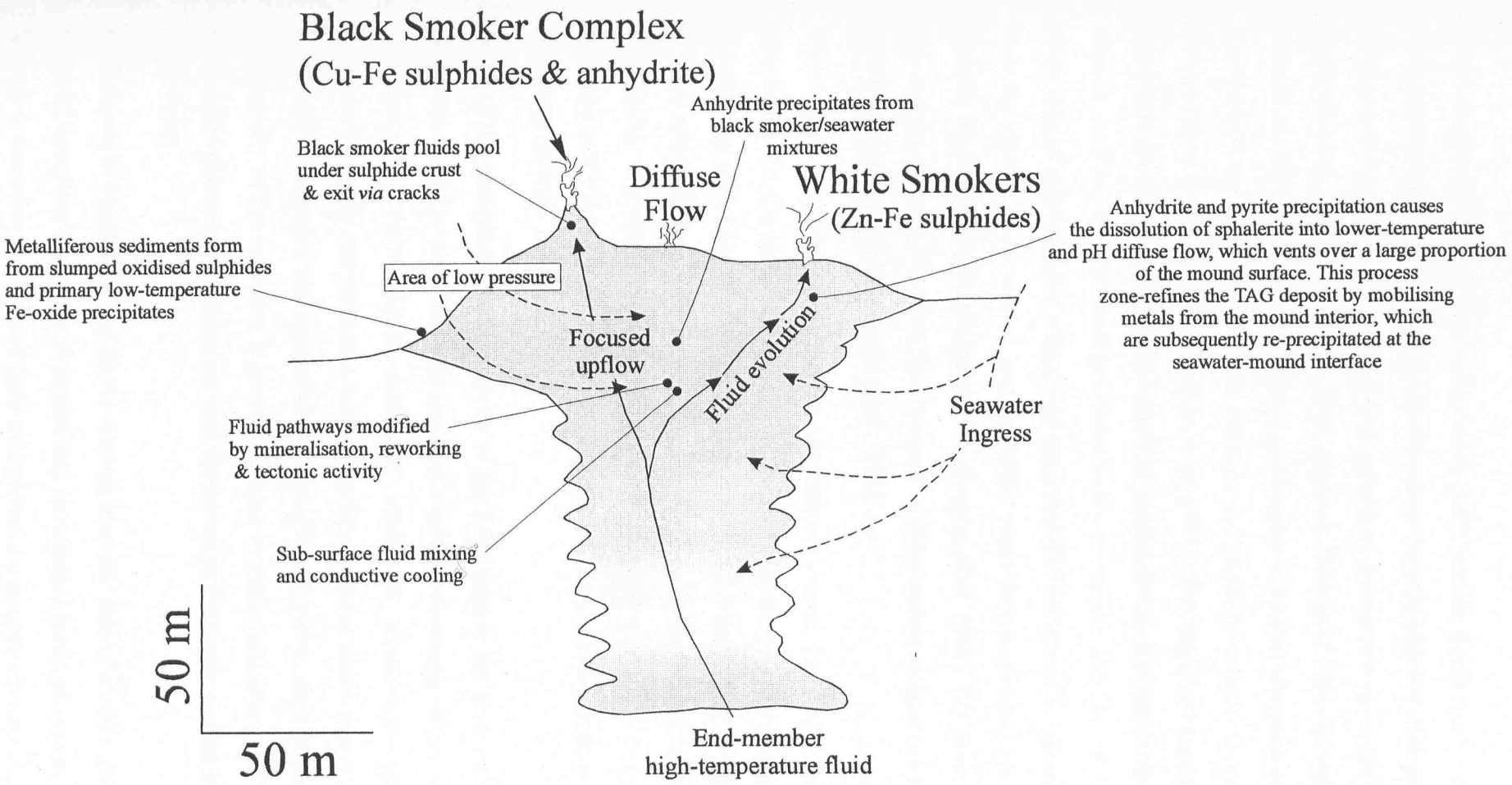

Figure 3.3: A schematic representation of sub-surface fluid flow and mineralisation processes within the active TAG mound, 26°N Mid-Atlantic Ridge. Fluid pathways within the mound are complex with seawater ingress and mixing to at least 120 mbsf, controlled by the subsurface permeability of the mound substrate. The abundance of anhydrite veins within the mound indicates significant seawater percolation into the mound interior, and the maintenance of temperatures in excess of 150°C in the fluid upflow zone.

lower-temperature fluids with end-member black smoker fluids has led to models of mound growth and fluid evolution that involves the precipitation of large amounts of silica, pyrite and anhydrite coupled with sphalerite dissolution and metal remobilisation [Edmond *et al.* 1995; Tivey *et al.* 1995; James & Elderfield 1996; Edmonds *et al.* 1996; Mills *et al.* 1996]. This is the probable mechanism of similar compositional zonation in Cyprus-type ore bodies that contain virtually no sphalerite in their interiors [e.g. Constantinou & Govett 1972; Franklin *et al.* 1981]. The degree of zone refining is dependant on the mixing-cooling history of mound fluids, and the thermal history of the deposit. At TAG steep thermal gradients within the mound and extensive hydrothermal reworking of sulphides has effectively separated Zn (and also Cd, Au, Ag, As and Sb) from the interior of the mound, and the higher temperature assemblages immediately beneath the Black Smoker Complex [Hannington *et al.* 1998]. The association of Zn with Ag, Au, As, Sb, and Pb reflect the transport of these metals as aqueous sulphur complexes at low temperatures [Hannington *et al.* 1991].

High temperature pyrite-chalcopyrite assemblages around the Black Smoker Complex are enriched in Cu, Co and Se. High Cu and Zn grades in the TAG surface sulphides reflects the maturity of the deposit, and is a result of repeated overprinting of high-temperature Cu-rich sulphides by lower-temperature Zn-rich assemblages [Hannington *et al.* 1998]. Bulk Cu/Cu +Zn ratios in surface material are generally less than 0.5 in surface deposits but close to 0.9 through the rest of the deposit, similar to Cyprus-type sulphide deposits [Hannington *et al.* 1998].

Much of the paragenesis of the interior of the TAG deposit has been obscured by processes related to seawater incursion and sulphide reworking. While sulphide textures in the upper part of the mound are dominantly colloform, sulphides from the mound interior are hydrothermally recrystallised, and fine-grained phases like marcasite and wurtzite are commonly overgrown and replaced by coarse-grained pyrite, chalcopyrite or sphalerite. The porosity of the sulphides is greatly reduced by recrystallisation and infilling of pore spaces, and chimney structures are only preserved in the upper mound debris [Hannington *et al.* 1998].

Differences in composition of fluids venting from the mound surface are a function of near-surface rather than deep hydrothermal processes [Hannington *et al.* 1995]. Microthermometric analyses of fluid inclusions in anhydrite crystals indicate that temperatures at depths greater than 100 mbsf are in excess of 380-390°C beneath the

Black Smoker Complex, while other areas on the mound have been affected by lower temperature fluids percolating through the mound or by local entrainment of seawater, displaying a wider and lower range of temperatures (187-337°C) [Petersen *et al.* 1998]. Salinities fall within the range for mid-ocean ridge vent fluids, but require phase separation to have occurred at depth to explain the observed compositions [Tivey *et al.* 1998].

3.2.4.3 Mound ochres

A carapace of Fe-oxides and gossanous sulphide talus is developed over much of the surface of the TAG mound to ~5 m depth, reflecting the extent of seawater alteration and penetration into the deposit [Hannington *et al.* 1998]. These surficial deposits accumulate from a combination of processes including slumping and oxidation of chimney material and the *in situ* precipitation of low-temperature phases from diffuse fluids that percolate through the cover of hydrothermal precipitates and soft sediments [Hannington *et al.* 1988, Hannington *et al.* 1991; Herzig *et al.* 1991; German *et al.* 1993; Mills & Elderfield 1995*a*; Mills *et al.* 1996; Goulding *et al.* 1998]. TAG ochres are compositionally diverse, comprising unconsolidated amorphous Fe-oxides and oxyhydroxides (hematite and goethite), often with minor amounts of quartz, carbonate, smectite and pyrite [Tivey *et al.* 1995; Mills & Elderfield 1995*a*; Mills *et al.* 1996]. The ochres are frequently underlain and cemented by cherty Fe-oxides produced by diffuse venting through the upper mound surface [Mills & Elderfield 1995*a*].

Weathering of the mound exterior is intense and produces a complex gossan assemblage of secondary Fe and Cu-rich minerals [Hannington *et al.* 1988; Herzig *et al.* 1991; Hannington *et al.* 1991, Hannington *et al.* 1998]. During seafloor oxidation or reaction with dilute hydrothermal fluids, metals such as gold are mobilised as chloride complexes by acidic pore fluids from primary mound sulphides and redeposited with secondary Cu-sulphides (covellite, diginite, chalcocite), hydrated Fe-sulphates (jarosite) and Cu-chlorides (atacamite) in gossanous crusts at the outer surface of the TAG deposit [Hannington *et al.* 1988, Hannington *et al.* 1991; Herzig *et al.* 1991]. These distinctive seafloor associations and secondary metal enrichments reflect the maturity of the TAG deposit, as ongoing sulphide reworking and gossanisation enhances the contrast between the mineralogical and chemical composition of the hot interior and cooler margins of the deposit [Hannington *et al.* 1998; Knott *et al.* 1998].

3.2.4.4 Metalliferous sediments

Metal-enriched sediments have been recovered from the TAG area since the early 1970s [Scott *et al.* 1978; Shearme *et al.* 1983; Metz *et al.* 1988; German *et al.* 1993; Mills *et al.* 1993]. Sediments at TAG have a patchy distribution, occurring as a veneer up to several metres thick on fault terraces on the walls of the rift valley, and in isolated ponds in the adjacent valley floor [Shearme *et al.* 1983; Mills 1995]. These sediments are pale-brown to yellow calcareous oozes (similar to normal Atlantic pelagic sediments), with anomalous metal enrichments attributed to hydrothermal plume and/or slumped sulphide inputs during episodes of high-temperature activity [e.g. Shearme *et al.* 1983; Metz *et al.* 1988; Mills *et al.* 1996].

The constant erosion, mass wasting and resedimentation of sulphide and oxide debris from the steep-sided flanks of the TAG deposit produces abundant metalliferous sediments that extend 50 m from the base of the mound [Hannington *et al.* 1988; Thompson *et al.* 1988]. Similarly, ponds of sediment several metres thick fill depressions in the valley floor down-slope from inactive *Mir* and *Alvin* deposits [Metz *et al.* 1988; Mills *et al.* 1993]. Hydrothermal inputs to near-vent sediments have been identified geochemically as slumped partially oxidised mound debris and fine-grained Fe-oxyhydroxide particles derived either from the neutrally buoyant TAG plume [German *et al.* 1993], or by direct precipitation from low-temperature diffuse fluids [Mills *et al.* 1996; Goulding *et al.* 1998]. The composition of the sulphidic sediment layers is controlled by the mineralogy of the mound inputs and their post-depositional history, that is typified by fairly rapid resedimentation [Metz *et al.* 1988; Mills *et al.* 1993].

Sediments dominated by plume fallout and mass wasting of sulphides are compositionally and texturally distinct [e.g. Mills *et al.* 1993; German *et al.* 1993]. Near-vent sediments commonly contain angular clasts of partially oxidised sulphides in a fine-grained Fe-oxide or -oxyhydroxide sedimentary matrix [Metz *et al.* 1988; Mills *et al.* 1993]. The composition and fine-grained texture of plume-derived sediments is less diverse, with a bulk geochemistry governed by scavenging interactions with large volumes of seawater [German *et al.* 1990*a,b*]. Fe-oxyhydroxide sediments formed *in situ* by direct precipitation from diffuse fluids at the surface of the TAG mound are also fine-grained, but with a "proximal" chemistry indicating precipitation from vent fluids with minimal, if any interaction with seawater (cf. section 2.9) [Mills & Elderfield 1995*a*; Mills *et al.* 1996; Goulding *et al.* 1998].

Various geochemical proxies of hydrothermal processes have been developed through studies of TAG sediments. These are discussed further and compared with Troodos metalliferous sediment compositions in Chapter 7 of this dissertation.

3.3 The Troodos ophiolite complex, Cyprus

The TAG deposit has been characterised by numerous studies, and following ODP drilling the processes controlling the structure, growth and composition of the sulphide mound are now better understood at TAG than any other seafloor vent site. The most recent models of sulphide mound formation at TAG are not only important for modern seafloor deposits, but have implications for on-land analogues such as Cyprus-type ore bodies. Many comparisons have been drawn between the active TAG mound and Cyprus-type ore deposits. For example, in terms of morphology and size, the TAG mound is more similar to Troodos ore deposits than it is to other known seafloor deposits [Tivey *et al.* 1995]. The composition of the TAG deposit is similar to that of some of the largest massive sulphide deposits in the Troodos ophiolite, which typically comprise massive brecciated pyrite ores, underlain by a quartz-pyrite-chlorite stockwork [Constantinou 1980; Constantinou & Govett 1973]. Similarly, the distribution of sulphide assemblages and textures throughout the TAG deposit is similar to that described for Cyprus ophiolite-hosted massive sulphide deposits [Brown & McClay 1998]. Additionally, the observation that surface of the TAG deposit is being modified by secondary diagenetic and weathering processes while still hydrothermally active has important implications for the timing of formation of the ochres that cap many Troodos ore bodies [Hannington *et al.* 1988; Hannington *et al.* 1991; Herzig *et al.* 1991].

One of the aims of this dissertation is to use the REEs as proxies of hydrothermal processes to determine if the current TAG model of sulphide mineralisation and metalliferous sediment formation is applicable to Troodos sulphide mound deposits. The following sections provide an introduction to the Troodos ophiolite, and the results of studies of the ore-forming processes operating at a Tethyan spreading centre.

3.3.1 Overview of the geological history of Cyprus

The island of Cyprus is located in the north-east Mediterranean Sea and comprises four arcuate E-W trending geological terranes with a surface area of 9251 km^2, of which the

Troodos ophiolite complex constitutes the main structural and topographical feature (Fig. 3.4). The ophiolite occupies an area of 3000 km^2 in the south-central region of the island and comprises upper Cretaceous (~85 Ma) basic and ultrabasic igneous rocks, formed by a pulse of late Cretaceous seafloor spreading [Gass 1980]. The Cretaceous Tethys ocean was a tectonic setting with few modern analogues, characterised by the opening and closure of many small, short-lived intracontinental ocean basins, and the creation and destruction of numerous spreading centres [Robertson & Woodcock 1980]. The ophiolite complexes of Cyprus and Oman define a suture zone formed by closure of the Tethys Ocean at the end of the Cretaceous, and the tectonic history of Troodos is complex due to its position in the oblique convergence of the African & Eurasian plates, and various microplates [Searle & Panayiotou 1980].

The ophiolite complex is succeeded to the north by upper Cretaceous to Pleistocene sedimentary rocks of the Mesaoria Plain [Bagnall 1964]. A generally undeformed sequence of circum-Troodos sedimentary succession in the southern part of the plain [Wilson 1959] is distinct from highly-folded flysch sediments derived from the Permian to middle Miocene allochthonous sedimentary formations of the Kyrenia Range to the north [Ducloz 1972; Dixey 1975]. In the Paphos district to the south-west of the ophiolite complex, allochthonous masses of Mesozoic age occur. The rocks of the Mamonia Complex are allochthonous, highly deformed rocks, including marine sediments, and an igneous-sedimentary sequence with pillow lavas and minor intrusives of alkaline affinity [Swarbrick 1980]. These rocks are interpreted to be remnants of a Mesozoic passive continental margin accreted onto the southern Troodos margin from a subducting slab in Maestrichtian times [Robertson & Woodcock 1980; Moores *et al.* 1984].

The ophiolite complex was rotated 90° anticlockwise after its formation and remained in a convergent tectonic regime during the closure of Tethys, which resulted in the deformation and uplift of the Kyrenia mountain range [Panayiotou 1987]. Palaeomagnetic vectors of lavas and overlying sediments indicate that the ophiolite has migrated northward 10-15° since formation, and that rotation of the ophiolite has occurred in the last 10 Ma [Shelton & Gass 1980]. The Troodos ophiolite was obducted onto the margin of the Afro-Arabian continental margin in the Late Cretaceous, although the geometry of the subduction zone responsible for obduction is still the subject of some debate [e.g. Moores *et al.* 1984; Taylor *et al.* 1992]. Late Tertiary uplift of ~2000 m is centred on a low-density serpentinite diapir beneath Mt. Olympus in central Cyprus [Searle &

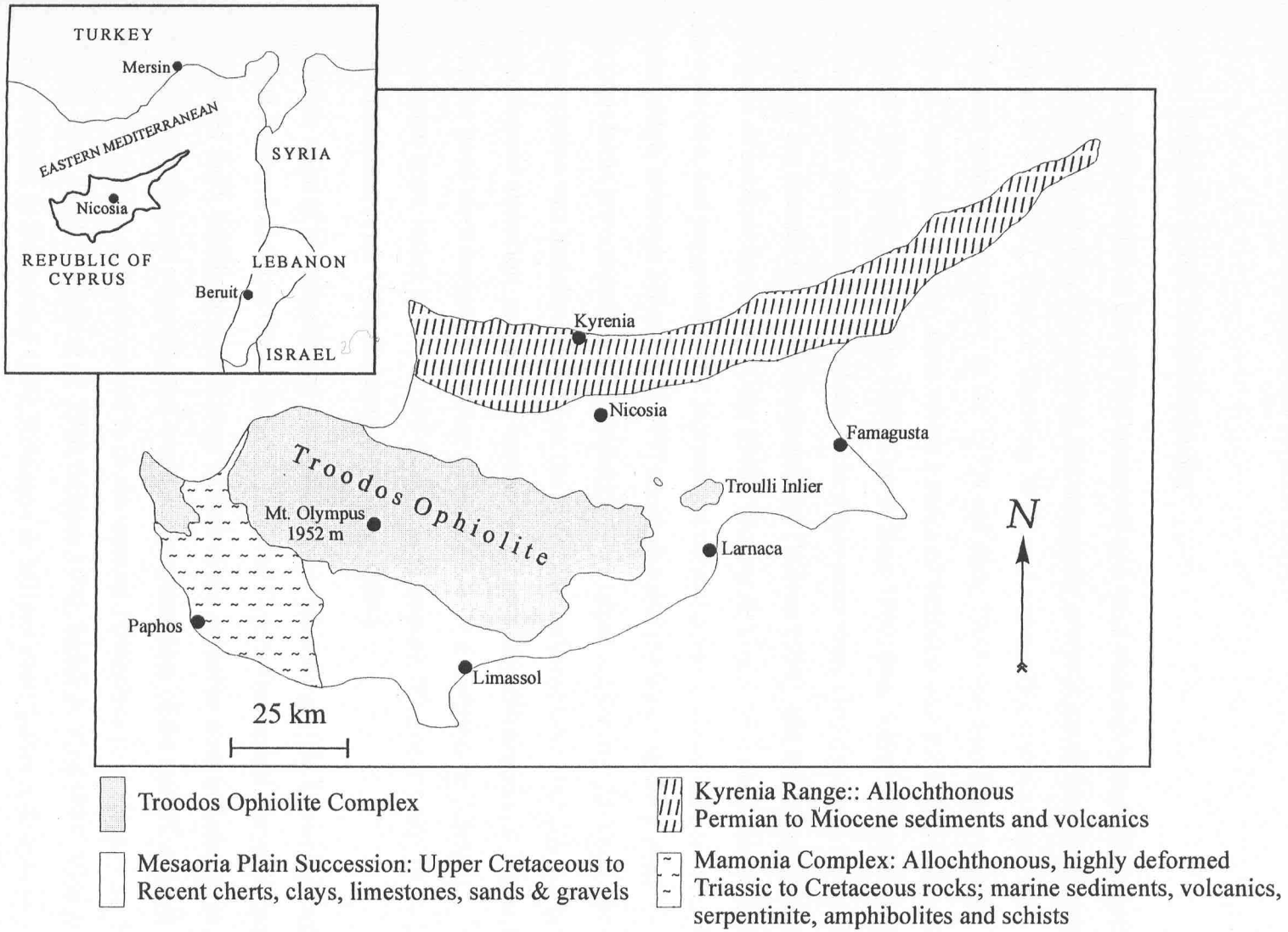

Figure 3.4: Location map of the island of Cyprus showing the main tectonostratigraphic terrains

Panayiotou 1980]. Uplift resulted in intensive erosion of the igneous rocks of the ophiolite complex, and the formation of undifferentiated gravels, sands and silts along the southern edge of the Mesaoria Plain [Wilson 1959].

3.3.2 Structure of the Troodos ophiolite

The Troodos ophiolite is one of best preserved and most thoroughly studied ophiolite complexes in the world. It is uplifted, but essentially *in situ* [Gass & Masson-Smith 1963; Moores & Vine 1971, Gass & Smewing 1973] and represents a complete and little-deformed ophiolite sequence. In the 1950s and early 1960s the massif was mapped by the Cyprus Geological Survey, from which a series of memoirs was published [Wilson 1959; Bagnall 1960; Bear 1960; Gass 1960; Carr & Bear 1960; Bear 1963; Pantazis 1967]. The composition and structural relations of the major units were identified, and the intrusive nature of the sheeted dykes was demonstrated [Wilson 1959], and subsequently interpreted in terms of seafloor spreading [Gass 1968]. Moores & Vine [1971] identified the massif as an ophiolite, and suggested that it represented normal oceanic lithosphere formed at a mid-ocean ridge, although Miyashiro [1973] concluded that the major element chemistry of Troodos lavas are compatible with formation in an island arc setting. Although this interpretation was initially disputed on the basis that the lavas have been subject to hydrothermal alteration, subsequent immobile element ratio determinations showed that Troodos lavas were erupted at a minor spreading axis in a marginal sea above a subduction zone, rather than in a mid-oceanic environment [Pearce & Cann 1973; Pearce 1975; Robinson *et al.* 1983; Rautenschlein *et al.* 1985].

A further stage of investigation of the ophiolite was initiated in 1981 by the International Crustal Research Drilling Group (ICRDG) and the Cyprus Geological Survey Department. Combined field, drilling and laboratory studies of the ophiolite were undertaken to resolve outstanding problems regarding the origin and emplacement of the massif, and test the applicability of the ophiolite model to *in situ* oceanic lithosphere [e.g. Cann *et al.* 1987; Malpas *et al.* 1989; Baragar *et al.* 1990; Malpas 1990; Smith & Vine 1987; Vine & Smith 1990; Bednarz & Schmincke 1990; Robinson & Malpas 1990; Gillis & Robinson 1990].

3.3.2.1 Mantle sequence

Differential uplift and subsequent erosion of the ophiolite has created an annular outcrop pattern, where the stratigraphically deepest rocks of the succession outcrop centrally,

surrounded by successively higher units, with pillow lavas occurring at the periphery of the massif (Figs. 3.5 and 3.6). A 1 km vertical succession of upper mantle rocks outcrop in the ultramafic core of the ophiolite (Mt. Olympus region), and the Limassol Forest area to the south of the Southern Troodos Transform Zone (STTZ) in south-east Troodos. The STTZ is a major east-west trending fault zone mapped by early workers [Wilson 1959; Bagnall 1960], and subsequently interpreted as an oceanic transform fault [Moores & Vine 1971; Allerton & Vine 1990; MacLeod 1990]. Troodos mantle rocks are (*c.* 50 to 80%) serpentinised and tectonised harzburgites (~80% of mantle outcrop), with associated lenticular dunite bodies of cumulate origin [Gass 1980]. The harzburgites are interpreted as the refractory residues of a plagioclase lherzolite mantle from which a basalt melt has been extracted to supply magma to the overlying sheeted dyke and extrusive sequences. They contain subordinate gabbroic and plagioclase lherzolite bodies, which are interpreted as trapped basaltic melts and less depleted mantle respectively [Wilson 1959; Greenbaum 1972; Menzies & Allen 1974; Allen 1975; George 1975; Greenbaum 1977].

3.3.2.2 Plutonic sequence

The plutonic sequence comprises high-level intrusives from ~50 to 800 m thick of gabbroic and more evolved compositions that overlie gabbros and peridotites of cumulate origin [Wilson 1959; Bear 1960; Moores & Vine 1971; Gass & Smewing 1973; Allen 1975; Coleman & Peterman 1975; Browning *et al.* 1989]. The textures of the high-level intrusives range on an outcrop scale from micro-textured to pegmatitic, and include silicic plagiogranites formed in the closing stages of crystallisation of basaltic magmas in spatially discrete multiple magma chambers [Wilson 1959; Bear 1960; Moores & Vine 1971; Gass & Smewing 1973; Allen 1975; Coleman & Peterman 1975; Greenbaum 1977; Malpas *et al.* 1989; Malpas 1990]. Detailed fieldwork and studies of ICRDG CY-4 drill core led to the recognition of an older series of deformed plutonic rocks intruded by a series of undeformed cumulate rocks, supporting a model of multiple magma chambers beneath the Troodos ocean floor [Malpas 1990].

3.3.2.3 Sheeted dyke complex

A mainly N-S striking sheeted dyke complex ~1 km thick forms an extensive concentric belt around the plutonic core of the ophiolite, necessitating formation in an extensional regime, regardless of the local plate geometry [Wilson 1959; Bear 1960; Gass 1960]. The contacts between the dykes and underlying gabbros and overlying volcanics are rapid and

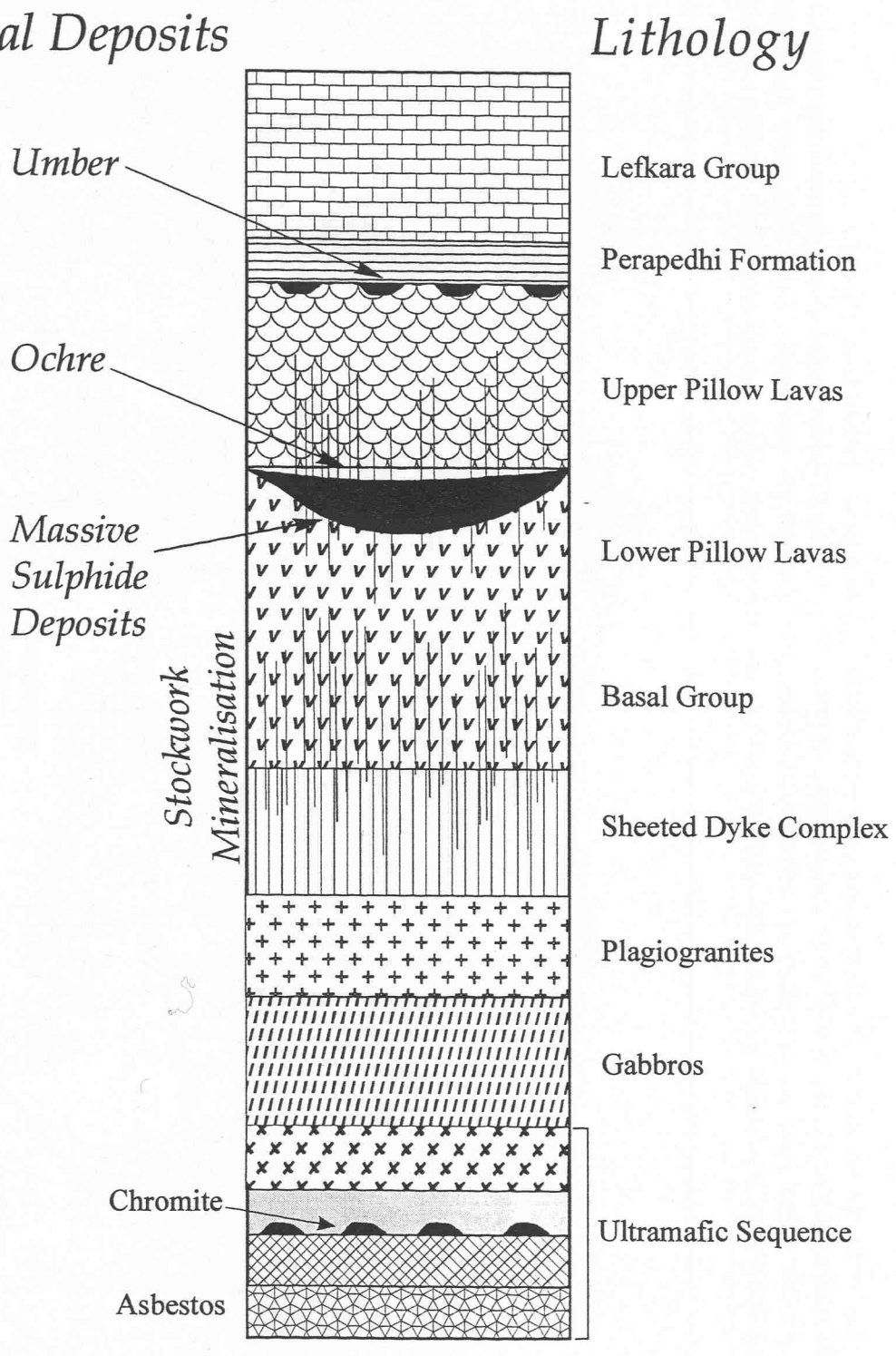

Figure 3.5: A schematic representation of the lithologic units of the Troodos ophiolite showing the spatial relationships between sulphide mineralisation, the occurrences of ochre and umber, and the Upper and Lower Pillow Lavas. Adapted from Constantinou [1980].

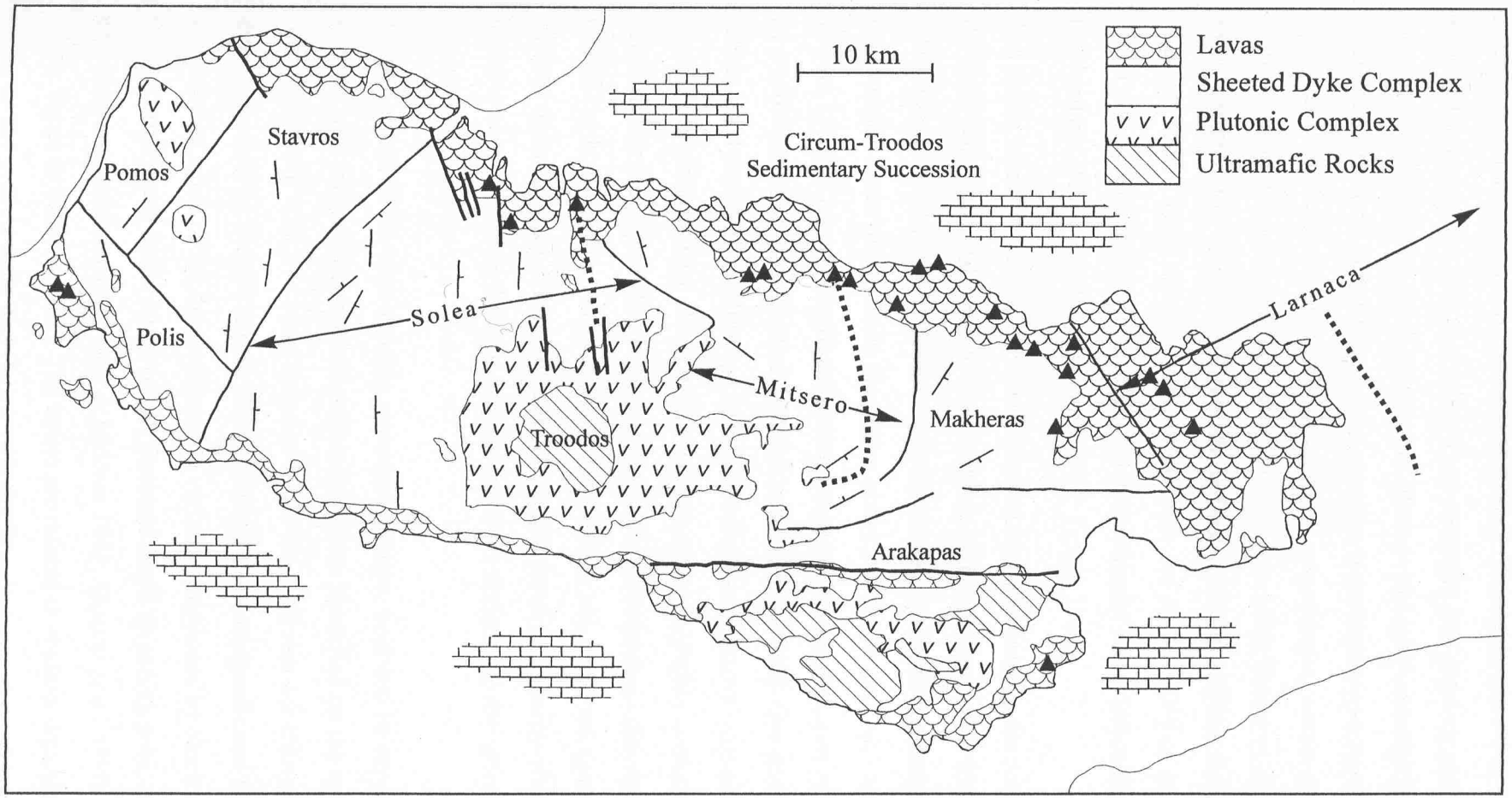

Figure 3.6: Simplified geological map of the Troodos Ophiolite, showing the internal structure within the Sheeted Dyke Complex. The boundaries of the Polis, Pomos, Stavros, Solea, Mitsero, Makheras, Arakapas and Larnaca dyke domains are delineated by fine solid lines. The attitude symbols show average dips of dykes within each domain. Dashed lines indicate approximate locations of the Solea, Mitsero and Larnaca graben axes. Triangles are major sulphide ore bodies. Heavy lines are high angle faults. Adapted from Moores *et al.* [1990].

transitional. The uppermost sheeted dykes contain screens of pillow lava; the lower parts screens of gabbro and microgabbro [Gass 1980]. The dykes are 0.1 to 5 m in width, although most are less than 2 m wide. They comprise fine grained, generally aphyric basalt and andesite with small amounts of olivine- and pyroxene-phyric basalt with ophitic or variolitic textures. The sheeted dyke complex is pervasively recrystallised to greenschist or lower amphibolite facies mineral assemblages, with frequent retrogression to lower temperature assemblages [Bickle & Teagle 1992; Bickle *et al.* 1998], in contrast to the variable, low temperature alteration of the volcanics and the mainly fresh plutonics [Baragar *et al.* 1990]. Original igneous textures and chilled margins are typically preserved, excluding the spectacularly altered epidosite zones (discussed in section 4.4.4) [Richardson *et al.* 1987; Baragar *et al.* 1990; Teagle 1993].

The dykes represent magma in transit from crustal reservoirs to the ocean floor, and span the same compositional range as the overlying lavas [Baragar *et al.* 1987; Baragar *et al.* 1989, Baragar *et al.* 1990]. However, the dykes do not record the sharp break in composition observed between the pillow lava suites in the extrusive sequence [e.g. Wilson 1959]. This compositional contrast may have been obscured in the sheeted dykes by hydrothermal recrystallisation [Robinson & Malpas 1990]. Compositional variability within the dykes can be attributed to high-level closed system fractionation except for some trace elements (e.g. REE) which indicate a more complex evolution, involving variable degrees of partial melting or open system fractionation [Baragar *et al.* 1990]. Unlike the lavas, the two magma suites do not show any preferred age relationship in the sheeted dyke complex. This indicates the simultaneous availability of magmas with variable composition in discrete magma chambers underlying the spreading axis [Baragar *et al.* 1990].

Three north to north-west trending structural grabens, bounded by inward dipping dyke swarms with relatively consistent strikes have been identified on the northern flank of the ophiolite, along with five other domains 10-20 km wide that are characterised by similar dyke attitude (Fig. 3.6) [Varga & Moores 1985]. Palaeomagnetic and structural data suggest that much of the dyke orientation variation originates by block rotation of newly formed crust along listric faults on the flanks of fossil spreading axes, rather than emplacement deformation [Varga & Moores 1985; Moores *et al.* 1990; Allerton & Vine 1990; Varga & Moores 1990]. The dykes are rotated to shallow dips along normal listric faults on the graben walls that flatten with depth and merge into a detachment surface

below each graben at or near the high-level gabbro-sheeted dyke interface. In places this detachment is cut by undeformed dykes, indicating that faulting occurred during crustal accretion near a spreading axis [Varga & Moores 1985]. From these structures it is inferred that the sheeted dyke complex formed at several separate and temporally distinct axes preserved by eastward migration of the ridge axis by ridge jumping [Varga & Moores 1985].

3.3.2.4 Volcanic sequence

Overlying the sheeted dyke complex is an extrusive sequence which outcrops in a discontinuous belt around the periphery of the ophiolite. Pillowed lava flows dominate the volcanics (80% of outcrop exposure), with lesser massive flows, thin sheet flows, breccias and hyaloclastites [Wilson 1959; Bear 1960; Malpas & Langdon 1984]. The extrusive sequence was initially divided by the Cyprus Geological Society into the Upper and Lower Pillow Lavas (UPL and LPL) on the basis of petrographic, field and geochemical criteria, and spatial relationships to the massive sulphide deposits (Fig. 3.5) [Wilson 1959]. The LPL have more evolved compositions than the UPL, and were interpreted as having formed near a spreading axis [Wilson 1959; Gass & Smewing 1973; Smewing *et al.* 1975]. The UPL outcrop around 60% of the perimeter of the massif. They cap many of the massive sulphide ore bodies, are interpreted as the products of off-axis volcanism [Gass & Masson-Smith 1963; Smewing *et al.* 1975; Malpas & Langdon 1984], and may be genetically related to off-axis plutons [Malpas 1990]. The boundary between the UPL and LPL suites was poorly defined in most localities. An unconformity was recognised to exist between the UPL and LPL in the south of the massif. However, in the north this boundary was interpreted to be a metamorphic discontinuity, with a geochemical overlap between the two groups [Wilson 1959; Gass & Smewing 1973; Smewing 1975; Smewing *et al.* 1985].

The lava suites were subsequently redefined by geochemical analyses of pristine volcanic glasses [Robinson *et al.* 1983; Rautenschlein *et al.* 1985], which occur throughout the volcanic section to the top of the sheeted dyke complex, excluding the narrow subvertical zones of pervasive alteration beneath the sulphide ore bodies [Robinson *et al.* 1983]. The compositions of these glasses have been used to define two major magmatic suites on Cyprus. A fractionated island-arc tholeiite (IAT) suite occurs in the basal 400-500 m of the lava pile on the northern flank of the ophiolite, comprising basalt-andesite-dacite-

rhyodacite assemblages [Robinson *et al.* 1983; Rautenschlein *et al.* 1985]. A later picrite-basalt-basaltic-andesite assemblage with boninitic affinities occurs on the west and southern flanks of the ophiolite [Robinson *et al.* 1983; Rautenschlein *et al.* 1985; Taylor & Nesbitt 1988; Taylor *et al.* 1992]. The IAT suite corresponds approximately to the LPL, and the boninitic lavas to the UPL, although the major compositional discontinuity lies at a much lower level than the traditional boundary between the two units, and lavas of the two suites are interfingered in several localities [Robinson *et al.* 1983; Schmincke *et al.* 1983; Robinson & Malpas 1990]. These lavas suites cannot be derived from each other or a common parental magma, and probably reflect successive melting episodes of a MORB source in a mantle wedge above a subduction zone [Robinson *et al.* 1983; Schmincke *et al.* 1983; Robinson & Malpas 1990]. Trace element compositions indicate all Troodos source regions have been affected by hydrous fluids and/or melts from subducted lithologies [Pearce 1975; Rautenschlein *et al.* 1985; Taylor & Nesbitt 1988; Robinson & Malpas 1990; Kostopoulos & Murton 1992; Taylor *et al.* 1992].

The Troodos volcanics have been affected by pervasive hydrothermal alteration in zones of hydrothermal recharge, with some superimposed higher-temperature alteration in zones of vent fluid discharge. This alteration is discussed in Chapter 4 of this dissertation.

3.3.2.5 Massive sulphide ore bodies

Troodos massive sulphide deposits occur within the extrusive sequence of the ophiolite complex, and display mineral associations, textures and zonations that place them among the best known ancient analogues of sulphide mineralisation at mid-ocean ridges. The ore bodies are located in five mining districts (Limni, Kalavasos-Mousoulos, Skouriotissa-Mavrovouni, Mitsero and Mathiati-Sha), each occupying an area of approximately 10 x 10 km [Wilson 1959; Bear 1960; Gass 1960]. The deposits have been worked for copper from near-surface exposure since 4000 BC, and for minor quantities of gold and silver which are enriched in Fe-rich gossans that cap many of the ore bodies [Wilson 1959; Gass 1960; Constantinou & Govett 1972], and are similar to those present on the active TAG mound [Hannington *et al.* 1988; Hannington *et al.* 1991; Herzig *et al.* 1991]. The deposits range from 50,000 tonnes to 16 Mt [e.g. Wilson 1959; Bear 1963; Constantinou 1980], but there are around 90 smaller, undeveloped prospects with <10,000 tonnes of ore, of a similar size to typical mid-ocean ridge vent deposits; indeed only half of the deposits are >1 Mt [Hannington *et al.* 1998]. Approximately 20 deposits containing on average ~1 Mt of ore of variable copper content have been worked on the island. Much of the copper

production was from three of the largest deposits: Mavrovouni (~15 Mt; 3.8 wt % Cu), Skouriotissa (~5.4 Mt; 2.3 wt % Cu) and Limni (~16 Mt; 1.4 wt % Cu) [Wilson 1959].

The five mining districts broadly correspond to the locations of three axial grabens preserved along the northern flank of the ophiolite that were produced by crustal extension processes, illustrated in Figure 3.6 [Varga & Moores 1985]. Of the three grabens, the excellent three-dimensional exposure of the Solea graben best illustrates the relationships between structural, magmatic and hydrothermal processes operating during seafloor spreading [Schiffman et al. 1987; Schiffman & Smith 1988; Varga & Moores 1985; Varga & Moores 1990; Moores *et al.* 1984; Moores *et al.* 1990; Schiffman *et al.* 1990]. The massive sulphide ore bodies were formed around seafloor hydrothermal vents on the flanks of the seafloor grabens [Spooner *et al.* 1977; Moores *et al.* 1990]. The high-temperature hydrothermal circulation responsible for the seafloor hydrothermal activity was driven by the off-axis magmatic intrusion of small plutons into crust previously thinned by extensional faulting on the graben valley walls [Varga & Moores 1985; Schiffman *et al.* 1987; Schiffman & Smith 1988; Varga & Moores 1990]. The three deposits associated with post-graben magmatic and hydrothermal activity in the Solea graben (Skouriotissa, Apliki and Mavrovouni) collectively represent the greatest sulphide accumulation in the Troodos complex [Varga & Moores 1990].

3.3.2.6 Ore deposit morphology and mineralogy

A typical Troodos massive sulphide bodies deposit is a single, discrete massive sulphide orebody underlain by a stockwork of hydrothermally brecciated and mineralised lavas, and overlain by unmineralised lavas [Constantinou & Govett 1972, Constantinou & Govett 1973; Constantinou 1980]. Most of the ore is mined from a zone of massive cupriferous pyrite deposited as a low-relief exhalative lenticular mound on the seafloor, although a significant proportion of the recoverable metals often occurs within the sub-seafloor stockwork.. Troodos sulphide mounds are typically a few tens of metres thick, although the largest bodies may have been over 100 m thick [Panayiotou 1987]. In contrast to the circular TAG mound (~200m in diameter), Troodos mound deposits have a typically elongate shape [Constantinou & Govett 1972]. For example, the Mathiati deposit (2.8 Mt) is comparable in tonnage to the active TAG mound (3.9 Mt), but the ore body is only 50 m wide and more than 250 m long [Lydon & Galley 1986]. The asymmetry of the ore bodies is attributed to their formation adjacent to a synvolcanic fault or graben wall. The ore

bodies thin away from, and are often dissected by late movement along these faults in a similar manner to the inactive sulphide mounds in the TAG vent field [Rona *et al.* 1993*a*]. Some of the largest deposits are replacive sub-seafloor stockwork-type deposits formed by mixing between black smoker-type fluids with seawater within the lava pile, and have modern oceanic counterparts [Edmond *et al.* 1979a; Honnorez *et al.* 1985; Richards *et al.* 1989]. In these deposits, stockwork-mineralised lavas grade upwards into less altered and mineralised lavas (e.g. the Pitharokhoma, Sha and Agrokipia B deposits).

The TAG model of sulphide reworking associated with seawater ingress, fluid mixing and sulphide precipitation and dissolution is the likely mechanism of a similar compositional zonation in Cyprus-type ore bodies, which contain virtually no sphalerite in their interiors [e.g. Constantinou & Govett 1972]. Cyprus mound sulphides are dominated by several generations of pyrite, that frequently accounts for >90% of the mineralised assemblage, with varying amounts of chalcopyrite, minor sphalerite and rare marcasite and pyrrhotite. Covellite, diginite, chalcocite and bornite are found in the massive ores in the upper parts of many ore bodies [Constantinou 1980]. The sulphides are Pb-poor, while Cu varies from 0.2-7.7 wt. % (averaging ~2 wt.%), with Zn generally <0.1 wt.%. The ore bodies typically have bulk compositions similar to the TAG mound, consisting of predominantly iron and sulphur, with minor Cu and Zn and traces of Co, Ag and Au [see review in Hannington *et al.* 1998]. The Zn content of sulphides is generally low (< 0.2 wt. %) but along with Cu (average ~2 wt. %), is concentrated in zones of secondary enrichment in the upper parts of some ore bodies [see review in Hannington *et al.* 1998]. Secondary Cu-rich sulphides such as covellite, diginite, chalcocite and bornite are found in the same associations as at TAG in the massive ores in the upper parts of many ore bodies [Constantinou 1980].

The ore deposits are characterised by a vertically-zoned assemblage of breccia units [Constantinou 1980] similar to those revealed by ODP drilling of the TAG mound [Humphris *et al.* 1995]. Although anhydrite is not preserved in the geological record, in view of the results of ODP drilling of the TAG mound, the brecciation that characterises the interiors of Troodos ore bodies can be attributed to internal anhydrite and sulphide reworking, rather than sulphide erosion and resedimentation at the mound surface [Constantinou 1980] or fragmentation as a result of sedimentary overburden pressure [Wilson 1959].

Sulphide breccias in the upper *c.*5 m of the Cyprus deposits are conglomeritic in nature, and comprise subangular porous blocks of compact or colloform pyrite occurring in a

matrix of dark sandy pyrite cubes with dimensions typically < 1 mm [Wilson 1959]. [Constantinou & Govett 1972; Constantinou 1980]. These are identical to the pyrite breccias in the uppermost drill core from the TAG mound (except for the absence of anhydrite), and represent the kinds of sulphide material from the Skouriotissa deposit analysed in Chapter 7 of this dissertation. Sulphide chimney structures are only rarely preserved in Cyprus ore bodies [Oudin *et al.* 1981; Oudin & Constantinou 1984] as in the active TAG mound [Hannington *et al.* 1998].

The conglomeritic ore overlies massive ('compact') ore comprising pyrite, chalcopyrite and sphalerite with lesser marcasite with localised secondary Cu enrichments (>5 wt % Cu) in covellite, chalcocite and bornite [Wilson 1959; Constantinou & Govett 1973; Constantinou 1980]. The compact ores are the product of the early brecciation of massive pyrite and later cementation by colloform pyrite. The compact ore consists of coarse, granular pyrite breccias or blocky ore cemented by porous pyrite with vuggy cavities lined with quartz and pyrite, and closely resemble sections of massive pyrite and pyrite-silica breccias from the TAG mound [Humphris *et al.* 1995]. These breccias are cut by late veins of colloform pyrite, and occasionally sphalerite. The compact ore is much less friable than the conglomeritic ore, and the sulphides are commonly extensively recrystallised to poikilitic euhedra (up to a cm in size) and do not show colloform textures [Constantinou & Govett 1972; Constantinou 1980]. Fossilised worm tubes and chimney fragments have been recognised in the pyrite breccias [Oudin & Constantinou 1984], but repeated hydrothermal recrystallisation and brecciation episodes means that these primary features are rarely preserved [Hannington et al. 1998].

The massive ores are underlain by chloritised and mineralised stockwork breccias, the thicknesses of which are often undetermined as drilling operations cease in low grade ore [Constantinou & Govett 1972]. In the stockwork zones, sulphide and quartz-sulphide veins cement lava breccias and fill fractures in altered pillow lavas. The size and abundance of these veins is highest in the upper stockwork. Away from sulphide veins, the amount and grain size of disseminated pyrite in lavas decreases abruptly [Constantinou & Govett 1972; Constantinou 1980]. Stockwork mineralised alteration pipes beneath the ore bodies have concentric alteration halos with characteristic mineral associations, which record fluid-rock interaction in zones of hydrothermal fluid upflow [Richards *et al.* 1989]. The relative mobility of REEs during axial and off-axis crustal alteration in the Pitharokhoma stockwork deposit is discussed in Chapter 6 of this dissertation.

3.3.2.7 Metalliferous sediments

The igneous rocks of the Troodos massif are overlain to the north and south by calcareous sediments of the circum-Troodos sedimentary succession. These are undeformed sediments of Maastrichtian to Tertiary age which have a gentle radial inclination imposed by the same central uplift that affects the massif [Wilson 1959]. The base of the succession is marked by the Perapedhi Formation of Campanian-early Maestrichtian age, which rests unconformably on the pillow lavas of the ophiolite (Fig. 3.5) [Wilson 1959]. This formation comprises a thin, intermittent layer of Fe-Mn oxide sediments which occur in hollows on the palaeo-seafloor, and are analogous to the metalliferous sediments of the MOR system [Robertson 1975]. The umbers locally grade into carbonate-free radiolarites and radiolarian mudstones that are overlain discontinuously by bentonitic clays. These sediments are overlain by Maastrichtian and Tertiary chalks of the Lefkara Formation [Wilson 1959]. Excluding the south-west region of Cyprus, these sediments have not been tectonically deformed, and they are physically and chemically little-altered [Robertson & Hudson 1973].

The metalliferous sediments that overlie the volcanic basement of the massif were deposited near a Cretaceous ocean ridge system, and are chemically and mineralogically comparable with the metalliferous sediments of the EPR and other active ocean ridges, being similarly enriched in iron, manganese and trace elements compared with overlying pelagic sediments [Robertson & Hudson 1973; Robertson & Fleet 1976]. Hydrothermal sediments in Cyprus include ochre (Fe-rich, Mn-poor sediment) and umber (Fe- and Mn-rich sediment). Fe-rich ochres occur at the surface of some of the sulphide ore bodies [e.g. Constantinou & Govett 1972; Robertson 1976], and are similar to the Fe-oxyhydroxide ochre deposits forming on the active TAG mound [e.g. Herzig *et al.* 1991]. In light of this similarity, the formation of the Troodos ochres is now attributed to sulphide weathering and oxidation, rather than by post-obduction leaching by meteoric groundwaters [Herzig *et al.* 1991].

Umbers show a wider spatial distribution across the palaeo-seafloor than the ochres, and generally overlie the boninitic lavas that are related to off-axis magmatism, hydrothermal circulation and ore deposition [Constantinou & Govett 1972]. The umbers were initially interpreted as hydrothermally-altered volcanic ash deposits [Wilson 1959], or as precipitates from Fe and Mn-rich solutions derived from the slow weathering of basaltic lavas by cold seawater [Constantinou & Govett 1972]. Other workers noted the similarity

between the umbers and metalliferous sediments on the EPR, and related their formation them to ridge-crest hydrothermal activity [Elderfield *et al.* 1972; Robertson 1975; Robertson 1976; Robertson & Boyle 1983; Boyle 1990]. The umbers have been interpreted as low-temperature precipitates around off-axis, low-temperature vents [Constantinou & Govett 1972; Robertson & Hudson 1973; Robertson 1975; Robertson 1976 Elderfield *et al.* 1972], or alternatively as distal accumulations sourced from high temperature vents [Corliss 1972; Boyle 1990].

3.4 Conclusions

Drilling by ODP has contributed to a greater understanding of the effect of seawater entrainment and fluid evolution on the geochemistry and composition of the TAG sulphide deposit [e.g. Humphris *et al.* 1995; Mills *et al.* 1998; Teagle *et al.* 1998; Tivey *et al.* 1998]. The most recent models of sulphide formation at TAG involve conductive heating of seawater in the mound-like sulphide structure, which causes anhydrite precipitation and effectively zone refines the sulphide to generate secondary pyrite phases and enrichment of Zn, Pb and trace metal-rich sulphide phases at the surface 'gossan' of the mound. [Edmond *et al.* 1995; Tivey *et al.* 1995; Humphris *et al.* 1995; Mills *et al.* 1998; Tivey *et al.* 1998].

Troodos sulphide mound deposits show many mineralogical and chemical similarities to the TAG ore body although they were formed in a supra-subduction rather than mid-ocean ridge environment. In contrast to MOR deposits they are easily sampled due to their on-land exposure by past mining operations [Oudin *et al.* 1981; Oudin & Constantinou 1984; Hannington *et al.* 1988; Hannington *et al.* 1991; Herzig *et al.* 1991; Hannington *et al.* 1998]. In view of these similarities, the REEs are used to test the applicability of the TAG model to processes of sulphide mound formation within the Troodos ophiolite, and to assess the extent of post-ore alteration in Chapter 7 of this dissertation.

Chapter 4

Hydrothermal alteration of the oceanic crust

4.1 Introduction

Our understanding of the physical and chemical processes occurring in the sub-surface of hydrothermal systems has developed through studies of dredged oceanic basalts [e.g. Irving *et al.* 1970; Corliss 1971; Muehlenbachs & Clayton 1971; Bonatti *et al.* 1975; Humphris & Thompson 1978; Delaney *et al.* 1987; Saccocia & Gillis 1995], drilling of the oceanic basement [e.g. Honnorez *et al.* 1985; Alt *et al.* 1986; Humphris *et al.* 1995; Honnorez *et al.* 1998; Humphris *et al.* 1998] and through inferences made from the altered rocks of ophiolites. In this respect, studies of the Troodos ophiolite have been of particular significance. Elevation of $^{87}Sr/^{86}Sr$ ratios from fresh rock towards seawater values and other geochemical changes in the Troodos ophiolite provided confirmation of the magnitude of hydrothermal circulation at mid-ocean ridges [Chapman & Spooner 1977; Spooner & Bray 1977; Spooner *et al.* 1977; Spooner & Fyfe 1973] that had been inferred from anomalous heat flow in the oceans [Lister 1972]. Subsequently, this ophiolite complex has proved particularly useful in characterising crustal evolution and ageing processes, as alteration related to emplacement of the massif is restricted to gypsum formation in the upper 500 m of the extrusive sequence [Staudigel & Gillis 1990]. All other crustal alteration can be related to seafloor processes occurring at a spreading ridge, and is broadly similar to that of *in situ* oceanic crust sampled to date from the ocean basins [e.g. Spooner & Fyfe 1973; Spooner *et al.* 1977; Spooner & Bray 1977; Gillis & Robinson 1988; Richards *et al.* 1989; Gillis & Robinson 1990*a,b*; Gillis *et al.* 1992].

A fundamental difference between ophiolitic and *in situ* ocean crust is that the rocks in ophiolites integrate the chemical effects of axial and off-axis alteration. Numerous studies have shown that the alteration in ophiolites attributed to axial black smoker systems is short-lived compared with the chemical exchange that occurs off-axis at lower-temperatures during ageing of the oceanic basement [Pflumio 1991; Bednarz &

Schmincke 1990; Gillis & Robinson 1988, Gillis & Robinson 1990*a,b*; Staudigel & Gillis 1990; Bickle & Teagle 1992; Bickle *et al.* 1998].

In this chapter the mineralogical and chemical effects of hydrothermal circulation within the oceanic crust are reviewed, within the conceptual framework of hydrothermal recharge, reaction and discharge zones [review by Alt 1995]. Some important differences between the styles of alteration of *in situ* ocean crust and ophiolites are discussed.

4.2 Thermal and alteration history of ODP Hole 504B

Hole 504B is the deepest basement hole in the oceans, and has been drilled over the course of seven Deep Sea Drilling Project (DSDP)/ODP legs since 1982 [Alt *et al.* 1996]. This hole has sampled a 2111 m continuous section of 5.9 Myr upper oceanic crust generated at the Costa Rica Rift in the eastern equatorial Pacific [e.g. Alt *et al.* 1996]. The hole penetrates 274.5 m of sediments, 571.5 m pillow basalts, a 209 m transition zone and 1056 m into a sheeted dyke complex [Alt *et al.* 1985; Alt & Emmerman 1985; Honnorez *et al.* 1985; Alt *et al.* 1986; Alt *et al.* 1996]. In the absence of any comparable drilling operations, Hole 504B has become a reference section for the petrology, geochemistry, hydrothermal alteration, magnetic and physical properties of the oceanic crust to near the base of the sheeted dyke complex [Alt *et al.* 1996]. The proximity to, and nature of the diabase/gabbro transition is not known, and our knowledge of this region is still restricted to analogies drawn with ophiolites [Alt *et al.* 1996].

While the chemical composition of the basalts from Hole 504B is strikingly uniform [Honnorez *et al.* 1985], hydrothermal alteration is highly heterogeneous on all spatial scales [e.g. Alt *et al.* 1996]. A history of crustal alteration has been constructed for Hole 504B on the basis of mineral assemblages and parageneses, summarised in Tables 4.1 and 4.2 [e.g. Honnorez *et al.* 1985; Alt *et al.* 1996]. Hydrothermal activity is inferred to have been initiated close to the axis of the Costa Rica Rift, with overall cooling of the system and multiple fracturing stages as the crust moved away from the ridge and/or during cooling of the magmatic heat source [Honnorez *et al.* 1985]. Initial alteration occurred in an axial discharge zone at temperatures of 250 to 350°C [Honnorez *et al.* 1985]. An overprinting, oxidising alteration occurred at lower temperatures (~150 to 250°C) as the crust moved off-axis into the recharge zone [Alt *et al.* 1996].

The physical properties of the crust sampled by Hole 504B vary with depth and lithology.

Table 4.1: Alteration zones within the Troodos ophiolite and ODP Hole 504B

	Troodos ophiolite, Cyprus					*ODP Hole 504B*		
	Depth[§] *(m)*	*T (degrees C)*	*W/R ratio*	*References:* 1-3	4	*Depth (m)*	*T (degrees C)*	*References:* e.g. 5,6
Volcanics:								
'Open' circulation	0-240	<50	>50	SWZ	CSA	0-320	<100	UPAZ
'Closed' circulation	240-680	<50-100	<5-50	LTZ	TZ & LTA	320-624	<150	LPAZ
Transition zone:	680-800	100-250	<5-50	TZ	HTA I	624-780	250-350	TZDZ
Upper sheeted dykes:	>800	>200	<5-10	UDZ	HTA I	780-1326	>350	TZDZ
Lower sheeted dykes:	-	<440	<1	-	HTA II,III	>1326	400-500	TZDZ

§Depth intervals for the alteration zones are from ICRDG Hole CY1/1A, but vary considerably across the ophiolite complex [Gillis & Robinson 1988]

[1]Gillis & Robinson [1988]; [2]Gillis & Robinson [1990*a*]; [3]Gillis & Robinson [1990*b*]; [4]Bednarz & Schmincke [1990]; [5]Alt *et al*. [1986]; [6]Alt *et al.* [1996]

Key to alteration zones:

SWZ = seafloor weathering zone; LTZ = low temperature zone; TZ = transition zone; UDZ = upper dyke zone

CSA = cold seawater alteration; TZ = transition zone; LTA = low temperature alteration; HTA I, II and III = high temperature alteration types I to III

UPAZ = upper pillow alteration zone; LPAZ = lower pillow alteration zone; TZDZ = transition zone and dyke complex

Table 4.2: Mineralogical and chemical characteristics of hydrothermal alteration zones in the Troodos ophiolite and ODP Hole 504B

A. Troodos ophiolite, Cyprus

	SWZ [1-3], *CSA* [4]	*LTZ* [1-3], *TZ* [4] & *LTA* [4]	*TZ* [1-3], *HTA I* [4]	*UDZ* [1-3]	*HTA II* [4]
Comments:	-Pervasive oxidising alteration -Reddish oxidation halos on pillow margins -Mg-smectite forms in pillow interiors from relatively O-depleted fluids	-Less reaction with host rock -Precipitation of 2° phases in voids -Enhanced Mg-uptake into smectite at <200°C; chlorite at >200°C -the TZ[4] is a zone of Na and K enrichment	-Upper boundary marked by appearance of laumentite and mixed layer chlorite-smectite -Lower bounday marked by development of greenschist facies assemblage (chl-qtz-py-epi)	-Near complete groundmass recrystallisation -Phenocrysts moderately to completely altered	-Pervasive alteration in upper dykes - Plagioclase mainly fresh with increasing depth
1° phases altered:	ol, cpx, 1° sulphides & plag	ol, cpx, 1° sulphides & plag	cpx, plag	cpx, plag, Ti-mag	plag, cpx, Ti-mag
2° phases:	smec, celad, Fe-ox, calc & K-feld	smec, celad	smec, chl-smec & albite	chl, albite, epi, qtz, py, sphene	albite , chl, sphene, actinolite at higher-T
Void-filling:	smec, Fe-ox (calc & palyg)	smec, celad (Na- & Ca-zeo, qtz, calc & palyg)	smec, chl-smec, qtz, py (laum, calc)	chl, epi, qtz, py (calc)	
Chemical changes:	+ K_2O, CO_2, Rb, Ba, Fe^{3+}/Fe^{T} - SiO2, Sr	+ K_2O, Na_2O, Rb, Ba -CaO, SiO_2	+ Na_2O, K_2O, Ba, MnO, Zn, Cu -CaO, Sr, Rb	+Na_2O, MnO, Cu, Zn -CaO, K_2O, Rb, Sr, Ba	+Na_2O, CaO (in lower dykes) -K_2O, Rb, Fe

B. ODP Hole 504B

	UPAZ [5,6]	*LPAZ* [5,6]	*TZDZ* [5,6]
Comments:	-Reddish alteration halos around cracks & veins -Light grey host rocks relatively fresh -Zeolites last phases to form in veins & vugs with rare anhydrite	-Basals are uniformly dark grey in colour -Primary phases more extensively altered than in the UPAZ, but recrystallisation is incomplete - cpx unaltered; anhydrite occurs in veins	-Greenschist and zeolite facies assemblages -Phenocrysts partially to totally altered -Anhydrite occurs in veins and replacing plag in the sheeted dykes
1° phases altered:	ol, plag	ol, plag,	ol, plag, cpx, Ti-mag
2° phases:	Fe-ox, celad, smec, goethite, calc, K-feld	sap, talc, albite, calc, py	chl, chl-smec, py, albite, zeo, chl, ep, calc, act, sphene
Void-filling:	Fe-ox, celad, smec	sap, py, calc, qtz, zeo & rare anhydrite	

[1] Gillis & Robinson [1988]; [2] Gillis & Robinson [1990*a*]; [3] Gillis & Robinson [1990*b*]; [4] Bednarz & Schmincke [1990]; [5] Alt *et al*. [1986]; [6] Alt *et al.* [1996]

Key to alteration zones:

SWZ = seafloor weathering zone; LTZ = low temperature zone; TZ = transition zone; UDZ = upper dyke zone

CSA = cold seawater alteration; TZ = transition zone; LTA = low temperature alteration; HTA I, II and III = high temperature alteration types I to III

UPA = upper pillow alteration zone; LPA = lower pillow alteration zone; TZD = transition zone and dyke complex

Key to minerals:

ol = olivine; cpx = clinopyroxene; plag = plagioiclase; smec = smectite; celad = celadonite; Fe-ox = Fe-oxyhydroxides; calc = calcite; palyg = palygorkite; feld = feldspar; zeo = zeolites; qtz = quartz; chl = chlorite; chl-smec = mixed layer chlorite-smectite; py = pyrite, laum = laumentite; mag = magnetite, epi = epidote; act = actinolite

void-filling phases in parentheses were the last phases to form

The porosity and permeability are highest in the uppermost volcanics, which contain abundant open fractures in which seawater circulated at low temperatures as the crust moved off-axis [Becker *et al.* 1989]. The porosity decreases into the lower volcanics, because during axial alteration fractures in the lower volcanics were sealed by secondary minerals such as smectite [Pezard 1990]. The porosity decreases dramatically by around an order of magnitude into the sheeted dykes [Becker *et al.* 1989]. This profile is similar to that estimated from measurements of the veins in the Semail ophiolite, Oman [Nehlig & Juteau 1988].

Measured heat flow for 504B crust falls close to the theoretical conductive cooling curve for ocean crust, indicating that the 274.5 m of sediment cover has created an impermeable seal between the oceanic basement and seawater [Honnorez *et al.* 1985]. This is atypical of 5.9 Myr oceanic lithosphere, as the average 'sealing' age of the oceanic crust is 65 ± 10 Myr [Stein & Stein 1994]. The sediment at 504B is particularly thick for such a young age, because crust formed at the Costa Rica Rift moves through the equatorial high productivity zone [Honnorez *et al.* 1985]. By analogy with Troodos and other drilled sections of *in situ* oceanic crust, sealing of the oceanic basement by a thick sediment cover will restrict the extent of seawater penetration and off-axis alteration of the 504B section.

4.3 Thermal and alteration history of Troodos crustal rocks

Early studies of hydrothermal alteration in the upper ~2 km of the Troodos ophiolite proposed that both the metamorphic grade and pervasiveness of alteration increases regularly with stratigraphic depth in the crust [Gass & Smewing 1973; Smewing *et al.* 1975]. However, later studies showed that thermal gradients in Troodos, like *in situ* oceanic crust, were not linear and that the distribution of alteration zones is controlled by a combination of the rate of sediment accumulation on the oceanic basement, permeability, temperature and patterns of former hydrothermal fluid flow [Gillis & Robinson 1988].

The volcanic section of the Troodos ophiolite is characterised by heterogeneous permeability, due to variations in the lateral distribution of pillows, flows, hyaloclastites and breccias units on scales ranging from 10's to 100's of metres [Gillis & Robinson 1988; Gillis & Robinson 1990*a,b*]. These units are characterised by pervasive low-temperature hydrothermal alteration in zones of hydrothermal recharge, with superimposed patterns of hydrothermal alteration that correlate to focused high-temperature fluid upflow at ancient spreading centres [Gillis & Robinson 1988; Gillis &

Robinson 1990*a,b*; Bednarz & Schmincke 1990]. Massive sulphide bodies accumulated where these fluids vented at the seafloor, and are underlain by intensely altered pipe-like stockworks [e.g. Richards *et al.* 1989]. On the basis of surface mapping, five zones with distinct mineralogies and intensities of alteration have been identified in the extrusive sequence, summarised in Table 4.1 [Gillis & Robinson 1988, Gillis & Robinson 1990*a,b*]. The alteration reflects evolving temperature, permeability and fluid regimes within the crust following accretion at the ridge axis [Gillis & Robinson 1988, Gillis & Robinson 1990*a,b*]. The five alteration zones display a constant stratigraphic relationship, but are laterally discontinuous, and the depth of the boundaries between them is variable [Gillis & Robinson 1988, Gillis & Robinson 1990*a,b*].

Examination of ICRDG drill core from holes CY-1, CY-1A (extrusive series) and in the upper parts of hole CY-4 (sheeted dyke complex) led to the identification of 6 alteration zones distinguished by characteristic chemistries and alteration minerals, with inferred temperatures ranging from <20° to >350°C (Table 4.1) [Bednarz and Schmincke 1990]. These alteration zones broadly correlate with those determined by surface mapping of the extrusive sequence [Gillis & Robinson 1988, Gillis & Robinson 1990*a,b*], and with those identified in ODP Hole 504B (Table 4.1) [e.g. Alt & Emmerman 1985; Alt *et al.* 1985; Alt *et al.* 1986; Honnorez *et al.* 1985; Alt *et al.* 1996].

Beneath the extrusive sequence, Troodos sheeted dykes are characterised by variable degrees of alteration, and often show regression to lower temperature assemblages [Bickle & Teagle 1992]. The metamorphism of the dykes is the product of heat derived from underlying plutons, and alteration by small volumes of water derived from a more copious circulation through the overlying lava pile [Baragar *et al.* 1990]. Consistent with measurements in Hole 504B, the sheeted dykes in ophiolites are less permeable than the lavas, and fluid circulation through them is inferred to be dominantly dyke-parallel [e.g. Nehlig & Juteau 1988; Gillis & Robinson 1990*a*]. Beneath the sheeted dykes, the upper plutonics show only limited interaction with ~350°C fluids in the high-temperature portion of the hydrothermal system [Bickle & Teagle 1992; Kelley *et al.* 1992; Kelley & Robinson 1990]

4.4 Chemical and mineralogical transformations during crustal alteration

4.4.1 Alteration of the volcanic section

The upper oceanic basement undergoes reactions with large volumes of seawater at a range of temperatures and water/rock ratios, which vary with time and position relative to the spreading axis [Thompson 1983]. The main processes affecting the crust in recharge zones include low-temperature oxidation, low-temperature alkali fixation, Mg-fixation, anhydrite formation, and alkali loss from the crust at higher temperatures [review by Alt 1995]. These processes are illustrated schematically in Figure 4.1.

Studies of ophiolites and drill core show that the upper ~300 m of the volcanic pile is altered by cold (<40°C), oxidising seawater at high water/rock ratios (≥50) [e.g. Alt *et al.* 1985; Gillis & Robinson 1988; Pflumio 1991; Teagle *et al.* 1996]. The main alteration processes operating here are oxidation and alkali fixation [review by Alt 1995]. On Troodos, this alteration characterises the seafloor weathering zone (SWZ) of Gillis & Robinson [1988] and cold seawater alteration (CSA) of Bednarz & Schmincke [1990] (Table 4.1). The chemical and mineralogical changes associated with this alteration in Troodos and Hole 504B are summarised in Table 4.2. These reactions are part of a general circulation in the volcanic section that continues for up to 20 Myr following crustal accretion [Thompson 1983; Staudigel *et al.* 1986; Staudigel & Gillis 1990], consistent with predictions that most of the heat advection occurs on the ridge flanks (section 1.4.2.4) [Morton & Sleep 1985]. The development of this zone in Troodos and *in situ* oceanic crust is well-developed at seafloor topographic highs and absent where the lavas are overlain by impermeable sediments [e.g. Davis *et al.* 1989; Mevel 1985; Teagle *et al.* 1996; Gillis & Robinson 1988]. On Troodos, the oxidative front represented by the base of the SWZ migrates downwards into the volcanic pile during crustal ageing, overprinting earlier, less oxidative alteration occurring in closer proximity to a ridge axis [Gillis & Robinson 1988].

The lower part of the volcanic pile (>300 m) is altered under a more rock-dominated 'restricted' regime as seawater circulation becomes limited by ongoing fracture sealing by secondary clay minerals and/or the deposition of a sedimentary cover [Alt *et al.* 1986]. On Troodos, this alteration is analogous to the low-temperature zone (LTZ) of Gillis & Robinson [1988] and the low-temperature alteration (LTA) of Bednarz & Schmincke [1990]. Seawater in these alteration zones is hotter than in the upper volcanics (~100 to 200°C) and has a more reacted composition (having lost oxygen and alkalis to the upper

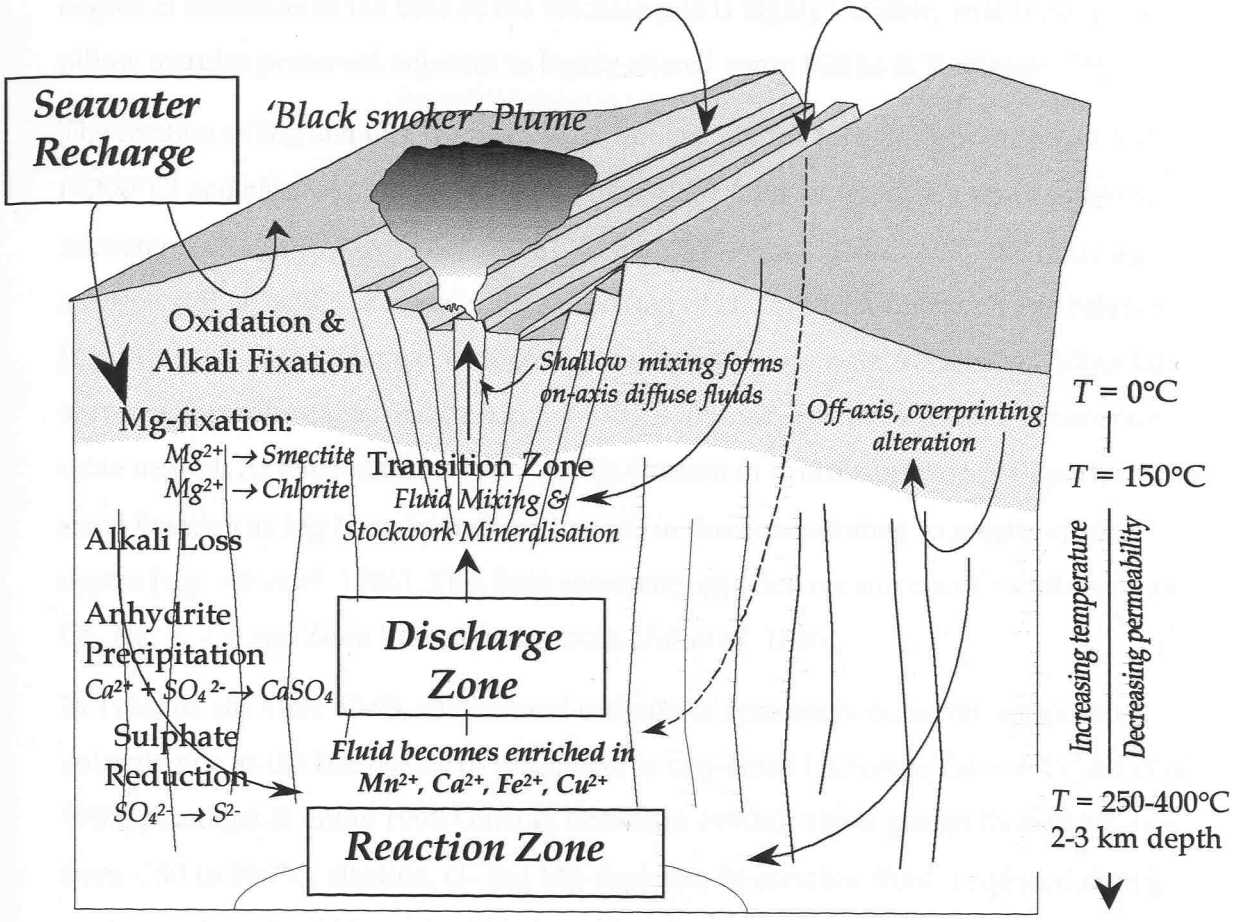

Figure 4.1: A schematic representation of the major chemical processes occurring during hydrothermal circulation. Chemical reactions and fluid compoistions change as seawater is heated and penetrates downwards into the crust at progressively lower water/rock ratios. The upper volcanics are affected by low-temperature alteration at high water/rock ratios; the lower volcanics are altered during a more retricted low-temeprature alteration. The lower sheeted dykes are altered at temperatures >250°C with fluids in partial equilibrium with greenschist facies mineral assemblages. Adated from Alt [1995].

volcanics) which in Troodos and Hole 504B favoured the formation of smectite over Fe-oxyhydroxides in the lower volcanics [Alt *et al.* 1985, Alt *et al.* 1986; Gillis & Robinson 1990*a*]. Consequently, increases in the ratio of ferric to total iron (Fe^{3+}/Fe^{T+} ratio) and alkali uptake is somewhat less than in the uppermost oceanic basement. In Troodos, the degree of alteration in the base of the volcanic pile is highly variable, with fresh glassy pillow margins preserved adjacent to highly altered zones [Gillis & Robinson 1990*a*].

The fixation of Mg and OH^- from seawater into mainly fracture-filling smectite at low (<200°C) and chlorite at higher temperatures (>200°C) is an important process during seawater recharge [e.g. Alt *et al.* 1986]. At high water/rock ratios (> 50) the resulting solution will be acidic because of the generation of H^+ ions to maintain charge balance [e.g. Alt *et al.* 1986]. During 'restricted' alteration at lower water/rock ratios, MgO from seawater is readily exhausted by reaction with wall rock, and the solution pH becomes more neutral. At temperatures > 300° C, Ca-fixation in hydrous silicates will perform the same function as Mg in maintaining a low pH in fluids penetrating to greater crustal depths [e.g. Alt *et al.* 1986]. This fluid represents an effective solvent of metals such as Ca, Na, K, Cu and Zn in lower crustal rocks [Alt *et al.* 1986].

In Troodos and Hole 504B, zeolites and carbonates commonly occur throughout the volcanic pile as the last phases to precipitate in clay-lined fractures (Table 4.2) [Alt *et al.* 1985; Staudigel & Gillis 1990 Gillis & Robinson 1990*a*]. These phases formed off-axis from □50 to 100°C, alkaline, O- and Mg-depleted, Si-enriched fluids produced during oxidative alteration [Alt *et al.* 1985; Staudigel & Gillis 1990; Gillis & Robinson 1990*a*].

4.4.2 Alteration of the sheeted dykes

Only a small (and as yet undefined) proportion of seawater penetrates deep into the oceanic crust to be transformed into a ~350°C black smoker fluid in proximity to an axial heat source [Alt 1995]. The record of alteration minerals in Hole 504B and the Troodos ophiolite defines a steep temperature gradient between the lower volcanics (*c.*100-150°C) and the upper sheeted dykes (*c.*250-350°C) over a few tens of metres [Gillis & Robinson 1990*b*; Alt *et al.* 1986]. Hydrothermal alteration in the sheeted dykes of Hole 504B is controlled by the permeability of the crust [Alt *et al.* 1985]. This alteration is characterised by incomplete recrystallisation to greenschist facies assemblages, with some superimposed lower-temperature off-axis zeolite facies alteration (Table 4.2) [e.g. Alt *et al.* 1986]. In the Troodos ophiolite, this alteration is analogous to the transition zone (TZ)

and upper dyke zone (UDZ) assemblages of Gillis & Robinson [1988], and the high temperature alteration I (HTA I) zone of Bednarz & Schmincke [1990] (Table 3.1). The level of the boundary between the LTA and TZ alteration zones in the Troodos crust varies from <150 m to >1400 m (indicating non-uniform thermal gradients) but generally occurs at a level that reflects the porosity and permeability contrast at the dyke/volcanics transition [Gillis & Robinson 1988].

In Hole 504B, the lower 500 to 600 m of dykes are altered at higher temperatures (>400°C) and are partially recrystallised to amphibolite facies assemblages [Alt *et al.* 1996; Vanko *et al.* 1996]. 504B lower dykes contain Mg-rich amphibole, display large whole rock $\delta^{18}O$ depletions, and are characterised by Zn, Cu and S depletions and the presence of secondary calcic plagioclase and clinopyroxene (rather than Na-rich albite found in the upper dykes). Similar metal losses have been noted in the lower sheeted dyke complex of the Troodos ophiolite [Richardson *et al.* 1987]. This alteration may be analogous to the HTA types II and III of the lower Troodos crust, that are characterised by the presence of amphibole, Ca enrichment and Fe depletion (Table 4.2) [Bednarz & Schmincke 1990].

4.4.3 Reaction zones

The reaction zone is that part of the hydrothermal system where recharge fluids acquire the characteristic chemical signature of black smoker fluids by partial-equilibrium reactions within the lower dykes and uppermost gabbros (refer to section 1.3) [e.g. Bischoff & Dickson 1975; Bowers *et al.* 1985, Bowers *et al.* 1988; Berndt *et al.* 1988, Berndt *et al.* 1989]. The fluids are heated to temperatures of ~350°C to 400°C in the vicinity of an axial heat source and rise rapidly to the seafloor (<1 yr) in a narrow discharge zone (refer to section 1.2) [Kadko *et al.* 1985]. The amount and type of alteration in the reaction zone is dependent on rock texture and mineralogy, water/rock ratio (discussed in section 4.5), fluid chemistry and the physical conditions and duration of alteration [Berndt *et al.* 1989]. Most of the constraints on these parameters come from studies of ophiolites, as *in situ* oceanic crust remains largely unsampled to these stratigraphic depths, although the lower 500-600 m of sheeted dykes in Hole 504B (~1.8 km sub-basement depth) exhibit chemical and mineralogical effects consistent with those attributed to a reaction zone [Alt *et al.* 1996]. The alteration assemblages in the lower dykes on Troodos and in Hole 504B are those predicted for reaction between lower crustal

rocks and fluids with decreased Sr/Ca, Na/Ca and Sr and Mg contents (due to chloritisation and albitisation of plagioclase and the precipitation of anhydrite in the overlying recharge zone) during an early, high-temperature phase of axial alteration (>400°C) [Berndt *et al.* 1988; Berndt *et al.* 1989]. While some experimental models of reaction zone processes have considered albite to be present in the equilibrium assemblage [e.g. Bowers *et al.* 1988, 1989], in Hole 504B albite in the lower dykes occurs as part of a later retrogressive greenschist facies assemblage [Alt *et al.* 1996; Vanko *et al.* 1996].

Upper gabbroic rocks recovered from ODP Hole 735B in the southwest Indian Ocean are also inferred to have been altered in the reaction zone of a hydrothermal system [Mevel & Cannat 1991]. The gabbros display varying degrees of early high-temperature plastic deformation, then brittle deformation associated with seawater penetration along fractures and partial alteration to amphibolite grade mineral assemblages (~500°C), with or without lower-grade retrogressive alteration [Mevel & Cannat 1991]. The upper few hundred metres of the Troodos plutonic section is hydrothermally altered, but passes downwards into less altered and fresh gabbro over a small depth interval [Cann & Strens 1982; Kelley *et al.* 1992; Kelley & Robinson 1990]. Fractures in the upper plutonics host inclusions formed at 200 to 400°C with salinities similar to modern vent fluids [Kelley *et al.* 1992; Kelley & Robinson 1990]. These inclusions are interpreted to reflect the migration of black smoker-like fluids into a crystallising pluton along fine networks of small fractures in a cracking front [Kelley *et al.* 1992; Kelley & Robinson 1990].

4.4.4 Discharge zones

High-temperature (350°C) fluids upwelling from the reaction zone may vent directly at the seafloor, but commonly mix with much larger volumes of cooler seawater within the permeable volcanic pile prior to their discharge at the seafloor [Honnorez *et al.* 1985; Nehlig & Juteau 1988; Richards *et al.* 1989]. Studies of ophiolites and Hole 504B indicate that this mixing commonly occurs at the transition between the sheeted dykes and overlying volcanics, and leads to a stockwork type mineralisation at this level within the crust [Honnorez *et al.* 1985; Nehlig & Juteau 1988; Richards *et al.* 1989]. In Chapter 6 of this dissertation, the REEs are used to evaluate the importance of axial versus off-axis alteration processes in one area of stockwork-mineralised lavas and dykes in the transition zone of the Troodos ophiolite.

Focused high-temperature upflow zones in ophiolites are marked by the development of

epidosites in the lower sections of portions of the sheeted dyke complex [e.g. Richardson *et al.* 1987; Schiffman *et al.* 1987; Schiffman & Smith 1988; Seyfried *et al.* 1988; Schiffman *et al.* 1990]. Epidosites are granular epidote, quartz and titanite assemblages which display no relict igneous textures. They are believed to form by the recrystallisation of greenschist and amphibolite alteration facies assemblages in diabase by ~400°C black smoker-type fluids at water/rock ratios of *c.*20 to 1000 (Table 4.3) [Richardson *et al.* 1987; Schiffman *et al.* 1987; Schiffman & Smith 1988; Seyfried *et al.* 1988; Schiffman *et al.* 1990; Bickle & Teagle 1992]. On Troodos, epidosites form dyke-parallel zones 100's of m wide, that are depleted in Cu, Zn, Rb, Na, K_2 and $\delta^{18}O$ and enriched in Ca, Al, Sr, Fe Fe_2O_3/FeO and H_2O [Richardson *et al.* 1987; Schiffman *et al.* 1987; Schiffman & Smith 1988; Schiffman *et al.* 1990]. Although no Troodos epidosite has been linked unequivocally to a particular ore deposit, calculations indicated that the metal depletions in epidosite zones can account for the formation of a major deposit, and they have been interpreted as the reaction zones of hydrothermal systems [Richardson et al. 1987]. However, experimental models of equilibrium assemblages in ridge crest reaction zones predict a great deal less alteration than is observed in epidosite zones [Berndt *et al.* 1989]. Fluids moving through the epidosite zones are inferred to have last equilibrated with relatively fresh lower dykes/upper gabbros. These fluids were probably not greatly modified (either chemically or isotopically) during their rapid passage through the dykes, although the diabase was completely transformed to a quartz-epidote assemblage [Berndt *et al.* 1988; Berndt *et al.* 1989].

It has been argued epidosites formed by alteration at higher water-rock ratios than non-epidotised dykes altered at the same temperature [Schiffman *et al.* 1987] but the Sr-isotope systematics of Troodos sheeted dykes do not indicate any preferential channelling of fluids in epidosite zones compared with adjacent diabase [Bickle & Teagle 1992; Bickle *et al.* 1998]. Rather, the sheeted dykes were pervasively altered with near equilibrium fluid-rock isotopic exchange [Bickle & Teagle 1992].

The epidosite zones in Troodos are discontinuous with the axis of the Solea graben, and recharge $\delta^{18}O$ and mineral zonations that are parallel to the ophiolite pseudostratigraphy [Schiffman & Smith 1988; Schiffman *et al.* 1987]. This is inferred to indicate a post-spreading, off-axis origin, with epidosite alteration driven by the intrusion of shallow stocks into previously deformed and tectonically thinned crust [Schiffman & Smith 1988; Schiffman *et al.* 1987]. However, other authors have argued for dyke by dyke

Table 4.3: Water/rock ratios in seafloor hydrothermal systems – a compilation of some published values for active vents, the Troodos ophiolite and experimental studies

Examples of:	Geochemical tracer:	Water/rock ratio:	References:
***A.* Seafloor vent sites**			
13°N EPR	Sr-isotopes	5	1
13°N EPR	Alkali elements	1-3	1
21°N	Alkali elements (Li and Rb)	<2	2
21°N	B-isotopes	0.28 to 0.66	3
21°N	Sr-isotopes	1.5	1
***B.* Experimental studies**			
21°N	Sr-isotopes (experimentally-supported reaction pathways)	10	4
-	Mg mass balance (conversion of diabase to chlorite-poor epidosite)	1000	5
***C.* Troodos ophiolite, Cyprus**			
Pillow lavas, dykes & gabbros	Sr-isotopes	15	6
Epidosite zones	Fe and Cu mass balance	20	7
Epidosite zones	Mg mass balance	500	8
Pillow lavas, dykes & gabbros	Sr-isotopes	Time integrated fluid flux of 2.9×10^7 kg m^{-2}	9

[1]Michard *et al.* [1984]; [2]Von Damm *et al.* [1985*a*]; [3]Spivack & Edmond [1987]; [4]Berndt *et al.* [1988]; [5]Seyfried *et al.* [1988]; [6]Spooner *et al.* [1977]; [7]Richardson *et al.* [1987]; [8]Schiffman *et al.* [1990]; [9]Bickle & Teagle [1992]

epidotisation shortly after intrusion at the ridge axis [Cowen & Cann 1988; Penwright pers. comm.].

Epidosites are inferred to extend upwards into zones of argillic alteration (alkali feldspar+quartz+chlorite±pyrite) beneath shallow stockwork feeder zones for sulphide deposits [e.g. Schiffman & Smith 1988; Richards *et al.* 1989; Cann *et al.* 1987; Lydon & Galley 1986]. The stockwork-mineralised zones contain abundant quartz and pyrite, and have distinctive sub-vertical pipe-like alteration facies that crosscut all other alteration zones [Gillis & Robinson 1990*a*]. A detailed appraisal of the REE geochemistry of the secondary minerals that have been used to define these alteration zones is presented in Chapter 6 of this dissertation.

4.5 Water/rock ratios in axial hydrothermal systems

The basis of the concept of the water/rock ratio is that highly soluble elements are leached from the crust during seawater circulation at mid-ocean ridges. If it is assumed that these elements are quantitatively leached from the crust, the concentration originally present in the rock divided by the net addition to the fluid can be expressed as the water/rock ratio [e.g. Von Damm *et al.* 1985*a*]. The concentration of the soluble element entering solution will fall as the rock reacts with greater volumes of fluid. The concept of water/rock ratio has a clear definition in experimental systems, but cannot be so clearly defined for an open system of hydrothermal circulation through ocean crust. At best, the water/rock ratio can be considered to be an integrative measure of how much water has flowed through a volume of rock [Von Damm 1995].

The alkali elements (particularly Li, Cs and Rb) and are the most suitable elements for calculating water/rock ratios, as in laboratory experiments they undergo almost quantitative removal from basalt at elevated temperatures, and undergo only minor secondary reactions [e.g. Bischoff & Dickson 1975]. The water/rock ratio is frequently calculated using oxygen and strontium isotope systematics [e.g. Spooner *et al.* 1997]. In particular, the Sr isotope ratios of altered rocks and fluids are used to provide a measure of the degree of interaction of seawater with the crust, because the $^{87}Sr/^{86}Sr$ ratios of seawater (0.7091) and fresh basalt (~0.7025) are distinct, and there is no temperature- or mineral-dependent isotopic fractionation of Sr. If the solubility of an element is controlled by equilibration reactions, or if it is readily incorporated into high-temperature secondary

phases, the water/rock ratio for that element is artificially raised, and is not a good indicator of fluid fluxes. The measurement of fluid/rock ratio is a species specific determination, and is only significant for those phases which contain the element under consideration. However, comparisons of the water/rock ratios for different elements in the same system can provide insights into processes occurring during sub-surface alteration of the crust [Berndt *et al.* 1989].

In studies of hydrothermal alteration in ophiolites, bulk water/rock ratios integrate a complex history of chemical exchange in channelled and pervasive flow regimes at a variety of temperatures [e.g. Bickle & Teagle 1992]. Similarly, at some active sites the water/rock ratio of the high-temperature axial alteration cannot be constrained. For example, at the MARK site on the MAR, vent fluids have reacted with seafloor-weathered basalts, hence variations in $\delta^{18}O$ relate to both the water/rock ratio of the high-temperature alteration, and the degree of interaction with previously altered crust [e.g. Campbell *et al.* 1988*b*].

Table 4.3 is a compilation of some calculated water/rock ratios for seafloor hydrothermal systems based on studies of vent fluids, altered rocks in ophiolites and experimental studies. Whole-system water/rock ratios are generally <5, indicating that the total extent of subsurface alteration of the oceanic crust is low [e.g. Michard *et al.* 1984; Von Damm *et al.* 1985*a*; Spivack & Edmond 1987; Berndt *et al.* 1988]. The high concentrations of 'soluble' elements such as Li, Rb, Cs and B in black smoker fluids requires a continuing abundance of fresh rock in the reaction zone [review by Von Damm 1995], although geochemical exchange during hydrothermal circulation is predicted to be dominated by reactions at locally higher ratios along the recharge paths of the fluids [Bickle & Teagle 1992].

4.6 Differences in the style of hydrothermal alteration in the Troodos ophiolite and *in situ* oceanic crust

Our knowledge of the deep portions of hydrothermal systems is from the altered rocks of ophiolites. However, some discrepancies exist in the style of alteration of *in situ* oceanic crust and ophiolites, that may reflect important differences between ophiolite-hosted and modern vent systems, related to the tectonic setting of crustal accretion in ophiolites [e.g. Bickle & Teagle 1992; Alt *et al.* 1996].

It is noteworthy that despite the common occurrence of epidosite zones in ophiolites [e.g.

Schiffman *et al.* 1990; Schiffman & Smith 1988; Richardson *et al.* 1987] and experimental predictions of epidote formation at high temperatures in hydrothermal systems [Berndt *et al.* 1988], no epidosite has been recovered from the ocean floor. In Hole 504B reactions in the lower sheeted dyke complex at high temperatures (>400°C) lead to only limited diabase alteration at low water/rock ratios, without any epidosite-like alteration [Vanko *et al.* 1996]. However, Hole 504B is a single section of *in situ* oceanic crust, so this difference may be a sampling artefact.

A further contrast between *in situ* ocean crust and ophiolites is the absence of anhydrite in the ancient setting. ODP drilling of Hole 504B and the active TAG mound has revealed abundant subseafloor anhydrite, consistent with experiments that predict anhydrite precipitation from conductively heated (>150°C) seawater [Bischoff & Dickson 1975; Alt *et al.* 1986; Humphris *et al.* 1995]. The absence of anhydrite in the ancient setting is unlikely to be related to fundamental differences in the style of alteration, but rather to the retrograde solubility of anhydrite at low temperatures [Gillis & Robinson 1990*a*].

A major discrepancy between *in situ* oceanic crust and ophiolites is that is that ophiolitic rocks have reacted with large volumes of seawater and are significantly elevated towards seawater Sr compositions [e.g. Chapman & Spooner 1977; Spooner *et al.* 1977; Bickle & Teagle 1992]. Mid-ocean ridge vent fluids are rock dominated, indicating less fluid reacting with fresh rock in the subsurface of the system [e.g. Michard *et al.* 1984; Campbell *et al.* 1988*b*]. Troodos black smoker fluids would have vented with a $^{87}Sr/^{86}Sr$ ratio elevated significantly above rock values, contrasting with the near MORB-like ratios of active high temperature vents at mid ocean ridges [Bickle & Teagle 1992]. Rather than using the dimensionless water/rock approach, Bickle & Teagle [1992] modelled fluid flow in the upper ~2.5 km of Troodos ocean crust by kinetically limited fluid-solid Sr-isotope exchange. Their calculations generate an inferred time-integrated fluid flux for Troodos of 2.9×10^7 kg m^{-2} [Bickle & Teagle 1992], compared with ~5×10^6 kg m^{-2} from thermal models of hydrothermal circulation at ocean ridges [e.g. Morton & Sleep 1985].

Comparison of the Troodos results (90 Myr crust) with Hole 504B (5.9 Myr crust) can shed light on whether there are important differences between Troodos and seafloor hydrothermal systems. In Hole 504B, the sheeted dykes are heterogeneously altered with $^{87}Sr/^{86}Sr$ ratios only slightly elevated above MORB values, with a trend towards elevated $^{87}Sr/^{86}Sr$ ratios with increasing alteration [Alt *et al.* 1996]. This signature reflects a mixture of secondary phases that record the isotopically heavy composition of the

hydrothermal fluid, and igneous phases that retain their MORB isotopic composition [Alt *et al.* 1996]. The extent of this sub-surface alteration is consistent with the MORB-like $^{87}Sr/^{86}Sr$ composition of modern vent fluids. In contrast, Troodos sheeted dykes are more thoroughly recrystallised [Richardson *et al.* 1987; Schiffman *et al.* 1987; Schiffman *et al.* 1990; Bickle & Teagle 1992]. Epidosite and adjacent diabase have identical $^{87}Sr/^{86}Sr$ ratios, that are strongly elevated towards Cretaceous seawater values, indicating that equilibrium existed between the rock and fluid [Bickle & Teagle 1992]. Sr-isotopic exchange in pore fluids on the flanks of hydrothermal systems is not significant [Hess *et al.* 1991], so it has been inferred that much of the Sr-alteration in Troodos was achieved by fluids that vented at the seafloor [Bickle & Teagle 1992]. The ophiolitic and thermal model fluxes could be reconciled if modern seafloor vents are in an early (high-temperature) phase of their evolution, and Troodos underwent a protracted phase of lower-temperature circulation (perhaps ~75% of the time-integrated fluid flux) during which fluids were no hotter than ~150°C but still capable of Sr-isotopic exchange [Bickle & Teagle 1992]. This circulation would probably carry a dominant fraction of the total geochemical fluxes [Bickle & Teagle 1992]. Alternatively, the structure of hydrothermal systems may be substantially different in supra-subduction zone environments, where underplating or intrusion of magmas is sufficient to drive the hydrothermal circulation for longer within the crust [Bickle *et al.* 1998].

4.7 Summary

There are many similarities between the alteration of *in situ* oceanic crust and ophiolites, although in the modern setting comparisons are mainly limited to ODP Hole 504B, which represents a single 2 km section through the ocean crust to near the base of the sheeted dyke complex. Additionally, the inferred time-integrated hydrothermal circulation for Troodos is ~6 times greater than inferred from thermal models of the ocean ridge circulation [Bickle & Teagle 1992]. This may reflect the maturity of the Troodos alteration profile, which provides a cumulative record of fluid-rock interaction and fluid pathways not available from surface observations of active systems [e.g. Gillis & Robinson 1988; Gillis & Robinson 1990*a,b*; Bickle & Teagle 1992; Bickle et al. 1998]. This is in comparison to active vents, that may be in an early, high-temperature stage of their evolution [Bickle & Teagle 1992].

The studies of *in situ* and ophiolitic ocean crust reviewed in this chapter have contributed

to our understanding of how the thermal and chemical composition of the crust evolves during ageing of the oceanic basement. The thermal and chemical constraints provided by these studies indicate that the chemical fluxes in transient black smoker systems must be small compared with the bulk chemical exchange between the oceanic crust and seawater during off-axis alteration (even if the chemical exchanges during individual reactions are small) [Bickle & Teagle 1992]. In Troodos, these low-temperature crustal ageing processes continued for ~20 My following crustal accretion [Staudigel & Gillis 1990]. In Chapter 6 of this dissertation, the REE compositions of low- and high-temperature secondary minerals in the stockwork-mineralised Pitharokhoma deposit have been used to document the evolution of hydrothermal fluids within the oceanic crust in these contrasting alteration regimes.

Chapter 5

Analytical Methods

5.1 Laboratory Materials

5.1.1 Laboratory Conditions

Inductively coupled plasma mass spectrometry (ICP-MS) and thermal ionisation mass spectrometry (TI-MS) sample preparation was carried out at the Southampton Oceanography Centre (SOC) in a clean laboratory over-pressured with filtered air to minimise airborne contaminants. Sample dissolutions were carried out in closed *Teflon* vessels or *Savillex* vials on a hot plate in a fume cupboard. Sample evaporations were undertaken on a hot plate in a fume cupboard with a scrubber system attached to the air outlet in order to extract acid vapours. All column separations were performed in the clean laboratory.

5.1.2 Reagents

High purity reagents were used throughout the experimental procedures. Laboratory grade water was generated by reverse osmosis then further purified by a *Millipore Milli-Q* mixed-bed de-ioniser. Nitric and hydrochloric acids used in sample dissolution and ion-exchange procedures were prepared by the appropriate dilution of *Aristar* grade reagents with *Milli-Q* water. Hydrofluoric acid used in silicate dissolutions was concentrated *Aristar* grade.

A Tm spike and an in-house 10 x chondrite REE standard solution were prepared by the dilution of 1000 ppm standard solutions (Johnson Matthey and Co. Ltd) for each rare earth element. The stage 1 (clean-up) Nd columns were calibrated using an appropriate dilution of the basalt standard BHVO. The stage 2 Nd columns were calibrated using either a dilute solution of a 100 ppm mixed REE standard (Johnson & Matthey and Co. Ltd), or the REE fraction of basalt standard BCR-1 after pre-concentration of the REE fraction with the stage 1 (clean up) Nd columns. The composition of the in-house 10 x chondrite REE standard is given in Table 5.1. Nd standard JMC 321 was used in Nd-isotope analyses.

	REE concentration in 10 x chondrite standard (ppm)
La	3.15
Ce	8.13
Pr	1.16
Nd	5.97
Sm	1.92
Eu	0.72
Gd	2.59
Tb	0.49
Dy	3.26
Ho	0.73
Er	2.13
Tm	0.23
Yb	2.08
Lu	0.32

Table 5.1: Concentrations of individual REEs in the in-house standard

	Column construction	Ion-exchange resin	Internal diameter (mm)	Resin height (mm)	Resin volume (ml)
Separation:					
REE	Polypropylene	*AG 50W-X8*	3	35	0.25
Nd 1	Polypropylene	*AG 50W-X8*	8	60	3
Nd 2	Pyrex Glass	*Teflon* powder coated with HDEHP	5	70	1.4

Table 5.2: Ion-exchange column specifications

Two types of resin were used in the ion-exchange procedures. For the REE and stage 1 (clean-up) Nd columns Bio-Rad AG-50W-X8 cation-exchange resin (200-400 mesh, capacity 1.7 meq ml^{-1}) was used. For cleaning, the resin was placed on a glass fibre filter paper on a *Teflon* holder fitted onto a glass Buchner funnel. The resin was stored in *Milli-Q* water until use. The resin was cleaned in 25 g batches by cleaning alternately (~15 times) with 50 ml *Milli-Q* and 50 ml 6 M Analar grade HCl.

The material used for the stage 2 Nd separation was a reverse phase cation-exchange resin consisting of a fine *Teflon* powder coated with 10 wt % di-2-ethyl-hexyl-ortho-phosphoric acid (HDEHP). The columns were stored in *Milli-Q* water to prevent resin dehydration.

5.1.3 Apparatus

All laboratory ware in contact with samples was made of polythene, polypropylene, low-density polyethylene (LDPE), high density polyethylene (HDPE), polymethylpentene (PMP) or *Teflon*. *Teflon* vessels were cleaned by soaking for at least 12 hours in hot (~50°C) 10 M *Analar* grade HNO_3 followed by 12 hours in hot (~50°C) *Milli-Q* water. *Savillex* vials used for Nd-isotope analysis were similarly cleaned and stored partially filled with *Aqua Regia* (3:1 concentrated HCl:HNO_3) on a hot plate at 50° C. Sample solutions were stored in HDPE bottles, that were cleaned by repeat rinsing with 6 M HCl followed by *Milli-Q* water. Polythene pastettes used for loading samples onto the stage 2 Nd columns were stored in 0.17 M HCl (the column loading acid) in HDPE bottles.

REE columns were constructed from polypropylene funnels with a 4 cm stem (3 mm internal diameter) fitted with polyethylene frits. Each column contained 0.25 ml of Bio-Rad AG-50W-X8 cation-exchange resin with a bed height of 3.5 cm. Stage 1 (clean-up) Nd columns were constructed from polypropylene funnels, containing 6 ml of the Bio-Rad AG-50W-X8 cation-exchange resin. Stage 2 Nd columns were constructed from *Pyrex* glass. The specifications of the ion-exchange columns used in the REE pre-concentration procedures are detailed in Table 5.2.

5.2 Sample digestions

5.2.1 Metalliferous oxides

Selected areas of basaltic and siliceous samples recovered from the TAG vent field were carefully scraped to remove any metalliferous oxide coating. From these scrapings, 10 mg

samples of pure metalliferous oxide were obtained by picking with the aid of a binocular microscope. These sub-samples were crushed using an agate mortar and pestle. Cleaning of the agate between samples was effected by repeat grinds with *Aristar* grade acid, followed by rinsing with *Milli-Q* water. Samples were oven-dried at 110° C for 12 hours then weighed and transferred to *Teflon* digestion vessels. Complete sample dissolution was achieved with the addition of 3 ml 6 M HCl and a few drops of *Aristar* grade H_2O_2 (to reduce the insoluble Mn^{4+} to soluble Mn^{2+}). Solutions were diluted to a known weight (~10 g) with 6 M HCl and stored in clean HDPE bottles.

5.2.2 Metalliferous sediments, sulphides and altered basalts

Before grinding to powders, samples were trimmed to remove any surface oxidation. Around 200 g of each rock sample was powdered using tungsten carbide-lined *Tema* pots. Mineralised samples were roasted at 600°C prior to digestion to oxidise any sulphide phases present, and the weight loss on roasting recorded for incorporation into a final dilution correction.

Approximately 0.3 g of dried homogenised sample powder was dissolved in closed *Teflon* vessels using a combined hydrofluoric acid/perchloric acid digest technique. Samples were initially left to reflux in a mixture of 3 ml concentrated HF and 5 drops of concentrated perchloric acid for 24 hours at ~150° C. An analytical blank was obtained for each batch of dissolutions by refluxing the analytical reagents in closed Teflon vessels in the absence of any sample material. The *Teflon* vessels were removed from the hot plate, and when cool, the lids carefully loosened to release any gas pressure. If complete dissolution was not achieved, a further 2 ml concentrated HF was added to the mixture, and a corresponding second blank solution prepared. These vessels were closed and returned to the hot plate until complete sample dissolution was achieved. Satisfactorily digested samples and the analytical blanks were evaporated to complete dryness, then taken up in 6 ml 3 M HCl. The closed vessels were then returned to the hotplate. When a true solution was achieved, the solutions and blanks were evaporated to near dryness and diluted to a known weight with 6 M HCl and stored in clean HDPE bottles.

5.3 Rare earth element analysis

The REEs are well suited to determination by ICP-MS, as they lie in an area of the mass spectrum (^{139}La to ^{175}Lu) characterised by minimal interferences (each REE has at least

one isotope free from elemental isobaric overlap) and a high, relatively uniform level of machine sensitivity [review by Jarvis *et al.* 1992]. Interferences that occur during ICP-MS analysis are due to spectroscopic and matrix effects. Of the former, the major problem for the REEs is refractory oxide formation. Barium oxide and hydroxide formation during ICP-MS analysis can produce significant isobaric interferences on some of the LREEs and MREEs, that in particular cannot be easily corrected for Eu [Jarvis *et al.* 1992]. High-precision Eu analyses are important because this element displays anomalous behaviour in seafloor hydrothermal systems (refer to section 2.2). A further spectroscopic interference results from the formation of refractory LREE oxides which can cause serious interferences on the HREEs.

Several measures were taken to compensate for these spectroscopic effects and to minimise matrix interferences. The REEs were separated from their major-ion matrix using a cation exchange chromatographic technique described in section 5.3.1. The separation procedure facilitated the measurement of low (<1 ppb) levels of REEs in Troodos sulphide samples, and REEs in very small (*c.* 10 mg) ferromanganese oxide samples from the TAG vent field, MAR. Additionally, an in-house standard was prepared containing REEs in chondritic proportions, that was broadly similar to the REE composition of the majority of samples under investigation (Table 5.1). This REE standard is inferred to be affected by similar spectroscopic interferences as the sample solutions, resulting from refractory LREE oxide and hydroxide formation in the plasma during analysis. The in-house standard was additionally able to offer a superior calibration of the HREEs (often present in the samples at around an order of magnitude lower concentrations than the LREEs), by ensuring that for each REE, the samples and standards are producing similar levels of counts during analysis.

5.3.1 Ion-exchange separations

The REEs were separated from whole-rock solutions using a modified cation-exchange procedure of Greaves *et al.* [1989] by a single passage through the small (0.25 ml) cation-exchange columns described in section 5.1.3. An initial column calibration was accomplished with a solution containing the radioactive isotopes ^{133}Ba, ^{144}Ce, ^{154}Eu and ^{155}Eu, and ^{137}Cs. To ensure a meaningful calibration the solution also contained Mn and Fe at concentrations comparable to samples. Successive eluate fractions were monitored by gamma-ray spectroscopy. The elution of yellow Fe-chloride complexes from the

columns was self-indicating. A typical elution profile for selected elements is shown in Fig. 5.1. Cerium and Eu were the only REEs monitered in the calibration runs. Barium and Eu showed a consistent separation in repeat calibration runs. By comparison with the data of Greaves *et al.* [1989], this was inferred to represent the effective separation of all the REEs from Ba. The published elution profiles for this separation scheme show that the MREEs (including Eu) and HREEs are eluted first, followed by Ce and La [Greaves *et al.* 1989]. In the column calibration experiment, both Ba and the REEs were eluted with 2M HNO_3. For the sample separations, the REEs were removed with 4M HNO_3, to ensure complete La recovery by minimising any 'tailing' effects. Column recovery was assessed by analyses of solutions spiked with a known quantity (~200 ng) of Tm that were loaded onto cation-exchange columns, and were typically better than 99%.

In a typical sample separation, the columns were cleaned with 5 ml of 6 M HNO_3, washed with 5 ml of *Milli-Q* water, and then conditioned with 3 ml of 1.75M HCl. Aliquots of each 6 M HCl sample solution, the analytical blank prepared during sample dissolution, and various international and in-house standards (section 5.3.3) were evaporated to incipient dryness and loaded onto the resin bed in 200 µl of 1.75 M HCl. Aliquots of sample solutions were taken to give the optimum REE yield without overloading the cation-exchange resin. The aliquot volume of sulphide solutions, that contain low levels of REEs, is limited by the capacity of the cation-exchange resin (1.7 meq ml^{-1}). Aliquots of each blank sample prepared during sample dissolution were also loaded onto the cation-exchange columns. Iron was eluted from the columns with 1.5 ml of 1.75 M HCl. This was followed by the removal of Ba with 3 ml of 2 M HNO_3. The REE were then eluted with 10 ml of 4 M HNO_3. The REE fractions and the dissolution/column blank were evaporated to dryness, then diluted to a known weight with 2% HNO_3 to bring REE concentrations to an optimum level for ICP-MS analysis.

5.3.2 Mass spectrometry

Sample and standard solutions were analysed for REEs using a VG Elemental Plasmaquad PQ2+ ICP-MS at the SOC. Instrument operating parameters are shown in Table 5.3. Operating conditions were adjusted for maximum count stability and machine sensitivity using a multi-element solution containing 0.1 ppb of Be, Co, Y, In, La, Re, Bi and Ba. The ion lens system was optimised on ^{139}La. Calibration of the results was achieved using appropriate dilutions of the in-house chondritic REE standard and a Johnson Matthey and

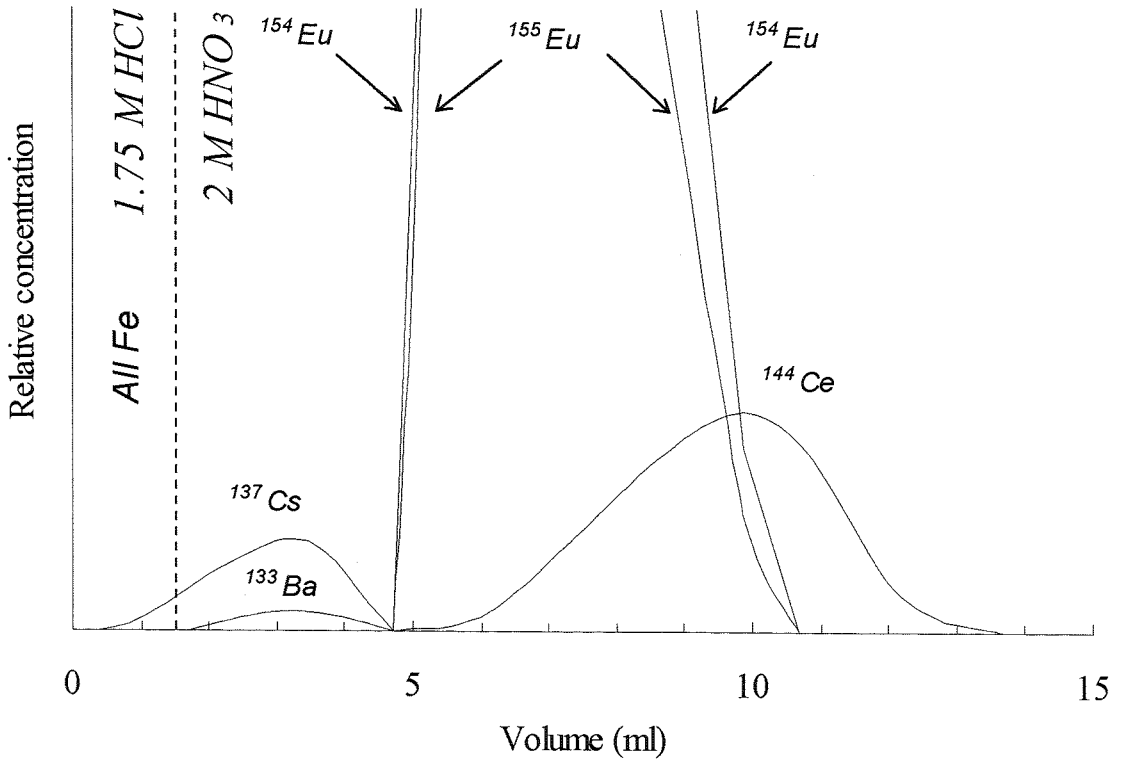

Figure 5.1: Elution curves for a small cation-exchange column loaded with a synthetic sample solution containing radioactive isotopes of Ba, Cs and selected REEs. Modified separation procedure of Greaves *et al.* [1989].

Operating parameter	Set-up
Plasma conditions:	
Forward power	1.35 kW
Reflected power	< 2 W
Gas flow rates:	
Plasma gas	Argon
Coolant gas-flow	14 litre min^{-1}
Auxiliary gas-flow	1.1 litre min^{-1}
Nebuliser gas-flow	1.0 litre min^{-1}
N_2 accessory gas (laser mode)	0.42 ml min^{-1}
Vacuum interface:	
Expansion chamber	2.0 mbar (0.8mbar with extra rotary pump)
Intermediate stage	$<10^{-4}$ mbar
Analyser	3.5×10^{-6} mbar
Sampling cone	Ni, 1.0 mm aperture
Skimmer cone	Ni, 0.7 mm aperture
Sample Introduction:	
Method	Gilson perilstaltic pump
Sample uptake rate	1 ml min^{-1}
Nebuliser type	De Gallen PTFE
Spray chamber	Scott-type, chilled to 0° C
Acquisition parameters:	
Detector type	Galileo Channeltron
Detector mode	Pulse counting
Analysis mode	Peak jumping
No. points per peak	3 (ΔM 0.069 amu)
Uptake	100 s
Acquisition	150 s
Wash time	>120 s
Dwell time per point	10. 24 ms
Time per sweep	0.65 s
Quad settle time	10 m

Table 5.3: ICP-MS instrument operating conditions

Co. Ltd mixed REE solution, both in a 2% HNO_3 matrix. The synthetic solution standards used for each run were chosen so that their concentrations bracketed the range expected in the unknown samples. This procedure effects a correction for any non-linearity in the count rate-concentration relationship.

Standards were run at the beginning and end of each procedure. Data were acquired in peak-jumping mode in 5 runs of 30 seconds for each sample, blank and standard solution. After each analysis, a wash solution containing 2% HNO_3 was run until background levels were achieved (typically after 1-2 minutes). The REE isotopes selected for measurement are given in Table 5.4. Signal drift was monitored by running a 1 ppb REE standard after every fifth sample, and a linear drift correction was applied to the count integrals. The data quality was monitored throughout the run by examination of the statistics produced after each analysis. Within-run precision was typically better than 3% (2σ). Following completion of the run, the raw integrated count per second data was exported from the ICP-MS software in text file format for subsequent manipulation by spreadsheet or other data handling program. An off-line custom written computer program, the "ICP-MS Data Manipulation Program", was used for data processing [A. Milton pers. comm.]. This program applies a drift and a blank correction to the raw data and produces a multi-standard calibration based on the concentration of REEs in the standard solutions.

5.3.3 Accuracy and precision of solution REE data

The accuracy and external precision of the REE data was assessed by the acquisition of ICP-MS REE data for (1) the BHVO-1 international basalt standard (2) an in-house REE standard and (3) a metalliferous core-top from the TAG vent field [Mills 1992]. These samples were subject to the REE separation procedures detailed above each time a batch of samples were analysed. The accuracy of these ICP-MS data was assessed by comparison with (1) recommended [Govindaraju 1996] (2) predicted [R. Boella pers. comm.] and (3) TIMS isotope dilution values obtained at Cambridge University [Mills 1992] respectively.

The REE data obtained for these standards are shown in Tables 5.5, 5.6, and 5.7. This is a relatively small data set, which ideally needs to be augmented with further analyses to build up a long-term evaluation of the precision and accuracy of the analytical techniques described. REE data for basalt standard BHVO-1 were on average accurate to within 4% of published values (Table 5.5). Repeat REE analyses of this solution showed the ICP-MS

Table 5.4 : Isotopes monitered for analysis by ICP-MS

	Masses monitored	% Abundance	Comment
Ba	135	6.59	Low-abundance Ba isotope to monitor isobaric overlaps
La	139	99.9	Most abundant isotope free from isobaric overlap
Ce	140	88.5	Most abundant isotope free from isobaric overlap
Pr	141	100	Mono-isotopic
Nd	146	17.2	Most abundant isotope free from isobaric overlap
Sm	149	13.8	-
Eu	151,153	47.8, 52.2	-
Gd	155,157	14.8, 15.7	Possibility of Ba oxide and oxyhydroxide isobaric overlaps
Tb	159	100	Mono-isotopic
Dy	161	18.9	-
Ho	165	100	Mono-isotopic
Er	166	33.6	Most abundant isotope free from isobaric overlap
Tm	169	100	Mono-isotopic
Yb	173	16.1	Most abundant isotope free from isobaric overlap
Lu	175	97.4	Most abundant isotope free from isobaric overlap

Table 5.5: Precision and accuracy of REE solution data for the international basalt standard BHVO-1

				*Internal Precision			
	‡BHVO-1	1a	1b	Mean	St.dev. (2σ)	RSD (2σ)	Accuracy
	ppb	*column separated REE, ppb*		*ppb*	*ppb*	*%*	*%*
La	14870	15469	14814	15142	926.3	6.1	2.2
Ce	37580	39432	36105	37769	4705	12	4.4
Pr	5030	5380.4	5209	5295	242.5	4.6	5.3
Nd	24240	24871	24407	24639	656.2	2.7	1.6
Sm	5980	5872	5887	5880	20.93	0.36	1.7
Eu	2050	1972	2006	1989	47.66	2.4	3.0
Gd	6020	5981	6174	6078	273.8	4.5	1.6
Tb	944	912.4	939.9	926.1	38.76	4.2	1.9
Dy	5190	5271	5453	5362	256.7	4.8	3.3
Ho	1000	935.9	971.2	953.5	49.81	5.2	4.6
Er	2490	2384	2517	2451	187.5	7.7	2.7
Tm	310	293.7	311.4	302.5	25.06	8.3	2.9
Yb	1900	1661	1868	1765	292.0	17	7.1
Lu	280	219.6	257.5	238.5	53.51	22	15
					Average:	7.3	4.1

‡ BHVO-1 is a basaltic international rock standard; recommended REE concentrations are from Govindaraju [1996]
*The internal precision is a comparison of columns 1a and 1b, that are repeat runs of the REE fraction from a single column separation

Table 5.6: Precision and accuracy of REE solution data for the in-house REE standard.

	¥10 x chondrite standard solution	1	2	3	*External Precision Mean	St.dev. (2σ)	RSD (2σ)	Accuracy
	ppb	*Column separated REE, ppb*			*ppb*	*ppb*	*%*	*%*
La	3151	3248	2978	2827	3018	426.8	14	6.3
Ce	8130.2	7607	7442	7104	7384	512.5	6.94	9.2
Pr	1160.5	1146	1119	1063	1110	84.71	8	4.4
Nd	5971.6	6090	5849	5516	5818	576.6	9.91	3.9
Sm	1919.9	1923	1876	1639	1813	304.9	16.8	5.7
Eu	719.7	699.9	699.8	642.2	680.6	66.63	10	5.4
Gd	2589.9	2544	2460	2150	2384	414.4	17.4	7.9
Tb	490.8	455.4	491.2	443.8	463.4	49.46	11	5.6
Dy	3257.5	3206.9	3211	2907	3108	348.8	11.2	4.6
Ho	729.9	664.9	724.2	646.8	678.6	80.99	12	7.0
Er	2131.1	2098	2137	1904	2046	250.0	12.2	4.2
Tm	299.8	-	300.91	252.4	-	-	-	5.4
Yb	2078.8	2086	2125	1686	1966	485.7	24.7	7.1
Lu	320.8	294.9	335.4	245.1	291.8	90.44	31.0	12.1
						Average:	14	6.3

¥ Predicted REE concentrations [R. Boella pers. comm.]
Dash indicates analyses excluded because solutions were spiked with Tm to assess column recovery
*The external precision is a comparison of columns 1, 2 and 3 (representing three column separations)

Table 5.7: Precision and accuracy of REE solution data for sample AMKG-1895

					External Precision			Internal Precision			
	§AMKG-1891	1a	1b	2	Mean	St.dev. (2σ)	RSD (2σ)	Mean	St.dev. (2σ)	RSD (2σ)	Accuracy
	ppb	*ppb*			*ppb*	*ppb*	*%*	*ppb*	*ppb*	*%*	*%*
La	13300	15564	16245	15320	15442	345.1	2.2	15905	963.1	6.055	18
Ce	16800	16067	16782	15864	15966	287.1	1.8	16425	1011	6.156	3.3
Pr		3219	3551	3171	3195	68.31	2.1	3385	469.2	13.86	
Nd	15900	14875	14898	14706	14791	239.0	1.6	14887	32.53	0.2185	6.8
Sm		2821	2969	2766	2794	77.07	2.8	2895	209.2	7.225	13
Eu	3270	542.2	763.8	509.3	525.8	46.60	8.9	653.0	313.3	47.98	27
Gd	830	3337	3525	3281	3309	79.34	2.4	3431	265.2	7.728	10
Tb	3760	448.0	543.7	444.5	446.3	5.063	1.1	495.9	135.3	27.29	
Dy		2830	3026	2712	2771	167.9	6.1	2928	276.2	9.433	11
Ho	3220	571.2	670.2	564.6	567.9	9.291	1.6	620.7	140.1	22.57	
Er		1526	1759	1472	1499	76.93	5.1	1643	329.9	20.09	12
Tm	1810	39851	39346	40280	40066	606.7	1.5	39599	714.2	1.804	
Yb		1158	1416	1119	1139	55.44	4.9	1287	364.0	28.29	16
Lu	1460	196.9	236.8	191.0	193.9	8.386	4.3	216.8	56.40	26.01	
						Average:	3.3			16	13

§ AMKG-1895 is a metalliferous core-top from the TAG vent field; TIM-ID REE data are from Mills [1992]

analyses to have an average external precision of 7% relative standard deviation (RSD) (2σ). The in-house chondritic REE standard was on average accurate to within 6% of predicted values (Table 5.6). Replicate column separations and ICP-MS REE determinations for this standard showed these results to be on average reproducible at a 14% RSD (2σ) level. REE data for the metalliferous core-top were on average accurate to within 13% of the TIMS-ID data (Table 5.7). Replicate column separations and ICP-MS REE determinations for this standard showed the entire analytical procedure to be on average reproducible at a 3% RSD (2σ) level. The accuracy of the ICP-MS data is expressed graphically in Fig. 5.2. Deviations from a hypothetical 1:1 line average 8 %.

The limit of quantitation (LOQ) can be defined as a concentration equal to 10 times the standard deviation of the background. The blank introduced by the sample dissolution and REE pre-concentration techniques described in this chapter gives a LOQ for the REE solutions between ~0.0005 and 0.013 ppb (Table 5.8). The precision on analyses of REEs at the low levels (<0.02 ppb) present in the procedural blank solutions varied from 1.5 % RSD for Ce to 18 % RSD for Eu (precisions quoted in Table 5.8 are 1σ).

5.3.4 Laser Ablation (LA) ICP-MS

Spatially resolved REE analyses of samples were obtained using a VG Elemental Plasmaquad PQ2+ ICP-MS with Fisons 'S' operation interface coupled to a frequency quadrupoled Nd-YAG UV Q-switched laser probe operating at 266 nm. REE data were acquired over 15 seconds, with 5 seconds pre-ablation, giving REE analyses from 10-20 μm ablation pits.

The general lack of well calibrated, matrix matched standards for use in laser ablation micro-analysis has led to the widespread use of National Institute of Standards and Technology (NIST) glass Standard Reference Materials (SRM). These synthetically manufactured wafers contain a range of trace elements (including the REEs) with nominal concentrations ranging from 0.02 ppm (NIST 616) to 500 ppm (NIST 610). The gas blank level is determined by acquiring data with the laser switched off. This establishes the effective background count-rate that is subtracted from subsequent analyses.

Data were calibrated by comparison with count rates for a synthetically manufactured NIST 612 glass wafer standard reference material (SRM) containing 40 ppm (nominal) of a range of trace elements including the REEs. Differences in the ablation characteristics of the sample and SRM (primarily due to matrix variations) can significantly influence the

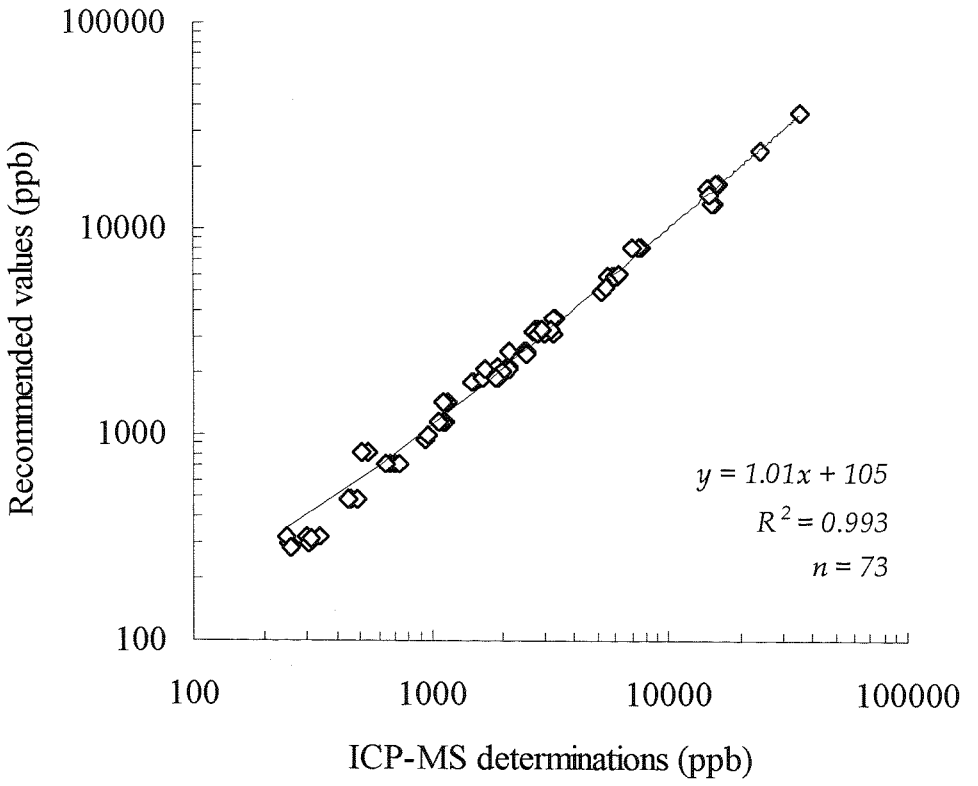

Figure 5.2: Predicted [R. Boella, pers. comm.], recommended [Govindaraju 1996] and TIMS-ID REE concentrations [Mills 1992] compared to REE results for two in-house and an international geological standard, determined by ICP-MS after cation-exchange REE separation.

Table 5.8: Quantitation limits for REEs in solution

§Isotope	1	2	3	4	5	Mean	St.dev. (1σ)	‡LOD	¥LOQ	#1 ppb	‡LOD	¥LOQ	RSD (1σ) (Procedural blank)
	procedural blank raw counts										ppb		%
La	1267	1410	1342	1364	1344	1345	52	155	517	94380	0.0016	0.0055	3.8
Ce	2765	2745	2823	2815	2727	2775	42	127	424	95480	0.0013	0.0044	1.5
Pr	410	472	472	491	448	459	31	93	312	116700	0.0008	0.0027	6.8
Nd	342	380	298	339	328	337	29	88	295	21610	0.0041	0.0136	8.7
Sm	180	147	170	120	175	158	25	75	249	18550	0.0040	0.0134	15.7
Eu	235	139	212	197	209	198	36	108	359	71660	0.0015	0.0050	18.1
Gd	169	140	190	189	179	173	21	62	205	21960	0.0028	0.0093	11.8
Tb	188	194	238	180	208	202	23	68	228	144500	0.0005	0.0016	11.3
Dy	191	176	184	184	168	181	9	26	88	37110	0.0007	0.0024	4.9
Ho	202	173	194	155	211	187	23	68	227	144700	0.0005	0.0016	12.2
Er	212	182	157	163	161	175	23	68	228	49420	0.0014	0.0046	13.0
Tm	197	215	205	199	197	203	8	23	77	147300	0.0002	0.0005	3.8
Yb	173	162	191	191	149	173	18	55	183	49410	0.0011	0.0037	10.6
Lu	185	163	208	208	181	189	19	58	192	141200	0.0004	0.0014	10.2

§Isotopes monitered as shown in Table 5.4
‡LOD is the Limit of Detection (3σ standard deviation on the procudural blank)
¥LOQ is the Limit of Quantitation (10σ standard deviation on the procedural blank)
#1 ppb standard solution made by the appropriate dilution of a Johnson & Matthey & Co. Ltd 100 ppm mixed REE standard

element concentrations determined. An element (or suite of elements) present in the sample and the standard at a known concentration can be used as an internal standard for LA ICP-MS analyses. By comparing the count-rate/concentration ratio for the chosen element in a sample and the SRM, the relative ablation characteristics can be established and a correction factor determined. The most frequently used elements for the internal standardisation of geological materials by LA ICP-MS are Ca, Mg, Al, and Ti, as they can be easily determined by alternative analytical methods. A graphical comparison of solution, LA and Ca-corrected LA ICP-MS REE data for REE in a basaltic glass from the Reykjanes Ridge is given in Fig. 5.3a. The Ca concentration in the basalt glass has been determined by XRF [R. Taylor pers. comm.] and in the NIST SRM by ion probe [Norman *et al.* 1996]. A correction factor can be applied to the basaltic glass REE data through a comparison of the Ca count rate/concentration ratios for the two materials. The data obtained by whole-rock dissolution followed by ion-exchange separation and solution ICP-MS can be regarded as the reference. The chondrite-normalised REE patterns produced by the NIST SRM calibration (with and without the Ca internal standard) represent the average of 10 laser shots, each producing a crater approximately 15μm in diameter (Fig. 5.3b). Although the accuracy and precision of the LA ICP-MS REE data is poorer than the whole-rock solution data, the inter-element ratios are similar; Yb_n/Nd_n = 1.70 for the uncorrected and Ca-corrected REE profiles, compared with Yb_n/Nd_n = 1.45 for the whole-rock solution data.

LA ICP-MS analyses of samples investigated in this thesis was achieved using broadly the method outlined above. However, an exploratory geochemical survey of the samples by LA ICP-MS revealed significant compositional heterogeneity at the <15 μm level. As no micro-scale compositional data was available for any samples, the LA ICP-MS REE data were calibrated using a NIST 610 SRM without an internal standard. Without internal standardisation of the data set, measured REE concentrations may be subject to an order of magnitude inaccuracy although inter-element ratios will be broadly unaffected (Fig.5.3a). Consequently, the degree of enrichment or depletion of Ce, Eu and the LREEs relative to the HREEs in the chondrite-normalised patterns acquired by LA ICP-MS can be interpreted in an equivalent manner to whole rock REE data. The reproducibility of 10 repeat laser shots for the REEs in a NIST SRM is typically 2-5% (2σ) [A. Milton pers. comm.].

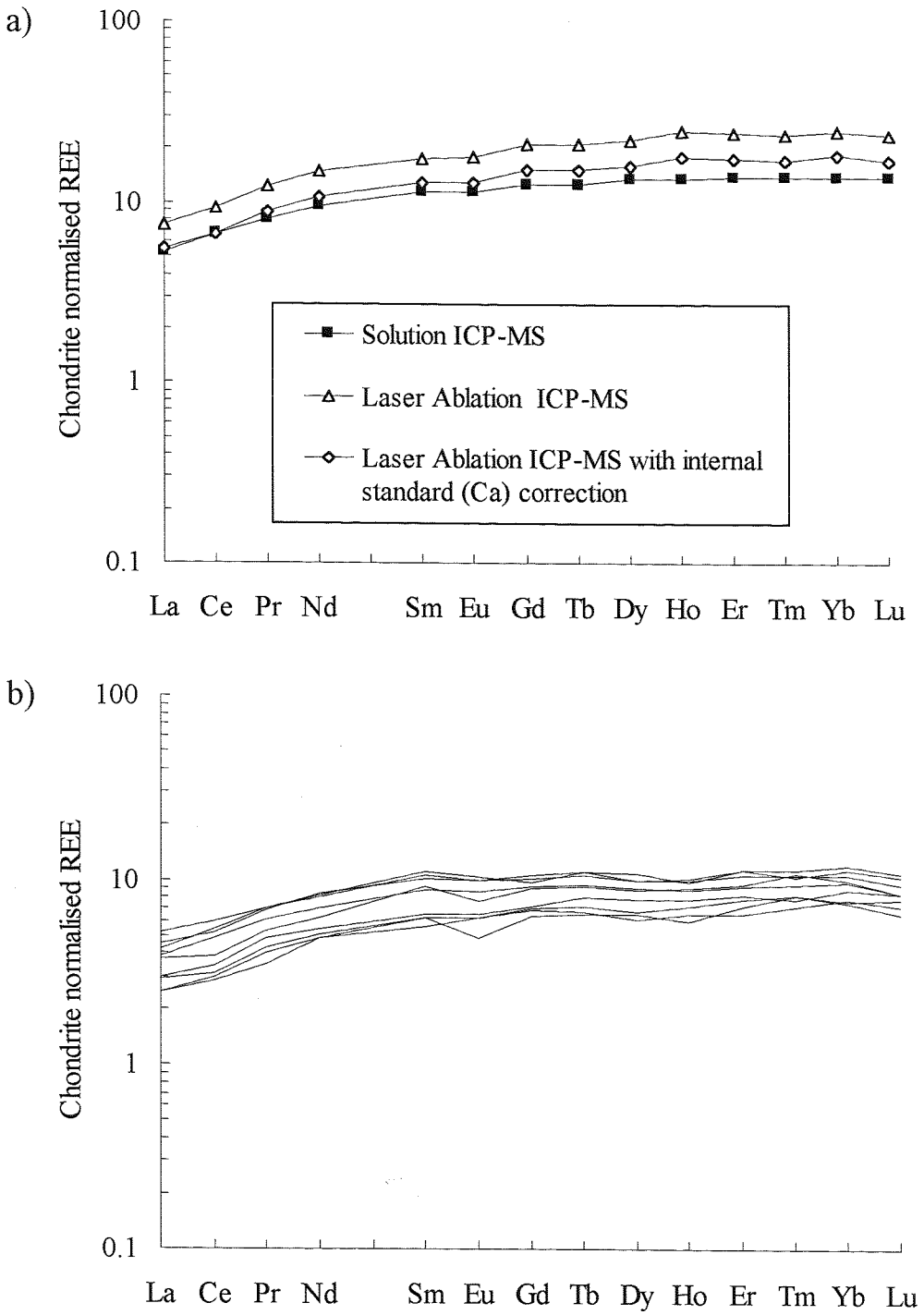

Figure 5.3: (a) Comparison of REE data for a basaltic glass from the Reykjanes Ridge determined by solution and LA ICP-MS. The solution ICP-MS pattern (squares) can be regarded as the reference. LA ICP-MS patterns represent the average of 10 repeat shots calibrated by NIST 612 SRM with (diamonds) and without (triangles) an internal standard (b) 10 repeat laser shots calibrated by NIST 610 SRM. The reproducibility of ten laser shots is typically 2 to 5% (2σ) [A. Milton pers. comm.].

5.4 Neodymium isotope ratio analysis

Aliquots of sample solutions were taken to give between 100 and 1000 ng Nd and evaporated to dryness. Separation of Nd from matrix elements was achieved by passage through stage 1 (clean-up) cation-exchange columns then HDEHP/*Teflon* reverse phase columns. The first column separates the REE from Groups I, II and III elements while the reverse phase column separates Nd from the other REE. In a typical stage 1 separation, columns were conditioned with 5 ml of 2.2 M HCl. Samples were loaded onto columns in 2 ml of 2.2 ml HCl, then washed on with a further 2 ml. Group I, II and III matrix elements were eluted with 24 ml of 2.2 M HCl and discarded. The REE were eluted into *Teflon* beakers with 24 ml of 6 M HNO_3 and evaporated to dryness.

The reverse phase ion-exchange columns were conditioned with 5 ml of 0.17 M HCl. The REE fraction eluted from the stage 1 Nd columns was redissolved in 10 drops of 0.17 M HCl and loaded onto the columns. Samples were washed on with a further 10 drops of 0.17 M HCl. La, Ce and Pr were eluted with 16 ml of 0.17 M HCl. Nd was eluted into *Savillex* vials with 7 ml of 0.17 M HCl. Sm and the HREE that were not separated in the first separation were stripped off the column during cleaning with 5 ml of 6 M HCl.

The Nd fraction was loaded in a few µl of *Milli-Q* water onto the side Ta filament of a Ta-Re triple filament assembly. Nd isotope ratios were determined using a V.G. Isomass 54E mass spectrometer. The Nd isotope ratios were determined as the average of >100 ratios by measuring ion beam intensities in multi-dynamic collection mode. Isotope ratios were normalised to $^{146}Nd/^{144}Nd = 0.7219$ to correct for fractionation occurring during isotope analysis. A filament loaded with Johnson & Matthey Nd standard JMC 321 was prepared to monitor the accuracy and precision of the isotope determinations within each turret of 20 samples. A mean value of $^{143}Nd/^{144}Nd = 0.511121$ ($N = 52$) was obtained for the JMC 321 standard compared with the recommended value of 0.511123 with an external reproducibility of 9 ppm on the isotope ratio during the period of time over which the samples were analysed (Table 5.9). Errors quoted on the isotope ratios are 2σ.

5.5 Major and trace element analysis

A Philips PW1400 fully automatic X-ray fluorescence spectrometer fitted with a 3 kW Rh-anode tube was used for major and trace element analyses. Major elements were determined on fused beads prepared with 10:1 or 20:1 mixtures of *Spectroflux* 100 and

Table 5.9: Reproducibility of Nd standard ¥JMC 321 analyses

From:	21/03/93	16/08/93	18/03/94	13/01/95	17/02/96	13/05/97	
To:	04/05/93	06/09/93	18/04/94	01/03/95	19/03/96	01/08/97	***Overall:***
	time interval						
Mean $^{143}Nd/^{144}Nd$	0.5111251	0.511128	0.511122	0.511124	0.5111341	0.5111213	0.511126
External reproducibility (2s)	0.000013	0.000014	0.000015	0.000019	0.000014	0.000009	0.000018
ppm error on isotope ratios (2s)	13	14	15	19	14	9	18
Number of analyses	21	23	22	31	25	52	174

¥Accepted $^{143}Nd/^{144}Nd = 0.511123$

ignited sample powder. Adsorption and enhancement matrix corrections are applied to all samples using influence coefficients supplied by Phillips. Precision of major element data is 1 to 5% (2σ) for SiO_2, Al_2O_3, Fe_2O3, CaO, K_2O; 5 to 10% (2σ) for TiO_2, MnO, MgO and over 10% (2σ) for Na_2O and P_2O_5 (Table 5.8).

Trace elements were determined on pressed powder pellets bound with an aqueous solution of polyvinyl alcohol. Precision of trace element data is better than 3% (2σ) when concentrations are well above detection limit. A modified Compton scatter technique was employed to correct for matrix effects for all wavelengths (Croudace & Gilligan 1990) resulting in detection limits which range from 4 ppm (Nb, Rb, Sr and Zr) to 60 ppm (Ti).

5.6 X-ray diffraction

X-ray diffraction (XRD) patterns were obtained for some powdered samples using an ENRAF-NONIUS PDS120 system with a position sensitive detector (PSD) at the Natural History Museum, London. An acquisition time of 900 s was used for each sample. Fe-fluorescence background was subtracted from the patterns of Fe-rich samples.

5.7 Transmission electron microscopy

The presence of crystalline phases on a micro-scale within X-ray amorphous samples of the ferromanganese oxide samples was investigated using transmission electron microscopy (TEM) techniques. Selected area electron diffraction patterns were obtained using a JEOL JEM-2000 RX electron microscope in transmission mode operated at 200 kV. One drop of an ultrasonically dispersed suspension of crushed sample was placed on a carbon film supported by a copper mesh TEM grid. This was allowed to air dry, and stored under vacuum until use. Semi-quantitative chemical analyses were obtained using energy dispersive X-ray analysis (EDS) with an acquisition time of 200 s from a spot size of 100 nm or less.

Table 5.10 Precision of XRF major element data

¥ *Rock standard:*	SiO_2	TiO_2	Al_2O_3	Fe_2O_3	MnO	MgO	CaO	Na_2O	K_2O	P_2O_5	Total
BE-N:											
December-97	39.51	2.84	9.74	13.41	0.2	13.95	14.58	2.86	1.54	1.16	100.2
June-97	39.45	2.79	10.48	13.42	0.21	13.99	14.64	2.69	1.58	1.14	100.4
May-97	40.16	2.78	10.53	13.70	0.20	14.20	14.62	2.90	1.55	1.16	101.8
May-97	40.20	2.82	10.56	13.48	0.20	14.04	14.61	2.84	1.56	1.14	105.4
May-97	40.10	2.82	10.61	13.55	0.20	14.18	14.59	2.91	1.56	1.16	105.7
June-97	39.00	2.72	10.41	13.21	0.21	14.19	14.80	3.17	1.50	1.18	103.5
August-97	38.63	2.81	10.40	13.38	0.19	13.41	14.33	2.75	1.59	1.17	101.8
mean	40	2.8	10	13	0.20	14	15	2.9	1.6	1.2	103
RSD (2σ)	**3.1**	**2.8**	**5.7**	**2.3**	**5.3**	**4.0**	**1.9**	**10.6**	**3.7**	**2.6**	
NIM-S:											
June-97	61.91	0.04	16.53	1.51	0	0.59	0.75	0.68	16.35	0.12	100.1
July-97	62.35	0.04	16.49	1.54	0	0.61	0.74	0.56	16.88	0.12	101
July-97	62.65	0.04	16.29	1.52	0	0.67	0.74	0.58	16.62	0.12	100.9
August-97	62.87	0.05	16.09	1.49	0	0.58	0.73	0.78	16.6	0.13	101
July-97	62.62	0.04	16.18	1.53	0	0.64	0.76	0.88	16.64	0.12	101.2
mean	62.48	0.04	16.32	1.52	0	0.62	0.74	0.70	16.62	0.12	100.84
RSD (2σ)	**0.16**	**0.005**	**0.10**	**0.02**	**0**	**0.04**	**0.01**	**0.13**	**0.02**	**0.004**	
GXR-1:											
June-97	49.94	0.06	6.82	37.97	0.13	0.48	1.35	0.6	0.07	0.15	99.2
July-97	50.31	0.07	6.8	37.87	0.13	0.69	1.37	1.24	0.07	0.17	100.4
July-97	50.06	0.08	6.73	37.95	0.13	0.6	1.35	0.49	0.1	0.15	99.2
August-97	50.54	0.07	6.69	37.46	0.12	0.58	1.37	0.89	0.07	0.17	99.6
July-97	49.17	0.07	6.99	37.62	0.13	0.59	1.35	0.60	0.07	0.15	98.3
mean	50.00	0.07	6.81	37.77	0.13	0.59	1.36	0.76	0.08	0.16	99.3
RSD (2σ)	**2.1**	**20**	**3.4**	**1.2**	**6.8**	**25**	**1.7**	**80**	**36**	**15**	
SY-2:											
December-96	60.90	0.15	11.85	6.50	0.33	3.37	8.13	5.62	4.50	0.55	101.9
December-96	60.979	0.147	11.6845	6.512	0.3235	2.6175	8.0015	4.4355	4.5155	0.434	99.7
mean	60.94	0.15	11.77	6.51	0.33	2.99	8.06	5.03	4.51	0.49	100.80
RSD (2σ)	**0.19**	**1.4**	**2.0**	**0.26**	**1.9**	**35**	**2.2**	**33**	**0.47**	**34**	
Mica-Fe:											
December-96	34.358	2.478	19.252	26.43	0.328	5.498	0.446	2.016	8.398	0.532	99.9
December-96	34.74	2.51	18.98	26.27	0.37	4.66	0.43	0.56	8.45	0.40	97.5
mean	34.55	2.49	19.12	26.35	0.35	5.08	0.44	1.29	8.42	0.47	98.70
RSD (2σ)	**1.6**	**1.7**	**2.00**	**0.84**	**16**	**23**	**3.90**	**159**	**0.86**	**38**	
JGb-1:											
May-97	42.41	1.61	16.39	14.77	0.18	7.81	11.62	0.27	0.19	0.03	95.6
May-97	42.31	1.60	16.23	15.10	0.18	7.93	11.69	0.41	0.19	0.04	95.7
May-97	42.41	1.61	16.39	14.86	0.18	7.81	11.62	0.27	0.19	0.03	95.7
May-97	43.20	1.61	16.11	14.92	0.18	7.94	11.58	0.39	0.18	0.04	96.5
June-97	40.83	1.50	16.02	13.97	0.18	7.91	11.37	0.51	0.18	0.05	93.1
mean	*42.23*	*1.58*	*16.23*	*14.72*	*0.18*	*7.88*	*11.57*	*0.37*	*0.19*	*0.04*	95.31
RSD (2σ)	**4.1**	**6.0**	**2.0**	**6.0**	**2.7**	**1.7**	**2.1**	**56**	**7.0**	**42**	

¥ Recommended data are from Govindaraju [1996]:

BE-N is a basalt from an old volcano near Nancy, France
NIM-S is a syenite from the Palabora Igneous Complex
GXR-1 is a jasperoid from the Drum Mountains, Utah, USA
SY-2 is a syenite from eastern Ontario, Canada
Mica-Fe is bioite from a two-mica granite, Massif Central, France
JGb-1 is an augite-hypersthene-hornblende gabbro from Utsushigatake

Chapter 6

REE mobility in a mineralised alteration pipe within the Troodos ophiolite, Cyprus[§]

6.1 Introduction

The significance of hydrothermal circulation on the chemistry of seawater and the oceanic crust is critically dependent on the degree, and nature of axial versus off-axis alteration of the oceanic basement following accretion at the ridge crest [review by Elderfield & Schultz 1996]. The aim of this study is to establish relative REE mobility during axial hydrothermal alteration and subsequent ageing of the oceanic basement in a Troodos stockwork-type massive sulphide deposit. Active ridge crest vent systems may be in an early (high-temperature) stage of evolution in comparison to the mature hydrothermal systems preserved within the Troodos ophiolite as superimposed alteration episodes, that provide a cumulative record of fluid-rock interaction and fluid pathways not available from surface observations of active systems [e.g. Gillis & Robinson 1988; Gillis & Robinson 1990*a,b*; Bickle & Teagle 1992; Bickle *et al.* 1998].

Studies of modern hydrothermal systems have elucidated numerous aspects of the ore-forming processes operating at oceanic spreading centres. Axial hydrothermal alteration of the oceanic crust gives rise to ~350° C black smoker fluids with a REE composition that exhibits little variability between vent fields, and is distinct from either basalt or seawater (Fig. 6.1) [Michard *et al.* 1983; Campbell *et al.* 1988; Klinkhammer *et al.* 1994; Mitra *et al.* 1994]. Seawater is chemically modified during low-temperature reactions with basalt within zones of hydrothermal recharge [Hellman & Henderson, 1977; Humphris *et al.* 1978; Ludden & Thompson 1978, Ludden & Thompson 1979; Juteau *et al.* 1979; Alt *et al.* 1986; Staudigal & Hart 1983; Gillis & Robinson 1990*a,b*; Minai *et al.* 1990; Gillis *et*

[§]WELLS, D. M., MILLS, R. A. & ROBERTS, S. 1998. Rare earth elements mobility in a mineralised alteration pipe within the Troodos ophiolite, Cyprus. *In:* MILLS, R. A & HARRISON, K. (eds) *Modern Ocean Floor Processes and the Geological Record,* Geological Society, London, Special Publication, **148**, 153-176.

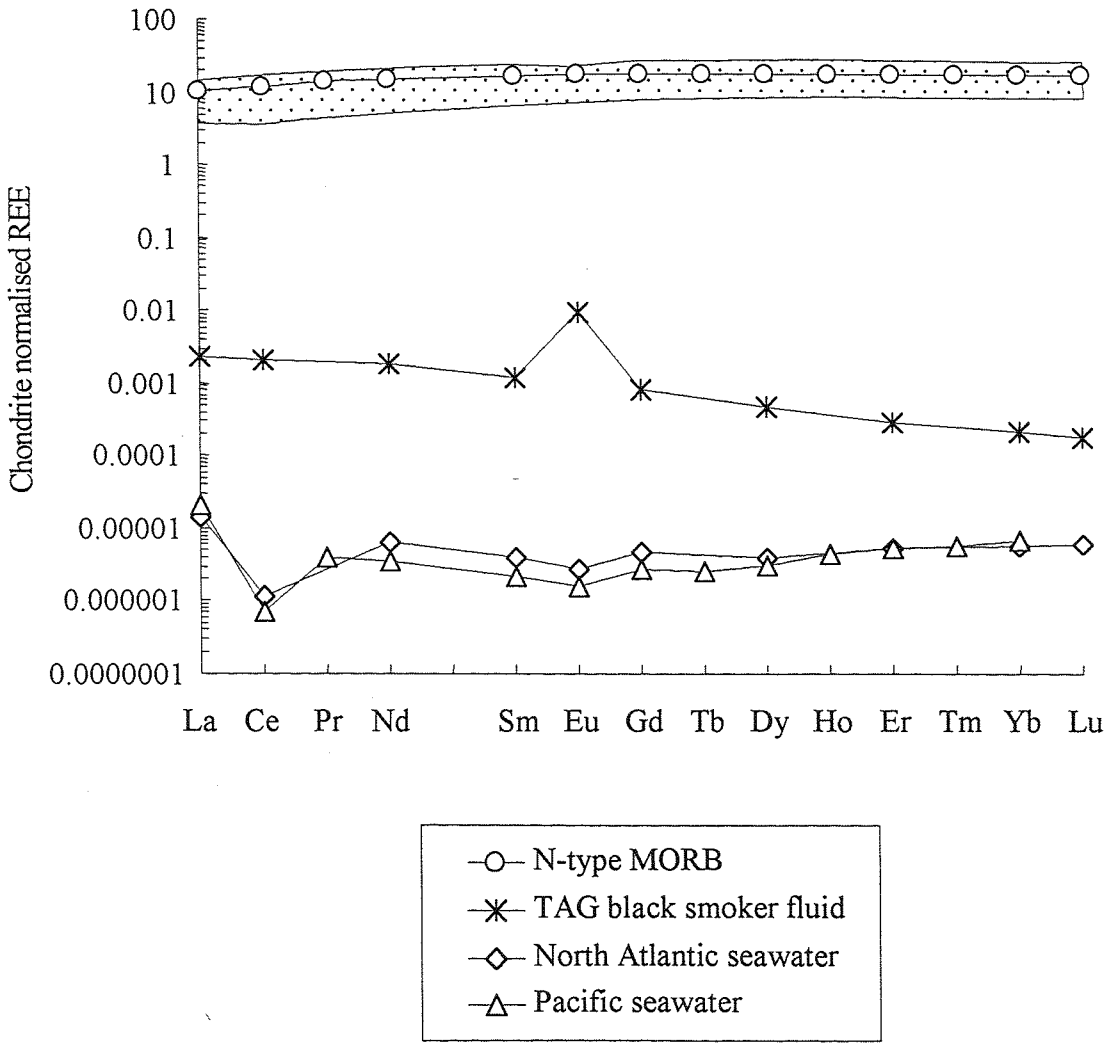

Figure 6.1: Chondrite normalised REE data for N-MORB, North Atlantic and Pacific seawater and a TAG black smoker fluid. Data are from Sun & McDonough [1989], Mitra *et al.* [1994] and Bau *et al.* [1996]. The shaded area shows the range in REE content of Troodos volcanic glasses, which are presumed to be free of the effects of any secondary alteration. Data are from Rautenschlein *et al.* [1985].

al. 1992]. However, experimental and theoretical studies have shown that black smoker fluids acquire their chemical signature at depths of 2 to 3 km within the crust, where plagioclase alteration in a reaction zone above an axial heat source generates fluids in equilibrium with greenschist facies mineral assemblages [Bischoff & Dickson 1975; Bowers *et al.* 1985, 1988; Berndt *et al.* 1988, 1989]. The striking similarities in the chondrite normalised REE patterns of black smoker fluids sampled from contrasting oceanic settings indicate that reactions between heated seawater and basalt exert a primary control on the REE composition of vent fluids [Klinkhammer *et al.* 1994], while complexation in solution may play a significant role in subsequent REE fractionation [e.g. Bau 1991; Haas *et al.* 1995].

The application of REEs to investigations of black smoker fluid-basalt interactions at mid-ocean ridges [e.g. Alt & Emmerman 1985; Gillis *et al.* 1990; Bach *et al.* 1996; Humphris *et al.* 1998] has been limited by infrequent sampling of the lithologies in the interiors of these systems. Therefore, ophiolite-based studies continue to provide important insights into those processes occurring in the sub-surface of active vent systems. The record of high temperature alteration minerals preserved in ophiolites attests to reactions between wall rock and black smoker fluids ascending from the reaction zone, that will modify their REE composition prior to venting [e.g. Regba *et al.* 1991; Gillis *et al.* 1992; Valsami & Cann 1992]. However, patterns of multistage hydrothermal alteration in ophiolites are the product of prolonged (~20 My) ageing of the oceanic basement in addition to axial hydrothermal circulation at ancient ocean ridges [Gillis & Robinson 1988, Gillis & Robinson 1990*a,b*; Staudigel & Gillis 1990; Bednarz & Schmincke 1990]. Consequently, studies of ophiolites have not generally been able to constrain hydrothermal fluid chemistries because they integrate a long history of alteration, which may or may not be dominantly related to axial venting processes. Consequently, in order to document the evolution of hydrothermal fluids within ophiolitic ocean crust, it is necessary to identify and geochemically characterise secondary mineral phases that have precipitated within the contrasting alteration regimes.

This study investigates REE mobility in the host volcanic rocks of a stockwork mineralised alteration pipe within the Troodos ophiolite. The distribution of REEs between high- and low-temperature secondary minerals within the lavas has been investigated by LA ICP-MS. This is an *in situ* technique that offers spatially resolved REE analyses from 10-20 μm ablation pits. Compared with mineral separate analysis, LA ICP-

MS has advantage of facilitating *in situ* REE analyses of often fine-grained and intimately intergrown alteration phases. These REE data have been used to infer fluid compositions and mixing in a hydrothermal upflow zone, and to establish relative REE mobility during axial hydrothermal alteration and subsequent ageing of the oceanic basement.

6.2 Oceanic hydrothermal upflow zones

The results of limited sampling suggest that the alteration of lavas directly beneath seafloor sulphide deposits is characterised by silicification, K-fixation, chloritisation and Mg-fixation [Alt *et al.* 1987; Delaney *et al.* 1987; Saccocia & Gillis 1995]. The oceanic database is presently restricted to hydrothermally altered basalts dredged from upflow zones exposed on fault scarps near oceanic fracture zones on the MAR and EPR [Delaney *et al.* 1987; Saccocia & Gillis 1995], samples from the mineralised transition zone of ODP Hole 504B [Honnorez *et al.* 1985] and the ~2.7 Mt hydrothermally active TAG mound located at 26° N on the Mid-Atlantic Ridge, that was recently drilled by Leg 158 of the Ocean Drilling Program [Humphris *et al.* 1995]. The 'stockwork-type' mineralisation in Hole 504B is typical of alteration observed at the transition between the sheeted dykes and overlying volcanic sequence in ophiolites [Honnorez *et al.* 1998].

6.2.1 Seafloor basalts

Oceanic faulting allows sampling of deeper parts of hydrothermal systems than are exposed at most seafloor vent sites. Samples dredged from the ocean floor comprise Fe- or Mg-rich chlorite-quartz-sulphide breccias [Delaney *et al.* 1987; Saccocia & Gillis 1995] and illitised basalts [Alt *et al.* 1987], indicating reactions with ~150 to 375°C alkali and metal-enriched hydrothermal fluids in near-surface upflow zones.

6.2.2 ODP Hole 504B

Stockwork-like sulphide mineralisation occurs at 910-928 mbsf in the pillow/dyke transition zone of ODP Hole 504B. Basalts in the transition zone are altered to a metal- and sulphur-enriched quartz-chlorite-albite-titanite assemblage. The mineralisation occurs in quartz-sulphide veinlets within the altered basalts [Honnorez *et al.* 1985; Alt *et al.* 1986]. The chlorite is relatively Mg-rich, reflecting incorporation of seawater Mg or preferential partitioning of Fe into pyrite. The greenschist facies alteration minerals are

inferred to have formed in veins and host rocks by reaction with partially reacted seawater circulating through the crust at temperatures of ~200 to 250°C. This alteration is overprinted by a 'stockwork-like' mineralisation where cooling/mixing of the circulating fluids induced the deposition of pyrite, chalcopyrite, sphalerite and rare galena from Mg-depleted, metal, Si and $\delta^{18}O$ enriched fluids at temperatures of ~230 to 340°C [Honnorez *et al.* 1985]. The $^{87}Sr/^{86}Sr$ ratios of the mineralised rocks are elevated towards seawater values, demonstrating the influence of seawater [Honnorez *et al.* 1985]. Fluctuations in fluid temperature and composition resulted in a complex sequence of sulphide mineral deposition [Honnorez *et al.* 1985]. The last alteration stage was zeolite formation in veins and host rocks from Mg-depleted and Ca-enriched fluids at temperatures <200°C [Honnorez *et al.* 1985].

6.2.3 TAG sulphide mound, 26°N MAR

Drilling of the actively forming TAG mound and stockwork deposit has provided important insights into those alteration processes occurring in the shallow sub-surface of a mature oceanic mineralising system [Humphris *et al.* 1995]. The surficial sulphide mound is 30-40 m thick and contains 2.7 Mt of pyrite-, quartz- and anhydrite-rich breccias (Fig. 3.2). A laterally and vertically zoned stockwork, ~100 m in diameter underlies the mound and extends to at least 125 mbsf [Humphris *et al.* 1995; Honnorez *et al.* 1998]. The stockwork does not extend beyond the perimeter of the mound, and to ~100 mbsf comprises silicified wall-rock breccias, which contain basalt clasts totally replaced by quartz, paragonite, pyrite and a Ti-bearing phase, in a matrix of quartz and pyrite. Below, and at the margins of the mineralised zone, the silicified wall-rock breccias grade abruptly into quartz- and pyrite-cemented chloritised basalt breccias [Humphris *et al.* 1995].

A sequence of alteration for the TAG stockwork has been determined by combining data for different samples in the 17 drill holes [Honnorez *et al.* 1998; Humphris *et al.* 1998]. Geochemical and mineralogical variations in altered basalts in different parts of the stockwork are indicative of interaction with hydrothermal fluids containing variable amounts of entrained seawater, reflecting the spatial and temporal evolution of the mineralising system [Honnorez *et al.* 1998; Humphris *et al.* 1998]. The earliest alteration is the chloritisation of the basaltic basement beneath the mound at temperatures of ~250 to 370°C. Chloritisation is pervasive in the deep stockwork underlying the centre of the

mound, to an assemblage of chlorite±quartz±pyrite with elimination of all primary igneous phases except Cr-spinel [Honnorez *et al.* 1998]. Chlorite under the south-east mound margin is Mg-rich and formed *via* reactions with Mg-bearing hydrothermal fluid-heated seawater mixtures, while chlorite under the north-west mound margin and in the deep chloritised stockwork is Mg-poor, and is inferred to have formed from black smoker fluids mixed with small amounts of seawater [Honnorez *et al.* 1998; Teagle *et al.* 1998]. Basalt chloritisation resulted in the uptake of Al, Fe, Mg, H_2O^+, Co, V, Cu, Ni and Zn while Ca, Na and Sr were lost during plagioclase alteration. Changes in Si content are variable in direction and small [Humphris *et al.* 1998].

The early chloritisation was followed by the replacement of basalt and chloritised basalt clasts by paragonite±quartz during reactions with upwelling alkali-enriched hydrothermal fluids. The clay mineral formed during these reactions is a Na-rich mica (paragonite) rather than K-rich mica (sericite/illite) found in the alteration pipes underlying some land-based [Richards *et al.* 1989] and oceanic massive sulphide deposits [Alt *et al.* 1987]. This is due to the high Na/K ratio of the ~360°C black smoker fluids discharging from the mound [Edmonds *et al.* 1996] compared to other black smokers [e.g. Von Damm 1995]. Paragonite is observed to replace both relict primary minerals and clay minerals formed during chloritisation, and additionally precipitated directly from hydrothermal fluids in interstitial spaces within quartz-pyrite breccias. All primary minerals were replaced during this phase of alteration, which resulted in the uptake of Si, Fe, S and small amounts of K, Na, Ba and Zn. Mineralised basalts show gains in Cu and Zn. Basaltic textures and minerals were obliterated through repeated pyritisation and silicification, and the altered basalts are hard to discern from the directly precipitated quartz +pyrite +paragonite assemblage. The last stage of hydrothermal alteration in the TAG stockwork was the precipitation of anhydrite in open spaces in veins and voids [Honnorez *et al.* 1998].

The least altered basement rocks occur at the mound margins, in which chloritisation is restricted to mm- to cm-thick halos which formed at the edges of basalt clasts in contrast to the pervasive chloritisation in the deep stockwork closer to the centre of the upflow zone [Honnorez *et al.* 1998]. At the mound margin, basalt alteration by cold, oxidising seawater results in the partial replacement of olivine by smectite, while all other primary phases are unaltered. In some basalt fragments, the oxidative alteration is manifested as reddish Fe-oxyhydroxides which replace disseminated pyrite in green alteration halos associated with early chloritisation [Honnorez *et al.* 1998].

6.3 Troodos mineralised stockworks & alteration pipes

Since its recognition as a virtually undeformed fragment of Cretaceous oceanic lithosphere [Gass 1968], the Troodos ophiolite complex has been the focus of many important investigations over the last 30 years. Studies of the ophiolite have resulted in models for the generation and tectonic evolution of oceanic lithosphere at oceanic spreading centres [Gass & Smewing 1973; Schmincke *et al.* 1983; Varga & Moores 1985], and the incidence and geometry of axial hydrothermal systems [Spooner & Bray 1977; Spooner *et al.* 1977; Schiffman *et al.* 1987; Schiffman & Smith 1988] associated with the mobilisation [Richardson *et al.* 1987; Schiffman *et al.* 1990] and concentration of metals within sulphide ore bodies [Constantinou & Govett 1973; Constantinou 1980; Adamides 1990]. Further studies have emphasised the ubiquitous low-temperature alteration of the upper oceanic crust that occurs during waning hydrothermalism and crustal ageing [Staudigel *et al.* 1986; Staudigel & Gillis 1990; Gillis & Robinson 1988; Gillis & Robinson 1990*a,b*; Bednarz & Schmincke 1990].

Troodos volcanic-hosted sulphide ore bodies vary in size from ~50,000 tonnes to over 20 Mt, and are among the closest ancient analogues of seafloor sulphide deposits. Many of them are situated on hydrothermally mineralised lavas and are demonstrably exhalative [Constantinou 1980]. Stockwork-mineralised lavas occur at the centre of concentrically zoned alteration pipes beneath these ore bodies, and represent the channels of ascending black smoker fluids [Constantinou & Govett 1973; Constantinou 1980; Lydon & Galley 1986; Cann *et al.* 1987; Richards *et al.* 1989]. The mineralised alteration zones are produced by reaction of hot upwelling hydrothermal solutions with wall rock, often with seawater mixing at the periphery of the upflow zone [Cann *et al.* 1987; Richards *et al.* 1989]. The alteration pipes frequently have outer chloritic zones where rocks are enriched in Mg and Na and have lost Ca, K, Rb and Ba, and illitic or Fe-chlorite mineralised central zones enriched in K, Rb, Ba, Fe, Si and S [Lydon & Galley 1986; Cann *et al.* 1987; Richards *et al.* 1989]. Post-mineralisation alteration of the extrusive sequence of the ophiolite [Staudigel *et al.* 1986; Staudigel & Gillis 1990; Gillis & Robinson 1988, 1990*a,b*; Bednarz & Schmincke 1990] may have caused the retrogressive alteration of hydrothermal sericite to illite or rectorite [Richards *et al.* 1989].

Two types of Troodos alteration pipe have been distinguished on the basis of mineralogical and geochemical characteristics; P (Pitharokhoma) and M (Mathiati) types,

with minor variations in secondary mineralogy attributed to low-temperature overprinting effects [Richards 1987; Richards *et al.* 1989]. The two pipe types have similar chlorite-smectite mixed layer outer alteration zones. Further towards the pipe centre, layer-silicates are dominated by chlorite, and plagioclase is albitised, giving rise to a chlorite-albite-quartz-sphene assemblage. The significant differences between the two types of alteration pipes are in the intensely metasomatised and mineralised pipe centres. In the centres of P-type alteration pipes, the lavas are altered to a Mg chlorite-illite-quartz-pyrite-anatase assemblage. Chlorite tend to decrease towards the pipe centre, and is completely eliminated in the centre of some P-type pipes. The pipe centre is enriched in K, Rb and Ba, and depleted in Mg, Ca, Sr, Na and Al . This type of stockwork alteration is seen underlying the Memi and Kambia deposits, and in an alteration pipe cored by the ICRDG Holes CY-2 and CY-2a [Cann *et al.* 1987]. The M-type alteration pipes at Mathiati, Skouriotissa, Limni, Mousoulos and Kalavasos have outer parts altered to a Mg-chlorite-rectorite-quartz-pyrite-anatase assemblage and central parts altered to Fe-rich chlorite-quartz-pyrite-anatase assemblage. In both pipe types, the chloritic zones are enriched in Mg.

Around the axial alteration zone in both pipe types, Mg-chlorite and sericite were stabilised by vent fluids containing a small proportion of entrained Mg-bearing seawater [Richards *et al.* 1989]. Fluids upwelling in the pipe centres were Mg-deficient by analogy with black smoker fluids, so chlorite in the centre of M-type pipes is Fe-rich [Richards *et al.* 1989]. In P-type alteration pipes, illite was the only aluminosilicate phase stabilised [Richards *et al.* 1989]. The elimination of chlorite to form illite may have initiated pyrite precipitation at Pitharokhoma, by increasing the Fe-activity of the hydrothermal fluid [Richards *et al.* 1989].

Much of the variability in the alteration characteristics of Troodos stockwork deposits [Lydon & Galley 1986; Cann *et al.* 1987; Richards *et al.* 1989] is comparable to that observed in upflow-zone breccias recovered from the Mid-Atlantic Ridge and East Pacific Rise [Delaney *et al.* 1987; Saccocia & Gillis 1995]. This is interpreted to reflect the H_2S content of the ascending hydrothermal fluid, consistent with the measured variability of vent fluids [e.g. Von Damm 1990; 1995]. In P-type alteration pipes the ratio of S to Fe addition is greater than for pyrite addition, which implies mineralising solutions with high S/Fe ratios. In M-type alteration pipes the basalts were altered by solutions with low S/Fe ratios, that stabilised Fe-rich chlorite in the pipe centres [Richards *et al.* 1989].

6.4 The Pitharokhoma alteration pipe

The Pitharokhoma deposit is located on the northern flank of the Troodos ophiolite close to the transition between the sheeted dyke complex and overlying lavas (Fig. 6.2). It is one of many stockwork-type deposits within the ophiolite, some of which are structurally contiguous with exhalative ore bodies formed on the Troodos seafloor [Constantinou & Govett 1973; Constantinou 1980]. The deposit comprises 2.3 Mt of non-cupriferous disseminated pyrite and minor occurrences of massive pyrite, located within two originally vertical pipe-like zones (each ~100 m in diameter) of intense basalt metasomatism [Richards *et al.* 1989]. The altered zones are comparable in lateral extent with the intensely altered and mineralised upflow zone (~80 m in diameter) that underlies the TAG sulphide mound.

Drilling records indicate that the deposit is overlain by less altered and mineralised lavas [Richards *et al.* 1989]. It is inferred that the deposit formed in a zone of mixing between ascending black smoker fluids and relatively unreacted seawater below the contemporaneous seafloor [Jensenius 1984; Richards 1987; Richards *et al.* 1989], as has been proposed for some active vent systems [Corliss *et al.* 1979; Edmond *et al.* 1979*a*] and the mineralised 'stockwork' zone in the Ocean Drilling Program Hole 504B [Honnorez *et al.* 1985]. While Hole 504B is therefore a better modern analogue for the Pitharokhoma deposit than the TAG stockwork (which underlies a sulphide mound), to date the TAG stockwork is the best sampled oceanic upflow zone, due to the drilling of a total of 17 ODP holes through the sulphide deposit and into the underlying basalt basement.

This study builds on previous work that characterised the major and trace element geochemistry and alteration assemblages of the eastern alteration pipe of the Pitharokhoma deposit [Richards 1987; Richards *et al.* 1989]. This alteration pipe is essentially intact, and one of the most completely exposed within the ophiolite. It comprises a sequence of concentrically zoned alteration facies, each defined by a characteristic secondary mineral assemblage with the most intense alteration and mineralisation occurring in the pipe centre (Table 6.1). Mineralisation occurred chiefly by the preferential replacement of interstitial ferromanganoan oxide sediments, with some replacement of lavas in the centre of the pipe [Richards 1987]. During hydrothermal alteration of the lavas, interstitial sediments in the peripheral alteration facies were

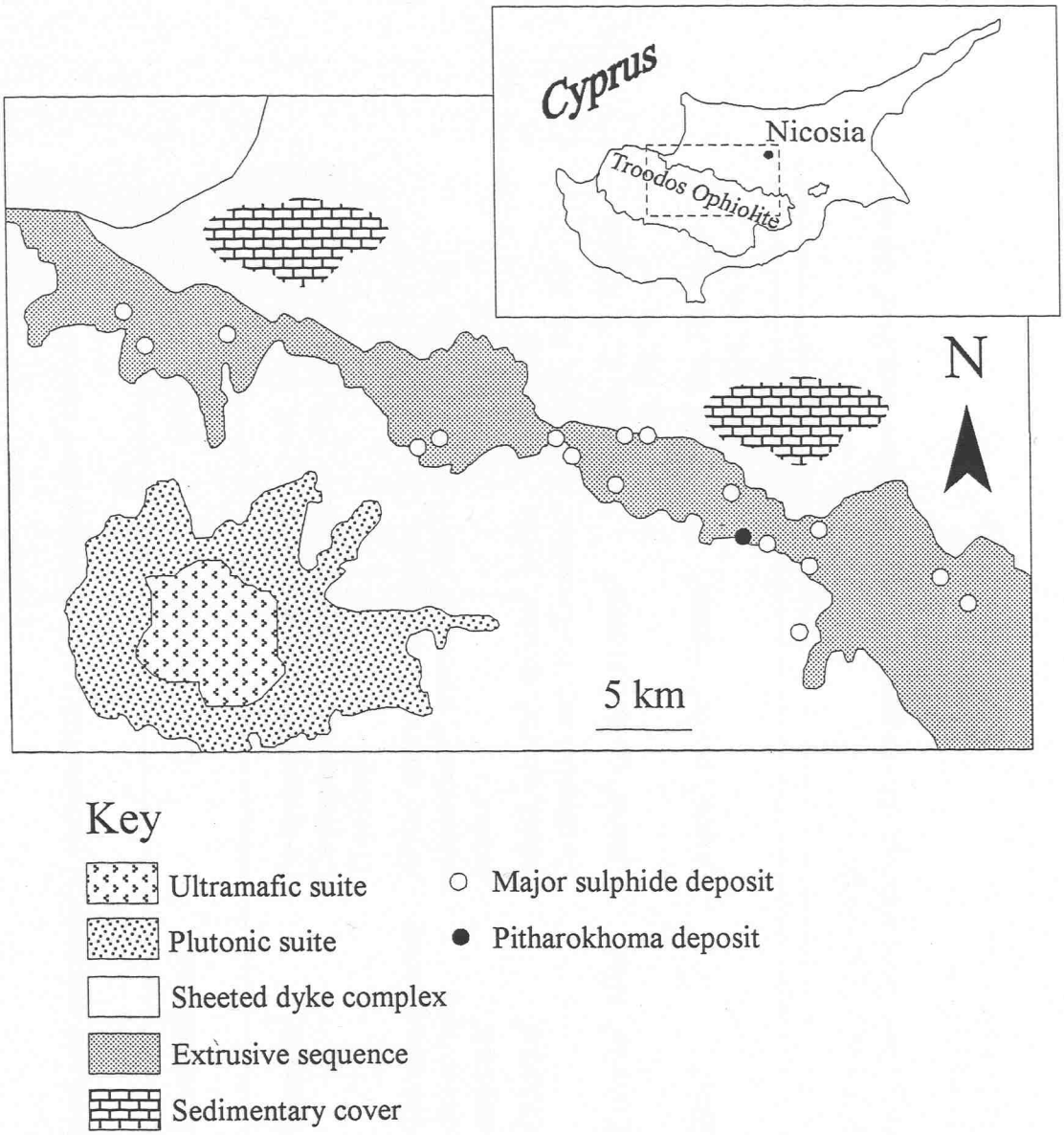

Figure 6.2: Simplified geological map of the northern flank of the Troodos ophiolite complex, showing the location of the Pitharokhoma deposit and other major sulphide deposits. Inset shows location of main figure within the island of Cyprus.

Table 6.1: Mineralogical and geochemical characteristics of lavas within the Pitharokhoma alteration pipe‡

	Layer silicates	Other minerals	Geochemical trends
Smectitic facies:	Smectite§	Fe-hydroxides, quartz, zeolites, Ca plagioclase*, pyroxene*, Fe-Ti oxides*	+K, Na, Rb, Ba¥ -Ca, Si¥
Chlorite-smectite mixed layer facies:	Chlorite-smectite mixed layer minerals§	Albite, quartz, sphene, pyrite, Ca plagioclase*, pyroxene*, Fe-Ti oxides*	+Na, Mg -Ca, K, Rb, Ba
Chlorite-albite facies:	Chlorite§	Albite, quartz§, sphene§, pyrite Ca plagioclase*, Fe-Ti oxides*	+Na, Mg -Ca, K, Rb, Ba
Chlorite-illite facies:	Chlorite§, illite§	Quartz§, pyrite§, anatase§	+Mg, K, S, Rb, Ba -Ca, Na, Sr
Leached facies:	Illite§	Quartz§, pyrite§, anatase§	+K, Ba, Rb, Fe, S -Mg, Ca, Na, Sr

‡Data summarised from Richards *et al.* [1989]
§Phase always present in a given facies (although chlorite may be absent in the pillow margins of chlorite-illite facies lavas)
¥Data from Gillis & Robinson [1988]
*Relict primary phase that may be present

converted to hematitic jasper [Richards *et al.* 1989], that is found associated with all Cyprus ore deposits [Richards & Boyle 1986]. Sulphide mineralogies and textures similar to modern vent sulphides have been described in sulphide scree from the western pipe of the deposit [Jensenius & Oudin 1983].

6.4.1 Wall rock alteration

Lavas at the periphery of the pipe are altered to a smectitic assemblage [Richards *et al.* 1989], which outside localised zones of upwelling is typical of the pervasive low temperature alteration of the extrusive sequence [Gillis & Robinson 1988; Bednarz & Schmincke 1990] and is similar to that reported for *in situ* upper oceanic basement [Alt & Emmermann 1985; Alt *et al.* 1985; Alt *et al.* 1986]. Lavas altered to chlorite-smectite mixed layer, chlorite-albite and chlorite-illite facies assemblages surround Mg depleted, illitised leached facies lavas at the pipe centre (Table 6.1). The leached facies lavas are inferred to have reacted with Mg deficient upwelling hydrothermal fluids [Richards 1987; Richards *et al.* 1989] by analogy with experimental studies [e.g. Bischoff & Dickson 1975] and modern black smoker fluids [e.g. Edmond *et al.* 1979*a*]. Metasomatic Mg enrichments in the chloritised lavas surrounding the pipe centre are attributed to mixing between black smoker fluids and relatively unreacted seawater at the margins of the zone of axial upflow [Richards 1987; Richards *et al.* 1989].

The alteration zones of the pipe produced by axial hydrothermal circulation are heterogeneously overprinted by K-feldspar and calcite attributed to lower-temperature alteration [Richards *et al.* 1989]. Similarly, illite in the pipe centre contains expandable smectite layers and is inferred to have formed from hydrothermal sericite in the waning stages of the ore-forming event, or during post-mineralisation alteration of the lavas [Richards *et al.* 1989].

Subaerial gossanisation due to the circulation of meteoric waters through the mine has degraded the exposure since exploratory mining in 1983. This supergene oxidation is unlikely to have had any significant effect on the REE inventory of the alteration pipe.

6.5 Sampling & Methods

18 samples were collected from across the eastern alteration pipe of the Pitharokhoma mine (Fig. 6.3). The sample set comprises variably altered and mineralised lavas and

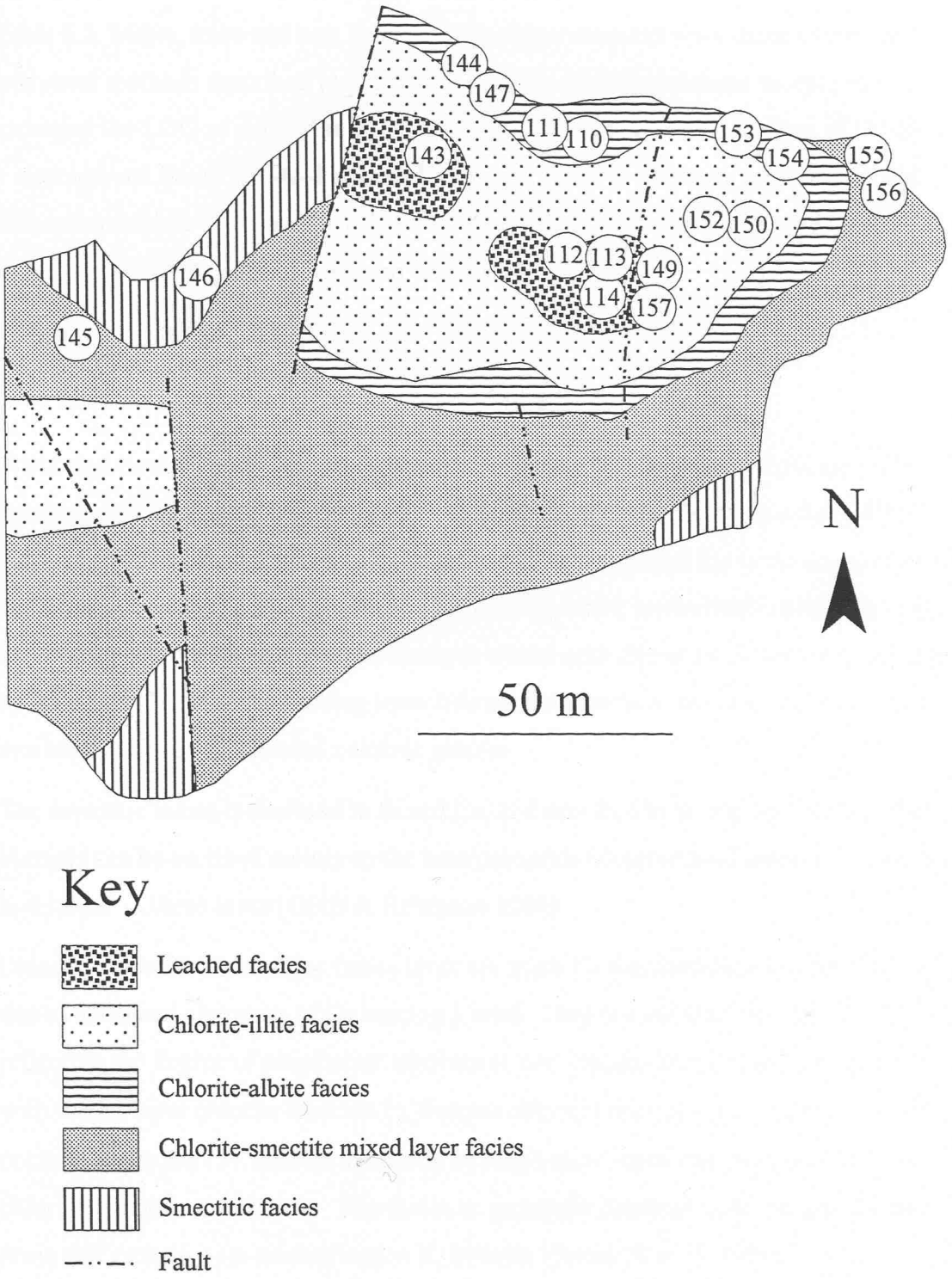

Figure 6.3: Map of the Pitharokhoma open pit with sample locations. Simplified alteration facies are from Richards *et al.* [1989].

dykes, hematised and mineralised interstitial sediments and massive pyrite, described in Table 6.2. Major, trace and rare earth element determinations were made using the analytical methods described in Chapter 5. REEs in all Pitharokhoma sample solutions exceeded the LOQ as defined in 5.3.3. Repeat analyses of the REE fraction of the BHVO-1 international basalt standard obtained using the above procedures were on average accurate to within 4% of published values (Govindaraju 1996) with an external precision averaging 7% (2σ) (refer to 5.3.3 and Table 5.6).

6.6 Results

Major and trace element data are presented in Table 6.3. Geochemical and alteration trends across the eastern pipe are similar to those reported by Richards *et al.* [1989], summarised in Table 6.1. Immobile element ratios indicate that the lavas were originally andesites or basaltic andesites with 60 to 55% SiO_2 and 2 to 6% MgO [Richards 1987; Richards *et al.* 1989]. Metasomatic changes within each alteration facies were calculated by Richards [1987] by comparing immobile element ratios in the altered lavas to those of available analyses of Troodos volcanic glasses.

The smectitic facies is depleted in Si and Ca, and enriched in K, Na, Rb and Ba. These changes can be ascribed mainly to the heterogeneous occurrence of secondary smectite and K-feldspar in these lavas [Gillis & Robinson 1988].

Chlorite-smectite mixed layer facies lavas are more Ca depleted than smectitic facies lavas due to enhanced alteration of Ca bearing phases. They are variably enriched in Na and Mg, reflecting the degree of plagioclase albitisation and replacement of the igneous groundmass with mixed-layer chlorite smectite (± discrete chlorite) respectively. The low Na and Sr content of sample 157 reflects the extent of plagioclase replacement by mixed-layer chlorite smectite and chlorite. This facies is generally depleted in K, Rb and Ba, except in lavas that contain post-mineralisation K-feldspar [Richards *et al.* 1989].

Towards the pipe centre, the enhanced albitisation of plagioclase (chlorite-albite facies) gives way to chlorite-illite facies alteration where albitised plagioclase is progressively replaced by illite and the igneous groundmass by quartz and Mg rich chlorite.

Leached facies lavas in the centre of the alteration pipe are altered to an illite-quartz-pyrite-anatase assemblage. The extent to which fluid flow was focused through the

Table 6.2: Description of Pitharokhoma samples

	Alteration facies‡	Description
Dykes:		
110	Chl-smec mixed layer	Qtz developed in mesostasis; qtz + chl-smec ± chl (cham) in vesicles; Fe-oxide after py
112	Chl-smec mixed layer	Fsp replaced by chl-smec ± chl (cham); sparse py; amorphous Fe-oxide in groundmass
154	Chl-smec mixed layer	Fsp replaced by chl-smec; qtz filled vesicles; disseminated euhedral py with minor sph; igneous texture absent in patches
156	Chl-smec mixed layer	Albitised fsp; mesostasis replaced by chl-smec ± minor chl (cham); sparse py; amorphous Fe-oxide in vesicles and after py
Lavas:		
146	Smectitic	Twinned fsp; fracture filling zeolites (mord + cowl); fibrous smec intergrown with zeolites; occasional cracked py; abundant matrix filling smec + amorphous Fe-oxide
145	Chl-smec mixed layer	Fe-oxide breccia with lava fragments partially replaced by equigranular qtz + chl-smec; sparse py
147	Chl-smec mixed layer	Enlarged vesicles lined with qtz + chl-smec and filled with finer chl-smec ± qtz; occasional twinned fsp partially replaced by chl-smec; amorphous vesicle and matrix-filling Fe-oxide; sparse py
153	Chl-smec mixed layer	Fsp partially replaced by chl-smec; abundant vein and matrix-filling amorphous Fe-oxides; relict igneous texture preserved; py absent
155	Chl-smec mixed layer	Partially altered twinned fsp and cpx; radiating orange/brown matrix and vesicle filling smec; sparse py
157	Chl-smec mixed layer	Amorphous Fe-oxide ± chl-smec ± chl (cham) replacing plag and mesostasis; eroded py with minor sph; qtz + py in vesicles
143	Leached	Relict igneous texture preserved; fsp replaced by ill + qtz; qtz in vesicles and veinlets replaces and is overgrown by py
150	Leached	Abundant qtz + py + fine grained ill; relict igneous texture absent; vesicles contain qtz ± py ± ill
114	Leached	Rare relict igneous texture; abundant py in mesostasis and associated with qtz in veinlets and vesicles; abundant fine grained matrix and vesicle filling ill

‡Alteration facies of Richards *et al.* [1989]
fsp = feldspar; cpx = clinopyroxene; smec = smectite; mord = mordenite; cowl = cowlesite; hem = hematite; chl-smec = chlorite-smectite; chl = chlorite; cham = chamosite; qtz = quartz; ill = illite; ser = sericite; py = pyrite; sph = sphalerite

Table 6.2 (continued): Description of Pitharokhoma samples

	Alteration facies‡	Description
Massive pyrite:		
113	Leached	Massive py
Interstitial sediments:		
111	Chl-smec mixed layer	Hematised jasper with void filling smec
144	Chl-smec mixed layer	Hematised jasper with abundant qtz and colloform textured hem; occasional basalt clasts partially altered to chl-smec
149	Leached	Granular qtz + py + minor ill/ser
152	Leached	Granular qtz + py + minor ill/ser

‡Alteration facies of Richards *et al.* [1989]
fsp = feldspar; cpx = clinopyroxene; smec = smectite; mord = mordenite; cowl = cowlesite; hem = hematite; chl-smec = chlorite-smectite; chl = chlorite; cham = chamosite; qtz = quartz; ill = illite; ser = sericite; py = pyrite; sph = sphalerite

Table 6.3: Major and trace element data for Pitharokhoma samples

	Dykes				*Lavas*									*Massive pyrite*	*Interstitial sediments*			
	110	112	154	156	146	145	147	153	155	157	114	143	150	113	111	144	149	152
SiO_2	55.9	54.1	50.2	51.8	56.8	54.3	50.9	53.2	53.2	52.0	52.8	54.2	46.6	3.88	90.6	83.6	68.6	5.94
TiO_2	1.1	1.2	1.0	1.1	1.2	1.3	1.2	1.3	0.81	1.4	0.59	0.42	0.58	0.01	0.04	0.04	0.02	0.03
Al_2O_3	13.4	13.6	14.3	14.9	14.2	13.2	15.5	18.7	14.9	15.9	5.81	7.18	3.78	0.01	0.82	1.25	0.49	-
Fe_2O_3	11.1	12.1	13.7	12.1	10.1	12.1	13.0	12.7	9.94	10.9	22.5	19.1	27.8	62.9	6.24	12.8	19.3	61.1
MnO	0.13	0.21	0.34	0.23	0.12	0.35	0.15	0.05	0.26	0.31	-	-	-	0.01	0.02	-	-	0.01
MgO	5.6	8.2	7.3	7.3	3.9	5.2	7.5	2.0	8.3	5.5	0.40	0.35	0.16	-	0.26	0.56	0.17	-
CaO	2.83	0.14	2.13	4.36	5.08	2.70	0.76	0.14	2.97	0.10	0.06	0.19	0.12	0.07	0.15	0.11	0.03	0.05
Na_2O	2.1	0.74	4.1	3.0	2.8	2.8	4.6	0.30	3.41	-	-	-	-	-	-	-	-	-
K_2O	0.11	0.71	0.38	0.13	0.79	1.52	0.34	0.42	0.74	0.47	1.39	1.88	0.95	0.02	-	-	0.04	-
P_2O_5	0.11	0.09	0.08	0.10	0.12	0.10	0.10	0.11	0.05	0.03	-	-	-	-	-	0.02	-	-
SO_3	0.64	0.45	0.35	0.23	0.22	0.16	0.30	0.40	0.55	0.94	0.48	0.10	0.26	0.19	0.50	0.09	0.11	0.11
CuO	-	-	-	-	-	-	-	0.21	0.01	0.03	-	-	-	-	-	-	-	-
LOI	3.9	7.6	5.0	3.8	3.3	3.7	4.8	9.5	4.3	11.8	15.3	15	18.8	32.2	1.1	1.1	11.0	32.3
Total	97.0	99.0	98.9	99.0	98.6	97.5	99.2	99.1	99.5	99.4	99.3	98.5	99.1	99.4	99.7	99.7	99.8	99.5
As	-	-	-	-	-	-	-	-	-	-	159	26.9	92.1	208	33.4	15	112	532
Pb	8.9	5	-	-		24.1	6.2	8.9	-	-	19.5		21.5	45.2	6.30	6.70	25.5	78.2
Zn	243	317	2240	343	94.5	237	619	379	98.8	314	142	284	237	3640	28.9	73.5	61.8	1050
Mo	-	-	-	-	-	-	-	-	-	-	9.4	-	5.5	79.7	-	-	22.8	32.4
Sb	-	-	-	-	-	-	-	-	-	-	14.2	-	-	11	-	-	-	18.1
Rb	-	5.5	-	-	8.1	12	-	-	4.4	5.6	16.7	20.5	12.2	-	-	-	-	-
Sr	70.8	12.4	78.2	77.6	120	128	62.9	15.8	84.4	5.1	6.5	7.3	7.7	-	15	9	-	4
Ba	33.5	59	92.1	-	123	239	83.2	33.2	74.1	35.5	554	463	661	91.4	44.5	47.9	65.6	-
V	242	306	390	326	198	236	368	494	267	367	222	236	199	-	92.3	305	33.8	-
Co	66.4	55.5	80.7	75.6	55.3	65	79.3	48.1	64.8	103	140	648	447	334	109	91.2	1330	603
Ga	17.3	16.4	17.1	16.3	17	16.7	16.5	16.9	14.3	16.5	-	5.2	-	-	-	-	-	-
Ni	-	6.5	15	17.7	-	7.4	14.9	8.4	27.1	14	8.8	16	11.8	-	-	9	25	-
Zr	82.9	68.7	45.4	58.3	76.9	71.5	53.3	61.7	34.8	61.6	27.9	18.1	25.6	-	-	-	-	-
Cr	16.6	20.3	23.9	29.4	35.9	-	20.8	29.3	35.6	24.7	17.5	28.3	19.2	-	-	19.3	26.8	-

Major elements are in wt %; Volatiles are determined as loss on ignition (LOI)
Trace element concentrations are in ppm
Dash indicates element not detected

alteration pipe during axial hydrothermal circulation is evident in the magnitude of major and trace element metasomatism of these lavas [Richards *et al.* 1989]. The chemical changes in this facies are due to illitisation at the expense of Mg rich chlorite. The lavas are highly depleted in MgO (up to -3.8 g /100 g) [Richards *et al.* 1989]. The elimination of feldspar results in depletions in Ca, Na and Sr with K, Ba and Rb added through illitisation [Richards *et al.* 1989]. Lava compositions indicate considerable mobility of Al_2O_3 (up to -10.5 g/100 g), V and P. Only Ti, Zr and Y are judged to have been immobile during axial alteration [Richards *et al.* 1989]. Similar trends are noted for leached facies samples analysed in this study. For example, sample 150 has a TiO_2/Al_2O_3 ratio of 0.15, compared with values typically less than 0.1 for most Troodos Ti-rich lavas [Robinson *et al.* 1983].

Whole rock REE data are shown in Table 6.4, with additional REE data for TAG black smoker fluids [Mitra *et al.* 1994], North Atlantic and Pacific seawater [Mitra *et al.* 1994; Bau *et al.* 1996], Troodos smectites [Gillis *et al.* 1992] and Troodos volcanic glasses analysed by Rautenschlein *et al.* [1985]. These glasses are presumed to be free from the effects of secondary alteration, and have a REE composition similar to N-MORB (Fig. 6.1). The Ce anomaly, Eu anomaly, and the fractionation between the LREE and the HREE in the Pitharokhoma samples have been quantified according to the methods outlined in Chapter 2. All ratios are shown in Table 6.4.

6.6.1 Pitharokhoma Dykes

Approximately 20% of the rocks exposed in the pit are dykes. Some of these were probably intruded after the peak of hydrothermal activity, as they are differentially altered with respect to their host lavas [Richards 1987]. The alteration of samples 110, 154 and 156 is equivalent to adjacent lavas, hence their intrusion is inferred to pre-date axial hydrothermal alteration. They are altered to chlorite-smectite mixed layer facies assemblages, but are less albitised and chloritised than the lavas they intrude (e.g. 155) This implies the dykes were less susceptible to hydrothermal alteration than the enclosing lavas. The most altered dyke analysed (112) intrudes illitised lavas at the pipe centre (e.g. 114), but contains secondary chlorite and mixed layer chlorite-smectites rather than illite.

Chondrite normalised whole rock REE patterns for dyke samples are shown in Fig. 6.4. Absolute REE concentrations (5.51-9.10 ppm Nd) are comparable to Troodos glasses (2.43-10.41 ppm Nd). They exhibit LREE depletions and Eu anomalies (La_n/Sm_n = 0.31-

Table 6.4: REE data for Pitharokhoma samples

	La	Ce	Pr	Nd	Sm	Eu	Gd	Tb	Dy	Ho	Er	Tm	Yb	Lu	Ce/Ce*	Eu/Eu*	Eu_n/Sm_n	La_n/Sm_n	Nd_n/Yb_n
	all values ppm																		
Dykes:																			
110	2.93	10	1.64	9.10	3.08	1.03	4.18	0.775	5.32	1.1	3.1	0.439	2.8	0.42	1.1	0.88	0.89	0.60	1.1
112	1.29	5.1	0.996	6.27	2.64	0.920	3.70	0.730	5.24	1.1	3.3	0.490	3.3	0.52	1.0	0.90	0.93	0.31	0.66
154	2.09	6.2	0.987	5.51	1.98	0.888	2.78	0.519	3.63	0.78	2.3	0.320	2.1	0.31	1.0	1.2	1.2	0.66	0.92
156	2.18	7.3	1.20	6.84	2.45	0.948	3.52	0.662	4.72	1.0	2.9	0.426	2.8	0.44	1.1	0.99	1.0	0.56	0.85
Lavas:																			
146	3.08	9.2	1.51	8.45	2.79	1.05	3.90	0.735	5.12	1.0	3.0	0.414	2.6	0.38	1.00	0.97	1.0	0.70	1.1
145	2.52	8.1	1.36	7.66	2.78	1.10	3.75	0.701	4.87	1.0	3.0	0.440	2.9	0.45	1.0	1.0	1.0	0.57	0.91
147	1.92	6.6	1.11	6.42	2.32	0.828	2.98	0.548	3.73	0.79	2.3	0.337	2.2	0.35	1.06	0.96	0.95	0.52	1.00
153	0.387	1.5	0.328	2.13	1.16	0.454	1.54	0.366	2.82	0.60	1.9	0.321	2.5	0.37	0.91	1.0	1.0	0.21	0.30
155	1.50	4.4	0.760	4.24	1.51	0.592	2.09	0.412	2.92	0.62	1.8	0.246	1.6	0.22	0.98	1.0	1.0	0.63	0.95
157	1.28	4.6	0.836	5.22	2.18	0.953	2.86	0.566	4.02	0.85	2.5	0.379	2.6	0.41	1.0	1.2	1.2	0.37	0.71
143	0.428	1.1	0.219	1.27	0.534	0.143	0.928	0.196	1.41	0.31	0.94	0.141	0.91	0.14	0.80	0.62	0.71	0.50	0.49
150	1.21	3.0	0.515	2.56	0.754	0.186	1.23	0.267	1.88	0.40	1.2	0.159	0.97	0.14	0.91	0.59	0.65	1.0	0.92
114	0.952	2.3	0.422	2.29	0.892	0.214	1.47	0.295	2.06	0.46	1.4	0.204	1.4	0.22	0.88	0.57	0.64	0.67	0.59
Massive pyrite:																			
113	0.0523	0.12	0.0189	0.0836	0.0158	0.00311	0.0246	0.00567	0.0375	0.0074	0.020	0.00242	0.014	0.002	0.90	0.48	0.52	2.1	2.1
Interstitial sediments:																			
111	1.81	2.7	0.420	1.97	0.521	0.170	0.697	0.121	0.856	0.20	0.62	0.0912	0.62	0.10	0.66	0.86	0.86	2.2	1.1
144	1.48	2.5	0.497	2.62	0.851	0.316	1.09	0.196	1.34	0.29	0.86	0.123	0.79	0.13	0.66	1.0	0.99	1.1	1.2
149	0.263	0.60	0.0995	0.441	0.0790	0.0167	0.0700	0.011	0.0610	0.011	0.029	0.00419	0.026	0.0038	0.91	0.67	0.56	2.1	6.0
152	0.681	1.5	0.254	1.08	0.185	0.0486	0.143	0.0175	0.0858	0.014	0.034	0.00442	0.024	0.0036	0.93	0.88	0.70	2.3	15
*Black smoker fluid	5.68E-04	1.32E-03		8.68E-04	1.87E-04	5.42E-04	1.70E-04		1.23E-04		4.93E-05		3.60E-05	4.41E-06	0.96	9.1	7.7	1.9	8.4
*North Atlantic Seawater	3.54E-06	7.62E-07		3.09E-06	6.21E-07	1.61E-07	9.83E-07		1.03E-06		9.15E-07		9.38E-07	1.54E-07	0.10	0.63	0.69	3.6	1.1
‡Pacific Seawater	5.13E-06	4.62E-07	3.71E-07	1.68E-06	3.25E-07	8.97E-08	5.65E-07	9.44E-08	7.93E-07	2.52E-07	9.03E-07	1.48E-07	1.12E-06		0.048	0.63	0.73	9.9	0.53
§Troodos glass 345	0.88	2.39		2.43	1.03	0.419	1.63		2.16		1.44		1.44	0.217	0.91	0.98	1.1	0.54	0.59
§Troodos glass 353	3.56	10.94		10.41	3.85	1.35	5.55		6.98		4.68		4.59	0.689	1.0	0.89	0.93	0.58	0.79
¥Smectite CY1:86.1	0.262			0.717	0.288	0.066				0.083	0.384						0.61	0.57	
¥Smectite CY1:437	0.802			1.948	0.777	0.214			1.38	0.389							0.73	0.65	

*Data from Mitra *et al.* [1994]; black smoker fluid data is recalculated to Mg = 0, white smoker is recalculated to Mg = 4 mmol kg^{-1}. Seawater data is for TAG (3400 m)

‡Data from Bau *et al.* [1996]; average of six samples from between 1000 - 2000 m depth

§Data from Rautenschlein *et al.* [1985]; data represent the range in REE content of Troodos volcanic glasses

¥Data from Gillis *et al.* [1992]; data represent the range in REE content of secondary smectite in Troodos lavas

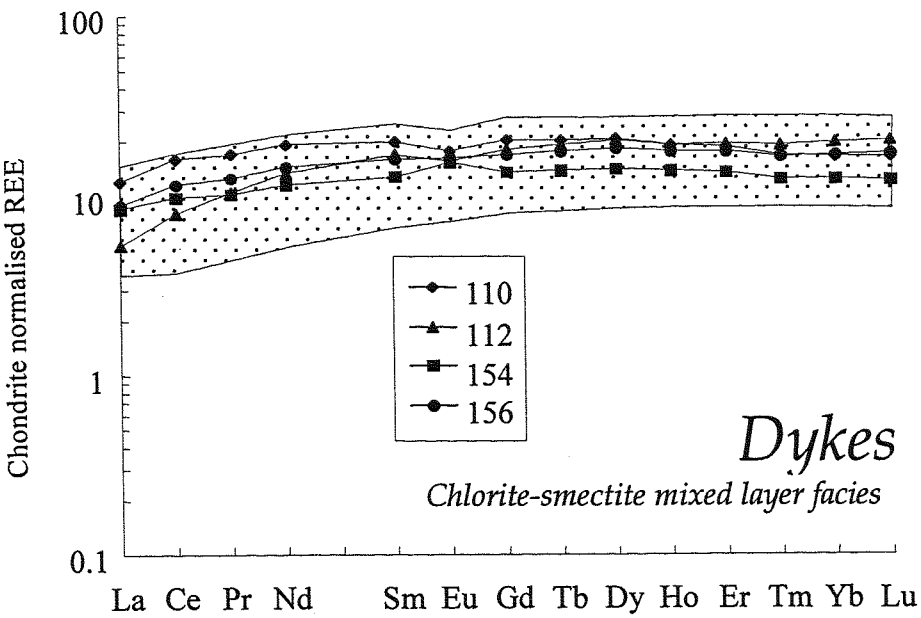

Figure 6.4: Chondrite normalised whole rock REE data for Pitharokhoma dykes. The shaded area shows the range in REE content for Troodos volcanic glasses. Data are from Rautenschlein *et al.* [1985].

0.66; Eu/Eu* = 0.88-1.2) that are slightly smaller or larger than those of Troodos glasses (La_n/Sm_n = 0.54-0.62; Eu/Eu* = 0.89-1.0). Hydrothermal alteration of these lavas has not caused any significant net REE mobilisation. There is no correlation between the degree of LREE depletion and the shape or magnitude of the Eu anomaly.

6.6.2 Pitharokhoma lavas

Smectitic and chlorite-smectite mixed layer facies lavas at the periphery of the alteration pipe (Fig. 6.5a) and leached facies lavas at the pipe centre (Fig. 6.5b) display contrasting REE patterns.

Smectitic and chlorite-smectite mixed layer facies

Chondrite normalised REE patterns for lavas from the smectitic and chlorite-smectite mixed layer alteration facies generally parallel Troodos glasses with some variability in the LREEs (Fig. 6.5a). There is little evidence for net REE mobilisation in smectitic (146) and most of the chlorite-smectite mixed layer facies lavas (145, 147, 155). They have REE concentrations (4.24-8.45 ppm Nd) and ratios (La_n/Sm_n = 0.52-0.63; Eu/Eu* = 0.96-1.0) similar to Troodos glasses (2.43-10.41 ppm Nd; La_n/Sm_n = 0.54-0.62; Eu/Eu* = 0.89-1.0). Two samples from the chlorite-smectite mixed layer facies (153, 157) are more LREE depleted (La_n/Sm_n = 0.21 and 0.37) than Troodos glasses (La_n/Sm_n = 0.54-0.62) indicating a net mobilisation of LREEs during crustal alteration.

The REE content of secondary alteration phases in some of these lavas was determined by LA ICP-MS. The minerals analysed were identified petrographically and/or by XRD analyses. Sample 146 from the periphery of the mine is altered to a smectitic alteration assemblage, that is inferred to post-date axial mineralisation [Richards *et al.* 1989]. Twinned feldspars in this lava are essentially unaltered. Smectite is the principal secondary phase and occurs replacing the mesostasis and intergrown with fracture filling zeolites. LA ICP-MS analyses show void filling smectite to be slightly LREE enriched (La_n/Sm_n = 0.44-0.58) and Eu depleted (Eu_n/Sm_n = 0.52 and 0.55) relative to the whole rock (Fig. 6.5c). Intergrown zeolites (mordenite and cowlesite) which fill vesicles and fractures are LREE enriched compared to the whole rock (La_n/Sm_n = 1.9-3.8 cf. 0.70) and variably Eu depleted (Eu_n/Sm_n = 0.14-0.74 cf. 1.0). Intimately associated smectite and amorphous Fe-oxides which replace much of the igneous groundmass are typically more LREE and Eu depleted (La_n/Sm_n = 0.42-0.72; Eu/Eu* = 0.64-0.84) than the whole rock (La_n/Sm_n = 0.70; Eu/Eu* = 0.97).

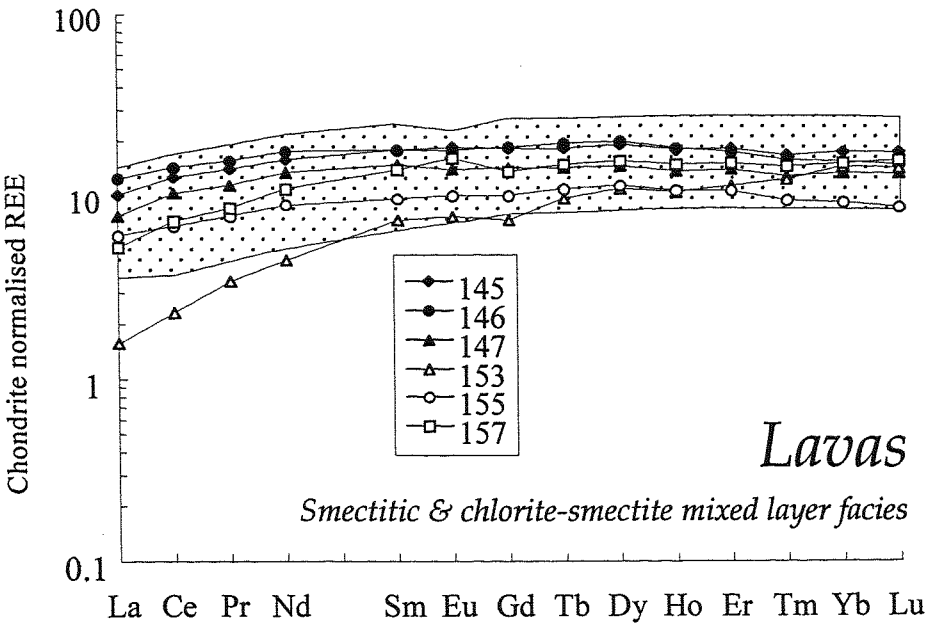

(a)

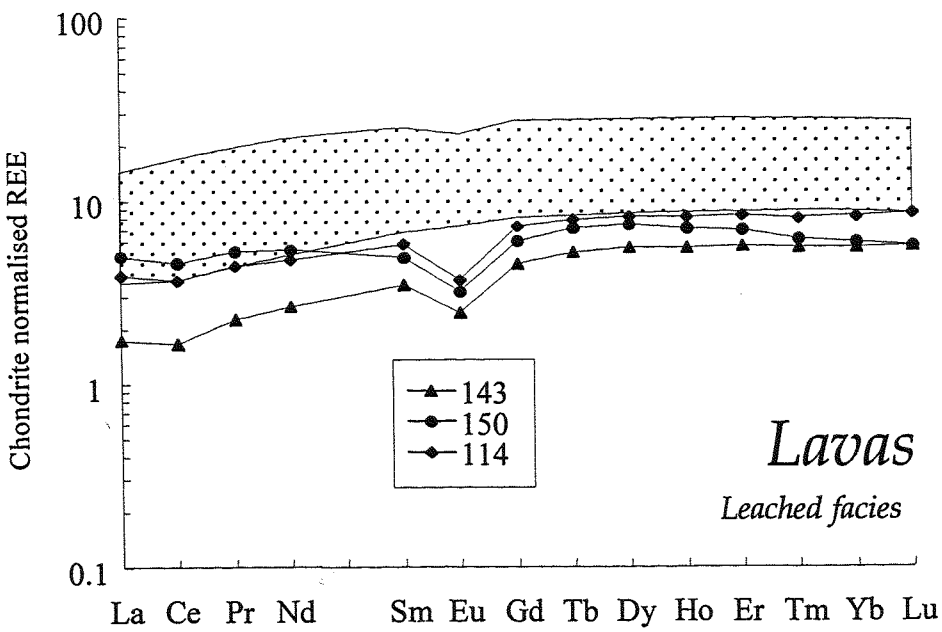

(b)

Figure 6.5 (a) & (b): Chondrite normalised whole rock REE data for (a) Pitharokhoma lavas from the smectitic and chlorite-smectite mixed layer facies (b) Pitharokhoma lavas from the leached facies. The shaded areas in (a) and (b) shows the range in REE content for Troodos volcanic glasses. Data are from Rautenschlein *et al.* [1985].

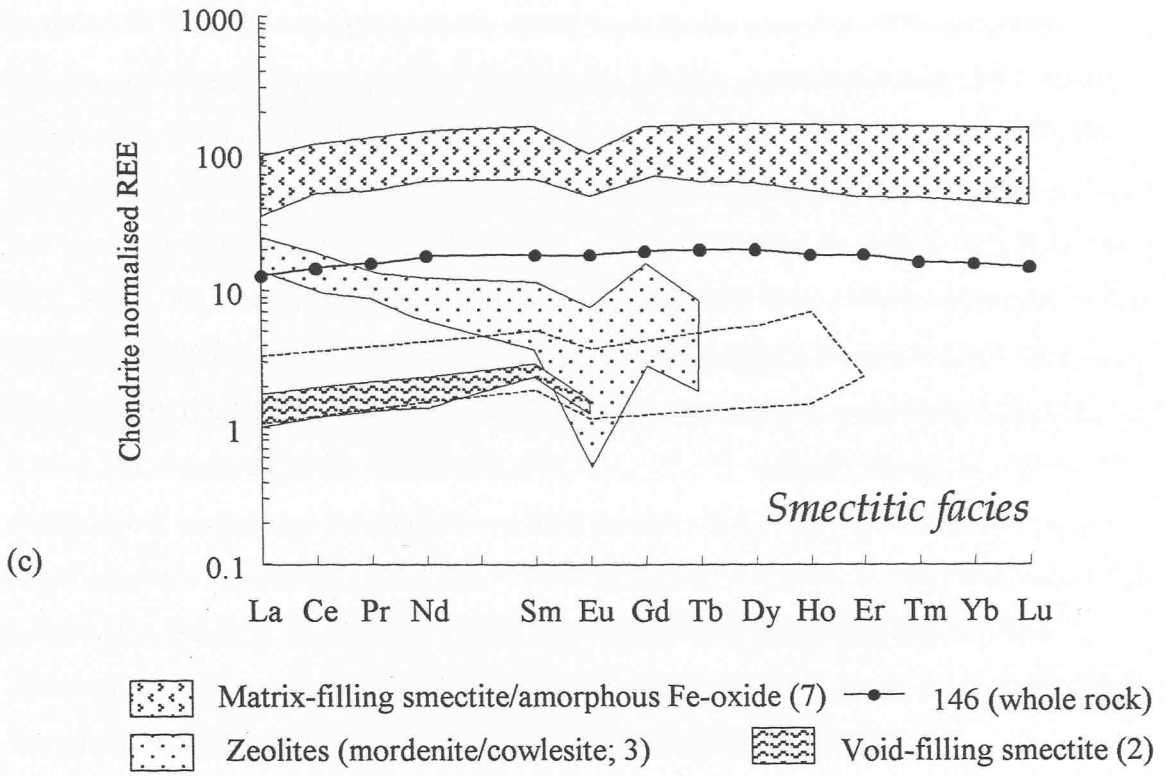

(c)

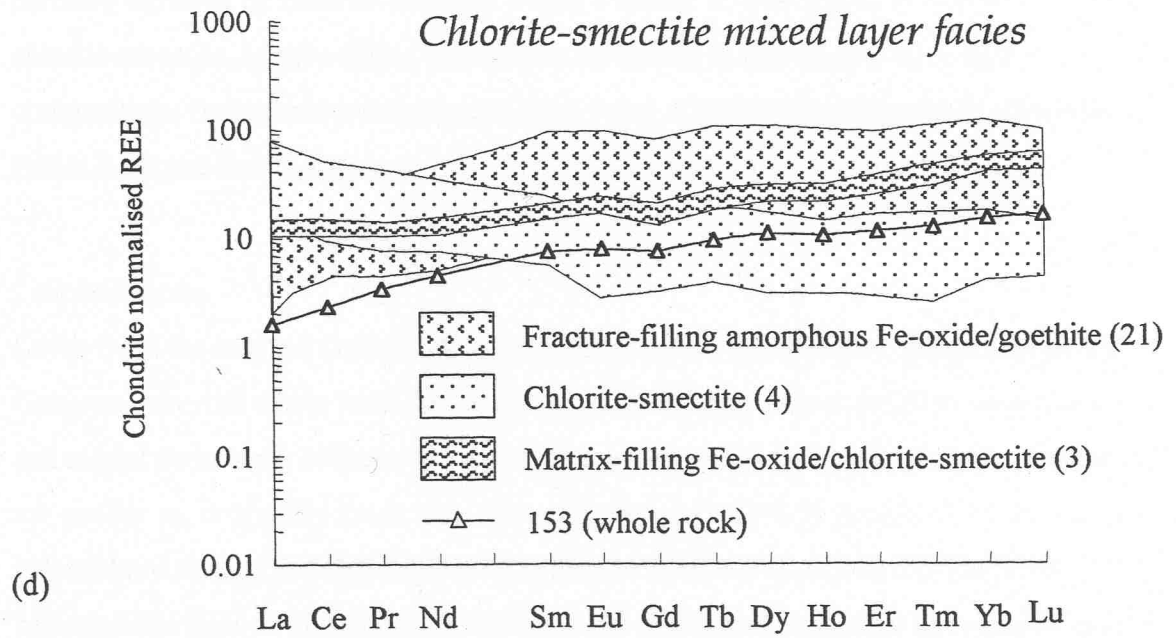

(d)

Figure 6.5 (c) & (d): Chondrite normalised LA ICP-MS REE data for alteration phases in (c) 146 from the smectitic facies lavas. The dashed line shows the range in REE content of secondary smectite in Troodos lavas [Gillis *et al.* 1992] (d) 153 from the chlorite-smectite mixed layer facies lavas. The numbers in parentheses indicate the number of analyses represented by each compositional field. Whole rock data are shown for reference.

Sample 153 from the chlorite-smectite mixed layer facies contains ~40% secondary chlorite-smectite developed primarily within the igneous groundmass and ~10% matrix- and fracture-filling amorphous Fe-oxides with minor goethite (Table 6.2). LA ICP-MS REE patterns of fracture-filling amorphous Fe-oxides are relatively flat to HREE enriched and generally more LREE depleted (La_n/Sm_n = 0.09-0.53) than the whole rock (La_n/Sm_n = 0.21; Fig. 6.5d). Poorly crystalline Fe-oxide stained mixed layer chlorite-smectites replace both igneous feldspars and groundmass adjacent to amorphous Fe-oxide filled fractures. They display flat LREEs (La_n/Sm_n = 0.67-1.0) and some HREE enrichment (Nd_n/Yb_n = 0.25-0.28) compared to the whole rock (Nd_n/Yb_n = 0.30). Chlorite-smectites without overprinting amorphous Fe-oxides have REE patterns that are LREE enriched with a larger negative Eu anomaly (La_n/Sm_n = 2.7-4.4; Eu/Eu* = 0.62-0.79) than the whole rock pattern (La_n/Sm_n = 0.21; Eu/Eu* = 1.0). The LA ICP-MS data reveal that the REE composition of amorphous Fe-oxides that overprint the chloritic alteration is dominating the whole rock pattern of this lava, due to their elevated REE content.

Sample 145 from the chlorite-smectite mixed layer facies comprises lava fragments partially replaced by chlorite-smectite within a matrix of amorphous Fe-oxides, quartz and chlorite-smectite. Matrix-filling amorphous Fe-oxides in this sample have REE compositions that mimic pristine basalt (Fig. 6.5e). Chlorite-smectites show somewhat flatter REE patterns (La_n/Sm_n = 1.0-1.5) than in sample 153 (La_n/Sm_n = 2.7-4.4).

Leached facies

Lavas from the leached facies (114, 143, 150) comprise chiefly illite, quartz and pyrite. Consequently, the whole rock REE patterns of these lavas reflect the REE composition and modal abundance of these secondary phases. They have whole rock REE contents that are similar to, or slightly lower than Troodos glasses (1.27-2.56 ppm cf. 2.43-10.41 ppm Nd) and are similarly LREE depleted (La_n/Sm_n = 0.50-1.0 cf. 0.54-0.62; Fig. 6.5b). Metasomatic gain of SiO_2 and FeS_2 during axial alteration manifested as replacive quartz and pyrite [Richards *et al.* 1989] will tend to dilute the whole rock REE concentrations and account for a degree of the observed depletion. Europium is significantly more depleted than the other REEs (Eu/Eu* = 0.57-0.62 cf. 0.89-1.0 for Troodos glasses).

Quartz and pyrite in sample 114 have REE contents below the detection limit of the LA ICP-MS technique. Thus, illite is inferred to be the major repository for REEs in the centre of the alteration pipe. Fine-grained illite in sample 114 occurs in a granular matrix of

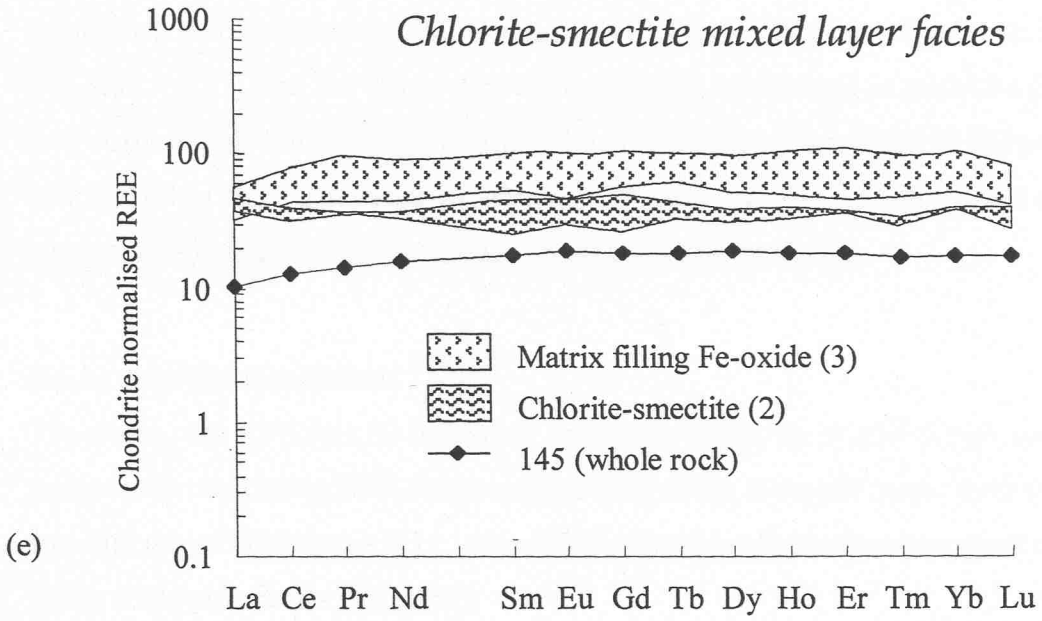

(e)

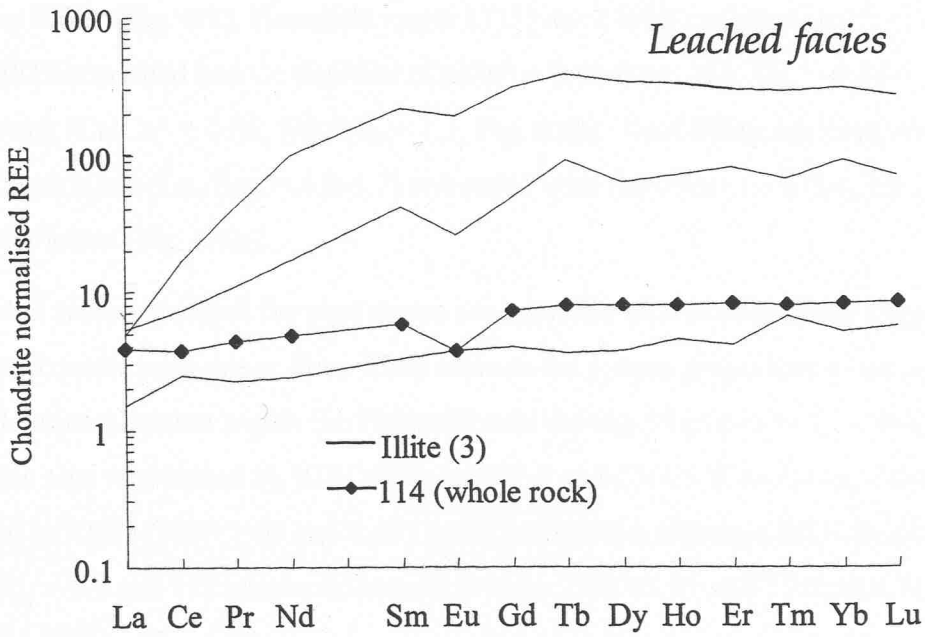

(f)

Figure 6.5 (e) & (f): Chondrite normalised LA ICP-MS REE data for alteration phases in (e) 145 from the chlorite-smectite mixed layer facies lavas (f) 114 from the leached facies lavas. The numbers in parentheses indicate the number of analyses represented by each compositional field. Whole rock REE data are shown for reference.

quartz and pyrite with rare preservation of igneous textures, and shows a range of REE compositions (Fig. 6.5f). HREE enriched illite (Nd_n/Yb_n = 0.19) with a Eu depletion comparable to the whole rock (Eu/Eu* = 0.56 cf. 0.57) can be inferred to dominate the whole rock REE composition. Another composition is slightly more HREE enriched (Nd_n/Yb_n = 0.47) than the whole rock without any Eu enrichment or depletion (Eu/Eu* = 1.0). A third illite composition is extremely LREE depleted (La_n/Sm_n = 0.02) and HREE enriched (Nd_n/Yb_n = 0.32) relative to the whole rock, with a REE composition similar to low temperature amorphous Fe-oxides in sample 153 (Fig. 6.5d).

6.6.3 Interstitial sediments

The whole rock REE data for interstitial sediments within the alteration pipe defines two groups with contrasting REE characteristics (Fig. 6.6a); hematitic jasper from the chlorite-smectite mixed layer facies (111, 144) and highly mineralised sediments from the leached facies at the pipe centre (149, 152).

Interstitial hematitic jasper has a relatively flat REE pattern (Nd_n/Yb_n = 1.1 and 1.2) with a pronounced negative Ce anomaly (Ce/Ce* = 0.66), demonstrating the influence of seawater REEs (Fig. 6.1). Hematitic jasper (111) has a REE composition that is slightly more HREE enriched and Ce depleted (Ce/Ce* = 0.46-0.50; Nd_n/Yb_n = 0.58-1.1) than the whole rock (Ce/Ce* = 0.66; Nd_n/Yb_n = 1.1; Fig. 6.6b). Void filling smectite in this sample is LREE enriched (La_n/Sm_n = 4.0-5.7) compared with the whole rock (La_n/Sm_n = 2.2) with no Ce depletion (Fig. 6.6b).

Interstitial sediments from the pipe centre are intensely altered to granular aggregates of pyrite and quartz with minor illite. They account for a large proportion of the total sulphide mineralisation within the Pitharokhoma deposit [Richards *et al.* 1989], and in the alteration pipe intersected by ICRDG Holes CY-2 and CY-2a [Cann *et al.* 1987]. They are depleted in REEs (Nd = 1.08 and 0.441 ppm) and show a striking LREE enrichment (Nd_n/Yb_n = 6.0 and 15) relative to hematitic jasper (Nd =1.97 and 2.62 ppm; Nd_n/Yb_n = 1.1 and 1.2).

Quartz and pyrite in sample 149 have REEs below the detection limit of LA ICP-MS. A compositionally insignificant phase was identified by Scanning electron microscopy (SEM) as a K-Al silicate, inferred to be illite or possibly hydrothermal sericite [Richards *et al.* 1989]. The REE content of the illite/sericite evidently controls the whole rock REE

(a)

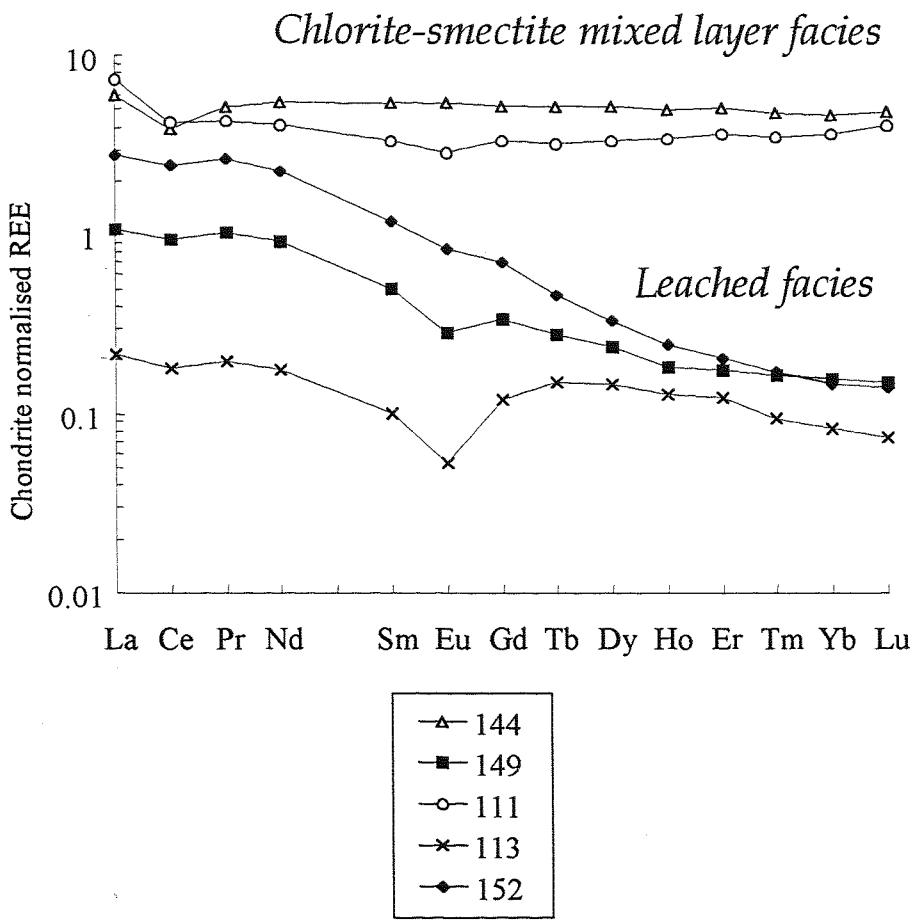

Figure 6.6 (a): Chondrite normalised whole rock REE data for massive pyrite (113) and altered interstitial sediments from the chlorite-smectite mixed layer and leached alteration facies.

(b)

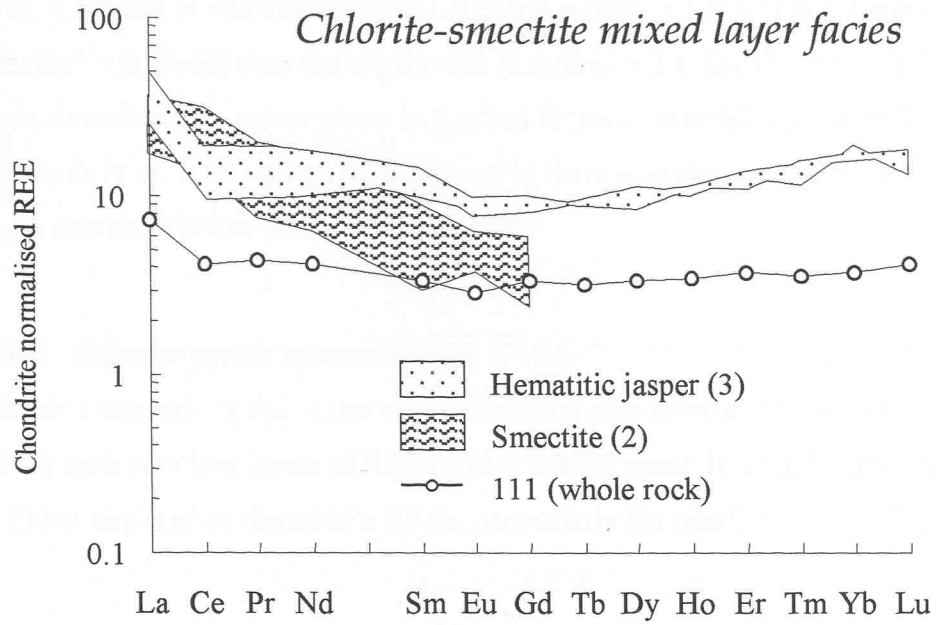

(c)

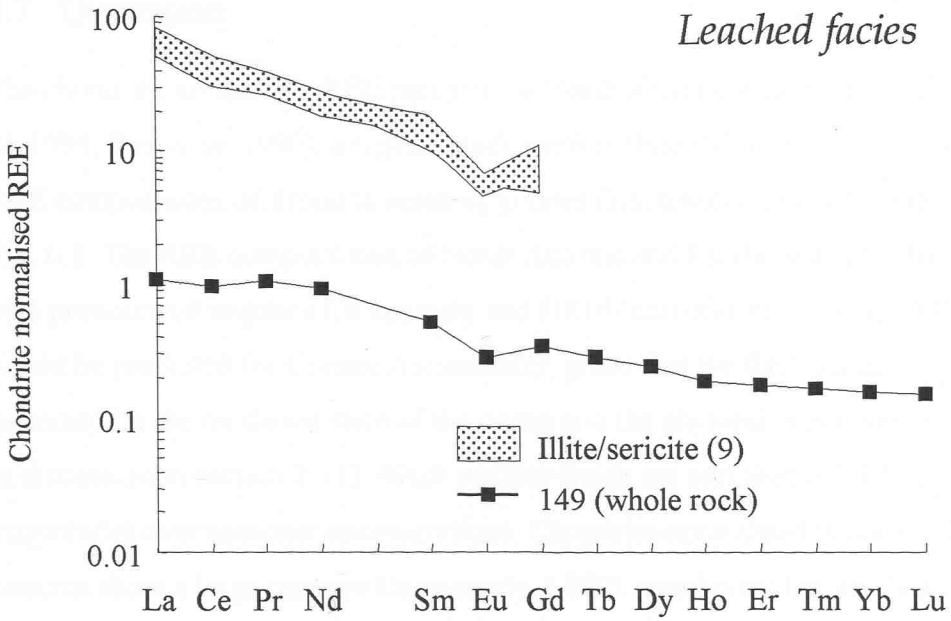

Fig. 6.6 (b) & (c): Chondrite normalised LA ICP-MS REE data for alteration phases in interstitial sediments in (b) 111 from the chlorite-smectite mixed layer facies lavas (b) 149 from the leached facies lavas. Numbers in parentheses indicate the number of analyses for each field. Whole rock REE data are shown for reference

composition, despite its low modal abundance (less than 5%). It contains abundant REEs (Fig. 6.6c) and is more enriched in LREEs (La_n/Sm_n = 3.5-7.5) and depleted in Eu (Eu/Eu* = 0.45-63) than the whole rock (La_n/Sm_n = 2.1; Eu/Eu* = 0.67). While apatite has been described as a minor phase in leached facies interstitial sediments [Richards 1987; Richards *et al.* 1989] it was not observed in these samples, consistent with low measured P_2O_5 contents (below detection limit).

6.6.4 Massive pyritic mineralisation

Massive sulphide in the centre of the alteration pipe consists of monomineralic pyrite (113) with very low levels of REEs (Nd = 0.0836 ppm). It is LREE enriched (Nd_n/Yb_n = 2.1) but depleted in the middle REEs, particularly Eu (Eu/Eu* = 0.48; Fig 6.6a).

6.7 Discussion

The chondrite normalised REE patterns for North Atlantic and Pacific seawater [Mitra *et al.* 1994; Bau *et al.* 1996], a typical black smoker fluid [Mitra *et al.* 1994] and the range of REE compositions of Troodos volcanic glasses [Rautenschlein *et al.* 1985] are shown in Fig. 6.1. The REE compositions of North Atlantic and Pacific seawater are characterised by a pronounced negative Ce anomaly and HREE enrichment. Similar REE characteristics would be predicted for Cretaceous seawater, given that the REE pattern of seawater is governed by the oxidation state of the ocean and the physical properties of the REEs (refer to discussion in section 2.11). Black smoker fluids are enriched in REEs (1 to 3 orders of magnitude) over seawater concentrations. Chondrite-normalised black smoker REE patterns show a large positive Eu anomaly, LREE enrichment but no Ce anomaly. This pattern is common to all known high-temperature fluids from sediment-free ridges, although there is a some variation in the size of the Eu anomaly between different vent sites [Klinkhammer *et al.* 1994; Mitra *et al.* 1994].

Lavas and dykes from the alteration pipe show either no change in REE content or a depletion in the LREE ± Eu. Quantification of REE mobility in the Pitharokhoma samples is problematic because all lavas and dykes analysed have been subject to a degree of hydrothermal alteration. Immobile element ratios indicate significant primary geochemical variability within the Pitharokhoma lavas [Richards 1987] hence the REE content of a pristine lava or dyke cannot be assessed with confidence.

6.7.1 Leached facies

Secondary illite is the primary repository for REEs in the leached facies lavas and interstitial sediments at the centre of the alteration pipe. Illite in the lavas (e.g. 114; Fig 6.5f) and illite/sericite in the mineralised sediments (e.g. 149; Fig 6.6c) show contrasting REE patterns, that are interpreted to reflect the REE signatures of fluids they have been altered by, or precipitated from. It is inferred that LREE enriched pattern of illite/sericite in the mineralised interstitial sediments was acquired from upwelling LREE enriched hydrothermal fluids, akin to modern black smoker fluids (Fig. 6.1). This interpretation is consistent with extreme Mg depletion of the lavas and inferred alteration temperatures of 300 to 370° C within the pipe centre [Jensenius 1984; Richards 1987].

In contrast, illite in the lavas that enclose these sediments has REE compositions similar to amorphous Fe-oxides and intergrown amorphous Fe-oxides/smectite in chlorite-smectite mixed layer and smectitic facies lavas (e.g. Figs. 6.5c & d). It is inferred that any high-temperature (LREE enriched) signature has been overprinted by REEs sourced from a lower-temperature hydrothermal fluid. This supports the inference of Richards *et al.* [1989] that illite in the pipe centre formed from non-expandable sericite during the waning stages of axial alteration, or during off-axis alteration at temperatures <260° C [Richards *et al.* 1989]. The different illite REE compositions in sample 114 (Fig. 6.5f) may indicate variable degrees of crystallographic control on REE uptake from the fluid, or differences in fluid composition arising from retrograde precipitation-dissolution reactions within the lavas.

The LA ICP-MS REE data indicate that the low-temperature phyllosilicates are the major repository for REEs in leached facies lavas in the core of the alteration pipe. LREE enriched illite/sericite in the mineralised interstitial sediments with a REE composition derived from ~350° C axial hydrothermal fluids was apparently stable during lower-temperature alteration, conceivably due to its occurrence within a chemically and physically robust granular quartz-pyrite assemblage.

6.7.2 Chlorite-smectite mixed layer facies

Mixed layer chlorite-smectites in the peripheral alteration facies of the pipe are inferred to have formed at temperatures of ~200° C by analogy with Icelandic geothermal systems [Richards *et al.* 1989]. Temperatures of formation of 80 to 240° C have been inferred for

chlorite in upper dyke zone of the Troodos ophiolite [Gillis & Robinson 1990*b*]. The alteration mineralogy of these lavas reflects mixing of upwelling black smoker fluids with relatively unreacted seawater at the periphery of the axial upflow zone [Richards *et al.* 1989]. The variably LREE enriched composition of chlorite and mixed layer chlorite-smectites in Pitharokhoma lavas (La_n/Sm_n = 1.0-4.4; Fig. 6.5d & e) is inferred to reflect precipitation from mixtures of entrained seawater and hydrothermal fluid, that would have been dominated by hydrothermal fluid rather than seawater REEs (refer Fig. 6.1).

Amorphous Fe-oxides that overprint chloritic alteration in these lavas are variably LREE depleted (Figs. 6.5d & e). These patterns are inferred to reflect the REE content of low-temperature hydrothermal fluids they were altered by or formed from, as Fe-oxides have the capacity to scavenge REEs from solution without significant fractionation [Koeppenkastrop & De Carlo 1992]. Large volumes of seawater circulate freely through the permeable volcanic section of oceanic lithosphere [Alt 1995]. Because basalt has a greater REE content than seawater (Fig. 6.1), even minor mobilisation of REEs during this circulation would produce solutions with rock-dominated REE compositions [Staudigel & Hart 1983]. The LA ICP-MS REE data show that the seawater-derived fluids responsible for low-temperature alteration were variably LREE depleted with a REE composition that mimics pristine basalt, as proposed by Gillis *et al.* [1992].

Dyke samples analysed in this study are altered to chlorite-smectite mixed layer facies assemblages, and excluding one sample (112) are hosted by similarly altered lavas. 112 contains secondary chlorite and mixed layer chlorite-smectites and intrudes illitised lavas in the pipe centre. It is inferred that this dyke was relatively impermeable to ascending hydrothermal fluids (resulting in the incomplete elimination of Mg-bearing phases), or was intruded following the peak of hydrothermal alteration. In the latter case, a degree of seawater entrainment into the axial upflow zone is implied by the presence of chlorite in the otherwise Mg depleted pipe centre.

The REE patterns of interstitial hematised jasper in chlorite-smectite mixed layer facies lavas (Fig. 6.6a) reflect uptake of REEs from seawater (Fig. 6.1) *via* scavenging mechanisms prior to, or following sedimentation on the Troodos seafloor, and are similar to ridge crest metalliferous sediments [Owen & Olivarez 1988; German *et al.* 1990] and Troodos umbers [Robertson & Fleet 1976].

6.7.3 Smectitic facies

Zeolite and smectite precipitation in voids is characteristic of low-temperature (<50 to 100° C) alteration of Troodos lavas [Gillis & Robinson 1990*a,b*]. The LREE enriched composition void-filling smectite in smectitic facies Pitharokhoma lavas is comparable to smectites in Troodos lavas analysed by Gillis *et al.* [1992], shown in Fig. 6.5c. However, void filling smectite in hematised jasper from the chlorite-smectite mixed layer facies is LREE enriched (Fig. 6b). Similarly, the REE compositions of mixed layer chlorite-smectites, amorphous Fe-oxides and illite vary between samples (Figs.6.5c-f; 6.6b&c). Thus, the REE content of a Pitharokhoma lava or interpillow sediment reflects the REE composition of hydrothermal fluids that have altered them at both high and low-temperatures, and is not a simple function of modal alteration mineralogy. Similar results have been obtained in previous oceanic and ophiolite-based alteration studies. Basalts from the transition zone of Hole 504B that display REE enrichments show a similar alteration mineralogy to non-enriched samples [Alt & Emmerman 1985]. Finely intermixed sulphides, sulphate and amorphous silica samples from the Southern Explorer Ridge with similar modal mineralogies show contrasting REE patterns [Barrett *et al.* 1990]. On Troodos, void-filling epidote and chlorite in sheeted dykes sampled by ICRDG Hole CY-1A have contrasting REE profiles to epidote and chlorite replacing the igneous groundmass, and are inferred to have precipitated from fluids with different REE compositions [Gillis *et al.* 1992].

Intergrown void filling mordenite and cowlesite shows a LREE enrichment and a striking Eu depletion, whereas void-filling smectite in the same sample is LREE depleted (Fig. 6.5c). Assuming the low-temperature fluid had a REE content depicted by amorphous Fe-oxides (Figs 6.5d & e) the zeolites have preferentially incorporated LREEs and discriminated against Eu.

6.7.4 REE composition of the mineralising fluid

Hydrothermal fluids venting at the seafloor at mid-ocean ridges share a characteristic LREE and Eu enrichment [e.g. Klinkhammer *et al.* 1994] (Fig. 6.1). Lavas and sediments in the centre of the alteration pipe were altered by ancient analogues of black smoker fluids in a zone of axial hydrothermal alteration [Jensenius 1984; Richards *et al.* 1989]. Secondary chlorite and chlorite-smectites that precipitated at the periphery of the upflow zone possess a LREE enrichment, that is inferred to reflect the REE composition of the

hydrothermal fluid. However none of the secondary phases analysed possess a striking Eu enrichment, although a small positive Eu anomaly has been noted in the REE pattern of chlorite from the sheeted dyke complex [Gillis *et al.* 1992].

Pyrite from the pipe centre is similarly LREE enriched and lacks a positive Eu anomaly (113, Fig. 6.6a). REE substitution into sulphide phases from the TAG sulphide mound and other oceanic deposits appears to be strongly influenced by crystallographic controls [Morgan & Wandless 1980; Alt 1988; Barrett *et al.* 1990; Mills & Elderfield 1995*a*]. Smaller HREE cations are more easily accommodated in the sulphide lattice than the larger LREEs. Therefore, the REE composition of sulphides reflects that of the parental hydrothermal fluid, albeit with a smaller positive Eu anomaly and a relative HREE enrichment [Mills & Elderfield 1995]. Given that the partitioning of REEs between hydrothermal fluid and sulphide is relatively well understood [e.g. Morgan & Wandless 1980], the REE composition of pyrite in the Pitharokhoma alteration pipe suggests that the parental hydrothermal fluid had a higher Nd_n/Yb_n ratio than the pyrite, and lacked the striking Eu enrichment that is characteristic of seafloor vent fluids

Preferential mobilisation of Eu in the divalent state has been invoked to explain the Eu enrichments of vent fluids [Sverjensky 1984; Wood 1990*b*; Bau 1991]. Divalent Eu dominates at temperatures in excess of 250° C, while at lower temperatures the relative stability of divalent and trivalent Eu will also depend on pH and complexing ligands in solution [Sverjensky 1984]. The absence of a Eu enrichment in the pyrite may reflect subsurface processes operating within the upflow zone relating to the temperature, pressure, E_h and pH of the mineralising system. This has been implied for the Snake Pit vent field on the Mid-Atlantic Ridge, where venting fluids are characteristically Eu enriched, but sulphides in hydrothermal sediments do not show a Eu anomaly, and are inferred to be precipitating from fluids with a different composition to those exiting at the seafloor [Gillis et al. 1990]. Alternatively, Troodos hydrothermal fluids may have differed in some fundamental respect to modern vent fluids (relating to redox conditions in the subsurface of the hydrothermal system) which is reflected in the REE composition of the alteration minerals.

6.7.5 Axial alteration versus crustal ageing processes

The LA ICP-MS REE data demonstrate that during high- and low-temperature

hydrothermal alteration there may have been some relative loss or gain of LREEs and HREEs, that did not necessarily cause any substantial net REE mobilisation.

Although leached facies lavas in the pipe centre were extensively altered by ~350° C hydrothermal fluids, their REE composition is dominated by retrogressive illite and records interaction with a low-temperature fluid. Interstitial hematised jasper at the periphery of the pipe has a similar REE composition to ridge crest metalliferous sediments and reflects seafloor sedimentation processes. Mineralised sediments have REE compositions that are inferred to reflect axial alteration by ~350° C LREE-enriched hydrothermal fluids.

The REE composition of chlorite-smectite mixed layer facies lavas comprises a component of the primary REE inventory (due to the incomplete alteration of igneous phases), with some high-temperature (mixed layer chlorite-smectites ± chlorite) and low-temperature REEs (amorphous Fe-oxides). The elevated REE content of overprinting amorphous Fe-oxides controls the whole rock LREE depletion of some lavas and dykes from the chlorite-smectite mixed layer facies (e.g. 153, 157, 112; Figs. 6.4 and 6.5a) although they also contain variably LREE-enriched mixed layer chlorite-smectites ± chlorite. The REE content of smectitic facies lavas at the periphery of the alteration pipe is chiefly a primary inventory, with low-temperature smectite and amorphous Fe-oxides having REE patterns that mimic fresh basalt.

Low-temperature alteration phases have been identified as the major repository for the REEs in many of the altered lavas. Lavas with net depletions in the LREE ± Eu have whole rock REE compositions dominated by low-temperature alteration phases (e.g. 153, Fig. 6.5a; 114,143, 150; Fig 6.5b). These data suggest that much of the REE signature of the alteration pipe reflects off-axis low-temperature crustal alteration rather than axial alteration by mineralising hydrothermal fluids.

6.7.6 REE mobility in hydrothermal systems

Contrasting trends in REE mobility have been noted in rocks altered at low (<100°C) and high (>300°C) temperatures at a variety of water/rock ratios during hydrothermal and crustal ageing processes in oceanic crust and ophiolites. These trends range from REE immobility to overall enrichment [Hellman & Henderson 1977; Ludden & Thompson 1978] or depletion of the REEs [Bach *et al.* 1996], to the selective uptake of LREEs

[Ludden & Thompson 1978, 1979; Juteau *et al.* 1979; Minai *et al.* 1990; Regba *et al.* 1991; Gillis *et al.* 1992]. From the results of these studies, REE mobility is understood to be dependant upon several factors, including the protolith crystallisation history [Humphris *et al.* 1978; Ludden & Thompson 1978; Gillis *et al.* 1992] the longevity of seawater exposure [Ludden & Thompson 1978, 1979; Juteau *et al.* 1979] and the water/rock ratio during alteration [Valsami & Cann 1992]. Further studies have shown that the REE patterns of altered rocks are controlled by their secondary mineral assemblages [Humphris *et al.* 1978; Regba *et al.* 1991; Valsami & Cann 1992].

REE depletions (~10 to 1200 ppm of the LREEs) are frequently observed in the alteration zones beneath ancient volcanic-hosted massive sulphide deposits, and often attributed to interaction with ore-forming fluids in the subsurface of the hydrothermal system [Graf 1977; Baker & de Groot 1983; Campbell *et al.* 1984; Bence & Taylor 1985; MacLean 1988; Whitford *et al.* 1988; MacLean & Hoy 1991; Regba *et al.* 1991]. Less frequently REE mobility has been implied to post-date ore formation [Schandl & Gorton 1991], or magmatic fluids have been invoked to account for some of the observed depletions [Schade *et al.* 1989]. A negligible capacity for hydrothermal fluids to mobilise REEs during hydrothermal circulation is inferred from the ubiquitously low REE inventories of seafloor vent fluids [e.g. Michard *et al.* 1983; Campbell *et al.* 1988*b*; Mitra *et al.* 1994] (Table 6.4). Studies of hydrothermal systems at mid-oceanic ridges predict that the REE budget of oceanic crust is unmodified during alteration at inferred water/rock ratios of ~1 [Michard *et al.* 1983; Michard & Albarède 1986; Bau 1991; Klinkhammer *et al.* 1994]. Furthermore, thermodynamic considerations suggest the observed REE depletions beneath ancient massive sulphide deposits are unlikely to have been achieved by ancient analogues of black smoker fluids, even for systems with water/rock ratios of ~1000 [Wood & Williams-Jones 1994]. The extreme REE mobility identified in the altered zones beneath some massive sulphide deposits [e.g. Baker & de Groot 1983; Campbell *et al.* 1984; Bence & Taylor 1985; MacLean & Hoy 1991; Schandl & Gorton 1991] is not evident in the stockwork mineralised lavas of the Pitharokhoma alteration pipe. Determination of the REE mineralogy of stockwork lavas by an *in situ* method such as LA ICP-MS might clarify the significance of the extreme REE mobility observed in many alteration pipes.

The inferred hydrothermal circulation for Troodos [Bickle & Teagle 1992, Bickle *et al.* 1998) is considerably greater than for typical mid-ocean ridges [e.g. Morton & Sleep 1985]. Hydrothermal alteration at water/rock ratios of ~20 to 1000 has been inferred for

the formation of epidosites (quartz-epidote-sphene assemblage) near the base of the sheeted dyke complex, that are considered to represent deep upflow zones of Mg-depleted hydrothermal fluids [Richardson *et al.* 1987; Seyfried *et al.* 1988; Schiffman *et al.* 1990]. Similarly, it is evident from the extreme metasomatism of Pitharokhoma leached facies lavas that large volumes of ~350° C hydrothermal fluid were focused through this fossilised upflow zone [Richards *et al.* 1989]. While studies of active vent systems predict little mobilisation of REEs during axial hydrothermal circulation [e.g. Klinkhammer *et al.* 1994; Bau 1991; Michard *et al.* 1983; Michard & Albarède 1986] these systems are in an early (high-temperature) stage of evolution in comparison to the mature hydrothermal systems preserved within Troodos as superimposed alteration episodes. It is not possible to assess the extent of REE mobilisation from the Pitharokhoma lavas by ancient analogues of black smoker fluids during axial hydrothermal alteration, as the REE inventory now observed is chiefly a low-temperature overprint, associated with ageing of the oceanic basement.

6.7.7 REE mobility in the TAG stockwork

ODP drilling of the TAG sulphide mound and stockwork deposit has provided the opportunity to test in the modern setting the model developed in this chapter for the relative loss or gain of light and heavy REEs during low- and high-temperature hydrothermal alteration of stockwork mineralised lavas, often without any substantial net REE mobilisation.

Figure 6.7 shows chondrite normalised REE data for chloritised basalts and pillow breccias from the TAG mound stockwork. Shown for comparison is the range in REE compositions of isotopically-unaltered "fresh" basalts from the TAG-2 and TAG-4 areas at the periphery of the mound [Alt & Teagle 1998; Teagle *et al.* 1998]. These basalts contain only minor amounts (5% to 15%) of secondary minerals, predominantly smectite that partially replaces olivine and interstitial areas and fills vesicles [Teagle *et al.* 1998]. Hydrothermally altered pillow breccias were recovered at ~20 mbsf in the TAG-2 area, located near the edge of the lower mound platform. They comprise glassy clasts replaced by Mg-rich chlorite cemented by quartz, chlorite and hematite [Honnorez *et al.* 1998; Humphris *et al.* 1998]. Bulk rock Sr-isotope ratios are near seawater, indicating that they were altered by interaction with large amounts of conductively-heated seawater at temperatures >200°C [Teagle *et al.* 1998]. The chondrite normalised REE patterns of the

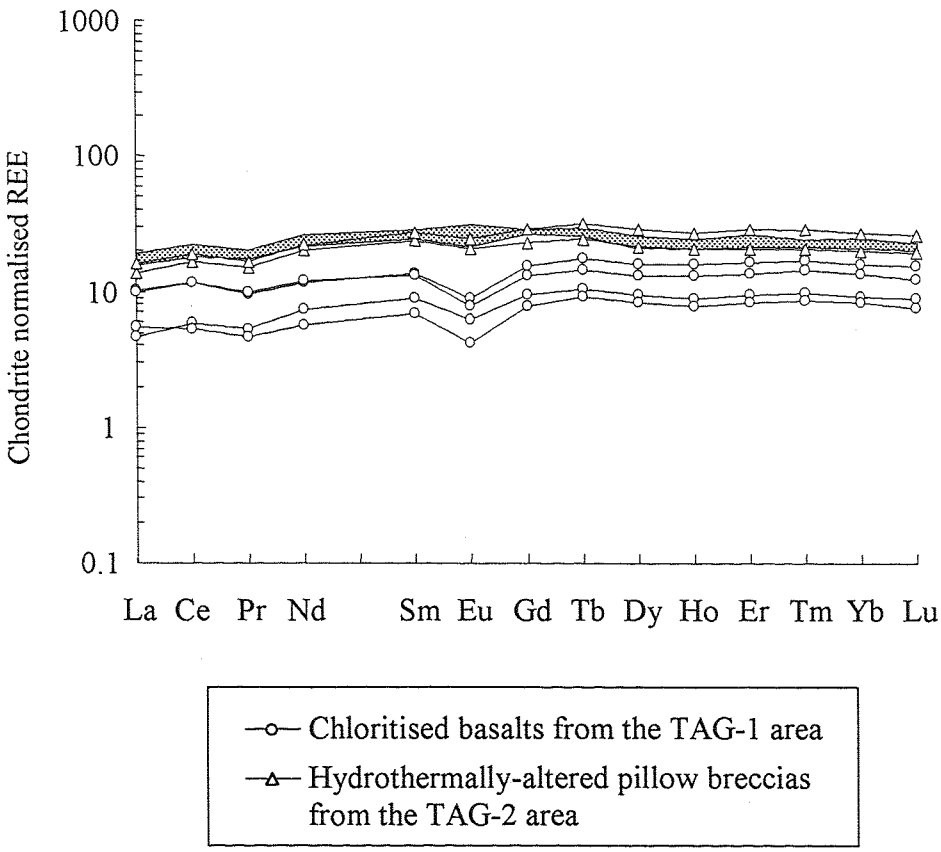

Figure 6.7: Chondrite normalised whole rock REE data for TAG stockwork samples. The shaded area shows the range in REE content of "fresh" basalts from the TAG-2 and TAG-4 areas. All data are from Humphris *et al.* [1998].

pillow breccias resemble "fresh" basalts, with slightly higher REE contents. Thus during high- and low-temperature seawater-dominated alteration, there has been some REE uptake without differential mobility of the LREE or HREE.

Chloritised basalt breccias were recovered at depths greater than 110 mbsf in the TAG-1 area, drilled to the SW of the black smoker complex. These samples are altered to a quartz-chlorite-pyrite assemblage [Humphris *et al.* 1998]. The fluid that caused recrystallisation of the basalt breccia was Mg-bearing, and inferred from whole rock Sr-isotope analyses to be a mixture of upwelling, black-smoker fluid (>300°C) with a minor proportion of entrained seawater (<10%) [Teagle *et al.* 1998]. The chondrite normalised REE patterns are lower than in "fresh" basalts, and are characterised by the development of a marked negative Eu anomaly [Humphris *et al.* 1998]. The REE pattern of a 90% black smoker fluid, 10% seawater mixture would be dominated by black smoker REEs. However, the REE pattern of these samples lacks the LREE and Eu enrichment that characterises TAG black smoker fluids (Fig. 6.1). They more closely resemble Troodos smectites (Fig. 6.5c) and illite from leached facies lavas in the Pitharokhoma alteration pipe (Fig. 6.5b) that are inferred to have a lower-temperature origin. The results of the Pitharokhoma study have shown that in the absence of REE analyses of individual alteration phases from the *same* samples for which isotope analyses and mineralogical descriptions are available, the significance of whole rock REE data for hydrothermally altered basalts is ambiguous, and will often display contrasting trends [e.g. Alt & Emmerman 1985]

6.8 Conclusions

REE mobility has been investigated in stockwork mineralised lavas and dykes that lie in a zone of former black smoker fluid upflow within Troodos oceanic lithosphere. The major and trace element geochemistry of the lavas of the Pitharokhoma deposit described by Richards *et al.* [1989] reflects increasing alteration towards the centre of a focused hydrothermal upflow zone, with heterogeneous overprinting by lower-temperature phases.

Most lavas from the Pitharokhoma alteration pipe have REE compositions similar to Troodos volcanic glasses, indicating that on- and off-axis hydrothermal alteration processes have not induced significant net REE mobilisation. A degree of REE mobility is inferred for some lavas which are depleted in the light REE ± Eu. LA ICP-MS REE data

for stockwork mineralised lavas, dykes and interstitial sediments from the eastern alteration pipe indicate that REE mobility was associated with the development of both high- (~200 to 350° C) and low-temperature (<100° C) alteration phases that precipitated within contrasting alteration regimes (discharge- and recharge-dominated respectively). Lavas and sediments in the centre of the alteration pipe were altered by ancient analogues of black smoker fluids upwelling in a zone of axial hydrothermal alteration [Jensenius 1984; Richards et al. 1989]. The LREE enriched composition of pyrite, chlorite and chlorite-smectite is inferred to reflect the composition of the ~350° C hydrothermal fluid and contrasts with the typically LREE depleted patterns of lower-temperature amorphous Fe-oxides and smectite. The whole rock REE compositions of altered lavas and dykes thus reflect the REE composition of hydrothermal fluids that have altered them at both high- and low-temperatures. During low- and high-temperature hydrothermal alteration of the lavas there may have been some relative loss or gain of LREEs and HREEs, that did not cause significant net REE mobilisation in most of the analysed lavas and dykes.

Low-temperature alteration phases are the major repository for the REEs in lavas that show LREE ± Eu depletions relative to pristine volcanic glass compositions. Hence much of the REE signature of the alteration pipe is a post-mineralisation overprint acquired in the waning stages of hydrothermal activity and during the protracted alteration of the oceanic basement which continued for ~20 million years following crustal accretion [Staudigel *et al.* 1986; Staudigel & Gillis 1990] rather than on-axis greenschist facies hydrothermal alteration.

This study has demonstrated the successful application of LA ICP-MS in identifying alteration phases which host REEs within complex matrices, although as of yet there is no accepted calibration protocol for the method [Norman *et al.* 1996].

Chapter 7

The rare earth element geochemistry of an ophiolitic sulphide mound deposit and associated metalliferous sediments

7.1 Introduction

Submersible and drilling studies of the TAG mound at 26°N, Mid-Atlantic Ridge have led to the development of models of mound growth and fluid evolution within an actively-forming seafloor sulphide deposit [e.g. Mills & Elderfield 1995*a*; Edmond *et al.* 1995; Humphris *et al.* 1995; Tivey *et al.* 1995; James & Elderfield 1996; Edmonds *et al.* 1996; Mills *et al.* 1996; Goulding *et al.* 1998; Mills *et al.*1998; Teagle *et al.* 1998; Tivey *et al.* 1998]. These studies have shown that the subsurface mixing of hydrothermal fluids with entrained seawater plays a crucial role in creating and modifying the TAG ore deposit, and the relevance of these models to hydrothermal mineralisation at other seafloor vent sites is now being investigated [Humphris *et al.* 1995]. The TAG models may also have important implications for on-land analogues such as Cyprus-type ore bodies. This chapter describes a study in which the REEs and other geochemical proxies have been used to determine if the processes described by the current TAG models of sulphide mineralisation and metalliferous sediment formation are identifiable in Troodos massive sulphide ore bodies, which are among the closest ancient analogues of the TAG sulphide mound. REE and other geochemical data were obtained for a suite of samples collected from the Skouriotissa ore body and other sites of hydrothermalism within the Troodos ophiolite. Sampling of Skouriotissa sulphides and associated metalliferous sediments was undertaken on a similar scale to that on the seafloor at TAG [e.g. Mills & Elderfield 1995*a*] to allow interpretation of the results within the framework of the TAG models.

Although not formed in a mid-ocean ridge setting [Pearce 1975; Robinson *et al.* 1983; Rautenschlein *et al.* 1985], the Skouriotissa ore deposit is similar to the TAG mound in terms of its size (~6 Mt), sulphide mineral associations and textures [Oudin 1984] and the occurrence of metal-enriched hydrothermal sediments and oxidised gossans spatially associated with the ore body [Herzig *et al.* 1991]. However, hydrothermal sediments in Cyprus differ from those in the modern setting by having distinctly bimodal Mn contents, and have been classified in the literature as Mn-rich, Fe-poor umbers and Mn-poor, Fe-rich ochres, both formed by hydrothermal processes occurring at a Tethyan spreading ridge [Corliss 1972; Elderfield *et al.* 1972; Robertson & Hudson 1973; Robertson 1975; Robertson 1976; Robertson & Fleet 1976; Gale *et al.* 1981; Boyle & Robertson 1984; Boyle 1990; Herzig *et al.* 1991; Robertson & Boyle 1993].

It is important to clarify how the terms 'umber' and 'ochre' in Troodos relate to the results of modern studies of metalliferous sediment formation. In the modern setting, the term ochre is used to describe oxidised gossans formed by low-pH reactions between the mound sulphides and seawater and/or diffuse hydrothermal fluids (section 3.2.7.3) [Hannington *et al.* 1991; Herzig *et al.* 1991; Tivey *et al.* 1995], in addition to primary Fe-oxyhydroxide sediments forming in areas of diffuse flow on seafloor sulphide mounds [e.g. Mills & Elderfield 1995*a*; Mills *et al.* 1996; Goulding *et al.* 1998]. Similar processes have been invoked to account for the formation of the surface gossan of trace metal-enriched secondary minerals and Fe-oxides on the Skouriotissa mound [e.g. Robertson 1976; Herzig *et al.* 1991].

Troodos umbers show a much wider distribution across the palaeo-seafloor than the ochres, occurring up to 10's of kms from the high-temperature vents [Boyle 1990]. In contrast to the Fe-rich ochres, Troodos umbers are mostly Mn-rich oxyhydroxide sediments which have been described as low-temperature precipitates from off-axis diffuse fluids [Robertson 1975; Robertson 1976], or alternately attributed to distal plume fall-out from high-temperature vents [Boyle 1990]. However, Troodos umbers are significantly different from TAG plume-derived sediments. The umbers are dark brown to black manganiferous sediments (2 to 16.3 wt.% Mn, averaging 8 wt.%) [Robertson 1976], unlike the metal-enriched pale-brown calcareous oozes that accumulate on the seafloor at TAG (296 ppm to 1.06 wt.% Mn, averaging 0.11 wt.%) [Scott *et al.* 1978; Shearme *et al.* 1983; Metz *et al.* 1988; Mills *et al.* 1993]. The TAG sediments comprise hydrothermal Fe-oxyhydroxide sediments (11.3 to

40.5 wt.% Fe) variably diluted by detrital (1.16 to 12.5 wt.%) and biogenic (<1 to 58.2 wt.%) components [Metz *et al.* 1988; Mills *et al.* 1993]. Within these sediments, Mn-enriched layers containing up to 1.06 wt.% Mn are marked by black Mn-oxide crusts [Mills *et al.* 1993], which may be more akin to the Mn-rich Troodos umbers. Additionally, one sediment core from the southern periphery of the TAG mound contains a ~10 cm thick zone of Mn (as well as Cu, Zn and Pb) enrichment (up to 15.2 wt.% Mn), which is inferred to be controlled by sharp redox gradients within the core, consistent with REE evidence for seawater ingress and overprinting in this core [Goulding *et al.* 1998]. However, perhaps the most similar sediments to umbers at TAG are the Fe- and Mn-rich oxide crusts (containing up to 39 wt.% Mn) that are found in the relict *Mir* and *Alvin* zones and the low-temperature field [M. Scott *et al.* 1974; Thompson *et al.* 1985; Rona *et al.* 1993*a,b*]. The origin of these Mn-rich crusts is investigated in Chapter 8 of this dissertation.

7.2 Geochemical proxies of hydrothermal processes at TAG

The TAG models of mound growth and evolution as inferred from the results of drilling and submersible studies of the active TAG deposit are described in section 3.2.4. The results of these studies indicate that diffuse flow is important in stripping metals soluble at lower temperatures from the interior of the deposit to generate secondary pyrite phases and enrichment of Zn- and trace metal-rich (Cd, Au, Ag, As and Sb) sulphide phases in gossanous crusts at the outer surface of the deposit [Edmond *et al.* 1995; Tivey *et al.* 1995; James & Elderfield 1996; Edmonds *et al.* 1996; Mills *et al.* 1996]. Drilling by ODP has extended the sampling to three dimensions and confirmed that the mound is zone-refined on a deposit scale, due to ongoing sulphide reworking in the mound interior [Hannington *et al.* 1998]. For example, sulphides at the surface of the mound contain up to 12 wt.% Cu compared with an estimated value of 2 wt.% Cu for the bulk deposit [Hannington *et al.* 1998]. These dynamic mound processes are summarised in Fig. 3.3.

The REEs have been used as an important tool in the investigations of the formation and evolution of the TAG deposit [German *et al.* 1993; Mills & Elderfield 1995*a*; James & Elderfield 1996; Mills *et al.* 1996; Humphris 1998; Goulding *et al.* 1998]. They are effective geochemical proxies of hydrothermal processes because the REE compositions of high-temperature hydrothermal fluids and seawater are well-characterised and distinct (refer to Fig. 2.1) [e.g. Klinkhammer *et al.* 1994; Mitra *et al.* 1994]. Consequently, fluid mixing and

evolution by processes related to mound growth are recorded in the REE compositions of mound precipitates and a range of fluids that exit from the mound surface (refer to sections 2.5 to 2.9) [e.g. Mills & Elderfield 1995*a*; James & Elderfield 1996; Mills *et al.* 1996; Goulding *et al.* 1998; Humphris 1998].

The REEs have been used to elucidate mechanisms of metalliferous sediment formation at TAG *via* plume fallout, mass wasting of sulphides and low-temperature precipitation, as these sediment sources have distinct REE signatures which reflect the degree of seawater exposure during sedimentation [German *et al.* 1993; Mills *et al.* 1993; Mills & Elderfield 1995*a*; Mills *et al.* 1996; Goulding *et al.* 1998]. Ochreous Fe-oxide sediments which precipitate from diffuse fluids at the surface of the TAG mound have vent fluid-like REE patterns, that indicate direct precipitation from, or alteration by a modified hydrothermal vent fluid [Mills & Elderfield 1995*a*; Mills *et al.* 1996]. One core sampled from the southern periphery of the mound provides evidence of seawater ingress and REE overprinting (i.e. development of a negative Ce anomaly; Fig. 2.4) [Goulding *et al.* 1998].

Fine-grained oxyhydroxide sediments deposited from the neutrally buoyant plume have seawater-like REE patterns and REE/Fe ratios that are elevated over vent fluid values due to scavenging interactions with large volumes of seawater [German *et al.* 1990; Rudnicki & Elderfield 1993]. The extent of REE uptake depends on the degree of seawater exposure, both prior to and following sedimentation on the seafloor. Consequently, the REE/Fe ratios of plume particles and sediments increases with time/distance from the vent source [German *et al.* 1990].

Investigations of geochemical interactions in the TAG plume have characterised the behaviour of the oxyanions (As, P, V, U and Mo) and chalcophile elements (Cu, Zn and Pb), [German *et al.* 1991*a*; German *et al.* 1993; Mills *et al.* 1993]. Oxyanions are conservative in seawater and underlying metalliferous sediments, and are co-precipitated with Fe-oxyhydroxides in the buoyant hydrothermal plume [German *et al.* 1991*a*]. Consequently As/Fe, P/Fe, V/Fe, U/Fe and Mo/Fe ratios tend to be constant in hydrothermal plume particulates and in sediments underlying areas of plume dispersion, with some modifications due to alteration processes occurring on the seafloor [Trefry & Metz 1989; Feely *et al.* 1991; German *et al.* 1991*a*; German *et al.* 1993; Mills *et al.* 1993].

Chalcophile elements such as Cu, Zn and Pb enter sulphide phases which accumulate on the TAG mound without significant interactions with seawater. Sulphides eroded from vent

structures are rapidly resedimented in surrounding sediments with relatively little interaction with seawater. They typically occur as distinctive layers of fragmented clasts of mound sulphides in a fine sedimentary matrix of plume particles. Even when partially oxidised, the original sulphide elemental associations remain. The composition of these sulphidic sediments is distinct due to their elevated U/Fe ratios (although complete oxidation leads to U dissolution and correspondingly lower U/Fe ratios), high chalcophile element content and vent fluid-like REE patterns [Metz *et al.* 1988; German *et al.* 1993; Mills *et al.* 1993; Mills *et al.* 1994].

The results of the TAG studies have shown that the geochemistry of hydrothermal deposits allows the identification of their processes of formation, in addition to post-depositional modifications. The aim of this chapter is to investigate these geochemical associations in the ancient setting.

7.3 Troodos sulphide mound and metalliferous sediment deposits

The characteristic morphology and mineralogy of the Troodos massive sulphide deposits, and their relationship to axial graben structures preserved within the ophiolite complex is discussed in detail in sections 3.3.2.5 and 3.3.2.6 of this dissertation.

7.3.1 Umbers

Troodos metalliferous sediments are preserved spatially and genetically associated with Troodos seafloor sulphide mound deposits. They occur overlying the ore bodies, inter-calculated with off-axis boninitic lavas that overlie many of the sulphide deposits, and additionally accumulated in fault-bounded grabens and half-grabens in the uppermost surface of the volcanic pile up to 10's of km from the high-temperature vents [Wilson 1959; Corliss 1972; Constantinou & Govett 1972; Robertson 1975; Robertson 1976; Boyle & Robertson 1984; Boyle 1990; Robertson & Boyle 1993]. The fault-bounded deposits are up to 50 m thick and locally grade into pelagic sediments [Karpoff *et al.* 1988; Robertson & Boyle 1993]. The absence of terrigenous material and siliceous microfossils in the majority of the umbers indicates they accumulated relatively rapidly [Boyle 1990].
The distribution of hydrothermal sediments across the upper surface of the Troodos lava pile is more similar to the rift valley-confined deposits of the MAR, rather than sediments formed at faster-spreading ridges [Boyle 1990]. At EPR spreading centres there is fairly

uniform sediment cover and a smooth decrease in hydrothermal enrichment away from the ridge axis [e.g. Böstrom & Peterson 1966; Böstrom & Peterson 1969; Dymond *et al.* 1973; Barrett *et al.* 1987] due to the lateral dispersion of hydrothermal plumes in the mid-depth circulation [Edmond *et al.* 1982]. However in Cyprus, like the rift valley floor at TAG, umber did not accumulate uniformly at the ridge axis. Boyle [1990] has invoked the absence of any mid-depth circulation to account for the short (*c.* 10 km) range of influence of the high-temperature vent sources.

Troodos umbers comprise massive or poorly bedded goethite and poorly crystalline Mn-oxides with small amounts of quartz and calcium apatite, with some additional terrigenous and biogenic inputs [Elderfield *et al.* 1972; Robertson 1975; Boyle 1990]. They are typically enriched in Mn and trace elements (Ba, Co, Cu, Ni, Pb, V, Zn and Zr) relative to ochres and overlying pelagic sediments [Robertson 1975, Robertson 1976]. Seawater and hydrothermal sources have been invoked to account for the characteristic trace element enrichment of the umbers [Elderfield *et al.* 1972; Robertson 1976]. The lead isotopic composition of Troodos metalliferous sediments indicates that a significant proportion of Pb in these sediments was derived from the underlying oceanic basement, while the strontium isotope ratios are indistinguishable from Late Cretaceous seawater [Gale *et al.* 1981]. Some basal umbers and interpillow metalliferous sediments are notably Mn-deficient, and contain volcaniclastic material which is mainly converted to smectite [Robertson 1976; Robertson & Fleets 1976]. The Mn-deficient umbers resemble ochres in the field, but are chemically more similar to the Mn-rich umbers [Robertson 1976].

The majority of Troodos ore bodies are directly overlain by the unmineralised UPL [Constantinou 1980]. However, the Skouriotissa mound and associated ochres were not completely buried by lavas, so that Mn-poor umbers occur directly above the mound ochres (or conglomeritic ore, where the ochres are absent) at some localities along the north margin of the pit [Robertson 1976]. Data from early boreholes indicate that metalliferous sediments formed a near-continuous cover over unconsolidated conglomeritic ore at the upper surface of the Skouriotissa orebody [Wilson 1959]. Mn-poor umbers pass upwards suddenly, but conformably into Fe- and Mn-rich umbers [Robertson 1976]. This transition is inferred to reflect sudden changes in E_h during mixing between hydrothermal fluids and seawater at the mound surface, or the diagenetic remobilisation and diffusion of redox-mobile Mn [Elderfield *et al.* 1972; Robertson 1976].

The Mathiati deposit is inferred to have formed towards the margin of the Tethyan rift valley [Boyle & Robertson 1984]. The Mathiati-Margi area is one of a number of areas of the Troodos which are metal enriched at many levels within the extrusives, indicating that hydrothermalism was locally persistent [Boyle & Robertson 1984]. Umbers were dispersed over the seafloor up to *c.* 10 km from the site of high-temperature venting (marked by the Mathiati deposit), including the Margi area [Boyle & Robertson 1976]. Margi umbers have been interpreted as low-temperature proximal precipitates [Robertson 1975], as dispersed oxidised sulphides [Boyle & Robertson 1984] or alternately as distal plume fall-out [Boyle 1990]. The basal sediments at Margi resemble Mn-poor basal umbers at Skouriotissa [Robertson 1975].

Umbers are commonly altered to siliceous jasper in proximity to mineralised faults, and in mineralised stockworks beneath the ore bodies [Boyle 1990]. However, Troodos metalliferous sediments are inferred not have undergone any significant diagenetic alteration, as their radiogenic isotope ratios are analogous to those of modern metalliferous sediments, and opaline silica in the umbers is not completely recrystallised to quartz [Gale *et al.* 1981].

7.3.2 Ochres

The Skouriotissa deposit is one of the classic localities for ochreous sediments within the Troodos ophiolite [Wilson 1959; Robertson 1976; Herzig *et al.* 1991]. In the Skouriotissa Mine, ochres are interbedded with conglomeritic sulphides, and separated from overlying umbers by a gentle angular conformity [Robertson 1976; Constantinou & Govett 1973]. The ochres are compositionally and texturally diverse, ranging from fine-grained, laminated goethite (formed from amorphous Fe-oxides) to oxidised and resedimented sulphides in a matrix of coarse-grained crystalline goethite, jarosite and quartz, with amorphous Fe-oxides and traces of hematite and gypsum [Robertson 1976; Herzig *et al.* 1991]. The laminated ochres have chemistry more like umbers, and are interpreted to be low-temperature hydrothermal precipitates [Robertson 1976]. Some of the ochres contain alternating dark, Fe-oxide rich bands and lighter, jarosite-rich bands which may represent original layering in the sulphide debris [Herzig *et al.* 1991]. Some of the ochres are partly silicified and show small scale sedimentary features [Robertson 1976]. The gossanous caps

of Cyprus ore deposits have been extensively mined for precious metals [Wilson 1959]. Skouriotissa ochres exhibit gold enrichments averaging 7 ppm which are similar to TAG ochres, and a common enrichment mechanism has been implied (refer to section 3.2.7.3) [Herzig *et al.* 1991].

7.4 Sampling

Figure 7.1 shows sampling localities for the 24 metalliferous sediment and sulphide samples analysed in this study. The sulphide samples are dominated by pyrite (>95%), and show a range of textures. The ochres and umbers are fine grained and homogeneous in appearance, with the exception of the Margi umber sample (33), which has a fragmental texture and is pervasively silicified, and a metal-enriched radiolarite from Kambia (159) which contains siliceous microfossils. The sampling localities are described in the following sections.

Skouriotissa Mine

The Skouriotissa sulphide deposit is located on the northern flank of the ophiolite in the axial valley of the Solea seafloor graben identified by Varga & Moores [1985]. The Skouriotissa area contains half (*c.* 4 Mt) the total ancient slag in Cyprus, indicating that it was an important mining district in antiquity [Constantinou 1987]. The deposit was discovered in 1914 during prospective drilling by the Cyprus Mines Corporation. Production and export of ore began in 1920 [Wilson 1959]. The ore body was a flat-lying mound 671 m long and 213 m wide with a concave upper and convex lower surface, and a maximum thickness of 150 m thinning to a few metres at the mound periphery [Wilson 1959]. Over 6 Mt of massive ore was extracted from the deposit averaging 48 wt. % S and 2.5 wt. % Cu [Constantinou 1987]. Prior to mining, the Skouriotissa deposit displayed the vertical array of breccia units that is characteristic of Troodos massive sulphide deposits [Wilson 1959], and similar to that revealed during ODP drilling of the TAG mound [Humphris *et al.* 1995]. Currently the deposit is being exploited by *in situ* acid-leaching to produce copper cement with up to 65-70% Cu metal [Constantinou 1987].

Specimens of sulphide, bedded ochre and umber were sampled from an exposed section through the upper surface of the Skouriotissa ore body and additional sites in the mine (Fig.

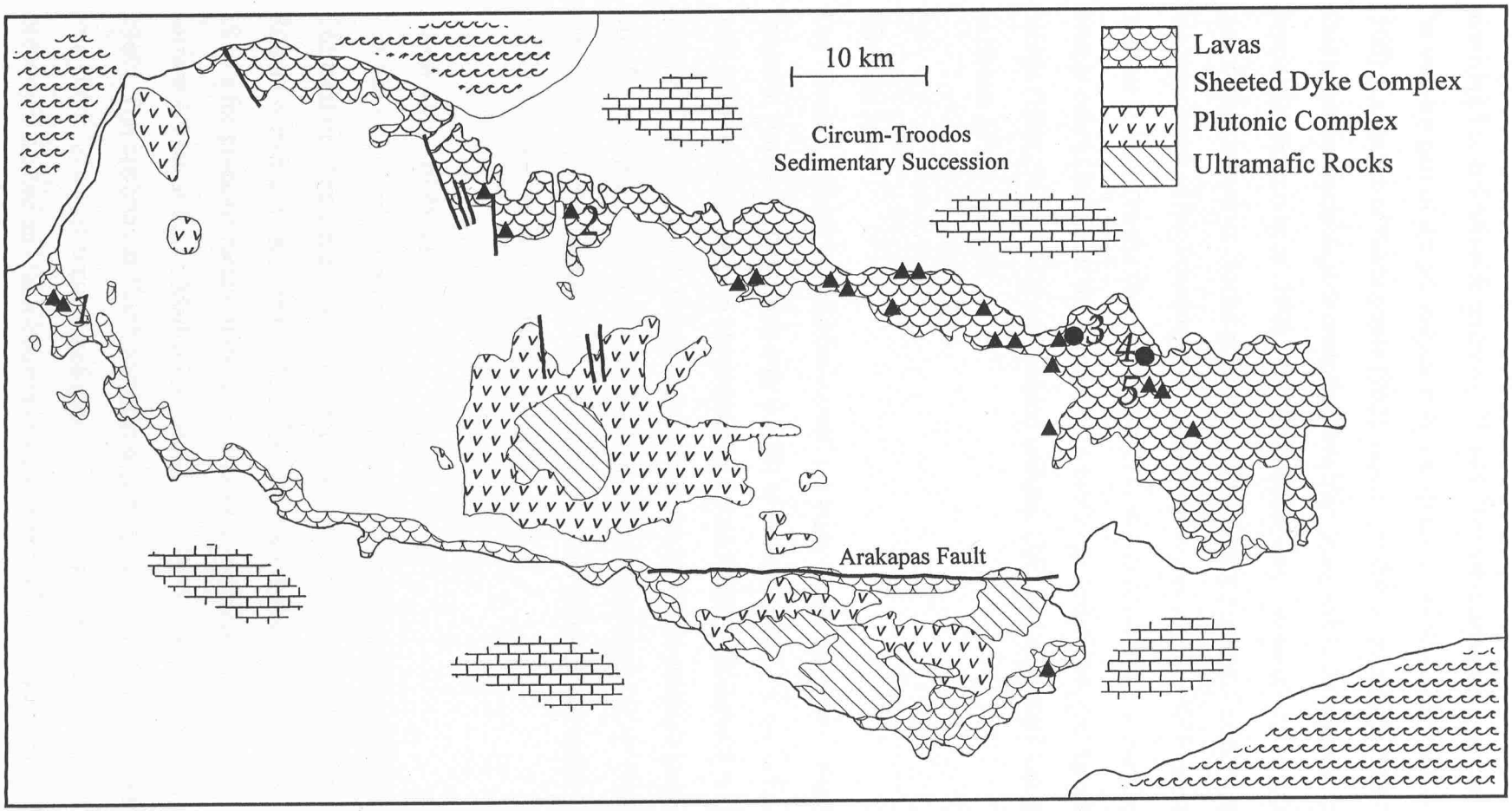

Figure 7.1: Simplified geological map of the Troodos Ophiolite, Cyprus. Sampling localities for the sulphide, umber and ochre specimens analysed in this study are indicated by triangles (mines) and circles (other localities). *1* = Kinousa Mine; *2* = Skouriotissa Mine; *3* = Kambia area; *4* = Margi area; *5* = Mathiati Mine. Black triangles show the locations of major sulphide ore bodies. Heavy lines represent high angle faults.

7.2). *In situ* quartz-pyrite ore (171) and overlying basal Fe-rich (172 and 213) and overlying Fe- and Mn-rich umbers (170 and 214) were sampled from the north margin of the western part of the pit. Adjacent to the open pit, massive (162) and colloform pyrite (168) in a matrix of sandy pyrite (163) overlain by Mn-rich umbers (169) were sampled. This sulphide assemblage is comparable to that observed in the upper *c.* 5 m of the TAG deposit [Humphris *et al.* 1995]. On the TAG mound, the sandy pyrite is being weathered out of large anhydrite blocks at the base of the Black Smoker Complex, and a similar origin has been invoked for Troodos pyrite sand [Hannington *et al.* 1998]. A piece of loose massive pyrite from the floor of the pit (211) was also collected for analysis. Massive orange ochre (165) near the contact with overlying bentonites, and light brown massive ochres (164a, 164b, 164c) and bedded umbers (167 and 166) were sampled to the northeast of the open pit.

Kinousa Mine

The Kinousa deposit is a relatively small ore body located in the northeastern part of the ophiolite complex from which only 0.3 Mt of ore averaging 2.4 wt.% Cu has been mined, with 4 Mt of *in situ* reserve ore averaging 1.5 wt.% Cu. This deposit is close to the Limni deposit (Fig. 7.1), which is the largest within the ophiolite complex and comprised *c.* 14.5 Mt of stockwork and mound sulphides [review in Hannington *et al.* 1998]. A sample of *in situ* massive pyrite (sample 179) was collected from Kinousa ore body. This ore exhibits colloform textures, with some pyritohedra.

North Mathiati Mine

The leases for both North and South Mathiati Mines are held by Cyprus Mines Corporation. There are extensive dumps of Roman slag near Mathiati village, indicative of Roman workings [Gass 1960]. Both the North and South deposits were worked during the 1930's for precious metals in the gold- and silver enriched gossan [Gass 1960]. Beneath the surface gossan at South Mathiati is a small uneconomic disseminated ore body [Gass 1960]. The ore body at North Mathiati was discovered in 1937 upon the sinking of a shaft to a 700 ft level that encountered pyrite, but was not mined until 1957 [Gass 1960]. The orebody is a tilted and fault-bounded sulphide mound 50 m wide and >250 m long [Lydon

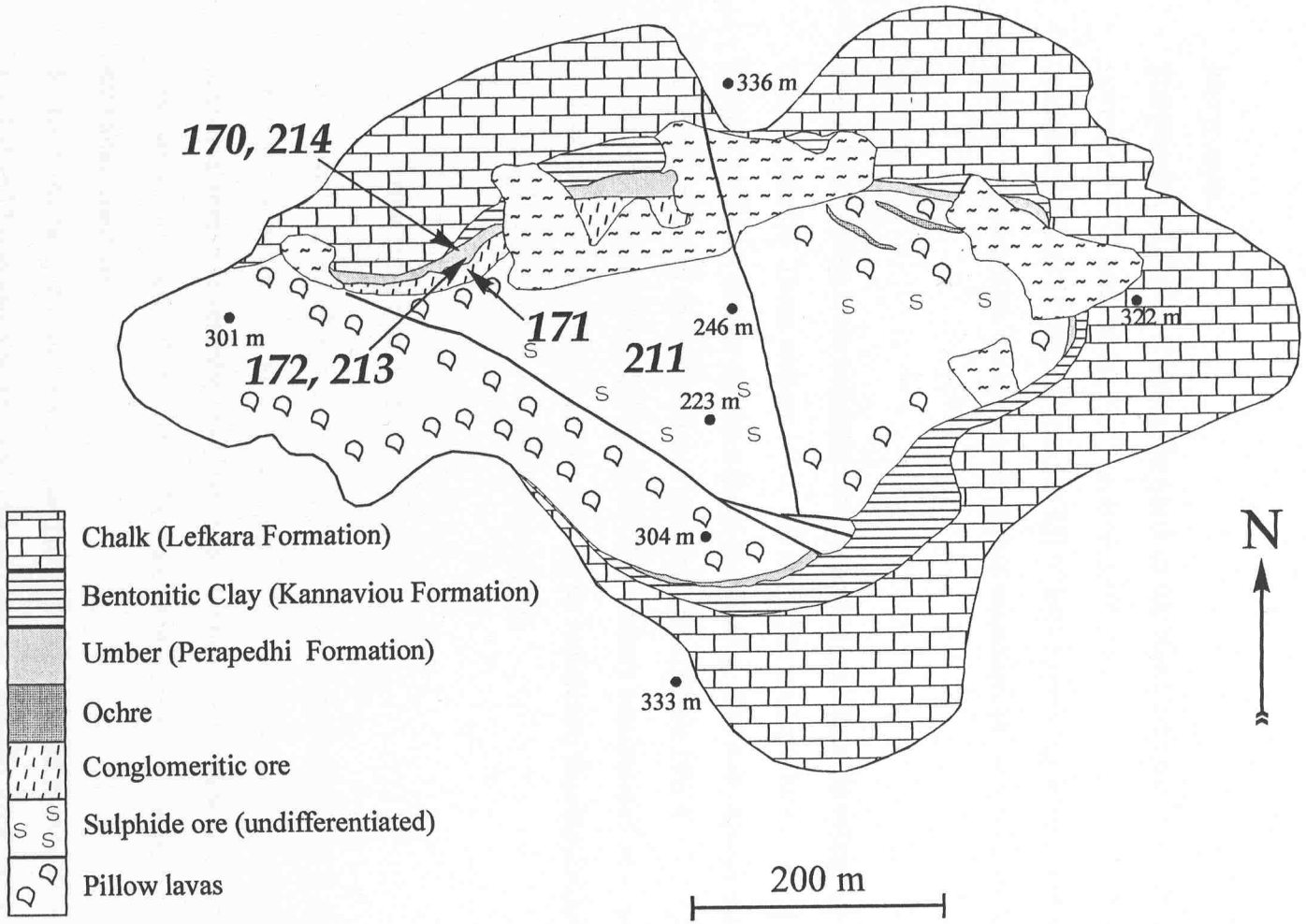

Figure 7.2: Geological map of the Skouriotissa Mine, Nicosia District after Robertson [1976]. Geological specimens collected from a section through the upper ore body in the western part of the open pit are indicated in italics. Samples 172 and 213 are Mn-poor basal umbers. Samples 170 and 214 are Mn-rich umbers. All samples were taken from *in situ* excluding sample 211. Additional sulphide, umber and ochre specimens were collected from exposure adjacent to the northwest area of the open pit. Mine slumps are indicated by the short horizontal dashed lines.

& Galley 1986]. The ore body is inferred to have formed in a fault-controlled bathymetric depression, and is overlain by unmineralised UPL [Constantinou 1980]. The sulphide mound and mineralised stockwork together contained 2.8 Mt of sulphides with 0.2 wt. % Cu. Two samples of brownish-yellow interpillow Mn-poor umber (95 and 99) were sampled adjacent to the mineralised stockwork of the North Mathiati deposit.

Margi area

The Margi area lies *c.*~5 km to the north of the North Mathiati ore body and contains extrusives (LPL and olivine-rich picrite basalts of the UPL) and high level intrusives first described by Gass [1960]. A sample (33) of light brown highly silicified Fe-rich pyrite-bearing sediment with a fragmented texture was collected from the Margi area.

Kambia area

Supra-lava umbers were collected from outcrops near Kambia village on the northern flank of the ophiolite. These umbers (116, 123 and 125) are dark brown in appearance, and contain sufficient clay to exhibit a shale-like parting. The outcrops have a rubbly appearance due to an abundance of swelling clays [Boyle 1990]. The underlying lavas are highly altered and light-green in colour. The umbers accumulated in a north-south striking fault-bounded half-graben, and are overlain by radiolarian mudstones (sample 159), then by Maastrichtian and Tertiary chalks [Boyle 1990].

7.5 Analytical methods

Whole-rock rare earth element determinations were made on *c.* 0.3 g samples of powdered metalliferous sediment and *c.* 0.5 g samples of powdered and roasted sulphide using the analytical methods described in Chapter 5. Aliquots of sulphide samples, which have low concentrations, were taken to give the maximum REE yield without overloading the cation exchange columns.

REEs in the sample solutions exceeded the LOQ as defined in section 5.5.3 except for Sm, Eu, Gd and Lu in samples 162 and 168 and Ho, Er, Tm and Yb in sample 168. These REEs were at, or above the LOD as defined in 5.5.3. Repeat analyses of the REE fraction of a Mn-rich core-top from the TAG vent field were on average accurate to within 13% of TIMS-ID values [Mills 1992] with an external precision averaging 3.3% (2σ) (refer to

Table 5.7).

LA ICP-MS REE analyses of the Margi umber (33) were performed according to the methods outlined in section 5.3.4, in order to provide spatially resolved REE analyses of the altered pyrite fragments and fine-grained Fe-oxides in this sample.

Major and trace elements were determined by XRF. Precision of major element data is 1 to 5% (2σ) for SiO_2, Al_2O_3, Fe_2O3, CaO, K_2O; 5 to 10% (2σ) for TiO_2, MnO, MgO and over 10% (2σ) for Na_2O and P_2O_5 (Table 5.10). Precision of trace element data is better than 3% (2σ) when concentrations are well above the detection limits, which range from 4 ppm (Nb, Rb, Sr and Zr) to 60 ppm (Ti) [Croudace & Gilligan 1990].

7.6 Results

Major and trace element data for the 18 sediments and 6 sulphide samples analysed in this study are shown in Table 7.1. The most comprehensive geochemical data sets for Troodos metalliferous sediments are those of Robertson [1976] and Robertson & Fleet [1976]. Robertson [1976] measured some major and trace elements (excluding the REEs) in metalliferous sediments from the Skouriotissa Mine and other localities within the ophiolite complex. Table 7.2 contains the data of Robertson [1976], along with equivalent data for the sediments analysed in this study (major elements were calculated from the XRF oxide determinations in Table 7.1). Robertson & Fleet [1976] measured REEs in metalliferous sediments associated with the Skouriotissa deposit, but did not present any major or trace element data for the same samples. There are no published REE analyses of Troodos massive sulphides.

7.6.1 Major and trace elements

Sulphides

Skouriotissa mound sulphides are dominated by Fe (48.6 to 65.7 wt.% Fe_2O_3) with Cu near, or at the limit of detection of the XRF method. The sulphides have lower As (29.6 to 89.8 ppm), and similar Pb (57.9 to 84.7 ppm) contents compared with overlying ochres (As = 142 to 361 ppm; Pb = 46.7 to 67.1 ppm). Sample 171 contains 24 wt.% SiO_2 (compared with very low levels for the other sulphides), which reflects the presence of

Table 7.1: Major and trace element data for Troodos metalliferous sediment and sulphide samples

	Skouriotissa sulphides					*Skouriotissa sediments*											*Mathiati sediments*		*Margi sediment*	*Kambia sediments*				*Kinousa sulphide*
	162	163	168	171	211	164a	164b	164c	165	166	167	169	170	172	213	214	95	99	33	116	123	125	159	179
SiO_2	0.332	n.d.	-	24.0	0.0462	3.76	3.15	2.50	4.01	64.7	5.01	12.0	9.98	14.1	14.3	15.2	1.61	32.7	87.7	10.9	19.8	n.d.	86.0	n.d.
TiO_2	0.020	n.d.	0.0066	0.025	0.013	0.049	0.016	0.023	0.022	0.046	0.044	0.14	0.13	0.17	0.18	0.16	0.028	0.15	0.05	0.088	0.15	n.d.	0.17	n.d.
Al_2O_3	0.186	n.d.	-	0.088	-	0.262	-	-	0.195	0.373	0.404	0.837	2.55	3.65	4.01	3.24	0.534	12.5	0.607	2.17	3.46	n.d.	3.58	n.d.
Fe_2O_3	65.3	n.d.	65.7	48.6	65.5	73.1	75.5	71.9	67.6	17.3	82.2	56.7	46.2	63.5	63.4	49.8	3.35	9.52	9.24	59.9	37.6	n.d.	2.62	n.d.
MnO	0.007	n.d.	0.66	0.030	0.007	0.073	0.024	0.031	0.045	-	0.088	2.0	13	2.2	2.1	16	0.24	0.42	0.069	1.5	20	n.d.	0.28	n.d.
MgO	-	n.d.	-	-	-	-	-	-	0.052	0.21	0.088	0.22	1.8	0.84	0.85	0.79	1.1	3.5	-	2.0	2.6	n.d.	1.1	n.d.
CaO	0.0332	n.d.	0.00660	0.0882	0.0198	0.125	0.0400	0.0307	0.329	0.109	0.114	0.113	6.38	0.386	0.430	0.510	48.6	16.2	0.465	6.20	1.76	n.d.	0.596	n.d.
Na_2O	-	n.d.	-	0.33	-	1.4	0.048	0.68	1.7	-	-	0.94	2.9	1.0	0.86	-	0.29	5.3	0.52	0.42	-	n.d.	0.89	n.d.
K_2O	-	n.d.	-	0.017	-	0.18	0.15	0.17	0.20	0.20	-	0.91	0.48	0.58	0.65	0.72	0.016	0.68	0.12	0.19	0.53	n.d.	0.55	n.d.
P_2O_5	0.0066	n.d.	-	0.032	-	1.2	0.61	1.1	0.55	7.5	1.6	1.0	4.1	0.58	0.56	0.39	0.075	0.053	0.25	4.0	1.1	n.d.	0.12	n.d.
SO_3	0.16	n.d.	0.21	0.03	0.30	-	0.39	0.30	-	0.61	0.47	0.45	-	0.036	-	0.49	0.51	0.068	-	-	0.24	n.d.	0.0068	n.d.
CuO	0.46	n.d.	0.020	-	-	-	0.048	0.023	0.052	0.018	0.053	0.13	-	-	-	0.29	-	-	-	-	0.035	n.d.	-	n.d.
LOI	33.6		34.0	26.5	33.9	20.5	20.1	23.2	25.2	8.9	12.2	24.6	11.7	12.9	11.8	12.0	39.5	17.9	1.9	12.6	12.5		3.2	
Total	100.1		101	99.7	99.7	100.8	100	100	99.98	100	102.6	100.01	99.5	100.1	99.2	100.0	93.1	98.8	100.9	99.9	100		99.1	
As	89.8	29.6	55.6	n.d.	-	361	142	173	171	556	244	237	356	363	134	424	7.1	7.2	70.7	387	255	294	-	95.9
Pb	-	58	57.9	n.d.	84.7	54.4	46.7	67.1	47.1	908	51.3	175.9	223.4	164.1	139.7	216.8	BDL	BDL	24.3	79.6	174	51.6	27	24.6
Zn	45.4	146	1660	n.d.	4290	710	423	377	992	40.4	468	183	316	522	533	300	22.5	64.7	49.4	303	302	454	42	1110
Mo	188	70.3	50	n.d.	17.8	38	20.1	26	32.4	61.2	44.3	12.6	33.8	49.3	68.1	32.7	-	-	-	15.2	11.4	26.6	-	9.9
Sb	-	9.2	BDL	n.d.	BDL	BDL	BDL	BDL	BDL	24.4	-	BDL	BDL	BDL	BDL	BDL	BDL	BDL	BDL	BDL	BDL	BDL	BDL	56.2
Rb	BDL	BDL	BDL	n.d.	BDL	BDL	BDL	BDL	BDL	BDL	BDL	36	16.9	20	23.3	23.8	BDL	10.1	4.9	7.3	20.6	16.3	23.4	BDL
Sr	BDL	BDL	-	n.d.	-	28.4	8.3	20.7	31.3	80.5	18.5	303	845.3	41.5	72.2	897.3	84.4	40	9.2	101	179	38.4	63.4	-
Ba	BDL	BDL	-	n.d.	45.3	BDL	BDL	-	BDL	BDL	BDL	446	1764.2	84.9	53.3	2211.6	-	-	BDL	-	1340	60.7	40.3	-
V	-	-	3.2	n.d.	4.8	1820	651	833	555	86.6	872	970	1020	778	743	851	138	419	138	2490	1120	3850	38.7	16.8
Ni	135	32.4	44.1	n.d.	141	28.8	28.8	30	38.2	15.1	62.5	153	344	338	363	343	25.3	39.3	45.5	232	247	370	52.7	172
Zr	-	-	-	n.d.	-	10.9	4.5	6.7	5.5	62.6	19.7	70.6	64.6	90.6	99.3	66	9.1	20	14.1	52.2	86.9	74.7	27.9	-
Cr	-	-	-	n.d.	-	111	46	58.5	43.2	22	72.3	52.3	44.8	39.3	33.7	51.1	BDL	22.9	50.5	74.1	125.6	132.5	42.6	-
Nb	-	-		n.d.	-	-	-	-	-	-	-	BDL	BDL	5.8	4.5	-	-	-	-	BDL	BDL	4	BDL	-
Bi	BDL	BDL	BDL	n.d.	BDL	BDL	BDL	BDL	BDL	11.3	BDL	-	BDL	BDL	BDL	BDL	BDL	BDL	-	-	BDL	-	BDL	104
Th	7.9	BDL	BDL	n.d.	BDL	BDL	BDL	BDL	BDL	-	BDL	-	BDL	BDL	BDL	BDL	BDL	-	-	BDL	BDL	BDL	BDL	50
U	-	-	-	n.d.	-	BDL	-	-	BDL	-	BDL	-	BDL	BDL	BDL	BDL	-	-	-	BDL	BDL	-	BDL	-
Y	-	-	-	n.d.	-	-	-	-	5.1	-	4.7	5.9	275	39.7	47.8	76.3	18.8	18.2	21.6	163	130	82.5	19.1	-

Major elements are in wt. %
Trace elements are in ppm
n.d. indicates element not detected
BDL indicates element below dection limit

Table 7.2: Comparison of umber and ochre data with sediment data of [§]Robertson [1976] and [‡]Robertson & Hudson [1973].

	Skouriotissa sediments											*Mathiati sediments*		*Margi sediment*	*Kambia sediments*			
	164a	164b	164c	165	166	167	169	170	172	213	214	95	99	33	116	123	125	159
Al	0.0694			0.0515	0.0988	0.107	0.222	0.676	0.965	1.06	0.857	0.141	3.30	0.161	0.575	0.915		0.946
Ca	0.0892	0.0286	0.0220	0.24	0.0781	0.0816	0.0809	4.6	0.3	0.31	0.365	34.7	11.6	0.33	4.43	1.26		0.426
Fe	25.6	26.4	25.2	23.7	6.07	28.7	19.8	16	22.2	22.2	17	1.17	3.33	3.23	20.9	13		0.915
K	0.1	0.063	0.1	0.08	0.1		0.4	0.2	0.24	0.27	0.30	0.007	0.284	0.05	0.1	0.2		0.227
Mg				0.032	0.126	0.053	0.132	1.11	0.507	0.512	0.478	0.7	2.1		1.21	1.58		0.657
Mn	0.057	0.019	0.024	0.035		0.068	1.54	10.3	1.71	1.66	12.67	0.2	0.3	0.053	1.2	15.7		0.215
Ti	0.030	0.010	0.014	0.013	0.027	0.026	0.081	0.08	0.10	0.11	0.09	0.017	0.1	0.027	0.05	0.09		0.103
Ba	BDL	BDL	-	BDL	BDL	BDL	446	1764.2	84.9	53.3	2212	-	-	BDL	-	1340	60.7	40.3
Bi	BDL	BDL	BDL	BDL	11.3	BDL	-	BDL	BDL	BDL	BDL	BDL	BDL	-	-	BDL	-	BDL
Co	645	708	508	885	198	1170	356	822	1380	1440	588	98.1	456	885	1248.3	776	1850	316
Cr	111	46	58.5	43.2	22	72.3	52.3	44.8	39.3	33.7	51.1	BDL	22.9	50.5	74.1	125.6	132.5	42.6
Mo	38	20.1	26	32.4	61.2	44.3	12.6	33.8	49.3	68.1	32.7	-	-	-	15.2	11.4	26.6	-
Ni	28.8	28.8	30	38.2	15.1	62.5	153	344	338	363	343	25.3	39.3	45.5	232	247	370	52.7
Pb	54.4	46.7	67.1	47.1	908	51.3	175.9	223.4	164.1	139.7	217	BDL	BDL	24.3	79.6	174	51.6	27
Sr	28.4	8.30	20.7	31.3	80.5	18.5	303	845.3	41.5	72.2	897	84.4	40	9.2	101	179	38.4	63.4
V	1820	651	833	555	86.6	872	970	1020	778	743	851	138	419	138	2490	1120	3850	38.7
Zn	710	423	377	992	40.4	468	183	316	522	533	300	22.5	64.7	49.4	303	302	454	42
Zr	10.9	4.50	6.70	5.5	62.6	19.7	70.6	64.6	90.6	99.3	66	9.1	20	14.1	52.2	86.9	74.7	27.9

	Skouriotissa umbers and ochres[§]						*Typical umber*[‡]	
	Mn-rich umbers		Mn-poor umbers		Ochres			
	average	*range*	*average*	*range*	*average*	*range*	*average*	*range*
Al	4.4	1.9-6.2	5.2	4.4-5.8	3.6	0.1-9.3	2.3	0.9-6.6
Ca	5.4	1.6-15.8	1.8	0.1-4.5	0.8	0.1-7.1	1.14	0.21-3.07
Fe	30.9	15.8-47.1	53.2	30.1-63	47.6	19.7-61.5	27.9	9.6-44
K	1.8	1.2-2.3	1.3	0.75-2.1	0.6	0.1-0.15	0.72	0.17-2.07
Mg	1.6	0.9-2.1	1.1	0.5-1.5	0.5	0.1-1.1	0.7	0.2-2.3
Mn	9.9	4.3-12.0	0.3	0.07-0.69	0.8	0.04-2.3	5.8	2.0-16.3
Ti	0.1	0.06-0.16	0.13	0.06-0.15	0.05	0.01-0.1	0.15	0.06-0.38
Ba	1454	756-3794	34	1-81	16	1-38	427	2-1250
Bi	20	19-24	20	15-24	9	3-16	-	-
Co	120	78-191	139	110-177	47	18-64	101	60-145
Cr	14	8-36	12	8-17	38	8-62	31	8-69
Mo	122	85-227	57	3-110	33	6-54	-	-
Ni	337	198-483	283	72-368	126	48-364	212	104-368
Pb	215	145-291	216	150-360	59	32-135	161	26-246
Sr	1316	966-1598	111	54-204	63	19-89	414	56-1200
V	419	331-781	968	529-1500	872	491-1113	755	186-1500
Zn	350	194-471	337	490-844	592	372-849	235	186-480
Zr	541	233-803	731	450-1102	272	49-134	370	65-1102

quartz in this sample. Sample 211 comprises euhedral pyrite with minor sphalerite, and is correspondingly Zn-enriched (4290 ppm). Mo concentrations are either similar, or elevated above (17.8 ppm to 188 ppm) those of overlying ochres and umbers (20.1 to 68.1 ppm). Ni concentrations in the Skouriotissa sulphides (32.4 to 135 ppm) are comparable to overlying ochres (15.1 to 62.5 ppm), but less than in the umbers (153 to 363 ppm). Chromium is below the limit of detection in the Skouriotissa sulphides, but present at concentrations between 22 ppm and 111 ppm in the overlying umbers and ochres. Sample 179 from the Kinousa Mine has a similar trace element composition to the Skouriotissa sulphides (Table 7.2).

Skouriotissa ochres and umbers

Skouriotissa ochre samples 164a, 164b, 164c and 165 have similar compositions to those from the north face of the west pit analysed by Robertson [1976] (Table 7.3). They are enriched in Fe_2O_3 (17.3 to 82.2 wt. %) and contain lower and more variable amounts of SiO_2 (2.5 to 64.7 wt. %) and MnO (0.024 to 16 wt. %). They generally exhibit lower trace element concentrations (particularly Pb, Ba, Ni and Sr) than overlying Mn-rich and Mn-poor umbers. The ochre samples analysed in this study have lower Zr contents (4.5-10.9) than those analysed by Robertson [1976] (Zr = 49 to 134 ppm), as do the umbers (Zr = 19.7 to 99.3 compared with 233 to 1102 ppm). Robertson [1976] also found Skouriotissa ochres to be enriched in Cr, V and Zn relative to Mn-rich umbers. These trends were not apparent in this sample set presented here.

Samples 166 and 167 have chemical attributes of both ochres and Mn-poor umbers, as defined by Robertson [1976]. They both have low Ni, Ba, Rb and Sr contents, which are similar to Skouriotissa ochres. Sample 166 has an ochre-like Pb content (47.1 ppm compared with 46.1 to 67.1 ppm) while Pb in sample 167 (908 ppm) is considerably greater then in the Mn-poor umbers analysed by Robertson [1976] (145 to 291 ppm) and in this study (140 to 223 ppm).

Samples 172 and 213 are basal Mn-poor umbers (1.71 and 1.66 wt. % Mn respectively) sampled approximately 15 cm below a sharp contact with overlying Mn-rich umbers (1.54 to 12.67 wt. %), represented by samples 169, 170 and 214. The Mn-poor umbers are chemically more similar to umbers than ochres, as noted by Robertson [1976]. Compared with the Mn-rich umbers, they are depleted in Mn, Ba and Sr, with higher Ni, Pb and Zr

contents than ochres.

Metalliferous sediments from the Mathiati Mine, and Margi and Kambia areas

Sample 33 from the Margi area is a Mn-poor, pervasively silicified sediment (0.05 wt. % Mn; 87.7 wt. % SiO_2) that was sampled because it displays a distinctive fragmental texture and contains partially oxidised pyrite. The high silica content cannot be attributed to the presence of terrigenous or hydrothermal clays because the Al content of this sample is low (0.161 wt. %) compared with, for example, clay-rich umbers from the Skouriotissa pit (~8 to 10 wt. % Al) [Robertson 1976]. Because this sample is not genetically related to a massive sulphide ore body, it would be classified as an umber [Robertson, 1976]. However, chemically it is more similar to ochre as it contains low levels of Ni, Ba, Rb, Pb and Sr which are comparable to the Skouriotissa ochres analysed in this study (Table 7.2).

Interpillow sediments from the Mathiati Mine (95 and 99) are Mn-poor umbers, and display the highest Ca contents of all samples analysed (48.6 wt. % and 16.2 wt. %). Robertson [1976] found that calcium is enriched in those samples that contain apatite, but the P_2O_5 contents of samples 95 and 99 are low (0.075 and 0.053 wt. % respectively). This Ca is inferred to be due to the presence of calcite, that was observed rimming the pillow interstices. Nickel, Pb and Zn concentrations are similar to, or lower than ochre compositions.

Mn-rich umber in the Kambia area (samples 116, 123 and 125) is overlain by a siliceous radiolarite (sample 159) that contains 86 wt. % SiO_2 but only 0.92 wt. % Fe and 0.22 wt. % Mn, indicating only a small input of hydrothermal Fe-rich particulates into a dominantly pelagic sediment. Compared with ochre and umber, this sediment is depleted in Pb and V.

7.6.2 Rare earth elements

Rare earth element data for the 18 sediments and 6 sulphide samples are shown in Table 7.3. The Ce anomaly, Eu anomaly and the chondrite normalised Nd/Yb ratios (Nd_n/Yb_n) have been quantified according to the methods outlined in 2.2. All ratios are shown in Table 7.3. Also shown for comparison in Table 7.3 are REE data for Atlantic and Pacific seawater [Mitra *et al.* 1994; Bau *et al.* 1996], a TAG black smoker fluid [Mitra *et al.* 1994] and mound sulphide [Mills & Elderfield 1995*a*], and various Troodos [Robertson & Fleet

Table 7.3: REE data for Troodos sulphide and metalliferous sediment samples

	La	Ce	Pr	Nd	Sm	Eu	Gd	Tb	Dy	Ho	Er	Tm	Yb	Lu	Ce/Ce*	Eu/Eu*	Nd_n/Yb_n
	all values ppm																
Skouriotissa Mine sulphides:																	
162	0.0145	0.021	0.00345	0.0151	0.00357	0.00143	0.00595	0.00114	0.00794	0.0019	0.0055	0.000632	0.0039	0.00062	0.65	0.94	1.3
163	0.101	0.14	0.0772	0.471	0.145	0.0374	0.139	0.0192	0.100	0.014	0.030	0.00406	0.013	0.0019	0.35	0.80	13
168	0.0179	0.013	0.00383	0.0147	0.00288	0.00064	0.00338	0.00050	0.00304	0.00054	0.0016	0.000074	0.0012	0.00020	0.35	0.62	4.2
171	0.556	0.24	0.146	0.623	0.138	0.0347	0.160	0.0272	0.173	0.035	0.098	0.0136	0.079	0.011	0.19	0.71	2.7
211	0.121	0.069	0.0210	0.0798	0.0146	0.00463	0.0153	0.00238	0.0155	0.0031	0.0086	0.00159	0.0086	0.0012	0.28	0.94	3.2
Skouriotissa Mine sediments:																	
164a	1.61	0.28	0.229	0.950	0.221	0.0729	0.291	0.0529	0.379	0.085	0.27	0.0415	0.28	0.044	0.087	0.88	1.2
164b	0.656	0.15	0.117	0.488	0.113	0.0371	0.142	0.0257	0.187	0.040	0.13	0.0206	0.14	0.022	0.11	0.89	1.2
164c	1.05	0.24	0.139	0.575	0.132	0.0404	0.167	0.0302	0.222	0.050	0.16	0.0247	0.17	0.027	0.12	0.83	1.2
165	1.78	0.50	0.363	1.44	0.305	0.0800	0.344	0.0625	0.419	0.085	0.24	0.0338	0.19	0.026	0.13	0.75	2.6
166	7.87	2.3	0.923	2.14	0.147	0.0238	0.254	0.0518	0.449	0.12	0.39	0.0592	0.38	0.054	0.16	0.37	2.0
167	2.71	0.95	0.687	2.57	0.588	0.150	0.693	0.128	0.879	0.19	0.59	0.0882	0.58	0.088	0.16	0.72	1.5
169	67.6	20	7.48	23.2	2.43	0.477	2.19	0.268	1.66	0.31	1.0	0.154	1.1	0.18	0.16	0.62	7.2
170	285	31	61.7	262	49.7	12.7	55.3	7.89	48.1	9.6	26	3.38	20	2.9	0.050	0.74	4.6
172	56.2	26	15.9	65.4	13.6	3.30	12.9	2.07	12.9	2.4	6.8	1.00	6.7	0.97	0.20	0.75	3.4
213	48.2	22	16.2	70.0	15.1	3.87	15.7	2.63	16.8	3.1	8.9	1.27	8.3	1.2	0.19	0.76	2.9
214	104	40	22.1	90.0	19.2	5.30	21.3	3.45	21.4	4.1	11	1.53	9.5	1.4	0.18	0.80	3.3
Mathiati Mine sediments:																	
95	3.97	2.3199	1.16	5.49	1.62	0.518	2.25	0.421	3.03	0.68	2.1	0.333	2.3	0.38	0.25	0.83	0.83
99	4.13	1.7039	1.38	6.59	1.94	0.655	2.39	0.464	3.21	0.66	2.0	0.289	1.9	0.29	0.17	0.93	1.2
Margi sediment:																	
33	17.9	6.373	4.82	20.7	4.13	1.37	4.53	0.681	4.20	0.80	2.2	0.290	1.8	0.26	0.16	0.97	4.0
Kambia sediments:																	
116	185.0	25.093	39.3	160	30.7	8.10	33.6	5.16	32.3	6.4	18	2.43	15	2.2	0.064	0.77	3.7
123	119.62	34.1690	32.8	138	29.1	7.26	29.9	4.55	27.6	5.3	14	1.90	12	1.7	0.13	0.75	4.1
125	48.56	9.8662	16.7	76.5	16.9	4.44	18.5	2.86	18.0	3.5	10	1.39	9.1	1.4	0.083	0.76	2.9
159	12.8	19.773	3.61	15.0	3.13	0.739	3.21	0.475	2.88	0.55	1.6	0.211	1.3	0.20	0.68	0.71	3.9
Kinousa Mine sulphide:																	
179	0.095264	0.11211	0.0787	0.497	0.15441	0.0391	0.145	0.0202	0.107	0.015	0.032	0.00421	0.013	0.0020	0.29	0.79	14

Table 7.3 continued: REE data for Troodos sulphide and metalliferous sediment samples

	La	Ce	Pr	Nd	Sm	Eu	Gd	Tb	Dy	Ho	Er	Tm	Yb	Lu	Ce/Ce*	Eu/Eu*	Nd_n/Yb_n
	all values ppm																
¥EPR metalliferous sediment	66.9	3.78		54.2	11.6	3.05		1.53					5.89	1.24	0.027		3.2
§Bentonitic clay 341	78.6	138.2		73	14.3	3.5		2.4				0.9	5.9	0.9	0.82		4.3
§Bentonitic clay 342	43.3	75.3		39.9	7.9	1.8		1.2				0.7	3	0.5	0.81		4.6
§Skouriotissa umber 328	100.9	43.4		91.3	18.6	4.5		2.6				0.9	6.2	0.8	0.20		5.1
§Skouriotissa umber 323	86.7	135.7		92.4	16.5	4		2.8				1	6.7	1	0.71		4.8
§Troodos umber 718	535.8	72.7		319.7	45.7	13.6		7.9				3.1	19.6	2.6	0.068		5.7
§Mathiati ochres 303	55	17.2		66.1	14.4	3.5		2				1.1	5.9	1	0.14		3.9
§Mathiati ochres 2007	17.5	13		16.9	5	1.3		0.6				0.6	2.3	0.3	0.34		2.6
§Skouriotissa ochre 2001	57.38	21.3		56.9	12.2	3.4		1.8				0.6	5.2	0.7	0.17		3.8
*Black smoker fluid	5.68E-04	1.32E-03		8.68E-04	1.87E-04	5.42E-04	1.70E-04		1.23E-04		4.93E-05		3.60E-05	4.41E-06	0.96	9.1	8.4
*North Atlantic Seawater	3.54E-06	7.62E-07		3.09E-06	6.21E-07	1.61E-07	9.83E-07		1.03E-06		9.15E-07		9.38E-07	1.54E-07	0.10	0.63	1.1
‡Pacific Seawater	5.13E-06	4.62E-07	3.71E-07	1.68E-06	3.25E-07	8.97E-08	5.65E-07	9.44E-08	7.93E-07	2.52E-07	9.03E-07	1.48E-07	1.12E-06		0.048	0.63	0.53
⁂TAG plume derived sediment	16.8	25.4		17.6	3.81	0.962	3.79		3.44		1.88		1.6		0.68	0.77	3.8
‡TAG sulphidic sediment	5.91	8.46		6.49	1.46	1.027	1.366		1.368		0.818		0.731	0.097	0.64	2.2	3.1
#TAG mound ochre	1.44	3.88		3.63	1.04	2.72	0.709		0.463		0.191		0.164	0.0212	0.94	9.2	7.7
#TAG mound ochre	3.73	9.25		13.5	3.25	9.71	1.93		1.2		0.496		0.366	0.0346	0.74	11	13
#TAG mound sulphide	0.0098	0.0118		0.0081	0.0016	0.0034	0.0017		0.0017		0.0013		0.0012		0.57	6.3	2.4
○TAG mound ochre (upper core)	3.17	6.96	0.997	4.91	1.18	1.4	0.954	0.138	0.743	0.141	0.373	0.048	0.321	0.048	0.92	4.0	5.3
○TAG mound ochre (upper core)	14.9	26.6	3.98	18.4	3.9	3.41	3.68	0.538	3.1	0.663	1.87	0.249	1.56	0.252	0.80	2.7	4.1
○TAG mound ochre (lower core)	0.365	0.934	0.157	0.912	0.266	0.897	0.204	0.03	0.14	0.022	0.057	0.008	0.046	0.008	0.92	12.0	6.9
○TAG mound ochre (lower core)	0.643	1.94	0.306	1.84	0.594	1.39	0.417	0.05	0.238	0.042	0.108	0.014	0.09	0.013	1.00	8.2	7.1

§Data are from Robertson & Fleet [1976]. Samples 328 and 323 represent the range in REE content of Skouriotissa umbers. Samples 303 and 2007 represent the range in REE content of Mathiati ochres.

¥Data are from Ruhlin & Owen [1986]. Sample 598-5-6, 58-60 cm is a 15.9 Myr sediment sampled 9 km from the palaeo-rise crest.

*Data from Mitra *et al.* 1994; black smoker fluid data is recalculated to Mg=0, white smoker is recalculated to Mg = 4 mmol kg^{-1}. Seawater data is for TAG (3400 m)

‡Data from Bau *et al.* 1996; average of six samples from between 1000 - 2000 m depth

⁂Data are from Mills [1992]; sediment core collected *c.* 2 km NNE of the active TAG mound

‡Data are from German *et al.* [1993]; *Alvin* sediment core 2182-4 collected from the periphery of the TAG mound.

#Data are from Mill & Elderfield [1995]

○Data from Goulding *et al.* [1998]

1976], EPR [Ruhlin & Owen 1986] and TAG metalliferous sediments [Mills 1992; German *et al.* 1993; Goulding *et al.* 1998]. The REE systematics of these fluids and hydrothermal precipitates are described in Chapter 2 of this dissertation.

Existing REE data for Troodos umbers are plotted in Fig. 7.3a [Robertson & Fleet 1976]. They are strongly enriched in REEs relative to normal pelagic clays and exhibit seawater dominated REE patterns with large negative Ce anomalies (Ce/Ce* = 0.068-0.71), and are more similar to EPR (Ce/Ce* = 0.027) than TAG plume-derived sediments (Ce/Ce* = 0.68). Bentonitic clays that overlie the umbers have greatly reduced Ce anomalies due to the incorporation of greater amounts of detrital clays, which do not possess any Ce anomaly [Robertson & Fleet 1976]. These REE patterns have been interpreted to reflect REE uptake from seawater during particle sedimentation on the seafloor [Corliss *et al.* 1971; Robertson & Fleet 1976].

Existing REE data for Troodos ochreous sediments genetically associated with the seafloor-weathered caps of Cyprus ore bodies are plotted in Figure 7.3b [Robertson & Fleet 1976; Herzig *et al.* 1991]. Herzig *et al.* [1991] reported large positive Eu anomalies in a partially oxidised seafloor gossan at the top of the Skouriotissa ore body, that is inferred to be a vent fluid signature. However, ochres analysed by Robertson & Fleet [1976] have seawater-derived REE patterns, albeit with lower REE abundances than the umbers.

Skouriotissa and Kinousa sulphides

Chondrite normalised REE patterns for the sulphides analysed in this study are shown in Fig. 7.4. In the absence of any REE data for Tethyan seawater (refer to discussion in section 2.11), Atlantic and Pacific seawater compositions are plotted for comparison [Mitra *et al.* 1994; Bau *et al.* 1996]. The REE content of a typical TAG mound sulphide is also shown [Mills & Elderfield 1995*a*].

The REE patterns of the Skouriotissa and Kinousa sulphides from Cyprus ore are strikingly different to TAG mound and other oceanic sulphides. Pristine sulphides from active mid-ocean ridge settings typically contain extremely low REE contents with chondrite normalised patterns that largely reflect the parental fluid compositions (refer to section 2.6) [e.g. Mills & Elderfield 1995*a*]. Troodos sulphides have elevated REE

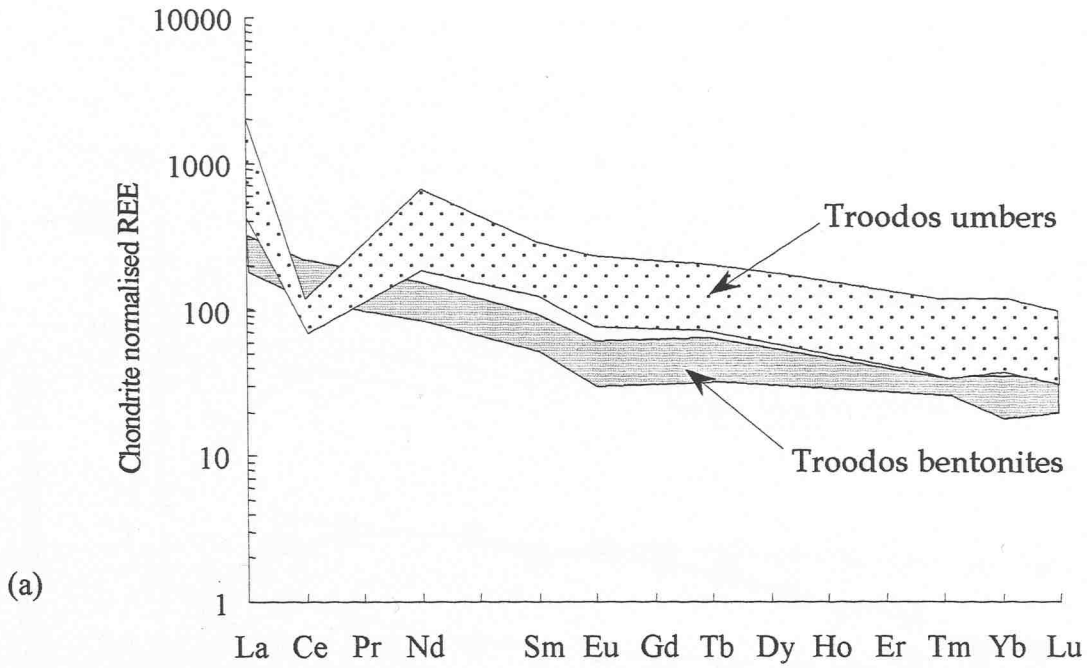

(a)

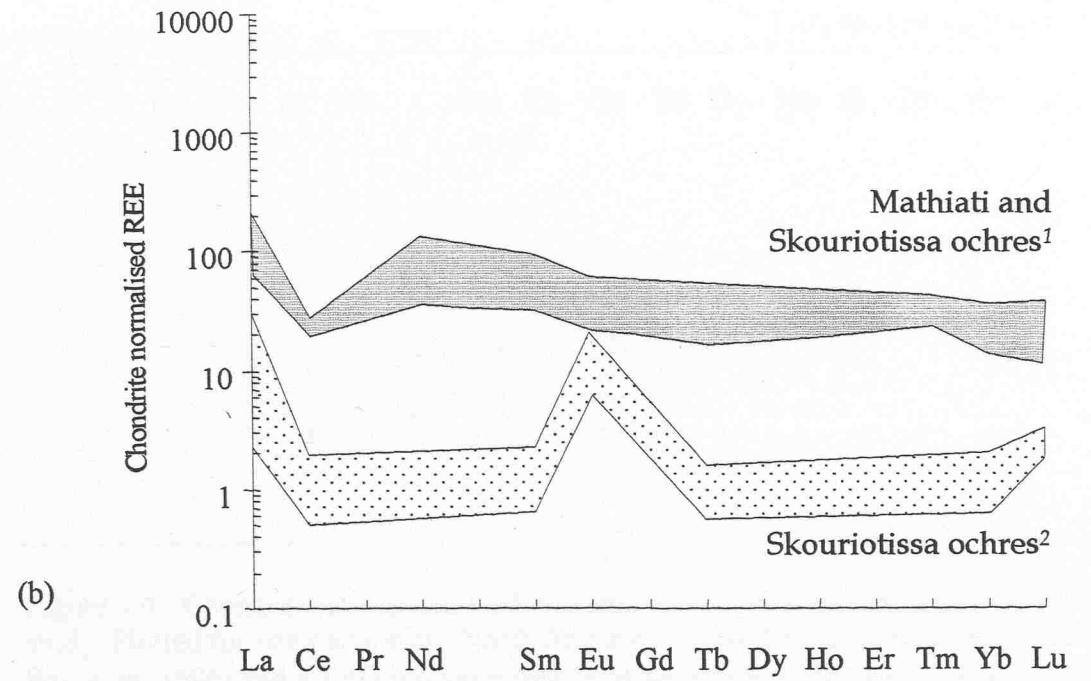

(b)

Figure 7.3 (a) & (b): Published REE data for (a) Troodos umbers and overlying bentonitic clays. Data are from Robertson & Fleet [1976] and Robertson & Hudson [1973] (b) Troodos ochres. Data are from [1]Robertson & Fleet [1976] and [2]Herzig *et al.* [1991]

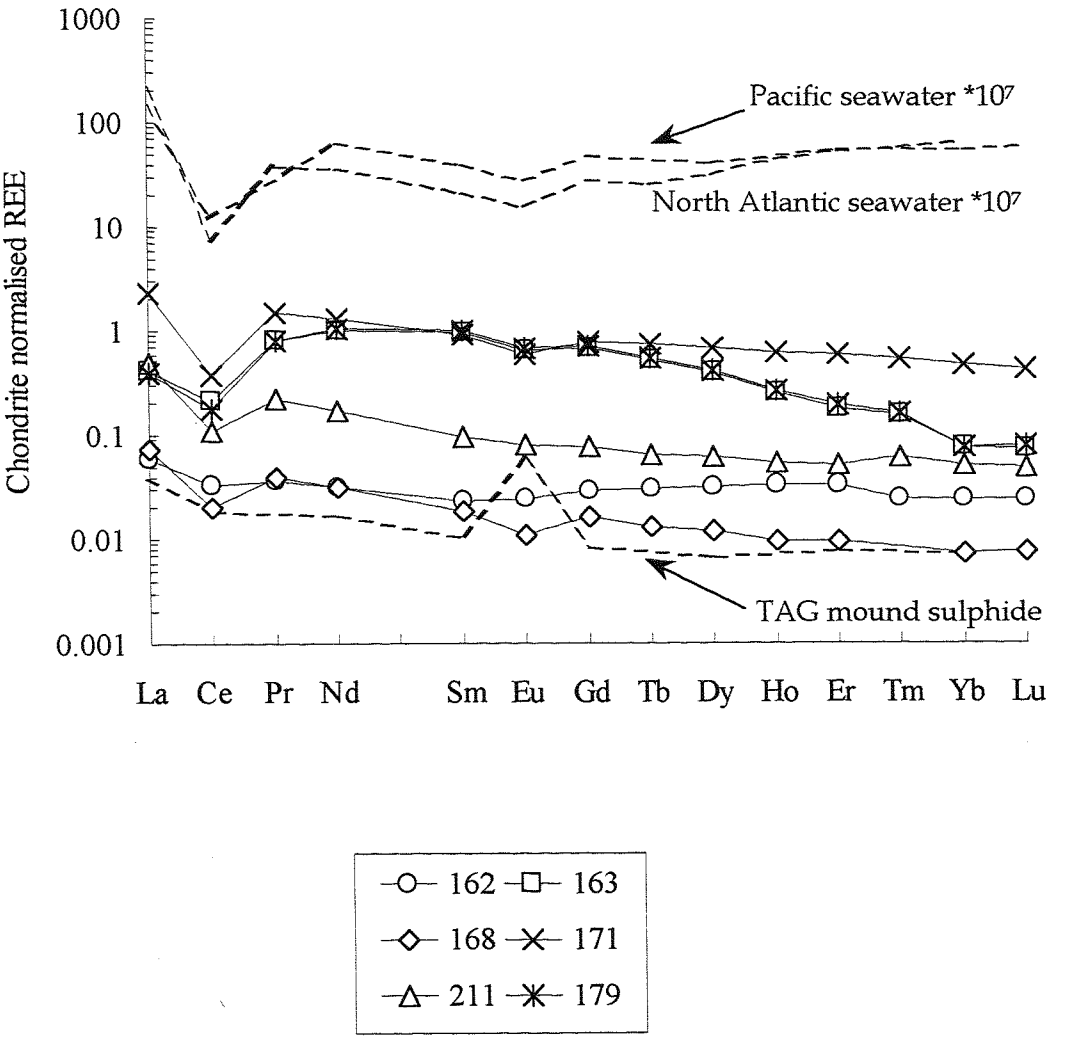

Figure 7.4: Chondrite normalised REE patterns for the sulphide ores analysed in this study. Plotted for comparison are North Atlantic and Pacific seawater [Mitra *et al.* 1994; Bau *et al.* 1996] and a TAG mound sulphide composition [Mills & Elderfield 1995*a*]. All sulphides are from Skouriotissa Mine, excluding sample 179 (Kinousa Mine). Compared with TAG mound sulphides, Troodos sulphides have elevated REE concentrations, no Eu anomaly and a pronounced negative Ce anomaly, demonstrating the influence of seawater-derived REEs.

concentrations (Nd = 0.0147 to 0.623 ppm) relative to a TAG mound sulphide (Nd = 0.0081 ppm) and have pronounced negative Ce anomalies (Ce/Ce* = 0.19 to 0.650), demonstrating the influence of seawater REEs. None of the sulphides analysed show the striking Eu enrichment that is characteristic of TAG and many other modern oceanic sulphides. Recrystallised quartz-pyrite ore (171) and pyrite ore (211) from the Skouriotissa deposit have high REE abundances (Nd = 0.623 and 0.0798 respectively) and REE patterns that are indistinguishable from Troodos umbers and ochres. Colloform (168) and massive pyrite (162) from the upper ore body contain lower levels of REEs (Nd = 0.0147 and 0.0151 ppm) than the pyrite-silica ore. The sandy pyrite (163) contains similar levels of REEs (Nd = 0.471 ppm) as the pyrite-silica ore, and has a REE composition which is identical to colloform pyrite from Kinousa Mine (179). These two samples are particularly enriched in the middle REEs and have higher Nd_n/Yb_n ratios (14 and 13 respectively) than the other sulphides (Nd_n/Yb_n = 4.2 to 1.3).

Metalliferous sediments

Chondrite normalised REE patterns for all umbers and ochres from the Skouriotissa Mine are shown in Fig. 7.5. The most striking feature of the REE concentration data is that it discriminates between the umbers (both Mn-rich and Mn-poor) and ochres. The umbers are enriched in REEs up to three orders of magnitude over ochre contents, consistent with their generally higher trace element concentrations (Table 7.2). Samples 166 and 169 show a slight enrichment in the LREE over the HREE (Nd_n/Yb_n = 7.2 and 2) and are somewhat depleted in the middle REEs.

Excluding samples 166 and 169, the umbers and ochres have similar REE patterns with pronounced negative Ce anomalies (Ce/Ce* = 0.087 to 0.2), that are more similar to EPR (Ce/Ce* = 0.027) than TAG plume-derived sediments (Ce/Ce* = 0.68). The umbers and ochres exhibit similar LREE enrichments to EPR and TAG plume-derived sediments (Nd_n/Yb_n = 3.2 and 3.8 respectively), although the umbers (Nd_n/Yb_n = 4.6 to 2.9) tend to be more LREE enriched than the ochres (Nd_n/Yb_n = 2.6 to 1.2).

Chondrite normalised REE patterns for umbers from other sampling localities are shown in Fig. 7.6. Umbers from the Kambia area have similar REE patterns to the Skouriotissa umbers, but exhibit larger negative Ce anomalies (Ce/Ce* = 0.064 to 0.13). The overlying radiolarite has lower REE concentrations, and a reduced Ce anomaly (Ce/Ce* = 0.68),

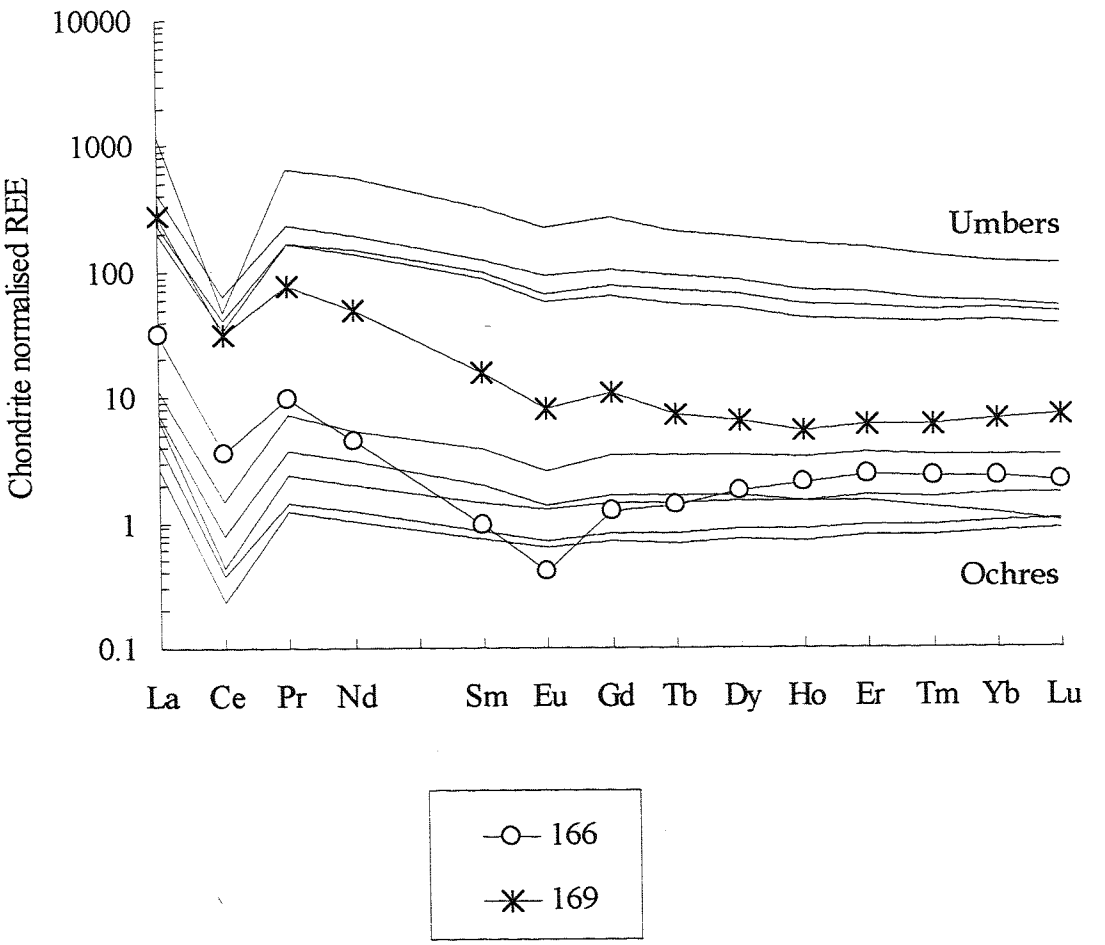

Figure 7.5: Chondrite normalised REE patterns for umbers and ochres from the Skouriotissa Mine. The REE data discriminate between umber and ochre, as REE concentrations in the umbers are up to 1000 times greater than ochre samples.

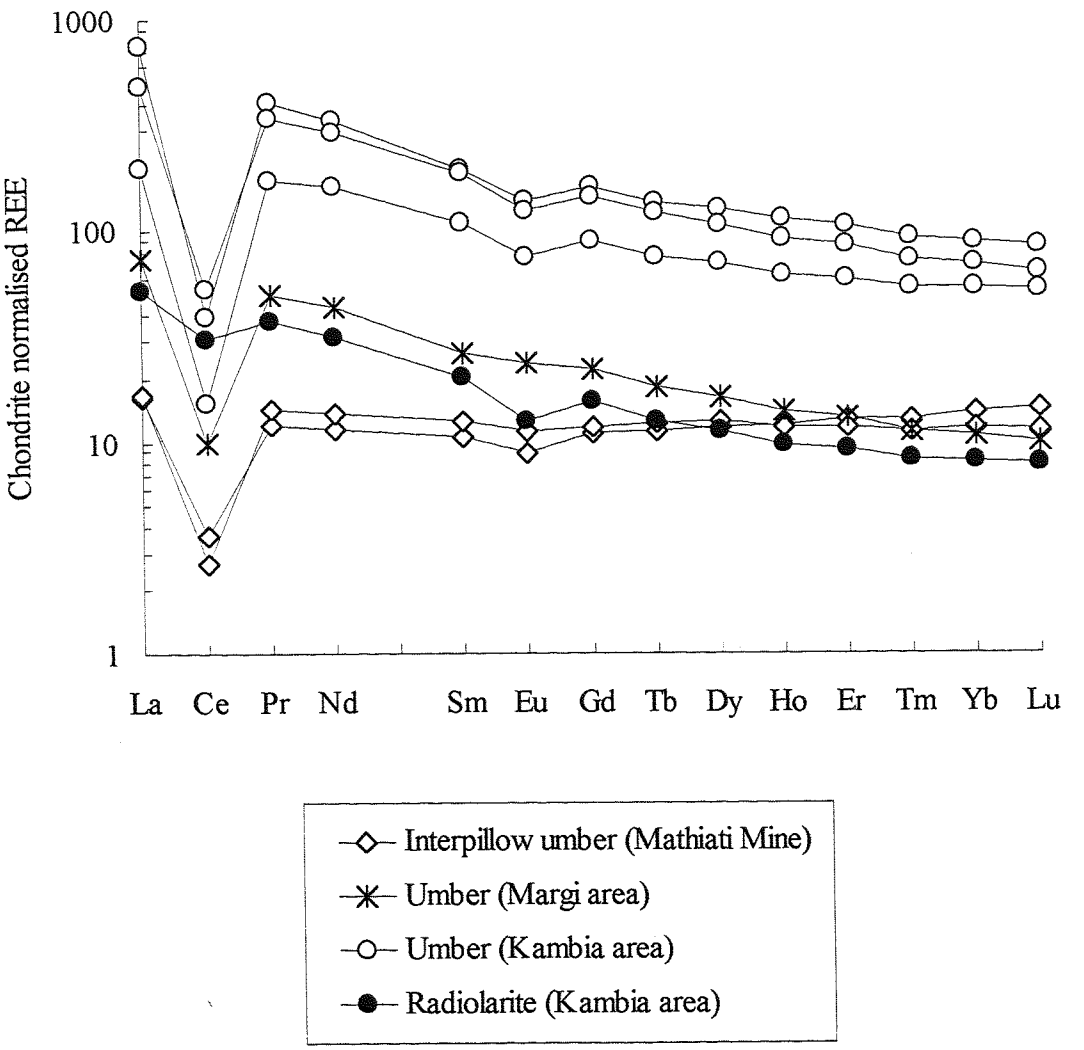

Figure 7.6: Chondrite normalised REE patterns for metalliferous sediments from Mathiati mine, and the Margi and Kambia areas.

reflecting inputs of detrital REEs with flatter REE distribution patterns.

Interpillow sediments adjacent to the mineralised stockwork at Mathiati Mine are enriched in Si, Al and Mg (presumably reflecting the presence of detrital or hydrothermal clays) and are depleted in REEs compared with typical umbers. They show a pronounced HREE enrichment (Nd_n/Yb_n = 0.83 and 1.2) and have somewhat reduced Ce anomalies (Ce/Ce* = 0.25 and 0.17) compared with the other sediments analysed in this study (Nd_n/Yb_n = 7.2 to 1.2; Ce/Ce* = 0.05 to 0.20).

The Margi sediment (33) contains much lower REE concentrations (Nd = 20.7 ppm) than typical Troodos umbers (Nd = 319.7 ppm) [Robertson & Fleet 1976], although it is similarly LREE enriched (Nd_n/Yb_n = 4 compared with 5.7). The low REE abundances in this sample are consistent with a trace element composition which is reminiscent of ochre rather than umber compositions (section 7.8.1). This sample exhibits a slight Eu-enrichment (Eu_n/Sm_n = 0.88) compared with typical umber compositions (Eu_n/Sm_n = 0.79). Unlike the other sediments, this sample has a heterogeneous, fragmental texture. In order to investigate its origin, spatially resolved REE analyses for this sample were obtained by LA ICP-MS. As no micro-scale compositional data were available for this sample, the LA ICP-MS REE data were calibrated using a NIST 610 SRM without an internal standard. Without internal standardisation of the data set, measured REE concentrations may be subject to an order of magnitude inaccuracy although inter-element ratios will be broadly unaffected (refer to section 5.3.4). The chondrite normalised LA ICP-MS REE patterns for sample 33 are shown in Fig. 7.7. The whole rock REE pattern, a typical umber [Robertson & Fleet 1976] and a TAG sulphidic sediment [German *et al.* 1993] are plotted for comparison. The LA ICP-MS REE data indicate that the sediment is composed of materials with a range of REE patterns. The fragmented layers in this sediment contain partially oxidised pyrite, and exhibit pronounced positive Eu anomalies (Eu/Eu* up to 2 compared with 0.97 for the whole rock) and smaller Ce anomalies than the whole rock (Ce/Ce* up to 0.27 compared with 0.16). These patterns resemble TAG sulphidic sediment (albeit with a more pronounced negative Ce anomaly). The fine-grained Fe-oxide sediment matrix is more Ce-depleted and Eu-depleted, and closely resembles the whole rock REE pattern. The fine-grained Fe-oxides appear to have higher REE levels, but this might be an artefact of the LA ICP-MS technique. For example, the sulphidic and Fe-oxide materials might have different ablation characteristics, perhaps related to

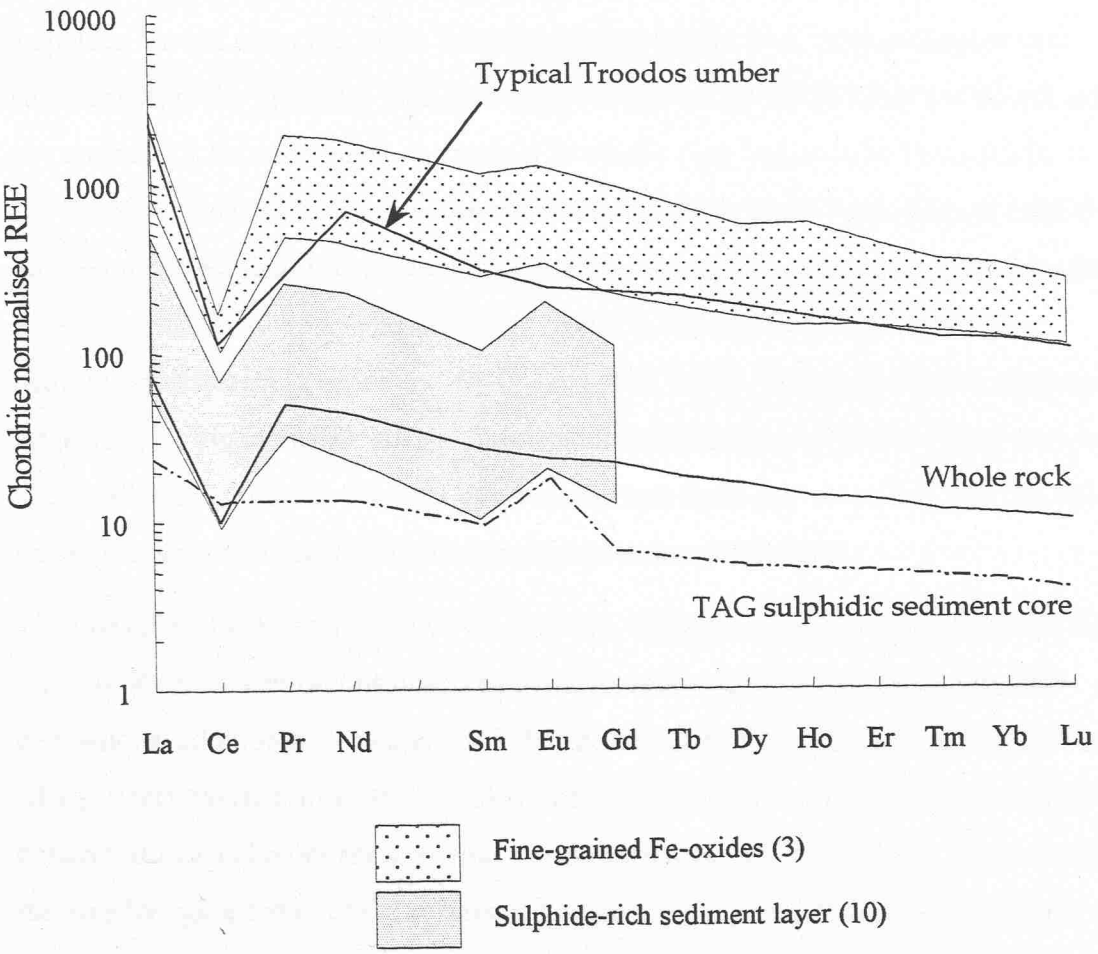

Figure 7.7: Chondrite normalised LA ICP-MS REE data for umber sample 33 from the Margi area. The numbers in parentheses indicate the number of analyses defining each compositional field. The whole rock REE pattern of sample 33 is shown for reference. Fine-grained Fe-oxides in this sample have REE patterns similar to a typical Troodos umber analysed by Robertson & Fleet [1976]. Sulphide-rich layers in sample 33 have REE patterns with a small positive Eu anomaly, and negative Ce anomaly indicative of the influence of seawater and hydrothermal fluid REEs. A similar REE pattern is observed in layers in a TAG mound sediment core (2182-4) which contain slumped sulphides in a matrix of plume-derived Fe-oxyhydroxides (data are from German *et al.* [1993]).

heterogeneous silicification of the sediment.

7.7 Discussion

7.7.1 Skouriotissa & Kinousa sulphides

The vent fluid-like patterns with large Eu enrichments that are characteristic of TAG sulphides are not observed in the Troodos sulphides (Fig. 7.4). Unconsolidated vent sulphides from the Snake Pit vent field on the MAR are LREE enriched but do not exhibit any anomalous Eu enrichment, in contrast to nearby high-temperature fluids [Gillis *et al.* 1990]. At the Snake Pit site, the absence of a Eu anomaly in the hydrothermal sulphides is inferred to reflect their precipitation from a fluid with a REE composition that is buffered by extensive modification *via* seawater entrainment in the shallow subsurface of the hydrothermal system [Sverjensky 1984; Gillis *et al.* 1990]. Consequently, the absence of large positive Eu anomalies in sulphides from Skouriotissa and Kinousa Mines does not necessarily imply that the Troodos mineralising vent fluids did not contain the anomalous Eu-enrichments that are ubiquitous in modern black smoker fluids.

The presence of a distinct negative Ce anomaly, the lack of any Eu-enrichment and the wide range of REE concentrations observed in the Troodos sulphides suggests that post-depositional addition of seawater REEs has occurred, and overprinted any original vent fluid REEs. Recrystallised ores from the Skouriotissa deposit (171 and 211) have elevated REE concentrations and more seawater-like Ce anomalies compared with the colloform and the massive 'conglomeritic' ore. The Troodos sulphides are scarcely altered or oxidised, which is not consistent with prolonged contact with seawater at the seafloor. Rather, seawater REE uptake is inferred to have occurred during pyrite recrystallisation within the sulphide mound. This interpretation is backed up by textural evidence for recrystallisation, which by analogy with the active TAG mound is inferred to be associated with seawater ingress and a subsequent drop in redox potential and pH during zone refinement of the deposit (refer to section 3.2.4) [e.g. Tivey *et al.* 1995; Edmond *et al.* 1995; Humphris *et al.* 1995]. At TAG, continued mineralisation within the sulphide mound results in evolution of the hydrothermal fluid *via* preferential discrimination of the LREEs [Mills & Elderfield 1995*a*]. The variable LREE and HREE enrichment of the Troodos sulphides suggests that also in the ancient setting, sulphide recrystallisation was associated with continued mineralisation that fractionated the REEs.

The similarity of the REE patterns in sulphide sand from the Skouriotissa deposit and a colloform pyrite ore from the Kinousa deposit indicates that processes of sulphide mineralisation and/or recrystallisation were comparable between these isolated mineralising systems.

7.7.2 Metalliferous sediments

Major and trace elements

In a combined mineralogical and geochemical study of hydrothermal sediments from the Mathiati-Margi area, Boyle [1990] found that the sediment compositions can be explained in terms of relatively few chemical components: volcanic debris, Mn- and Fe-oxides, silica and apatite. Rather than adopting the mineralogical source approach of Boyle [1990] the geochemical data presented in this chapter have been evaluated in terms of geochemical proxies determined from studies of modern ocean-ridge metalliferous sediments.

Major element data for alteration clays in Troodos lavas are scarce, but the published data are included in the following element plots. A positive correlation between SiO_2-TiO_2, TiO_2-Al_2O_3 and Al_2O_3-SiO_2 (Fig. 7.8a-c) in the majority of the sediments indicates that most of the Si, Al and Ti are within a relatively invariant aluminosilicate component. Figure 7.8a shows that most samples possess TiO_2/SiO_2 ratios similar to those of Troodos volcanic glasses (*c.* 0.013), which are presumed to be free from the effects of secondary alteration [Rautenschlein *et al.* 1985]. Secondary illite formed by hydrothermal alteration of the volcanic lavas exhibits somewhat lower TiO_2/SiO_2 ratios (*c.* 0.0023) than pristine basalts [Richards *et al.* 1989]. It is therefore inferred that most of the Al, Ti and Si in the metalliferous sediments represents locally-derived lava detritus, which in some sediments is observed to be converted to smectite [Robertson 1975; Robertson 1976], and has similar Al/Si ratios to pristine basalts (Fig. 7.8b) [Richards *et al.* 1989]. Samples 166 (bedded umber from Skouriotissa Mine), 33 (inter-lava umber from the Margi area), 159 (radiolarian mudstone from the Kambia area) and 99 (interpillow sediment from Mathiati Mine) are enriched in Si, and lie off the trend defined by the other samples in Fig. 7.8a. While the Si enrichment of sample 159 can be attributed to the presence of siliceous microfossils, a hydrothermal origin is implied for Si enrichments in the other samples. The

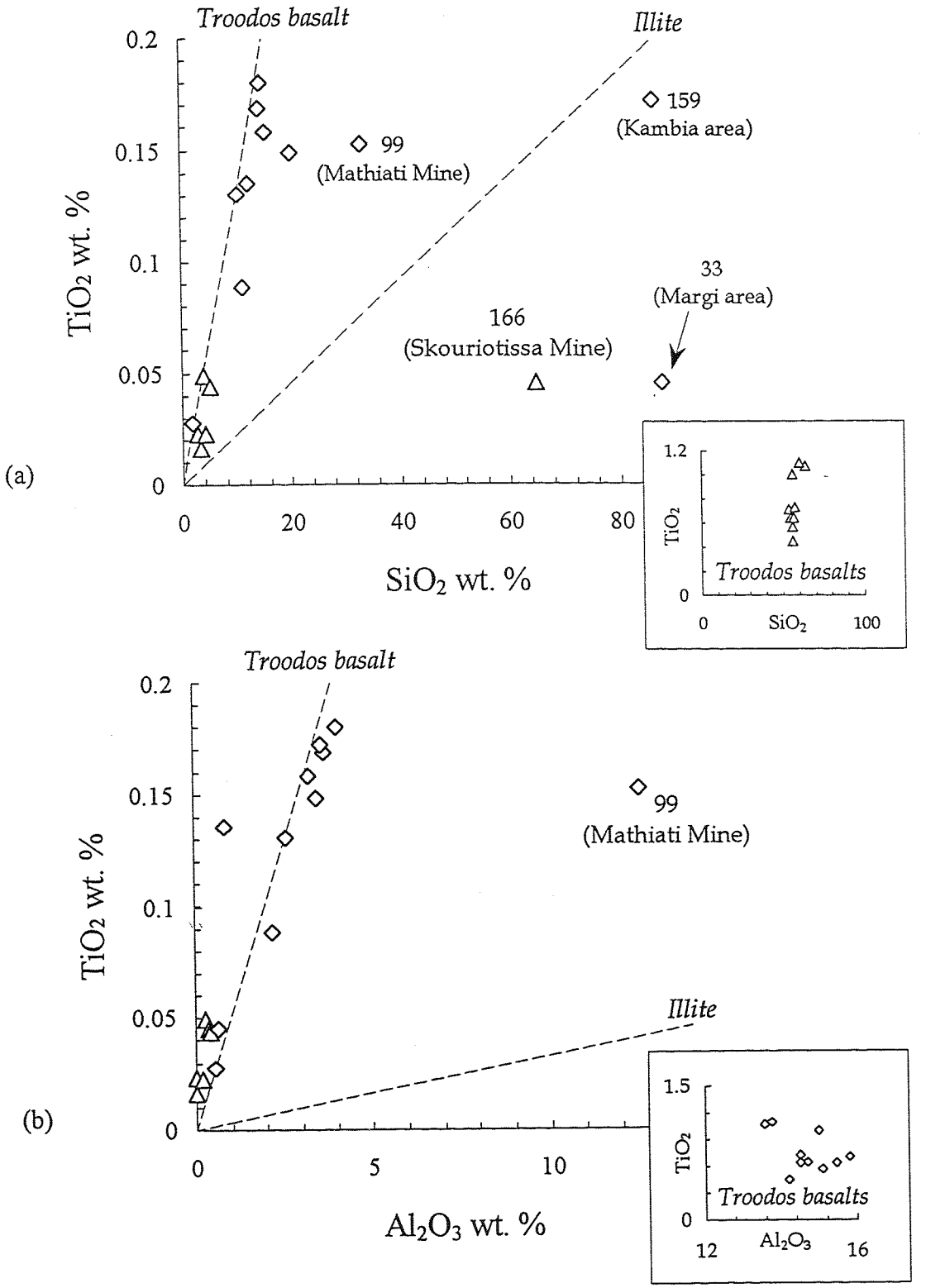

Figure 7.8 (a) & (b): Relationship between TiO_2 and (a) SiO_2 and (b) Al_2O_3 content in Troodos umbers (diamonds) and ochres (triangles). Insets show Troodos basalt compositions from glass analyses by Rautenschlein *et al.* [1985]. Secondary clay data are from Richards *et al.* [1989]. Marked samples are discussed in the text.

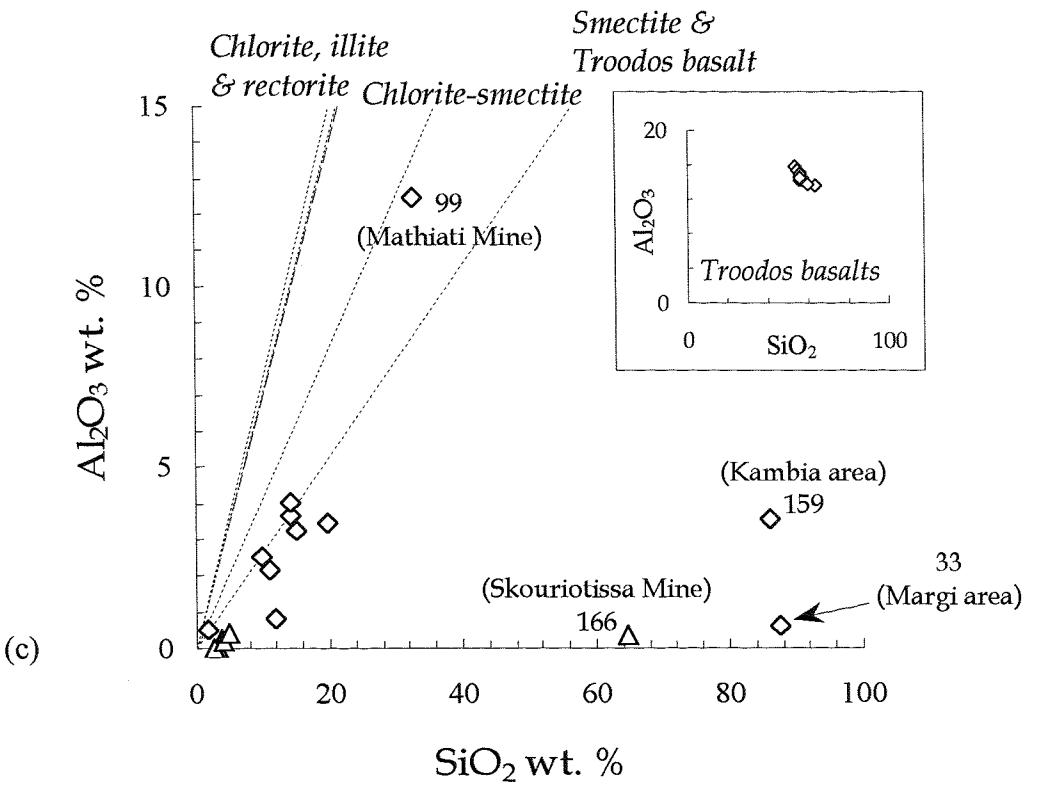

Figure 7.8 (c): Relationship between Al_2O_3 and SiO_2 in Troodos umbers (diamonds) and ochres (triangles). Inset shows Troodos basalt compositions from glass analyses by Rautenschlein *et al.* [1985]. Secondary clay data are from Richards *et al.* [1989]. Marked samples are discussed in the text.

nature of the Si enrichment is clarified by inspection of the TiO_2-Al_2O_3 and Al_2O_3-SiO_2 correlations (Figs. 7.8a & b). Figure 7.8b shows that excluding sample 99, the Ti and Al contents of the sediments is consistent with the presence of detrital clays which have similar Ti/Al ratios to Troodos basalts. It can therefore be inferred that the Si enrichments in samples 33 and 166 are not due to the presence of hydrothermal clays (such as illite, shown in Fig. 7.8b), as these have Ti/Al ratios that are lower than Troodos basalts. Sample 33 from the Margi area has a fragmental texture and is pervasively silicified, indicating that silicification was late-stage, possibly related to alteration by a Si-rich hydrothermal fluid. Sample 99 has a lower Ti/Al ratio that is lower than Troodos basalts (Fig. 7.8b). Fig. 7.8c shows that this may be due to the presence of secondary chlorite-smectite in this sample, which has a Al_2O_3/SiO_2 ratio of *c.*0.4, compared with 0.26 for Troodos glasses. This interpretation is consistent with the higher Mg content of sample 99 (2.1 wt. %) compared with the other sediments (0 to 1.58 wt.%; Table 7.3).

Figures 7.9a & b investigate the extent to which the LREE/HREE fractionation of the sediments correlates with detrital volcanic content, that can be represented by either the SiO_2 or TiO_2 content on the basis of the relationships observed in Figs. 7.8a & c. It is not possible to include any published data in Figs. 7.9 to 7.12, because there are no Troodos sediments for which major, trace and REE element data have been presented. The Nd_n/Yb_n ratios of the sediments generally increase with TiO_2 content, although the data show a large amount of scatter (Fig. 7.9a). There is a more significant correlation between SiO_2 content and Nd_n/Yb_n ratio (shown in Fig. 7.9b), although the Si-enriched samples discussed above plot separately on this graph. From Figs. 7.9a & b it can be inferred that the detrital component of the sediments is relatively LREE enriched (higher Nd_n/Yb_n ratios) compared with pristine Troodos basalts. The implication of this observation is that while the Ti, Al and Si contents of lava detritus have not been altered during sedimentation, the REEs have undergone some fractionation to compositions with higher Nd_n/Yb_n ratios. This is further investigated Figs. 7.10a & b, in which the TiO_2 content of the sediments (representing the detrital basalt component) is plotted against Nd content. A line representing the composition of pristine Troodos basalt is plotted for comparison [data from Rautenschlein *et al.* 1985]. The data exhibit a large amount of scatter. Figure 7.10a shows that the ochres and interpillow sediments contain less lava detritus (lower TiO_2) than the umbers, and plot more closely to the line representing an average Troodos basalt

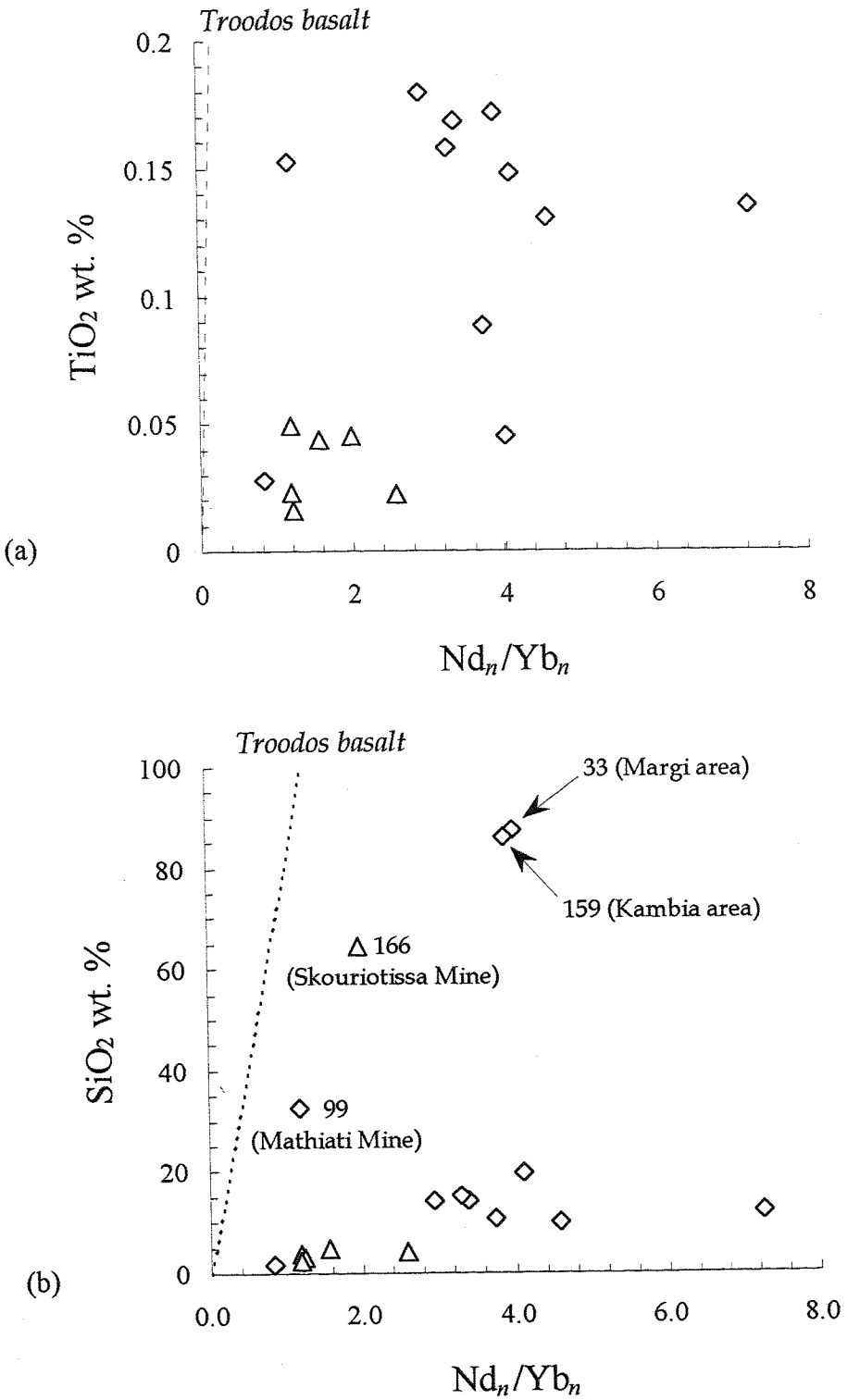

Figure 7.9 (a) & (b): Relationship between the chondrite normalised Nd/Yb ratio and (a) TiO_2 and (b) SiO_2 content in Troodos umbers (diamonds) and ochres (triangles). Troodos basalt compositions are from glass analyses by Rautenschlein *et al.* [1985]. Marked samples are discussed in the text.

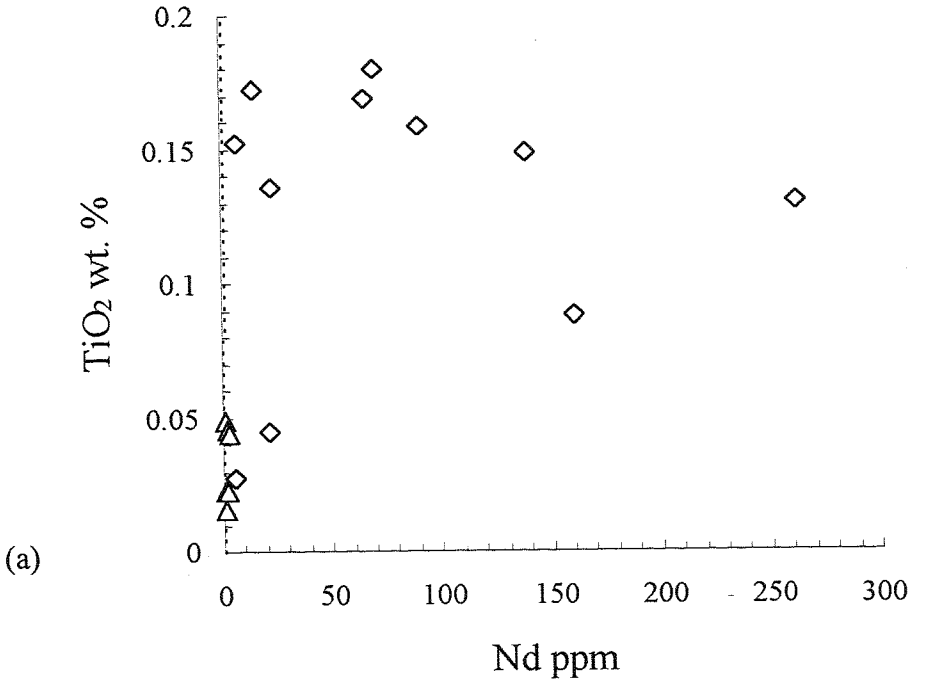

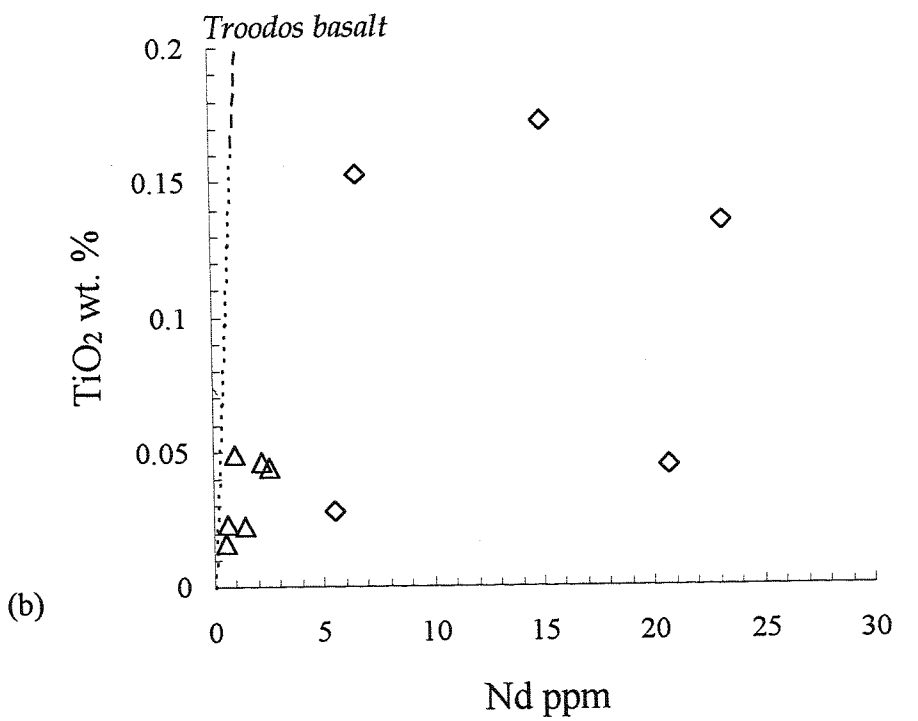

Figure 7.10 (a) & (b): Relationship between TiO_2 and Nd content for (a) all umber (diamonds) and ochre (triangle) samples (b) Expansion of Fig. 7.10a to include only those samples with <30 ppm Nd. Troodos basalt compositions are from glass analyses by Rautenschlein *et al.* [1985].

composition. This plot is expanded in Fig. 7.10b to show only those samples with <30 ppm Nd, which are mostly ochres. Figure 7.10b shows that the ochres lie to the right of the Troodos basalt line. Consequently there must be another source of Nd to the lava detritus in addition to basaltic REEs. The whole rock-REE patterns of the ochres are seawater-like (Fig. 7.5). This suggests that the increased Nd_n/Yb_n ratios of the lava detritus over pristine Troodos basalts compositions (illustrated in Fig. 7.9b) is due to the incorporation of LREEs (including Nd) from seawater. In Fig. 7.10a the umbers plot away from the line representing Troodos basalt compositions, indicating that the majority of the REEs in these samples are associated with hydrothermal oxides, rather than detrital clays.

Robertson & Fleet [1976] reported the purest umbers they sampled (i.e. lowest detrital clay content) to have the highest REE contents. The two umber samples with the lowest clay content (170 and 116) are the most Nd-enriched, while those with higher TiO_2 contents tend to have lower Nd contents (e.g. 213). This is the general relationship observed by Robertson & Fleet [1976], although the data in this study are somewhat scattered. Additionally there is no clear relationship between Fe_2O_3 (representative of hydrothermal particle input) and Nd content in the metalliferous sediments (Figure 7.11). This indicates that the sediments are composed of hydrothermal oxide particulates with varying REE contents. Given that the REE content of the umbers is not clearly related to either the 'detrital' (TiO_2) or 'hydrothermal' (Fe_2O_3) components, it is apparent that there has been varying degrees post-formation addition of REEs to the sediment particles, which is probably a function of hydrothermal plume dispersal and/or seafloor sedimentation rates (refer to sections 2.8 and 2.9).

Robertson & Fleet [1976] noted that the umbers with the highest clay content have the smallest negative Ce anomalies, because detrital clays have flatter REE patterns. Figures 7.12a & b show that no clear relationship exists between TiO_2 (detrital input) or Fe (hydrothermal input) concentrations and the size of Ce anomaly, indicating that other factors (for example, accumulation rate) are more important in controlling the Ce content of these sediments (discussed further in section 7.5.3).

Because silica can be sourced from biogenic as well as detrital sources, Al and Ti are generally more accurate proxies of detrital inputs. However, the observed correlations between Si-Ti and Si-Al for the majority of these sediments warrant the use of Si as a

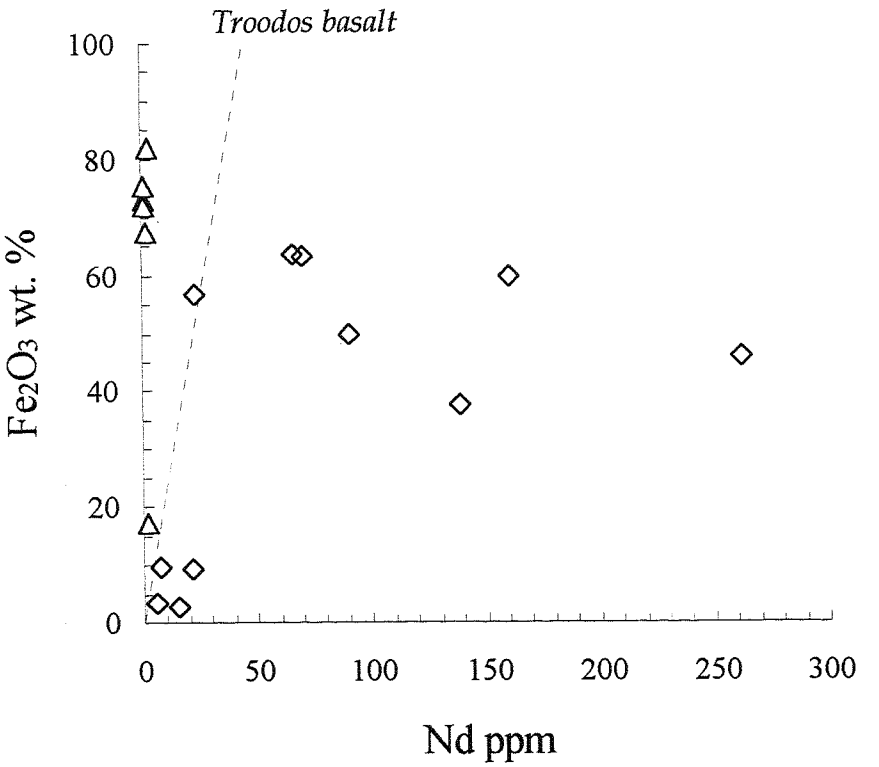

Figure 7.11: Relationship between Fe_2O_3 and Nd content in Troodos umbers (diamonds) and ochres (triangles). Troodos basalt compositions are from glass analyses by Rautenschlein *et al.* [1985].

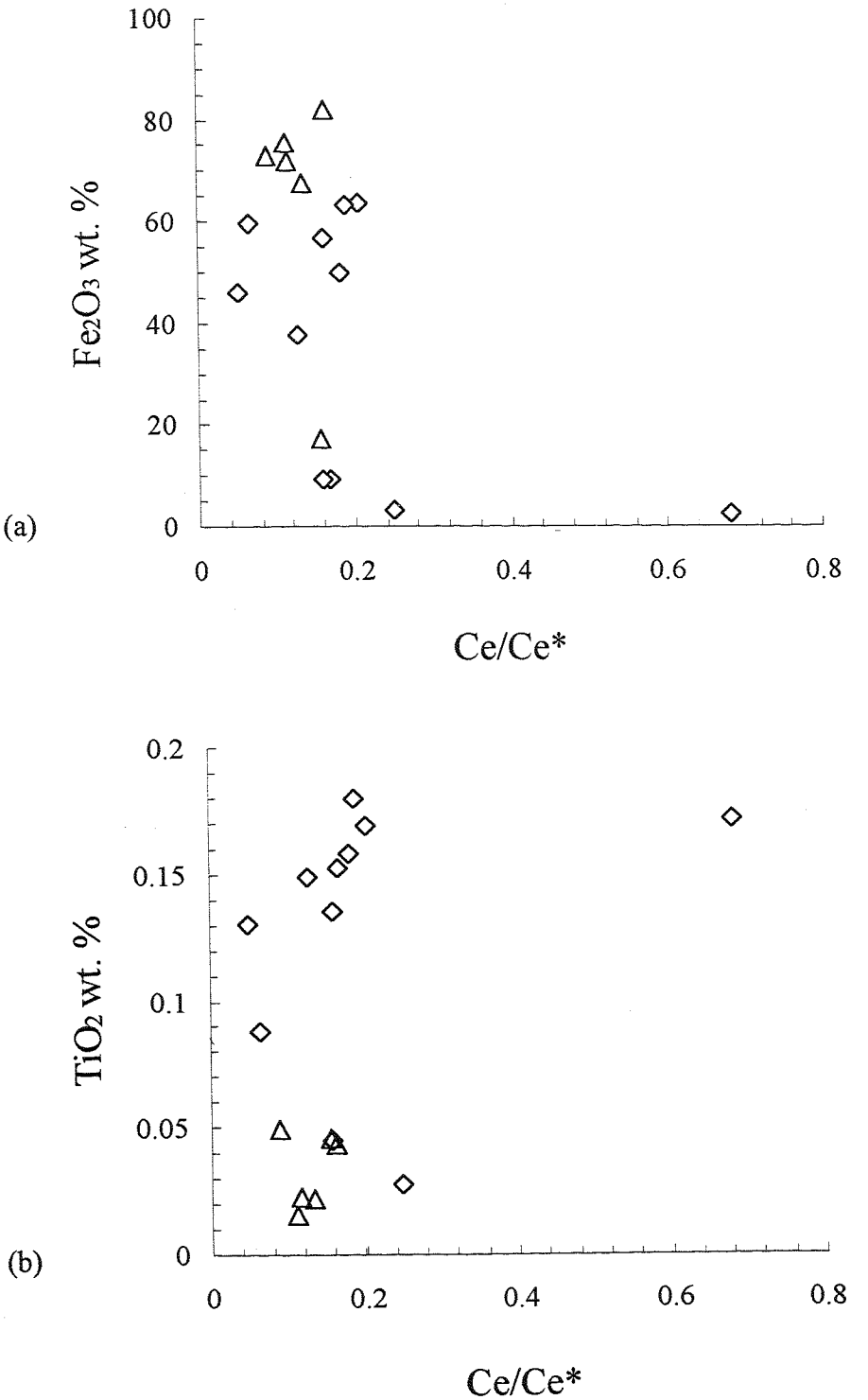

Figure 7.12 (a) and (b): Relationship between the Ce anomaly and (a) Fe_2O_3 content and (b) TiO_2 content in Troodos umbers (diamonds) and ochres (triangles).

proxy for detrital clays (Fig. 7.8). Figure 7.13 shows the Fe_2O_3 content of the metalliferous sediments plotted against SiO_2 content. Lines representing the composition of Troodos basalts [Rautenschlein *et al.* 1985] and a range of secondary hydrothermal clays [Richards *et al.* 1989] are shown for comparison. There is a negative correlation between Si and Fe content for the majority of samples which indicates that the majority of Fe is independent of the detrital sediment component. The negative correlation is therefore inferred to reflect the dilution of hydrothermal Fe-oxides by detrital clays. Samples that do not fall on this hypothetical mixing line are those that contain a significant amount of another component (e.g. sample 95 which contains abundant calcite) or are enriched in hydrothermal (samples 166 and 33) or biogenic (159) silica. Figure 7.14 indicates that excluding the Si- or Ca-enriched sediments, there is a negative correlation between Fe and Mn concentrations. This relationship indicates that Fe-oxide and Mn-oxides formed within the hydrothermal plume are separate sediment components.

Rare earth element patterns

There is a striking uniformity in the REE patterns for most of the Troodos umber and ochre samples. The REE content of the sediments is bimodal and discriminates between umber (both Mn-poor and Mn-rich) and ochre (Fig. 7.5). Both umbers and ochres have REE compositions indicative of extensive scavenging of seawater REEs. Similar patterns have been reported for EPR ridge crest metalliferous sediments [Dymond, 1973; Ruhlin & Owen 1986; Barrett & Jarvis 1988; Owen and Olivarez, 1988], for hydrothermal ferromanganese deposits [Toth 1980; Fleet 1983], and for metalliferous sediments accumulating on the seafloor beneath the TAG neutrally buoyant plume [Mills 1992; Mills *et al.* 1993; German *et al.* 1993]. The REEs are particle-reactive metals that are rapidly scavenged from the vent fluid and entrained seawater onto newly-formed hydrothermal oxyhydroxide particulates during plume dispersion (refer to section 2.8) [Klinkhammer *et al.* 1983; German *et al.* 1990; German *et al.* 1991*a*; Rudnicki & Elderfield 1993]. The enhanced REE concentrations of the umbers is inferred to reflect a greater extent of seawater contact prior to and/or following sedimentation from the hydrothermal plume. Prolonged scavenging of seawater REEs causes fractionation of the REEs because LREEs have a greater affinity for Fe- and Mn oxide surfaces than the more soluble HREEs [Koeppenkastrop & De Carlo 1992]. Consequently, the umbers have higher REE contents

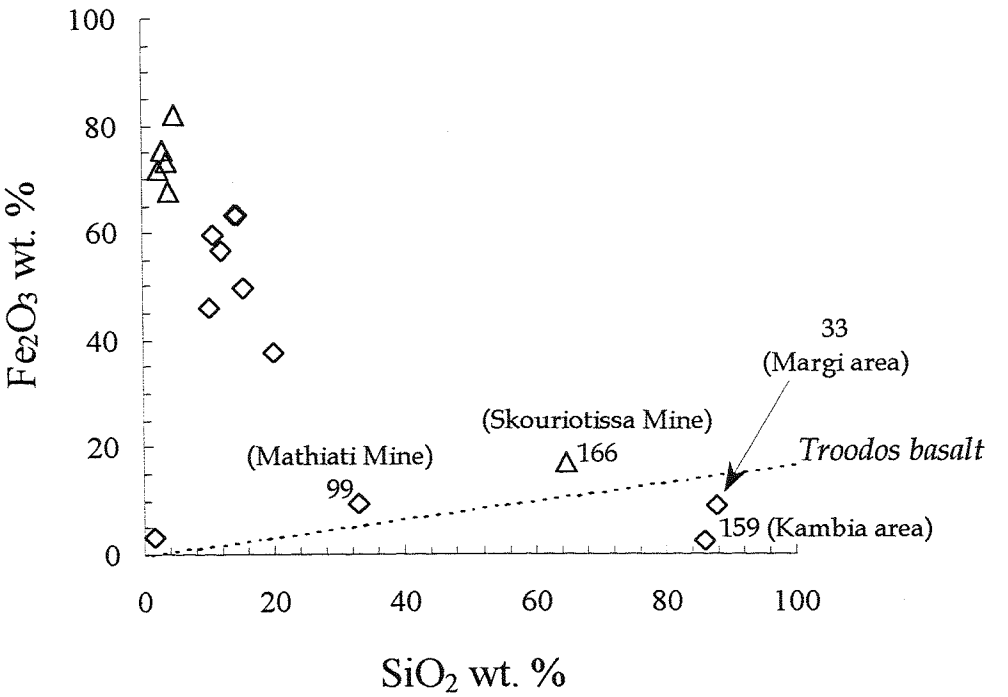

Figure 7.13: Relationship between Fe_2O_3 and SiO_2 in Troodos umbers (diamonds) and ochres (triangles). Troodos basalt compositions are from glass analyses by Rautenschlein *et al.* [1985]. Secondary clay data are from Richards *et al.* [1989]. Marked samples are discussed in the text.

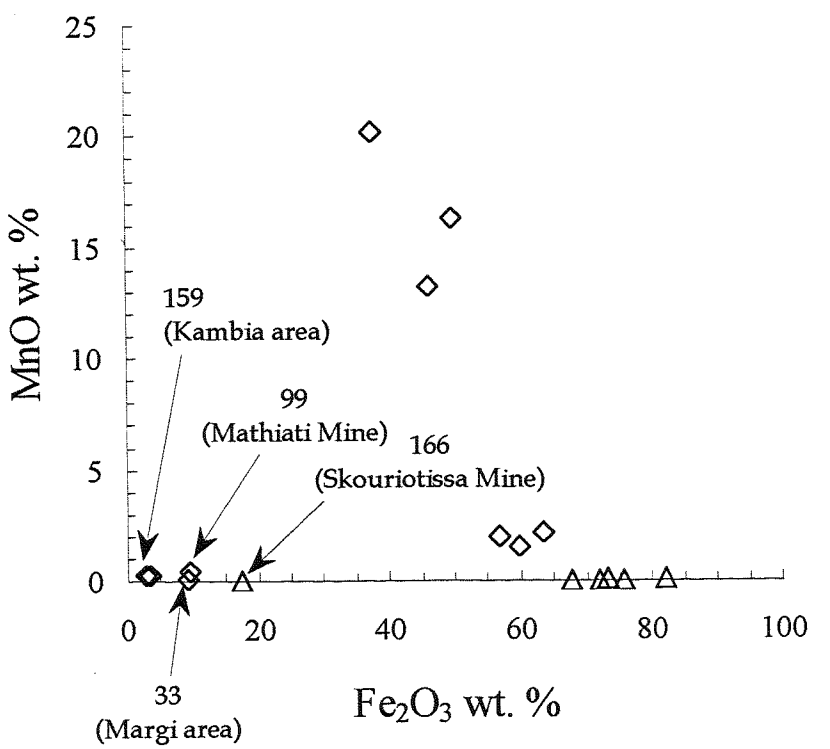

Figure 7.14: Relationship between MnO and Fe_2O_3 in Troodos umbers (diamonds) and ochres (triangles). Marked samples are discussed in the text.

and are generally more LREE-enriched than the ochres (Fig. 7.15).

7.7.3 Ce anomalies

All the umber and ochre samples possess negative Ce anomalies which are more pronounced than TAG plume derived sediment, but similar to REE patterns for EPR distal hydrothermal sediments (Fig. 7.3) [e.g. Ruhlin & Owen 1986]. The behaviour of Ce in seawater is dominated by preferential oxidative uptake onto manganese oxides in particular [Goldberg 1961], rather than the general scavenging processes which dominate the oceanic chemistry of the trivalent REEs [Elderfield 1988]. The characteristic Ce depletion of plume derived-particulates and metalliferous sediments is due to the rapid uptake of REEs from a Ce-depleted seawater source. Experimental studies have demonstrated that enhanced Ce scavenging is characteristic of manganese- rather than iron oxyhydroxide particulates [Koeppenkastrop & De Carlo 1992]. Mn-rich umbers might therefore be expected to have higher Ce contents than ochres, as Mn-oxides will scavenge Ce from seawater more effectively than Fe-oxide particles. However, like the Nd content (representative of the trivalent REEs), variations in the size of the Ce anomaly of the umbers and ochres do not correlate with either Fe or Mn contents (Fig. 7.12a). These observations may reflect variable sedimentation rates, that will lead to differing amounts of REE uptake from seawater in the hydrothermal plume and on the seafloor [e.g. Ruhlin & Owen 1986; Barrett & Jarvis 1988; Olivarez & Owen 1989; German *et al.* 1990].

All the umber samples show evidence for large amounts of seawater contact during sedimentation in their elevated REE contents and large negative Ce anomalies. In previous studies, the Mn-poor basal umbers have been inferred to form as a consequence of changes in either depositional or diagenetic Eh [Robertson 1976; Boyle 1990]. Fig. 7.6 shows that Mn-poor and Mn-rich umbers have similar REE concentrations. Therefore, if Mn was mobilised during reducing diagenetic reactions (e.g. 172 and 213), then the trivalent REEs were immobile during this alteration in addition to Eu and Ce, that like Mn display a redox chemistry (refer to section 2.2). Alternately, if the Mn depletion in the basal umbers is attributed to changes in depositional E_h by mixing between acidic hydrothermal solutions and oxic seawater during sediment formation [e.g. Elderfield *et al.* 1972; Robertson & Fleet 1976], then the REE patterns of the umbers indicate that then REE uptake was independent of the Mn/Fe ratios of the hydrothermal particles.

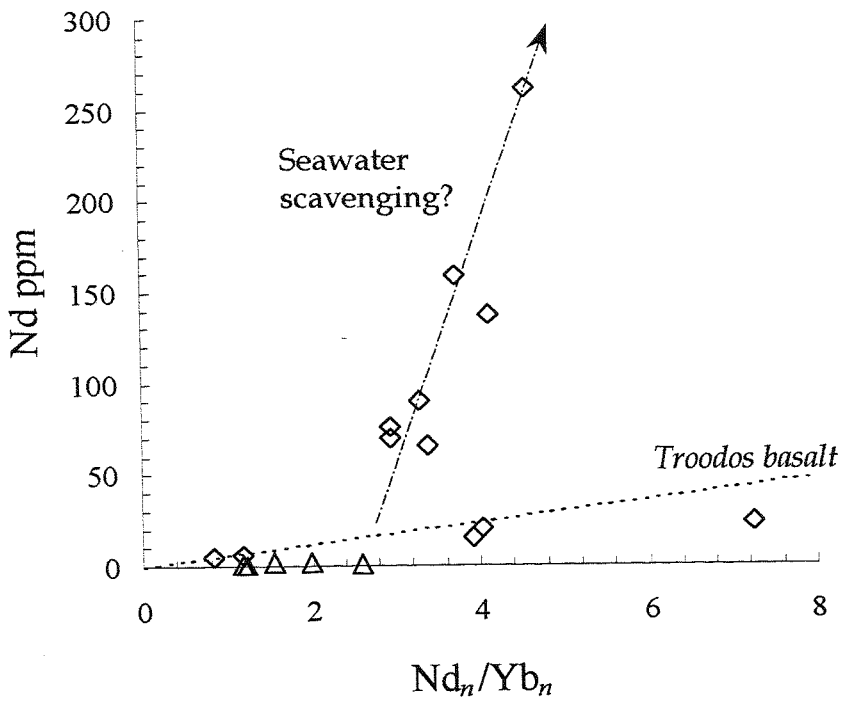

Figure 7.15: Relationship between Nd content and the chondrite normalised Nd/Yb ratio in Troodos umbers (diamonds) and ochres (triangles). Preferential scavenging uptake of the less soluble LREEs from seawater is inferred to simultaneously elevate the Nd content and the Nd_n/Yb_n ratio of the sediments. Troodos basalt compositions are from glass analyses by Rautenschlein *et al.* [1985].

7.7.4 Ochre formation

Skouriotissa ochres have been inferred to form by the submarine oxidation of mound sulphides in addition to the precipitation of Fe-oxyhydroxide sediments from diffuse vent fluids [Robertson 1976; Herzig *et al.* 1991]. At TAG, sediments formed by these two processes have distinctive, vent fluid-like REE patterns [German *et al.* 1993; Mills & Elderfield 1995*a*; Mills *et al.* 1996; Goulding *et al.* 1998]. While Herzig [1991] reported ochres from the Skouriotissa deposit with large positive Eu anomalies (Fig. 7.3a), the ochres analysed in this study possess seawater-derived REE patterns without any anomalous Eu-enrichment. These REE patterns are inferred to be associated with seawater ingress into the mound sediments, and overprinting of any hydrothermal REE signature with seawater derived REEs. This is a process that has been observed in its inception in an ochreous sediment core from the periphery of TAG mound [Goulding *et al.* 1998]. The lower 10 cm of the core displays fractionated vent fluid REE patterns, with no evidence of any seawater influence (Fig. 2.4). However, the upper 15 cm of the core has REE patterns with positive Eu anomalies and small negative Ce anomalies, demonstrating the influence of both vent fluid- and seawater-derived REEs [Goulding *et al.* 1998]. The REE patterns of this core provide evidence for low-temperature seawater overprinting of the TAG ochres while the TAG mound is still actively forming, and would be predicted to continue when the deposit becomes inactive. The seawater-like REE patterns of the Skouriotissa ochres provide evidence for extensive uptake of REEs from seawater on the seafloor following the peak of hydrothermal activity, and prior to uplift and emplacement of the ophiolite.

7.7.5 Origin of the Margi sediment

The silicified umber from Margi (sample 33) is reminiscent of some sediments within the TAG vent which contain slumped sulphides in a matrix of fine-grained plume derived sediment [German *et al.* 1993; Mills *et al.* 1993]. This origin is supported by the highly fragmented texture of the umber and the presence of partially oxidised pyrite, which was not observed in any of the other sediments. LA ICP-MS analyses show that the fragmented material displays negative Ce and small positive Eu anomalies, demonstrating the influence of both vent fluid and seawater REEs. The Fe-oxide matrix has REE patterns similar to the whole rock REE pattern (and other umbers), and is inferred to represent fall-out from a hydrothermal plume. The sulphides in this sediment would have been derived from a high-temperature vent source. The nearest sulphide body is the Mathiati deposit, that is located

~ 5km south of the Margi area. This implies transport of sulphides ~ 5km from the high-temperature vent to the site of deposition. At TAG, slumped sulphides are transported several km's from sulphide structures to sediments accumulating on the floor of the median rift valley [Metz *et al.* 1988; Mills *et al.* 1993].

7.7.6 Trace metal contents

Modern metalliferous sediments are enriched in elements that are mobilised from the oceanic crust during ridge crest hydrothermal activity, with some additional seawater sources for some elements that coprecipitate from seawater with Mn- and Fe-oxyhydroxides particles in hydrothermal plumes [e.g. Bender *et al.* 1971; Dymond & Veeh 1975; Trocine & Trefry 1988; Trefry & Metz 1989; German *et al.* 1991*a,b*]. Troodos umbers are highly enriched in Mn (2 to 16.3 wt.% Mn, averaging 8 wt.%), compared with metal-enriched calcareous oozes accumulating on the seafloor at TAG (296 ppm to 1.06 wt.% Mn, averaging 0.11 wt.%). It may be that Fe- and Mn-rich oxide crusts (containing up to 39 wt.% Mn) that are found in the relict *Mir* and *Alvin* zones and the low-temperature field at TAG [M. Scott *et al.* 1974; Thompson *et al.* 1985; Rona *et al.* 1993*a,b*] are better modern analogues of umbers. The trace element composition of Troodos umbers and a range of modern metalliferous sediments and nodules are shown in Table 7.4. Compared with TAG metalliferous sediments and hydrothermal ferromanganese crusts, hydrogenous ferromanganese deposits are particularly enriched in Co, Cu, Pb, Ni, Cr and Ba. Compared with TAG metalliferous sediments Troodos umbers are slightly enriched in Pb and Cr, and contain an order of magnitude higher concentrations of Ni (~220 ppm compared with ~20 ppm). At TAG, the distribution of chalcophile elements such as Cu, Zn, Co and Pb in metalliferous sediments is mineralogically controlled, as they are contained in sulphides that are deposited close to the high-temperature vents [Metz *et al.* 1988; Mills *et al.* 1993]. The contrasting compositions of plume- and sulphide-derived sediment layers at TAG is shown in Table 7.4 [Metz *et al.* 1988]. Because Troodos umbers are generally non-sulphide bearing oxide sediments, their Pb, Cu and Co enrichments cannot be explained in terms of the sulphide mineralogical controls of the TAG models of metalliferous sediment formation. Consequently, these trace metals are inferred to be incorporated into the umbers by slow

Table 7.4: Comparison of the trace element composition of Troodos umbers and a range of modern metalliferous sediments

Examples of:	Pb	Zn	As	Ni	Mo	V	U	Sr	Ba	Th	Cr
	All values ppm										
***A.* Troodos umbers:**											
This study (N = 11)	***114***	***454***	***230***	***227***	***22.7***	***1140***	***BLD***	***237***	***542***	***BLD***	***57.0***
[1]Typical umbers (*N* = 23)	161	235	-	212	-	755	-	414	427	-	31
***B.* TAG sediments:**											
[2]Plume-derived sediment (0-15 cm)	88	779	-	16.1	-	518	-	-	-	-	21.2
[2]Sulphidic mass flow (15-47 cm)	112	1768	-	16.4	-	354	-	-	-	-	26.3
[2]Average (whole core)	137	2830	-	25	-	560	-	-	-	-	29
***C.* Ferromanganese crusts:**											
[3]Galapagos Spreading Ridge (ht)	-	85-4860	-	58-500	-	-	0-6.9	-	-	0.01-	-
[4]Bauer Basin (ht)	-	-	-	5540	-	-	-	-	-	-	-
[5]Hawaiian Archipelago (hdg)	-	-	-	1910-6340	-	-	-	-	-	-	
[6]Central Pacific seamounts (hdg)	11-<50	240-460	300-320	43-270	<5-390	130-700		163-3299	22	-	150-560
[7]TAG vent field (ht)	-	87-1448	-	343-2200	-	-	-	-	400-1010	-	-
***D.* Ferromanganese nodules:**											
[4]Bauer Basin (hdg)	-	-	-	12100	-	-	-	-	-	-	-
[8]N. Equatorial Pacific (hdg)	-	600-1400	-	7200-16300	-	-	-	-	1100-2600	-	-
[9]Average nodule composition (hdg)	1500	3500	-	5700	-	590	-	-	-	-	10

[1]Robertson & Hudson [1973]; [2]Metz *et al.* [1988] (calculated on a carbonate-free basis); [3]Moore & Vogt [1976]; [4]Elderfield & Greaves [1981]; [5]De Carlo & McMurtry [1992]; [6]Hein *et al.* [1994]; [7]Toth [1980]; [8]Calvert *et al.* [1987]; [9]Chester [1990]

BDL indicates element below limit of detection; dash indicates element not reported

ht = hydrothermal origin; hdg = hydrogenous origin

adsorption from seawater, in an analogous manner to hydrogenous ferromanganese deposits [e.g. Toth 1980]. Implicit in this interpretation is that the umbers accumulated sufficiently slowly on the Troodos seafloor for hydrogenous processes to significantly affect their trace element composition. In light of this observation, the preservation of large negative Ce anomalies in these sediments is unclear. The preferential oxidative Ce uptake from seawater onto Mn-oxides in the umbers would be expected to produce the positive Ce anomalies that characterise hydrogenous ferromanganese sediments [e.g. Fleet 1983].

7.8 Conclusions

The REE patterns of the Troodos sulphides are strikingly different from TAG mound and other oceanic sulphides. Despite the many similarities between modern and ancient massive sulphide deposits, the data suggest that the Troodos ore bodies are dominated by seawater REE signatures introduced during the extensive entrainment and sub-surface circulation of Cretaceous seawater, which has resulted in the overprinting of any original hydrothermal signatures in both mound sediments and sulphides. Sulphides with seawater-dominated REEs have not been recorded at modern oceanic vent sites. Consequently, it can be inferred that the seawater overprinting of the Skouriotissa deposit is the end product of a process which we only see the initiation of on the modern seafloor [e.g. Tivey *et al.* 1995; Edmond *et al.* 1995; Goulding *et al.* 1998]. By analogy with the TAG models, it is inferred that these processes involve seawater incursion, and overprinting by lower temperature assemblages within hydrothermal mounds and stockworks (cf. Chapter 6). The present study has demonstrated that the geochemistry of the sulphide mound deposits continues to evolve following the peak of hydrothermal activity, and that the REE can be used to trace seawater entrainment, fluid evolution and ore formation processes in both the active setting and geological record.

Troodos umbers are essentially fine-grained oxide sediments which are analogous to modern hydrothermal ferromanganese sediments, and have seawater-like REE patterns reflecting extensive seawater exposure prior to/and or following sedimentation on the palaeo-seafloor. Exposure of fine oxides to seawater is inferred to have facilitated extensive scavenging of the REEs and preferential uptake of the less soluble LREEs.

TAG ochres have fractionated vent fluid-like REE patterns, because they precipitate from fluids which have evolved within the mound by the precipitation and dissolution of mound

sulphides and anhydrite [Mills & Elderfield 1995*a*; Mills *et al.* 1996; Goulding *et al.* 1998]. Although other Skouriotissa ochres have previously been described as the products of hydrothermal weathering of sulphides on the basis of textural, mineralogical and REE evidence [Herzig *et al.* 1991], the Troodos ochres analysed in this study display REE patterns indicative of REE scavenging from seawater by particulate phases. These REE patterns may be a primary (i.e. direct seawater precipitation) or secondary (i.e. overprinting) signature. At TAG, in addition to the REE evidence, the zone-refined nature of the sulphide mound, and the complex assemblage of anhydrite-pyrite-silica breccia units revealed by ODP drilling are interpreted to reflect ongoing processes of seawater entrainment and the formation of diffuse fluids within the ore body [Humphris *et al.* 1995; Hannington *et al.* 1998]. Troodos ore bodies are similarly zone-refined, displaying Cu-enrichments of up to 4 wt.% Cu in the upper parts of the ore bodies, compared with < 1 wt.% in the stockwork breccias [review by Hannington 1998]. By analogy with the TAG mound, cycles of anhydrite formation and dissolution have been inferred to have played an important role in the evolution of the sub-surface pyrite-silica breccias of the Troodos deposits [Humphris *et al.* 1995; Hannington *et al.* 1998]. In view of these observations, the Skouriotissa ochres might be expected to have had similar REE patterns to TAG ochres, reflecting continued sub-surface mineralisation and anhydrite precipitation associated with seawater ingress and circulation within the Troodos sulphide structures. However, the REE patterns of the ochres analysed in this study no longer signify their processes of formation. Rather, the REE patterns of umber, ochre and sulphide sampled from a section through the top of the Skouriotissa ore body clearly demonstrates extensive seawater ingress and circulation throughout the upper ore body.

Drilling and submersible studies of the TAG mound have formulated models in which seawater circulation and mixing within the mound is inferred to cause significant dissolution and re-precipitation (reworking) of mound sulphides, through the formation of diffuse hydrothermal fluids (section 3.2.7) [Tivey *et al.* 1995; [Mills & Elderfield 1995*a*; Edmond *et al.* 1995; Humphris *et al.* 1995; Tivey *et al.* 1995]. By analogy with the TAG models, a similar origin can be implied for the formation of multiple generations of pyrite ore within the Troodos mound deposits [e.g. Constantinou & Govett 1972].

At TAG, processes of fluid mixing and modification within the TAG mound involving seawater circulation, and the precipitation of anhydrite, pyrite and chalcopyrite, the

dissolution of sphalerite within the mound are reflected in the REE systematics of the various hydrothermal phases associated with the active mound [Mills and Elderfield, 1995*a*]. The integrated effects of seawater ingress into the Skouriotissa deposit during waning hydrothermalism, and subsequent sustained seawater alteration during cooling of the mound have obscured any such REE signatures in the sulphides and metalliferous sediments of this ophiolitic deposit.

Chapter 8

The origin of low-temperature hydrothermal deposits from the TAG vent field, 26° N, Mid-Atlantic Ridge

8.1 Introduction

A spectrum of hydrothermal deposits are observed to be associated with ridge-crest hydrothermal activity. Sulphide-rich, Mn-poor assemblages occur where black smoker fluids are sufficiently channelled to vent directly at the seafloor [e.g. Speiss *et al.* 1980*b*; Edmond *et al.* 1982; Rona *et al.* 1986; Fouquet *et al.* 1988; Scott *et al.* 1990]. The precipitation of dissolved hydrothermal manganese is kinetically limited, hence occurs at lower temperatures than for sulphide minerals and in distal localities relative to sites of high-temperature venting [e.g. Klinkhammer *et al.* 1986]. Consequently manganese is a sensitive tracer of plume dispersion as the hydrothermal end-member is a million times enriched (*c.*1 mmol kg^{-1}) relative to ambient seawater and displays a near-conservative behaviour for some time after discharge, in contrast to many other metals [Klinkhammer *et al.* 1986]. Dissolved Mn can persist in the water column as a detectable anomaly for 100's of km from Pacific vents [Klinkhammer & Hudson 1986], and has been frequently used as a prospective tool for locating new hydrothermal sites along the ocean-ridge system [e.g. Klinkhammer *et al.* 1977; Klinkhammer 1980; Lupton *et al.* 1980; Klinkhammer *et al.* 1983; Klinkhammer *et al.* 1985; Klinkhammer & Hudson 1986; Klinkhammer *et al.* 1986].

In contrast to sulphide chimneys and mounds that precipitate from ~350°C black smoker fluids, low-temperature metal-rich deposits of Mn- and Fe-oxides and Fe-silicates form around the discharge sites of diffuse hydrothermal fluids that have mixed with seawater in the subsurface of the hydrothermal system, and contain only a few per cent of the high-temperature fluid [e.g. Edmond *et al.* 1979*b*; James & Elderfield 1996]. These low-temperature fluids are effective at transporting manganese, that during seawater mixing is unaffected by processes of oxidation and sulphide formation which result in the removal

of many other metals (e.g. Fe, Cu, Ni, Cd, Cr, U) [Edmond *et al.* 1979*b*; James & Elderfield 1996; Mills *et al.* 1996].

At the TAG vent field, 26° N Mid-Atlantic Ridge, significant deposits of Fe-oxides, Fe-silicates and Mn-oxides are located in a 'low-temperature field' on the east median valley wall between depths of 2400 m and 3200 m (section 3.2.1). These metalliferous oxides have been described as a 'bath-tub ring' deposit, forming where the neutrally buoyant TAG plume impinges on the median valley walls [Elderfield & Rudnicki 1992], or alternately as hydrothermal precipitates forming where channelled, dilute hydrothermal fluids seep from faults on the eastern valley wall [Rona 1973; Scott *et al.* 1974; M. Scott *et al.* 1974; Thompson *et al.* 1985; Ravizza *et al.* 1996].

The origin of these low-temperature oxides has implications for the fate of hydrothermal manganese in the TAG vent field; specifically whether this element is behaving as a tracer of the hydrothermal plume sourced from black smoker activity on the TAG mound, or low-temperature 'diffuse' hydrothermal venting occurring high on the east rift valley wall. This chapter describes the distribution of REEs within some low-temperature metalliferous oxide crusts from different locations within the TAG vent field. These data are used to assess their mode of formation, in view of previously suggested models.

8.2 Hydrothermal ferromanganese deposits

Hydrothermal Mn- and Fe-oxide deposits are widespread in tectonically active areas of the ocean floor, and have been recovered from active spreading centres and seamounts in the Atlantic, Pacific and Indian oceans [e.g. Scott *et al.* 1974; Bonatti 1975; Thompson *et al.* 1975; Moore & Vogt 1976; Cann *et al.* 1977; Corliss *et al.* 1978; Bäcker et al. 1985; Alt *et al.* 1987; Alt 1988; Marchig *et al.* 1988; De Carlo & McMurtry 1992; Hein *et al.* 1994]. They represent one end-member of a spectrum of oceanic ferromanganese deposits that differ in the degree of influence of hydrothermal *versus* hydrogenous metal enrichment processes in their formation [e.g. Fleet 1983]. The hydrogenous end-member is represented by ferromanganese nodules, that are widespread in areas with low sedimentation rates including oceanic abyssal plains and topographic highs [Bonatti 1975]. The nodules form by a combination of direct metal precipitation from seawater, and diagenetic metal remobilisation and cycling *via* adjacent marine sediments [Bonatti 1975; Elderfield & Greaves 1981; Elderfield *et al.* 1981*a*,*b*].

In contrast to hydrogenous nodules, hydrothermal ferromanganese deposits are the final precipitates from ~350°C black smoker-like fluids that have mixed with cold, oxidising seawater in the subsurface of the system. While infrequently sampled, these diffuse fluids are probably analogous to the 3 to 13°C Galapagos 'hot springs' [Edmond *et al.* 1979*a,b*]. The Galapagos fluids are strongly enriched in reduced, divalent Mn (derived from the breakdown of silicate minerals during high-temperature basalt alteration), while Fe contents are low and variable [Edmond *et al.* 1979*a*]. Mn is fractionated from Fe because the Fe^{2+}/Fe^{3+} redox couple occurs under conditions of lower E_h than the Mn^{2+}/Mn^{4+} couple, and additionally because the kinetics of Mn oxidation are slow compared with those of Fe [Krauskopf 1957]. Consequently, Fe oxidation and precipitation occurs before that of Mn during mixing between reduced hydrothermal fluids and seawater [Krauskopf 1957]. If this mixing occurs below the seafloor, Fe precipitates as sulphides or hematite within the crust [Hajash 1975], generating fluids that seep from the seafloor with low Fe/Mn ratios [e.g. Edmond *et al.* 1979*b*; James & Elderfield 1996]. Although the oxidation of Mn^{2+} is extremely slow, it is autocatalytic, whereby newly formed insoluble MnO_2 provides reaction sites for further oxidation. Mn is therefore effectively scavenged from diffuse hydrothermal fluids to form crust-like accumulations of metalliferous oxides [Edmond *et al.* 1979*b*; Mills *et al.* 1996].

Compared with black smoker fluids, diffuse fluids sampled from the surface of the TAG mound are depleted in Fe, Cu, H_2S and silica, contain comparable amounts of Mn and are enriched in Zn [James & Elderfield 1996]. Although Mn enrichments of up to 15 wt.% have been reported in the upper part of an sediment core from the TAG mound [Goulding *et al.* 1998], ferromanganese crusts are not presently forming from these diffuse fluids at the surface of the TAG mound [Hannington *et al.* 1998], although they are present in the relict *Mir* and *Alvin* zones that lie to the north and north-east of the active TAG mound (section 3.2.1) [Rona *et al.* 1993*a,b*; Lalou *et al.* 1993].

Toth [1980] identified two distinct hydrothermal end-member deposits; crystalline birnessite and/or todorokite crusts and Fe and Si-rich crusts composed of Fe-rich nontronite or amorphous oxyhydroxides and silica. This suite of low-temperature metal-rich deposits is found associated with Galapagos diffuse fluids, and is inferred to reflect the degree of subsurface mixing of hydrothermal fluid with seawater prior to venting [Edmond *et al.* 1979*b*]. In general, Mn-oxides precipitate from extremely dilute fluids (seawater: hydrothermal fluid ratio >100:1), Fe-rich silicates from less dilute and

oxidising fluids (<1:1) and Fe- and Mn-rich sediments from fluids of intermediate composition [Edmond *et al.* 1979*b*].

Compared with hydrogenous ferromanganese nodules, hydrothermal deposits are characterised by extreme Fe/Mn ratios and low concentrations of trace metals and the REE. The trace element composition of these deposits is controlled by adsorption of elements onto MnO_2 and FeOOH surfaces [e.g. Koeppenkastrop & De Carlo 1992]. The metalliferous crusts incorporate hydrothermal Zn, As, Sb and Hg and adsorb minor amounts of Co, Cu, Ni, Pb Ba and REE from seawater [Toth 1980]. Hydrothermal ferromanganese deposits accumulate several orders of magnitude faster (*c.*250 mm Myr^{-1}) than hydrogenous ferromanganese nodules [e.g. M. Scott *et al.* 1974; Moore & Vogt 1976; Cann *et al.* 1977], which inhibits the hydrogenous enrichment of trace elements from seawater [Toth 1980].

8.3 Low-temperature hydrothermal deposits in the TAG vent field

Submersible investigations of the eastern rift valley wall at TAG by the deep-sea research vessel (DSRV) submersible *Alvin* in 1982 delineated the vertical extent of fault-controlled deposits of Fe-oxides and -silicates, and Mn-oxides that occur in discontinuous linear stripes subparallel to the rift axis, and cumulatively cover ~10% of the low-temperature field [McGregor and Rona 1975; Temple *et al.* 1979; Shearme *et al.* 1983]. These deposits are spatially distinct from the TAG sulphide mound located at the junction of the east wall and floor of the axial rift valley (Fig. 3.1), and their relationship to the high-temperature hydrothermal system is unresolved. Some of the Fe- and Mn-rich oxide crusts have compositions which preclude a hydrogenous mode of formation, but are consistent with direct precipitation from diffuse hydrothermal fluids containing large amounts of dissolved Fe, Mn and Si [Thompson *et al.* 1985]. No vent fluids have been sampled from the low-temperature field, but venting has additionally been inferred from water column temperature, ^{3}He and ^{222}Rn anomalies [R. Scott *et al.* 1974; Rona 1975; Rona 1978; Rona 1980; Jenkins *et al.* 1980; Elderfield *et al.* 1993], the occurrence of Fe-hydroxide vent-like protrusions (*c.*10 cm tall and 4 cm in diameter) on the surface of these deposits [Thompson *et al.*1985], and the presence of large amounts of suspended particulate Fe- and Mn rich matter above the seafloor [Scott *et al.* 1974; Nelson & Forde 1991].

Within the TAG vent field, the distribution of Mn is decoupled from Fe and other metals

enriched in the high-temperature end-member fluid. There is a gradient of manganese concentrations in hydrothermal deposits on the scale of the entire vent field. Copper, Zn and ~50% of the Fe in the vent fluid are deposited as sulphides either within, or in close proximity to the TAG mound [e.g. Tivey *et al.* 1995], while Mn and the remaining Fe is dispersed over several km in the hydrothermal plume, within the confines of the median rift valley [Klinkhammer *et al.* 1985; Klinkhammer *et al.* 1986]. Vent sulphides located at 3650 m depth contain <50 ppm Mn [Rona *et al.* 1986] while todorokite and/or birnessite crusts between depths of 2800 and 2400 m on the eastern rift valley wall contain up to 39 wt.% Mn [M. Scott *et al.* 1974; Thompson *et al.* 1985]. These crusts vary from thick, laminated- to loose earthy Mn-oxides to layered nontronite and/or amorphous Fe-oxides, which occur as discrete deposits ranging in size from ~1 to 20 m in diameter [Thompson *et al.* 1985; Rona *et al.* 1984]. They overlie and cement basalt talus and are accumulating 2 orders of magnitude faster (100 to 200 mm Myr^{-1}) than hydrogenous ferromanganese deposits [R. Scott *et al.* 1974]. Hydrothermally-enriched sediments occur on the valley floor and lower east wall up to the 3000 m isobath. These sediments contain Fe-, Cu- and Zn-enriched, Mn-poor layers which represent inputs of partially-oxidised slumped mound sulphides onto the floor of the median valley [Scott *et al.* 1978; Shearme *et al.* 1983; Metz *et al.* 1988; Mills *et al.* 1993]. Non sulphide-enriched calcareous oozes on the rift valley floor exhibit a correlation between Fe and Mn concentrations [Shearme *et al.* 1983], that also characterises EPR surface sediments [Böstrom & Peterson 1969]. Mn- and Fe-stained sediments occur from 3000 m and extend up the valley wall to the base of the low-temperature field at 2800 m water depth [Thompson *et al.* 1985]. The surficial Mn and Fe-enrichments may reflect either interaction with diffuse fluids [Thompson *et al.* 1985] or deposition from the TAG hydrothermal plume [Rudnicki & Elderfield 1993]. In the *Alvin* and *Mir* relict zones, Mn and Fe-rich deposits dated at around 125,000 years occur as dark stains on semi-consolidated carbonate ooze, and as coatings on fractured pillow lavas and basalt talus [Rona *et al.* 1993*a,b*; Lalou *et al.* 1993].

8.4 Physical and chemical properties of the TAG hydrothermal plume

The detection of manganese anomalies, and subsequent use as a tracer of hydrothermal venting [Klinkhammer *et al.* 1985, Klinkhammer *et al.* 1986; Trefry *et al.* 1986] led to the discovery of black smoker activity on the active TAG mound in 1985 [Rona *et al.* 1986]. Black smoker and diffuse fluids are entrained into the rising, buoyant hydrothermal plume

and mix with seawater before spreading laterally upon reaching density equilibrium with the surrounding seawater between 200 and 455 m above the TAG mound [Speer & Rona 1989; Rudnicki and Elderfield 1992]. Pacific hydrothermal plumes exceed the height of the valley walls at the ridge crest, and are dispersed tens to hundreds of kilometres from the ridge crest system [e.g. Lupton & Craig 1981]. At TAG, the hydrothermal plume is trapped by the MAR valley walls that rise to 1700 m above the rift valley floor, and both near- and far-field hydrothermal deposits are confined to the median valley [Klinkhammer *et al.* 1986].

The *c.*250 m thick neutrally buoyant TAG plume can be defined by various physical and chemical anomalies (e.g. temperature, salinity, particulate matter and elevated Mn content), and has a layered structure indicative of multiple sources [Nelson & Forde 1991; Rudnicki and Elderfield 1992]. Five main layers have been identified that reflect venting from different chimney structures on the mound and the degree of integration of the chemical and physical properties of black smoker and diffuse hydrothermal fluids [Rudnicki & Elderfield 1992]. Mapping of hydrothermal particulates [Nelson & Forde 1991] and a comparison of ^{222}Rn, He isotopes and Mn at the level of neutral buoyancy [Elderfield *et al.* 1993] indicate an additional low-temperature hydrothermal source region on the east wall that may be related to the formation of the Mn- and Fe-rich oxide deposits. Plume studies have lead to heat flux estimates of 500-940 MW for the TAG vent field, of which low-temperature fluids may contribute up to $^{6}/_{7}$ of the total heat loss [Rudnicki & Elderfield 1992; Elderfield *et al.* 1993].

The flux of elements into the ocean from vents is modified by chemical reactions within hydrothermal plumes. Fe does not persist in solution after venting [German *et al.* 1991*a*]. The molar ratios of total (i.e. dissolved and particulate) Fe to Mn in TAG hydrothermal fluids is *c.*10, whereas that of neutrally buoyant plume particles is *c.*5, because half of the iron in the high-temperature fluid is precipitated as sulphides within the first few minutes of mixing in the buoyant plume [German *et al.* 1990; Rudnicki & Elderfield 1993]. Fe has undergone ≥95% removal by the time it has reached plume height, where there are high levels of Fe-oxyhydroxide particulates (~250 nmol kg^{-1}) [Rudnicki & Elderfield 1993]. In contrast, Mn exhibits near-conservative behaviour, and its concentration in the neutrally buoyant plume is a function of the degree of seawater entrainment into the high-temperature vent fluid [Rudnicki & Elderfield 1993]. Dissolved manganese profiles over the TAG vent field are similar to those found over sites of high temperature venting on the

EPR [Klinkhammer & Hudson 1986] with maximum Mn anomalies of ~60 nmol kg^{-1} at a height of 330 m above the mound [Klinkhammer *et al.* 1986], indicative of an entrainment ratio of 10^4 [Elderfield *et al.* 1993]. In the near field, 100% of vent fluid Mn is in solution [Trocine & Trefry 1988]. Most of the dissolved Mn remains in solution as it is dispersed over the first 100-1000 m away from source [German *et al.* 1991*a*].

Increased microbial biomass relative to ambient seawater is a common feature of hydrothermal plumes [e.g. Jannasch 1995; Sudarikov *et al.* 1995]. Microbes provide a large and chemically suitable surface area for metal deposition, and there is evidence they influence the partitioning of Mn from Fe in the plume because they have direct metabolic role in Mn, but not Fe oxidation [Cowen *et al.* 1986]. Microbially-mediated removal of Mn from the plume has been demonstrated to occur in the near- [Mandernack & Tebo 1993] and to a greater extent in the far-vent field [Cowen *et al.* 1986]. This process additionally affects Co and Ni concentrations, because these metals are scavenged by Mn-oxide phases [Lilley *et al.* 1995].

Near-vent sulphides are enriched in Fe, Zn, Cu, Co, Cd and Pb. These particulates settle from the plume and undergo oxidative dissolution within the water column [German *et al.* 1991*a*]. Many hydrothermally- and seawater-derived trace elements are co-precipitated with newly formed oxide particles in the buoyant and neutrally buoyant hydrothermal plumes (e.g. V, As and Cr), while particle reactive elements such as the REEs, Th, Y and Be undergo additional uptake from seawater during plume dispersion [Trocine & Trefry 1988; Trefry & Metz 1989; Feely *et al.* 1990; German *et al.* 1990, 1991*a,b*]. Vent-derived REEs undergo quantitative removal from seawater by a combination of co-precipitation and scavenging uptake onto iron oxyhydroxide particles, and consequently do not become entrained into the ocean circulation or affect the seawater chemistry of the REEs [Rudnicki & Elderfield 1993; Olivarez & Owen 1991]. Moreover, the adsorption of vent- and seawater-derived REEs onto hydrothermal particle surfaces is capable of producing sub-ambient dissolved REE levels in the neutrally buoyant plume [Klinkhammer *et al.* 1983] where seawater-scavenged REEs account for >99% of total measured particulate REE concentrations [German *et al.* 1990]. Particle fall-out from the neutrally buoyant plume contributes to metalliferous deposits forming in the median valley.

The results of TAG plume studies have shown that sediments formed by deposition from the neutrally buoyant plume are dominated by fractionated seawater REEs, scavenged during interactions between newly-formed hydrothermal particles and large volumes of

seawater [German *et al.* 1990; Rudnicki & Elderfield 1993]. Metalliferous oxides that form from diffuse hydrothermal fluids show a more 'proximal' REE chemistry, reflecting a lesser degree of seawater interaction during deposition [e.g. Mills & Elderfield 1995*a*; Mills *et al.* 1996; Goulding *et al.* 1998]. This chapter describes the distribution of REEs within low-temperature metalliferous oxide crusts from different locations within the TAG vent field. In the TAG literature, these sediments have been described as forming by deposition from the TAG plume [Elderfield & Rudnicki 1992], or as precipitates from diffuse vent fluids seeping from eastern rift valley wall [Rona 1973; Scott *et al.* 1974; M. Scott *et al.* 1974; Thompson *et al.* 1985; Ravizza *et al.* 1996]. The aim of this chapter is to use the REEs to discriminate between the two suggested modes of formation

8.5 Sampling & Methods

Metalliferous oxide crusts were recovered from the TAG vent field in 1994 during the British-Russian Atlantic Vents Expedition (BRAVEX) cruise of the RV *Akademic Mstislav Keldysh*, that is equipped with two *MIR* deep-sea submersibles.

Basalt and indurated carbonate sediment with thin (mm-thickness) Mn- and Fe-rich oxide coatings were recovered from the 'low-temperature field' during dredge hauls 3386 and 3387 at depths of ~ 2400 m to 2800 m on the eastern wall of the axial rift valley, shown in Fig. 8.1. Siliceous samples with mm-thick Mn- and Fe-oxide coatings were collected from the inactive *Alvin* zone located 2 km north-east of the active TAG mound at 3450 m depth during dive 15 of the BRAVEX submersible program.

Additionally, five powdered samples of metalliferous oxide deposits collected in July 1982 by DSRV *Alvin* from dive sites located between 2500 and 2900 m within the low-temperature field [Rona *et al.* 1984] were obtained from G. Thompson at the Woods Hole Oceanographic Institute (WHOI) for REE analysis. These samples have previously been described by Thompson *et al.* [1985]. The osmium isotope composition of some of the *WHOI* samples has been described by Ravizza *et al.* [1996]. Sample descriptions are given in Table 8.1.

8.5.1 Rare earth elements

Rare earth element determinations were made on *c.* 10 mg samples of powdered metalliferous oxide using the analytical methods described in Chapter 5. REEs in all TAG

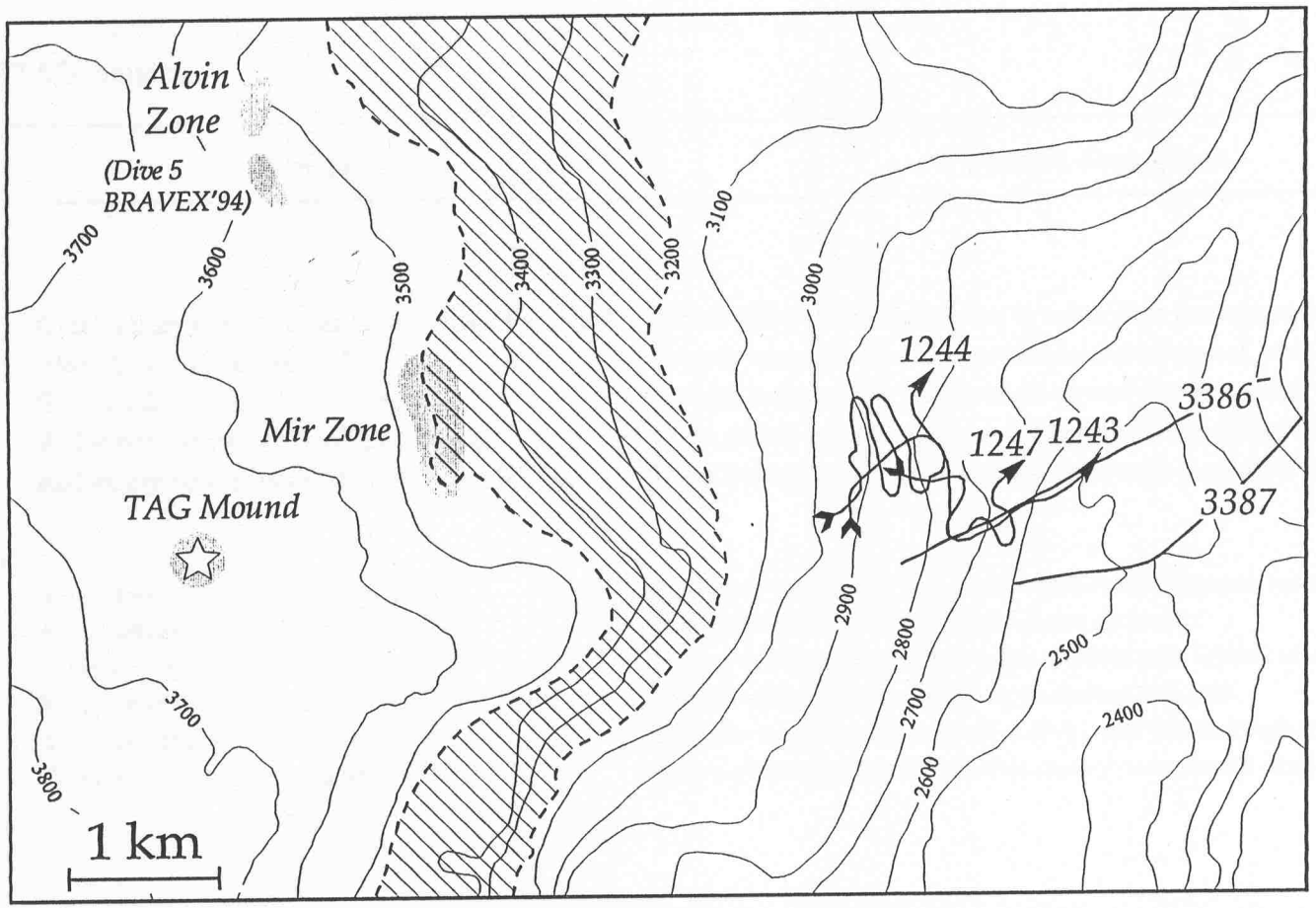

Figure 8.1: Map of TAG vent field showing sampling locations for the materials analysed in this study. The *WHOI* samples were collected by DSRV *Alvin* in 1982. Sample 1243-1 was retrieved during dive 1243, samples 1244-1B and 1244-1C during dive 1244 and samples 1247-2-2D and 1247-2-2B during dive 1247. BRAVEX'94 dredge tracks across the low-temperature field are also shown. Dive 5 of the BRAVEX'94 DSRV *MIR* submersible program was to the inactive *Alvin* zone (samples 3423-R-33 MnB and 3423-R-27 MnC). The dashed line represents the lower and upper limits of the neutrally buoyant hydrothermal plume sourced from the active TAG mound. At the level of neutral buoyancy the plume is 250 m thick and impinges on the eastern rift valley wall between 3200and 3450 m depth. The *Alvin* (3550-3450 m) and *Mir* relict zones (3450 m) lie beneath the neutrally buoyant TAG plume. The ferromanganese crusts in the low-temperature field occur higher on the rift valley wall (2400 to 3200 m). Hydrothermal plumes emanating from the now-inactive *Mir* and *Alvin* sulphide mounds might have impinged on the deeper parts of the low-temperature field. Map adapted from Karson & Rona [1990].

Table 8.1: Description of TAG samples

	Mineralogy	Sample description
Low-temperature field		
1982 *Alvin* samples:		
1243-1	Green earthy nontronite and amorphous Fe-oxide[¥]	Friable earthy nontronite, grading in colour from green through yellow to red[§]
1244-1B (top)	Black laminated birnessite[¥]	Irregular upper surface of a layered deposit composed of platy birnessite[§]
1244-1C (bottom)	Blue-black laminated birnessite[¥]	Smooth, lustrous lower surface of the layered platy birnessite[§]
1247-2-2D	Red earthy amorphous hydrated Fe-oxide [¥]	Loose deposit sampled from area of tubular vents comprised of the same Fe-rich material[§]
1247-2-2B	Red earthy amorphous hydrated Fe-oxide[¥]	Loose deposit sampled from area of tubular vents comprised of the same Fe-rich material[§]
1994 BRAVEX samples:		
3387-R-1 MnA	X-ray amorphous Fe- and Mn-oxides	Mixture of coarse- and fine-grained dark oxide coating on basalt
3387-R-1 MnA2	X-ray amorphous Fe- and Mn-oxides	Fine-grained dark-coloured oxide coating on basalt
3387-R-1 MnA3	X-ray amorphous Fe- and Mn-oxides	Coarse, friable coating of dark oxide admixed with minor carbonate on basalt
3387-R-1 MnB	X-ray amorphous Fe- and Mn-oxides	Medium-grained homogeneous oxide coating on basalt
3387-R-1 MnC	X-ray amorphous Fe- and Mn-oxides	Medium- to fine-grained coating of dark oxide admixed with minor carbonate on basalt
3386-R-1 MnD	X-ray amorphous Fe- and Mn-oxides	Coarse grained dark-coloured oxide coating on indurated carbonate
Relict Mir zone		
1994 BRAVEX samples:		
3423-R-33 MnB	X-ray amorphous Fe- and Mn-oxides	Heavily oxide-encrusted basalt
3423-S-27 MnC	X-ray amorphous Fe- and Mn-oxides with minor carbonate	Thick oxide coating on a highly porous block of Fe-stained silica

[¥]Sample mineralogy based on XRD as reported in Thompson *et al.* [1985]. Birnessite is a crystalline manganese oxide; nontronite is a crystalline iron-rich silicate

§Sample descriptions are from Thompson *et al.* [1985].

samples exceed the LOQ as defined in 5.5.3. Repeat analyses of the REE fraction of a Mn-rich core-top from the TAG vent field obtained using these procedures were on average accurate to within 13% of TIMS-ID values [Mills 1992] with an external precision averaging 3.3% (2σ) (Table 5.7).

Samples 3387-R-1 MnA1, 3387-R-1 MnA2, 3387-R-1 MnA3 and 3387-R-1 MnB were picked with the aid of a binocular microscope to obtain pure ~10 mg sub-samples. For the other samples, the mechanical separation of fine oxide from biogenic carbonate phases was not possible. Carbonate can be readily dissolved from a mixture of oxide and carbonate phases by acid leaching. However, this procedure was considered undesirable in view of the possibility of leaching REEs from the oxides if they occur as loosely adsorbed (rather than lattice-bound) species. Samples 3387-R-1 MnA1 and 3387-R-1 MnA2 were therefore analysed as picked and unpicked samples to assess any discrepancy in REE content. The REE determinations for these samples are shown in Table 8.2. The difference in REE content between picked and unpicked samples is typically less than occurs during replicate REE separations and ICP-MS analyses of the BHVO-1 and in-house standards (refer to section 5.3.3). The results for samples 3387-R-1 MnA1 and 3387-R-1 MnA2 demonstrate that in the unpicked samples, the REEs reside mainly in the oxide rather than calcite phases, and that separation of the carbonate detritus does not significantly affect the REE analyses. This observation corresponds with previous measurements of low (Nd = < 0.2 ppm) levels of REEs in foraminiferal calcite [Palmer 1985].

8.5.2 Neodymium isotopes

The Nd-isotope composition of the five *WHOI* samples and five of the BRAVEX samples was determined by TI-MS. Aliquots of dissolved sample were taken to give between 100 ng and 1000 ng Nd. The Nd fraction was separated using the cation-exchange procedures described in 5.4. Nd isotope ratios were determined using a V.G. Isomass 54E mass spectrometer. A mean value of $^{143}Nd/^{144}Nd = 0.511121$ ($N = 52$) was obtained for the JMC 321 standard compared with the recommended value of 0.511123. The external reproducibility of Johnson & Matthey JMS 321 Nd standard was 9 ppm on the $^{143}Nd/^{144}Nd$ isotope ratio during the period of sample analysis (Table 5.7). All Nd-isotope ratios are shown in Table 8.3. Errors quoted on the isotope ratios are 2σ.

Table 8.2: Comparison of the REE content of picked and unpicked sub-samples of TAG metalliferous oxides

	p	u	Mean	St.Dev. (2σ)	RSD (2σ)	p	u	Mean	St.Dev. (2σ)	RSD (2σ)
	3387-R-1 MnA1, ppm		*ppm*	*ppm*	*%*	*3387-R-1 MnA2, ppm*		*ppm*	*ppm*	*%*
La	232	231	231.3	1.4	0.60	264	241	116	33	13
Ce	1120	990	1055	180	17	1030	1060	620	43	4.1
Pr	62.6	59.0	60.8	5.1	8.5	64	60.224	33.0	5	8.7
Nd	253	236	244.8	24.0	9.9	256	231	134	36	15
Sm	54.0	50.4	52.2	5.1	9.9	53	49	28.7	4.7	9.1
Eu	12.8	12.2	12.49	0.87	6.9	12.6	12.3	6.68	0.47	3.7
Gd	59.6	57.1	58.4	3.6	6.1	60	55	31.0	7.6	13
Tb	8.49	8.08	8.3	0.6	7.0	8.6	8.4105	4.43	0.32	3.8
Dy	47.4	45.2	46	3	6.8	48.4	45	24.7	4.3	9.2
Ho	8.8	8.4	8.58	0.52	6.0	8.9	8.8	4.6	0.13	1.5
Er	24	23	23	1	4.3	24	23	12	1.8	7.9
Tm	3.28	3.16	3.2	0.2	5.3	3.281	3.2634	1.69	0.02	0.8
Yb	20	20	20	0.77	3.8	20	19	10	0.31	1.6
Lu	3.1	3.1	3.1	0.036	1.2	3.0	3.2026	1.6	0.34	11
			Average:		6.7			*Average:*		7.3

p = picked sample

u = unpicked sample

Table 8.3: Nd isotope composition of TAG samples

	Nd (ppm)	$^{144}Nd/^{143}Nd$	$^{\S}\varepsilon_{Nd}(0)$	$^{\Phi 187}Os/^{186}Os$
		all errors are 2 σ		
Low-temperature field				
1982 *Alvin* samples:				
1243-1	7.63	0.512009 ± 0.000164	-12.3 ± 3.2	7.14 ± 0.49
1244-1-1B (top)	0.669	0.512047 ± 0.000005	-11.5 ± 0.10	4.42 ± 0.03
1244-1C (bottom)	1.5	0.512089 ± 0.000150	-10.71 ± 2.9	4.24 ± 0.13
1247-2-2B	0.499	0.512044 ± 0.000031	-11.6 ± 0.60	-
1247-2-2D	0.912	0.512529 ± 0.000008	-2.13 ± 0.16	4.77 ± 0.06
1994 BRAVEX samples:				
3387-R-1 MnA2	256	0.512047 ± 0.000006	-11.53 ± 0.12	-
3387-R-1 MnA3	298	0.512013 ± 0.000046	-12.19 ± 0.90	-
3392-R MnA	-	0.512078 ± 0.000006	-10.92 ± 0.12	-
Relict Mir zone				
1994 BRAVEX samples:				
3423-27 MnC	274	0.512015 ± 0.000005	-12.15 ± 0.10	-
3423-R-33 MnB	334	0.512017 ± 0.000004	-12.11 ± 0.08	-

§The $^{144}Nd/^{143}Nd$ value of CHUR(0) is 0.512638

ΦOs isotope data are from Ravizza *et al.* [1996]

Isotope ratios were normalised to $^{146}Nd/^{144}Nd = 0.7219$

8.5.3 XRD analysis

X-ray diffraction patterns were obtained for powdered specimens using an ENRAF-NONIUS PDS120 system with a position sensitive detector (PSD) with an acquisition time of 900 s for each sample. Fe-fluorescence background was subtracted from all patterns.

8.5.4 TEM analysis

The presence of crystalline phases on a micro-scale within X-ray amorphous samples was investigated using TEM techniques. Selected area electron diffraction patterns were obtained using a JEOL JEM-2000 RX electron microscope in transmission mode operated at 200 kV. One drop of an ultrasonically dispersed suspension of crushed sample was placed on a carbon film supported by a copper mesh TEM grid. This was allowed to air dry, and stored under vacuum until use. Semi-quantitative chemical analyses were obtained using energy dispersive X-ray analysis (EDS) with an acquisition time of 200 s from a spot size of 100 nm or less.

8.6 Results

8.6.1 XRD and TEM results

XRD analysis identified all BRAVEX samples as X-ray amorphous oxides. There was insufficient sample powder to prepare fused glass beads and pressed powder pellets for XRF analysis. The results of published XRD analyses of the *WHOI* samples are shown in Table 8.1 [Thompson *et al.* 1985].

TEM investigations were made of BRAVEX samples 3386-R-1 MnA and 3387-R-1 MnA2 and the *WHOI* sample 1247-2-2B from the low temperature field , and BRAVEX sample 3423-R-33 MnB from the inactive *Alvin* zone. TEM energy dispersive X-ray spectroscopy identified particles (*c.*300 to 1000 nm in size) of 4 types with Fe-Si-, Fe-Mn-, Fe-Mn-Si- and Mn-rich compositions. These particles probably represent mixtures of Fe oxide and -silicate and Mn oxide. Fe-rich particles were dominant in sample 3423-R-33 MnB from the relict *Alvin* zone. Particles with Fe-Si- and Fe-Mn-rich compositions were identified in sample 3386-R-1 MnA. Particles with Fe-Mn-rich compositions were most common in sample 3386-R-1 MnA2, while of three particles analysed from sample 1247-2-2B two were Mn-rich and one had an Fe-Mn-Si-rich composition. This sample has previously been described as amorphous iron oxides [Thompson *et al.* 1985]. The limited number of TEM

analyses indicate that small-scale compositional heterogeneities exist in all the sample investigated.

Electron diffraction patterns for these samples vary from a regular array of spots for an Fe-Si-rich particle from sample 3386-R-1 MnA from the low-temperature field (indicative of a crystalline material) to diffuse rings with spots for an Fe-rich particle in sample 2423-R-33 MnB from the relict *Alvin* zone (indicative of crystalline domains within a dominantly micro-crystalline matrix). Mn-rich particles (sample 1247-2-2B) exhibit electron diffraction patterns with well-defined rings, indicative of a random array of ordered, but micro-crystalline material. The degree of crystallinity of the metalliferous oxides and silicate samples is significant because amorphous phases are characterised by higher surface area to volume ratios than the crystalline phase, and consequently possess relatively more surface sites available for REE complexation. This factor has been invoked to account for experimental variations in the REE-adsorptive properties of amorphous FeOOH and crystalline goethite [Koeppenkastrop & De Carlo 1992].

8.6.2 Rare earth elements

Rare earth element data for 11 samples from the low temperature field and 2 samples from the relict *Alvin* zone are shown in Table 8.4. The Ce anomaly, Eu anomaly and the chondrite normalised Nd/Yb ratios (Nd_n/Yb_n) have been quantified according to the methods outlined in 2.2. All ratios are shown in Table 8.4. Also given are published REE data for North Atlantic seawater [Mitra *et al.* 1994], and a range of hydrothermal deposits and fluids sampled from the TAG vent field [German *et al.* 1990; Mills 1992; German *et al.* 1993; Mitra *et al.* 1994; James & Elderfield 1996]. The REE systematics of these fluids and hydrothermal precipitates is described in Chapter 2 of this dissertation. Also shown in Table 8.4 is some unpublished REE data for pore fluids extracted from sediments forming in a zone of diffuse fluid upflow near the surface of the mound [M. Rudnicki pers. comm.].

REE patterns for all samples analysed in this study are shown in Figure 8.2. The REE data have been normalised to a composite chondrite composition [Evensen *et al.* 1978]. The REE data define two groups with differing REE concentrations. BRAVEX samples from the low-temperature field and the relict *Alvin* zone have greater REE contents (Nd = 231 to 334 ppm) than the *WHOI* samples recovered from the low-temperature field by DSRV *Alvin* (Nd = 0.499 to 7.63 ppm). The REE patterns of these two groups are discussed in

Table 8.4: REE data for TAG samples

		La	Ce	Pr	Nd	Sm	Eu	Gd	Tb	Dy	Ho	Er	Tm	Yb	Lu	Ce/Ce*	Eu/Eu*	Nd_n/Yb_n
		all values ppm[#]																
Low-temperature field																		
1982 *Alvin* samples:																		
1243-1		5.64	5.46	1.65	7.63	1.57	0.389	1.71	0.260	1.53	0.29	0.76	0.0949	0.56	0.088	0.41	0.72	4.8
1244-1B (top)		0.848	0.83	0.158	0.669	0.118	0.0355	0.210	0.0385	0.317	0.093	0.32	0.0429	0.26	0.052	0.47	0.68	0.88
1244-1C(bottom)		1.26	1.9	0.351	1.50	0.346	0.107	0.451	0.0880	0.634	0.17	0.56	0.096	0.64	0.12	0.65	0.83	0.82
1247-2-2D		1.06	1.1	0.221	0.912	0.159	0.0519	0.261	0.0518	0.382	0.11	0.34	0.0489	0.29	0.060	0.50	0.77	1.1
1247-2-2B		0.572	0.51	0.110	0.499	0.100	0.0313	0.157	0.0277	0.216	0.064	0.22	0.0323	0.21	0.044	0.42	0.76	0.82
1994 BRAVEX samples:																		
3387-R-1 MnA1		232	1120	62.6	253	54.0	12.8	59.6	8.49	47.4	8.8	24	3.28	20	3.1	2.2	0.69	4.3
3387-R-1 MnA1	u	231	990	59.0	236	50.4	12.2	57.1	8.08	45.2	8.4	23	3.16	20	3.1	2.0	0.69	4.2
3387-R-1 MnA2		264	1030	64.0	256	52.8	12.6	60.2	8.64	48.4	8.9	24	3.28	20	3.0	1.8	0.68	4.6
3387-R-1 MnA2	u	241	1060	60.2	231	49.5	12.3	54.8	8.41	45.4	8.8	23	3.26	19	3.2	2.0	0.72	4.1
3387-R-1 MnA3		282	1130	74.4	298	64.6	15.9	72.3	10.8	57.5	11.0	29	4.09	24	3.9	1.8	0.71	4.3
3387-R-1 MnB		291	1380	72.0	285	59.1	14.6	67.5	9.83	52.4	9.7	26	3.62	21	3.4	2.2	0.70	4.6
3387-R-1 MnC	u	256	953	61.8	246	53.2	12.7	59.0	8.41	47.0	8.8	24	3.33	20	3.1	1.7	0.69	4.2
3386-R-1 MnD	u	261	1260	67.6	269	57.0	14.2	63.88	10.0	52.7	10	26	3.72	21	3.4	2.2	0.72	4.5
Relict Mir zone																		
1994 BRAVEX samples:																		
3423-R-33 MnB	u	345	517	82.2	334	71.3	17.7	78.9	12.0	68.6	13	36	5.00	31	4.8	0.69	0.72	3.8
3423-R-27 MnC	u	295	408	67.9	274	56.7	13.9	62.4	9.41	54.5	10	28	3.78	23	3.6	0.64	0.71	4.1
*Black smoker fluid		5.68E-04	1.32E-03		8.68E-04	1.87E-04	5.42E-04	1.70E-04		1.23E-04		4.93E-05		3.60E-05	4.41E-06	0.96	9.1	8.4
+ Diffuse flow		3.90E-04	9.51E-04		6.43E-04	1.38E-04	1.48E-03	1.32E-04		8.58E-05		3.40E-05		3.15E-05	4.20E-06	0.98	33	7.1
§TAG pore fluid 2900-5			2.14E-04		9.61E-05	2.02E-05	1.79E-05	3.57E-05		4.66E-05		4.67E-05		7.61E-05	1.55E-05		2.0	0.44
§TAG pore fluid 2900-8			1.02E-03		4.60E-04	9.29E-05	6.05E-05	1.62E-04		1.72E-04		1.39E-04		1.11E-04	2.08E-05		1.5	1.4
*North Atlantic Seawater		3.54E-06	7.62E-07		3.09E-06	6.21E-07	1.61E-07	9.83E-07		1.03E-06		9.15E-07		9.38E-07	1.54E-07	0.10	0.63	1.1
✪ Pacific Seawater		5.13E-06	4.62E-07	3.71E-07	1.68E-06	3.25E-07	8.97E-08	5.65E-07	9.44E-08	7.93E-07	2.52E-07	9.03E-07	1.48E-07	1.12E-06		0.048	0.63	0.52
⌘TAG plume particulate		4.93E-07	3.28E-07	1.31E-07	5.74E-07	1.33E-07	4.00E-08	1.15E-07	2.30E-08		2.80E-08	7.44E-08				0.29	0.97	
⊛AMKG-1895		13.3	16.8		15.9	3.27	0.83	3.76		3.22		1.81		1.46		0.56	0.72	3.8
⊛TAG plume derived sediment		16.8	25.4		17.6	3.81	0.962	3.79		3.44		1.88		1.6		0.68	0.77	3.8
‡TAG plume derived sediment		5.91	8.46		6.49	1.46	1.027	1.366		1.368		0.818		0.731	0.097	0.64	2.2	3.1

u = unpicked sample; all other oxide samples were picked using a binocular microscope

*Data are from Mitra *et al.* [1994]; black smoker fluid data is recalculated to Mg=0, white smoker is recalculated to Mg=4 mmol kg^{-1}. Seawater data is for TAG (3400 m)

§Data are from M. Rudnicki [pers. comm.]

+ Data are from James and Elderfield [1996]

⊛Data are from Mills [1992]

⌘Data are from German *et al.* [1990]

✪ Data are from Bau *et al.* [1996]; average of six seawater samples from between 1000 and 2000 m depth

‡Data are from German *et al.* [1993]

#All REE concentrations are ppm except TAG plume particulates expressed as mg (of particulate REE) per litre of seawater [German *et al*.1990]

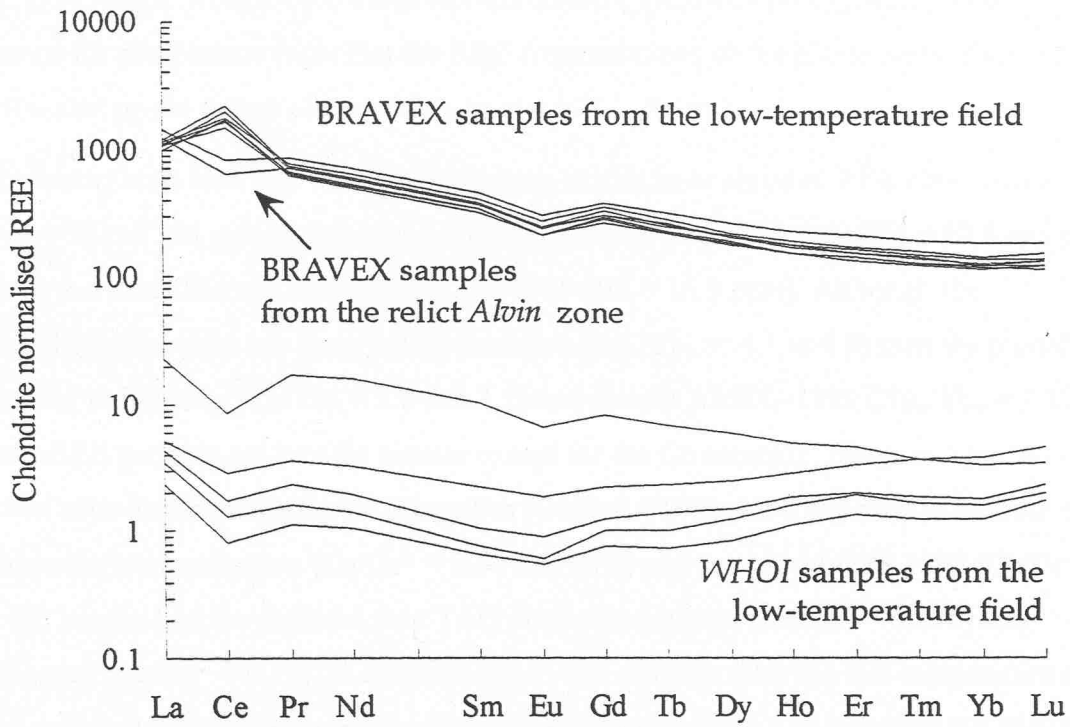

Figure 8.2: Chondrite normalised REE patterns for all ferromanganese crusts analysed in this study. The *WHOI* samples were collected by DSRV *Alvin* in 1982 and described by Thompson *et al.* [1985].

turn in the following sections.

BRAVEX samples (Alvin zone and low-temperature field)

Chondrite normalised REE patterns for BRAVEX samples from the low temperature field and the relict *Alvin* zone are shown in Fig. 8.3. The REE patterns of typical TAG plume particulate matter [German *et al.* 1990], plume derived sediments [Mills 1992; German *et al.* 1993] and a Mn-enriched metalliferous core-top (AMKG-1895) [Mills 1992] are shown for comparison (note that the REE concentrations of the plume particulate matter are scaled up six orders of magnitude to plot in this figure).

The amorphous Mn- and Fe-rich amorphous oxides have elevated REE concentrations (Nd = 231 to 334 ppm) compared with the plume derived sediments (Nd = 17.6 and 6.49 ppm) and metalliferous core-top AMKG-1895 (Nd = 15.9 ppm). Although the metalliferous oxides are more LREE-enriched (Nd_n/Yb_n = 4.1 to 4.6) than the plume derived sediments (Nd_n/Yb_n = 3.8 and 3.1) and sample AMKG-1895 (Nd_n/Yb_n = 3.8), their REE patterns are broadly similar except for the Ce anomaly. Samples from the relict *Alvin* zone display negative Ce anomalies (Ce/Ce* = 0.64 and 0.69) similar to those of plume derived sediments (Ce/Ce* = 0.64 and 0.68) and sample AMKG-1895 (Ce/Ce* = 0.56) but are less Ce-depleted than TAG plume particulates (Ce/Ce* = 0.296) and seawater (Ce/Ce* = 0.10). In contrast, BRAVEX samples from the low temperature field are enriched in Ce relative to the trivalent REEs (Ce/Ce* = 1.7 to 2.2). The BRAVEX samples are more depleted in Eu (Eu/Eu* = 0.68-0.72) than the plume derived particles and sediments (Eu/Eu* = 0.72 to 2.2).

WHOI samples (low-temperature field)

Chondrite normalised REE patterns for metalliferous oxides and silicates collected from the low-temperature field by DSRV *Alvin* are shown in Fig. 8.4. The REE patterns of North Atlantic seawater at 3400 m [Mitra *et al.* 1994] and the range of REE compositions of TAG mound pore fluids [M. Rudnicki pers. comm.] are shown for comparison. The pore fluids have negative Ce and positive Eu anomalies, indicating the influence of both seawater and vent-derived REEs (refer to Fig. 2.1).

The *WHOI* samples have REE concentrations (Nd = 0.499-7.36 ppm) that are two orders of magnitude lower than those recorded for the BRAVEX samples from the low temperature field. Sample 1243-1 has the highest REE abundances, and a distribution pattern that is

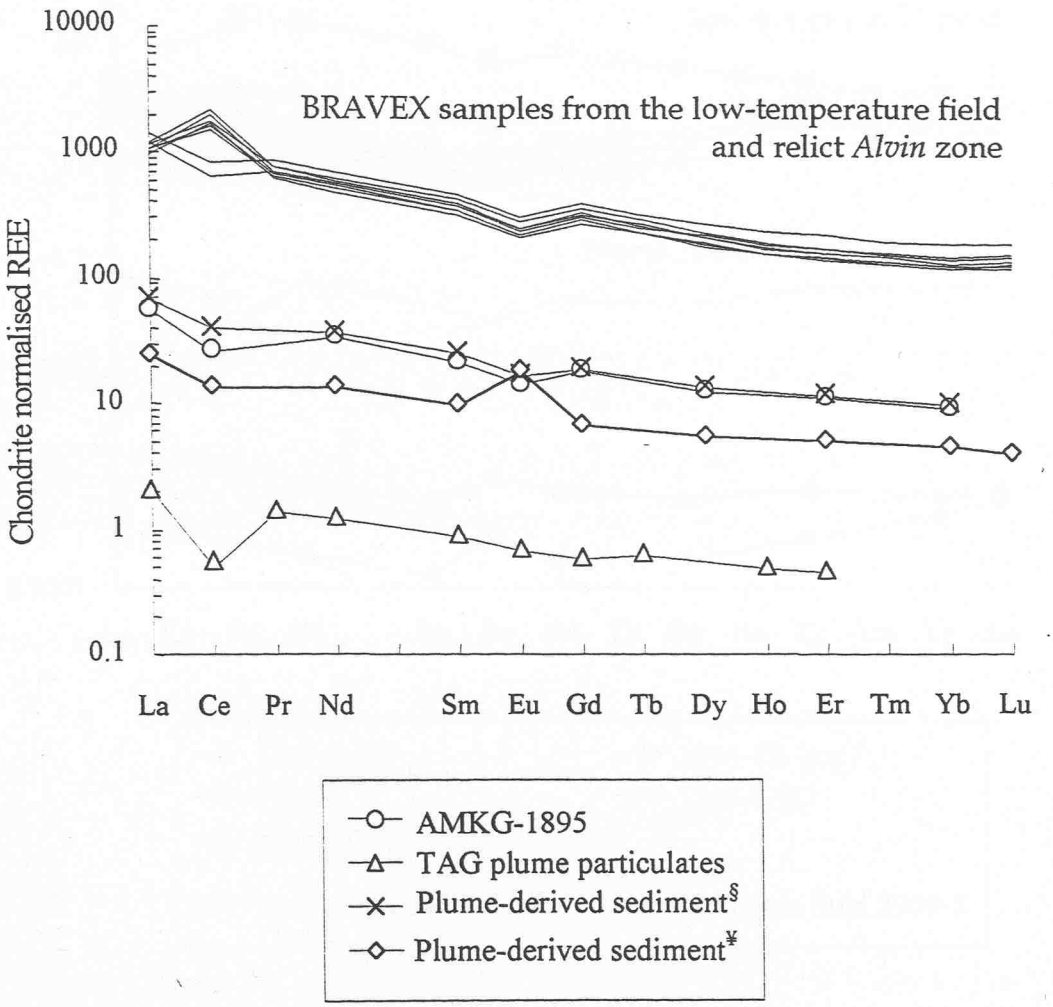

Figure 8.3: Chondrite normalised REE patterns for the BRAVEX samples from the low-temperature field and the relict *Alvin* zone. Plotted for comparison are the REE patterns of oxyhydroxide particles from the TAG neutrally buoyant plume (REE concentrations multiplied by 10^6), a manganiferous TAG core top (AMKG 1895) [Mills 1992], a plume-derived layer from a TAG sediment core§ [Mills 1992], and a plume-derived layer within a sediment core from the active TAG mound¥ (2182-4) [German *et al.* 1993].

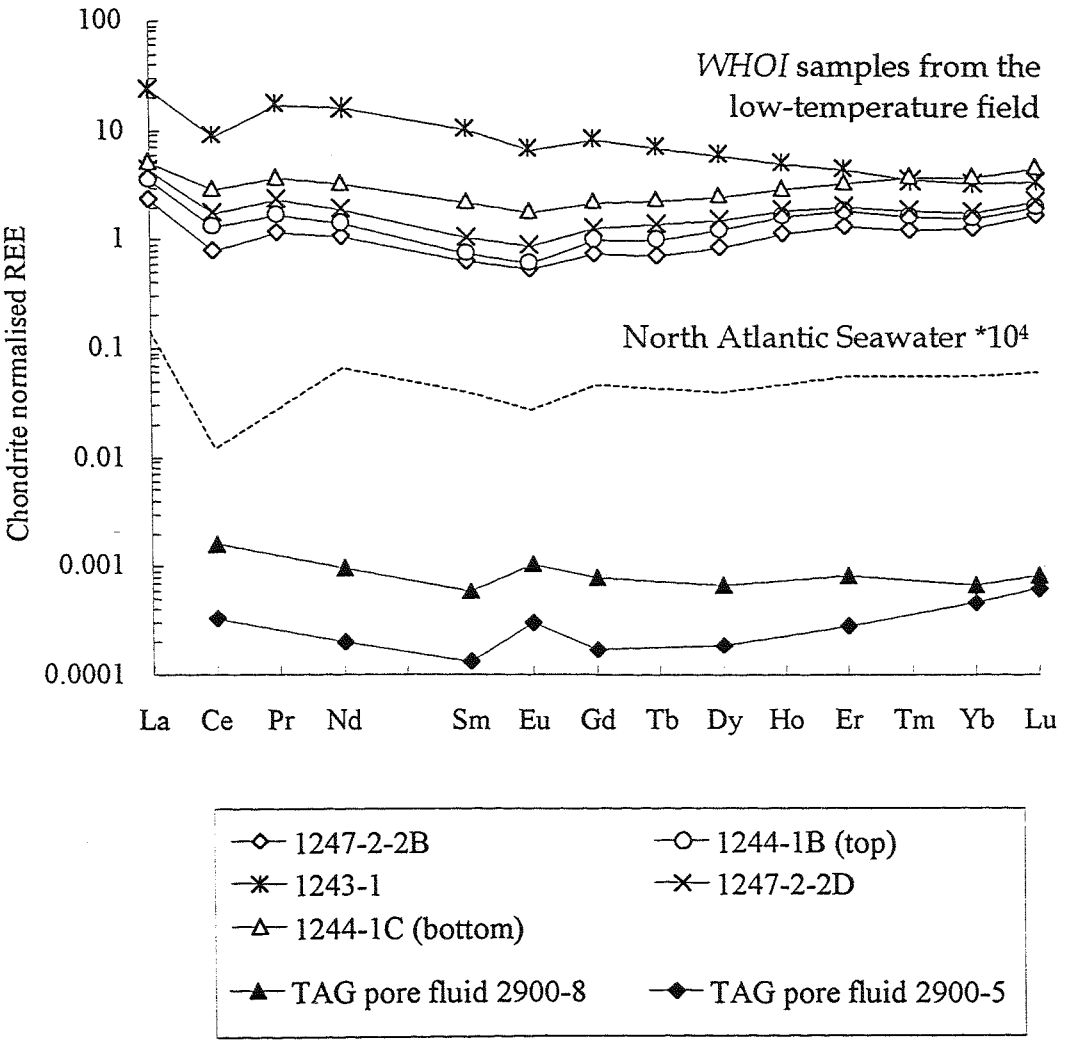

Figure 8.4: Chondrite normalised REE patterns from the *WHOI* samples collected from the low-temperature field by DSRV *Alvin* in 1982. Samples 1244-1B and 1244-1C are the top and lower surfaces of the same cm-thick birnessite crust, described by Thompson *et al.* [1985]. Plotted for comparison are the REE patterns of North Atlantic seawater (3400 m) at 26°N [Mitra *et al.* 1994], and TAG mound pore fluid samples 2900-8 and 2900-5 [M. Rudnicki pers. comm.]. These two samples represent the range in REE compositions of 8 pore fluids extracted from a sediment core sampled from the upper TAG mound.

similar to the plume derived particulates and sediments and BRAVEX samples from the relict *Alvin* zone, shown in Fig. 8.3 ($Ce/Ce^* = 0.41$; $Eu/Eu^* = 0.72$; $Nd_n/Yb_n = 4.8$). In contrast, the other *WHOI* samples show a degree of HREE enrichment ($Nd_n/Yb_n = 0.82$ to 1.1) that is greater than TAG plume derived sediments ($Nd_n/Yb_n = 3.8$ and 3.1) and seawater ($Nd_n/Yb_n = 1.1$) but within the range exhibited by TAG mound pore fluids ($Nd_n/Yb_n = 0.44$ to 1.4). The Eu anomalies of the *WHOI* samples ($Eu/Eu^* = 0.68$ to 0.83) are comparable to plume derived particulates ($Eu/Eu^* = 0.72$). In comparison the pore fluids are relatively enriched in Eu ($Eu/Eu^* = 2.0$ to 1.5).

8.4.3 Nd-isotopes

Radiogenic isotopic results for the ten analysed samples are recorded in Table 8.4, with the results of Os isotope analyses of four of the *WHOI* samples [Ravizza *et al.* 1996]. The $^{143}Nd/^{144}Nd$ ratios are expressed as parts per 10^4 deviation from the CHUR(0) value of $\varepsilon_{Nd}(0) = 0.512638$. The Nd-isotope results are also displayed as a histogram of $\varepsilon_{Nd}(0)$ values in Fig. 8.5, with the values of some Atlantic ferromanganese deposits (authigenic and hydrothermal) determined by Piepgras *et al.* [1979].

The $\varepsilon_{Nd}(0)$ values for four of the *WHOI* samples fall in the range -12.3 to –10.17. Sample 1247-2-2D has a considerably higher $\varepsilon_{Nd}(0)$ value of –2.13. The five BRAVEX samples exhibit much lower $\varepsilon_{Nd}(0)$ values that range from -12.19 to –10.92, and are similar to the other four *WHOI* samples.

8.7 Discussion

8.7.1 Seawater scavenging of REEs

The BRAVEX samples from the inactive *Alvin* zone and the low-temperature field (Fig. 8.3), and *WHOI* sample 1243-1 from the low-temperature field (Fig 8.4) have compositions indicative of extensive scavenging of seawater REEs. Similar patterns have been reported for EPR ridge crest metalliferous sediments [Dymond, 1973; Ruhlin & Owen 1986; Barrett & Jarvis 1988; Owen and Olivarez, 1988], for hydrothermal and hydrogenous oceanic ferromanganese deposits [Toth 1980; Fleet 1983], and for metalliferous sediments accumulating on the seafloor beneath the TAG neutrally buoyant plume [Mills 1992; Mills *et al.* 1993; German *et al.* 1993].

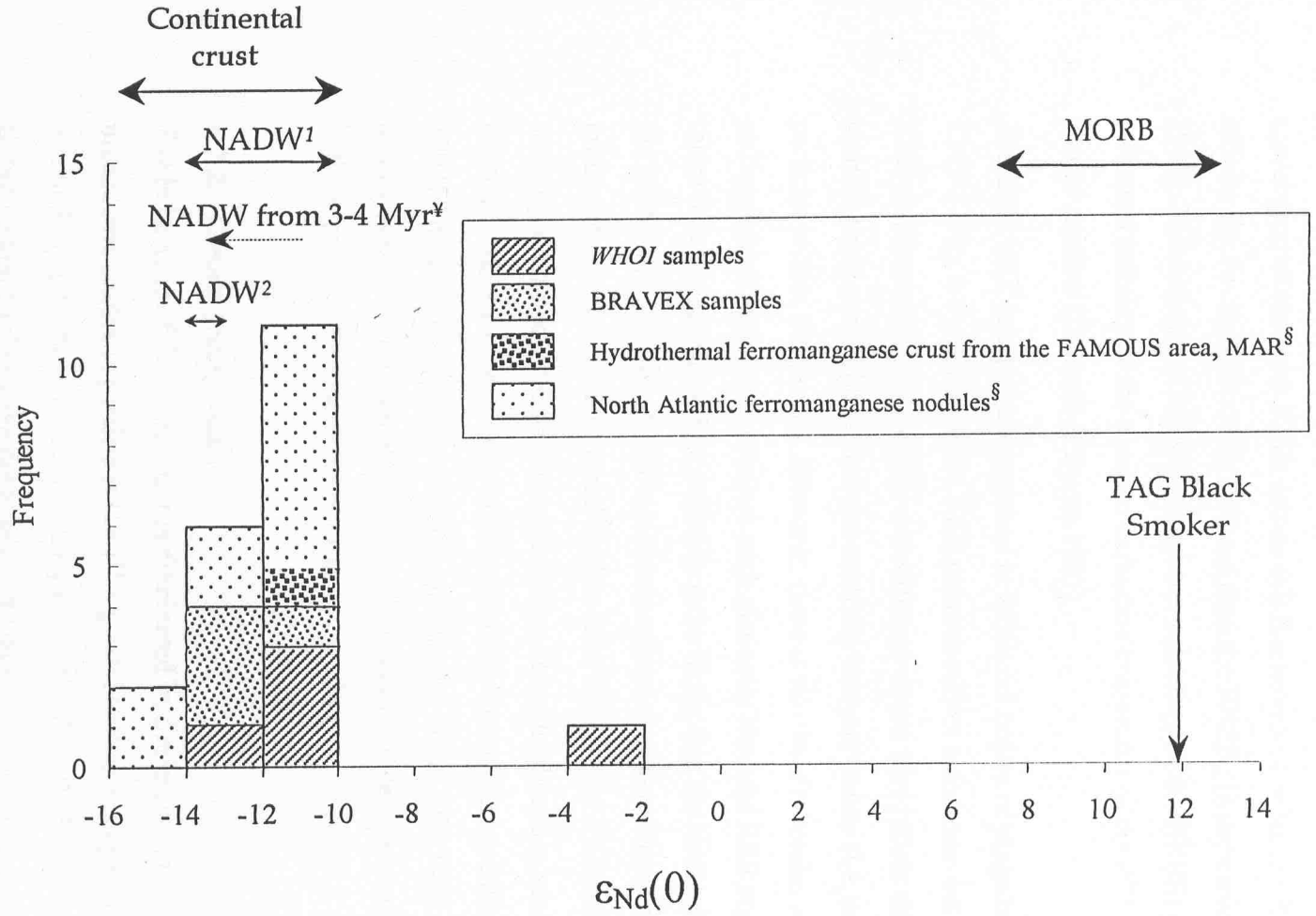

Figure 8.5: Histogram of $\varepsilon_{Nd}(0)$ values of the TAG ferromanganese crusts analysed in this study. The $\varepsilon_{Nd}(0)$ values represent the parts per 10^4 deviation from the CHUR(0) value of 0.512638. Data for an Atlantic hydrothermal crust and ferromanganese nodules [§Piepgras *et al.* 1979] are shown for comparison. Seawater below 1000 m depth in the North Atlantic is dominated by North Atlantic Deep Water (NADW). The data for NADW are from [1]Piepgras *et al.* [1979] (inferred from authigenic ferromanganese sediments) and [2]Piepgras & Wasserburg [1987] (direct seawater measurements). The $\varepsilon_{Nd}(0)$ values for MORB and continental rocks are from DePaolo & Wasserburg [1977]. The Nd-isotopic composition of NADW is inferred to have shifted to less radiogenic compositions over the last 3-4 Myr [¥Burton *et al.* 1998].

Sediments forming on the valley floor at TAG from the slow fall-out of oxyhydroxide particles from the neutrally buoyant plume have highly elevated REE/Fe ratios, due to continued uptake of REEs from seawater after deposition on the seafloor [German *et al.* 1993; Mills *et al.* 1993]. The BRAVEX samples and *WHOI* sample 1243-1 are enriched in LREEs compared with the plume particulates and underlying sediments. Prolonged scavenging of seawater REEs causes this fractionation because LREEs have a greater affinity for Fe- and Mn oxide surfaces than the HREEs [Koeppenkastrop & De Carlo 1992]. This behaviour reflects the greater solubility of the HREEs in seawater, due to the enhanced stability of the aqueous carbonate complexes of the REEs with increasing atomic number [Cantrell & Byrne 1987].

The BRAVEX samples are enriched in REEs *c.*3 orders of magnitude over *WHOI* sample 1243-1 (Fig. 8.4), although the REE patterns reflect a common enrichment process. The REE enrichment of some of the metalliferous crusts may reflect differences in the flux of hydrothermal particulates from the neutrally buoyant plume (i.e. exposure time of particles within the plume). However, there is no obvious reason why local variations in sedimentation rate would produce such distinctly bimodal REE contents, rather than a range of concentrations. It is probably more likely that the extreme REE enrichment of the BRAVEX over the *WHOI* samples is related to differences in the substrate in the two groups of samples. Experimental studies have shown that REEs are more effectively scavenged onto amorphous than crystalline Fe-oxyhydroxides because they have relatively more surface area available for REE uptake [Koeppenkastrop & De Carlo 1992] This may account for the REE enrichment of the BRAVEX amorphous oxides, in comparison to *WHOI* sample 1243-1, which has been described as crystalline nontronite with amorphous Fe-oxides [Thompson *et al.* 1985].

8.7.2. Cerium fractionation

The behaviour of Ce in seawater is dominated by preferential oxidative uptake onto manganese oxides in particular [Goldberg 1961] rather than general scavenging processes which dominate the oceanic chemistry of the trivalent REEs [Elderfield 1988]. Experimental studies have demonstrated that enhanced Ce scavenging is a feature of MnO rather than FeOOH systems [Koeppenkastrop & De Carlo 1992].

Hydrothermal ferromanganese deposits typically have Ce-depleted REE patterns because they incorporate particles that have scavenged seawater REEs and/or precipitate from

dilute hydrothermal fluids that have mixed with large amounts of seawater [e.g. Bonatti 1975; Toth 1980; Elderfield & Greaves 1981; Fleet 1983; De Carlo & McMurtry 1992; Hein *et al.* 1994]. Hydrogenous deposits, including ferromanganese nodules, form by direct precipitation from seawater and diagenetic interactions with surrounding sediments [Bonatti 1975; Elderfield *et al.* 1981*a,b*]. They are typically Ce-enriched and are the main repository for insoluble Ce that is depleted in seawater compared with the trivalent REE [Elderfield *et al.* 1981*a,b*]. While the trivalent REEs undergo some diagenetic cycling through surface sediments, Ce is incorporated directly from seawater into the nodules [Elderfield *et al.* 1981*a*]. Most ferromanganese deposits are formed by a combination of hydrothermal and hydrogenous processes [Fleet 1983], and atypical negative Ce anomalies in Pacific ferromanganese nodules have been attributed to formation in the vicinity a hydrothermal plume [Elderfield & Greaves 1981].

BRAVEX samples from the relict *Alvin* zone and the *WHOI* samples from the low-temperature field display negative Ce anomalies, while BRAVEX samples from the low temperature field are enriched in Ce relative to the trivalent REEs (Fig. 8.4). The contrasting Ce contents of these two groups of samples might be related factors such as deposit mineralogy or accumulation rate. However, the results of limited TEM analyses suggest that both the Ce-enriched BRAVEX low-temperature field samples and Ce-depleted relict *Alvin* zone samples comprise X-ray amorphous particles with similar compositions. Further evidence against a compositional control on Ce content is provided by the *WHOI* samples from low-temperature field. These samples display similar negative Ce anomalies, despite extreme differences in Mn content (52.3 wt. % Mn for sample 1244-1B to 0.67 wt. % for sample 1243-1) [Thompson *et al.* 1985]. It is therefore more likely that differences in the Ce anomaly are related to accumulation rate. The characteristic Ce depletion of plume derived-particulates and metalliferous sediments (e.g. Fig. 8.3) is indicative of the rapid uptake of REEs from a Ce-depleted seawater source. The negative Ce anomalies exhibited by samples from the inactive *Alvin* zone might reflect the rapid accumulation of Mn-Fe particles in a zone of fall-out from the neutrally buoyant TAG plume. However, these particles are presumably accumulating sufficiently rapidly to inhibit the development of large Ce-enrichments that are typical of hydrogenous ferromanganese deposits.

The Ce-enriched chondrite normalised REE patterns of the BRAVEX samples from the low temperature field are reminiscent of hydrogenous ferromanganoan sediments and

nodules [e.g. Bonatti *et al.* 1975; Elderfield et al. 1981*a,b*; Fleet 1983; De Carlo & McMurtry 1992]. The Ce-enrichment can be attributed to the preferential removal of Ce from seawater onto Mn-oxides [Goldberg 1961; Koeppenkastrop & De Carlo 1992]. These samples are inferred to be accumulating relatively slowly in the absence of a Ce-depleted particle flux from the neutrally buoyant plume. The accumulation rates of these samples might be more similar to hydrogenous ferromanganese deposits in the Atlantic (~3 mm Myr^{-1}) [Claude-Ivanaj *et al.* 1998] than to hydrothermal ferromanganese deposits in TAG vent field (100 to 200 mm Myr^{-1}) [Scott et al. 1974]. Ferromanganese crusts have been previously described from outside the TAG vent field that are similarly enriched in REEs and exhibit small positive Ce anomalies [Toth 1980].

Although the BRAVEX samples analysed exhibit variable Ce content, there is no fractionation of the trivalent REEs in these samples over the range of crystallinities inferred from TEM electron diffraction patterns, inferred accumulation rates, nor with depth (refer to Fig. 8.1).

8.7.3 REE evidence for diffuse venting within the low-temperature field

Excluding sample 1243-1 (section 8.7.1), the *WHOI* samples have REE compositions (Nd_n/Yb_n = 0.82 to 1.1) that are distinct from the other samples analysed in this study (Nd_n/Yb_n = 3.8 to 4.8) but are similar to TAG mound pore fluids (Nd_n/Yb_n = 0.44 and 1.4) in terms of the degree of LREE /HREE fractionation they exhibit. To assess if this fractionation can arise during uptake of REEs from a seawater source, the REE contents of the BRAVEX and *WHOI* samples are shown normalised to TAG seawater concentrations in Fig. 8.6. Also plotted in Fig. 8.6 (after appropriate scaling) are scavenging rate constants for REEs onto Fe-oxyhydroxides in the neutrally buoyant TAG plume calculated by Rudnicki & Elderfield [1993]. Scavenging rate constants REEs in the neutrally buoyant plume range between 3.5 to 16 $\times$ 10^{-11} $(nmol/kg)^{-1}$ s^{-1} (for Sm and Lu respectively) and are greater for the intermediate- than light- and heavy REE [Rudnicki & Elderfield 1993]. Consequently scavenging uptake of the REEs at these different rates within the neutrally buoyant plume leads to the addition of a fractionated (MREE-enriched) seawater REE pattern that is reflected in the fractionated (MREE enriched) seawater REE patterns of underlying plume-derived sediments [German *et al.* 1993; Mills *et al.* 1993].

The BRAVEX samples and *WHOI* sample 1243-1 have REE patterns (excluding Ce) that are similar in form to that predicted by the chemical plume model of Rudnicki &

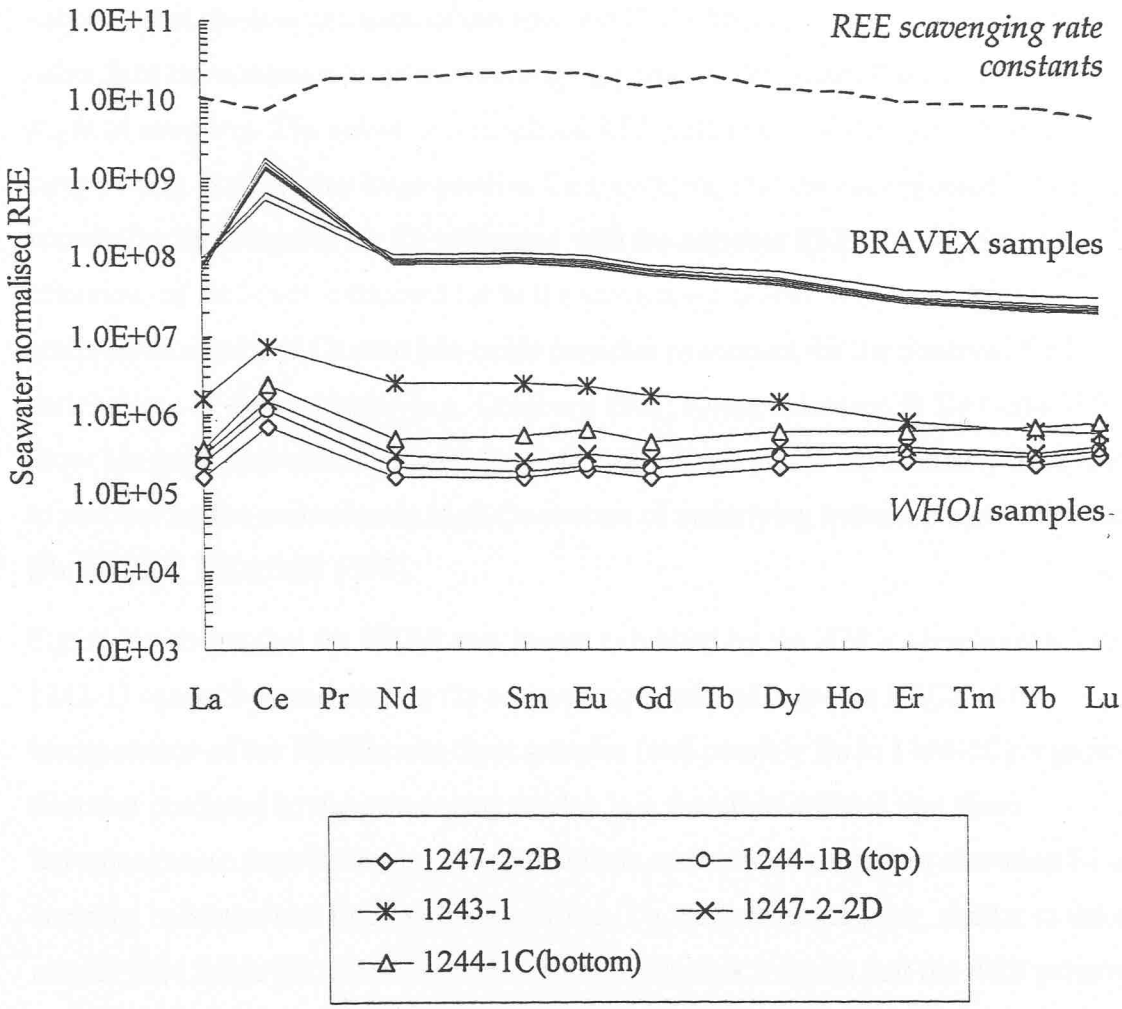

Figure 8.6: Seawater normalised REE patterns for the *WHOI* and BRAVEX ferromanganese crusts. Scavenging rate constants for REEs in the TAG neutrally buoyant plume from the chemical plume model of Rudnicki & Elderfield [1993] have been plotted for comparison, after appropriate scaling. These constants range from 16×10^{-11} $(nmol/kg)^{-1}$ s^{-1} for Sm to 3.5×10^{-11} $(nmol/kg)^{-1}$ s^{-1} for Lu, and are greater for the intermediate- than light- and heavy REE [Rudnicki & Elderfield 1993]. The scavenging model accounts for the relative abundances of the trivalent REEs in the BRAVEX samples and *WHOI* sample 1243-1, but cannot explain the HREE-enriched patterns of the other four *WHOI* samples. Ce concentrations are elevated above the trivalent REEs and not accounted for by the scavenging model (see discussion in text).

Elderfield [1993], confirming the scavenging uptake of seawater REEs onto hydrothermally produced metal-oxyhydroxides. The striking similarity of the REE fractionation patterns of the BRAVEX samples and *WHOI* sample 1243-1 (Fig. 8.4) indicates that the concentration of the trivalent REEs are controlled by uptake processes, rather than the composition of the scavenging particles, the inferred accumulation rates or depth of sampling. The seawater normalised REE patterns for the BRAVEX and *WHOI* samples (Fig. 8.6) display large positive Ce anomalies, that are not reflected in the scavenging rate constant for Ce compared with the adjacent REEs. This indicates that the behaviour of Ce is not accounted for in the scavenging model. It is necessary to invoke the preferential uptake of Ce onto Mn-oxide particles to account for the observed Ce enrichments of these samples [e.g. Goldberg 1961; Koeppenkastrop & De Carlo 1992]. Slow Mn particle production and fall-out from the TAG plume has similarly been inferred to account for the anomalously high Ce content of underlying hydrothermal sediments [Rudnicki & Elderfield 1993].

Figure 8.6 shows that the HREE enrichment exhibited by the *WHOI* samples (excluding 1243-1) cannot be generated by the scavenging uptake of seawater REEs, as the incorporation of the HREEs into these samples (and possibly Eu in 1244-1C) is greater than that predicted by the scavenging model. It is therefore inferred that these ferromanganese deposits have precipitated from and/or been subject to alteration by a Eu-enriched hydrothermal fluid with a lower Nd_n/Yb_n ratio than seawater, similar to the TAG mound pore fluids [M. Rudnicki pers. comm.]. Figure 8.7 shows that the REE pattern of this fluid cannot be replicated by any simple mixture of end-member black smoker fluid and seawater, as mixing alone cannot produce a fluid with low Nd_n/Yb_n ratios. The REE pattern of the pore fluids is also different from diffuse flow that has been sampled at the surface of the TAG mound, also shown in Fig. 8.7. The REE content of this diffuse flow has been explained as a dilute (*c.* 25 °C) black smoker fluid containing 0.12 mmol of dissolved anhydrite per kilogram of fluid, and is not enriched in HREEs (Nd_n/Yb_n = 7.1) [James & Elderfield 1996]. Ochreous sediments in zones of diffuse (*c.* 46°C) fluid upflow on the TAG mound have more fractionated (evolved) REE patterns with high Nd_n/Yb_n ratios (8.2 to 14), and are inferred to form from fluids with similarly LREE-enriched compositions [Mills *et al.* 1996]. The contrasting REE patterns of these diffuse fluids are inferred to reflect the complexity of fluid mixing and evolution processes occurring within the sulphide mound [Mills *et al.* 1995*a*; James & Elderfield 1996; Mills *et al.* 1996].

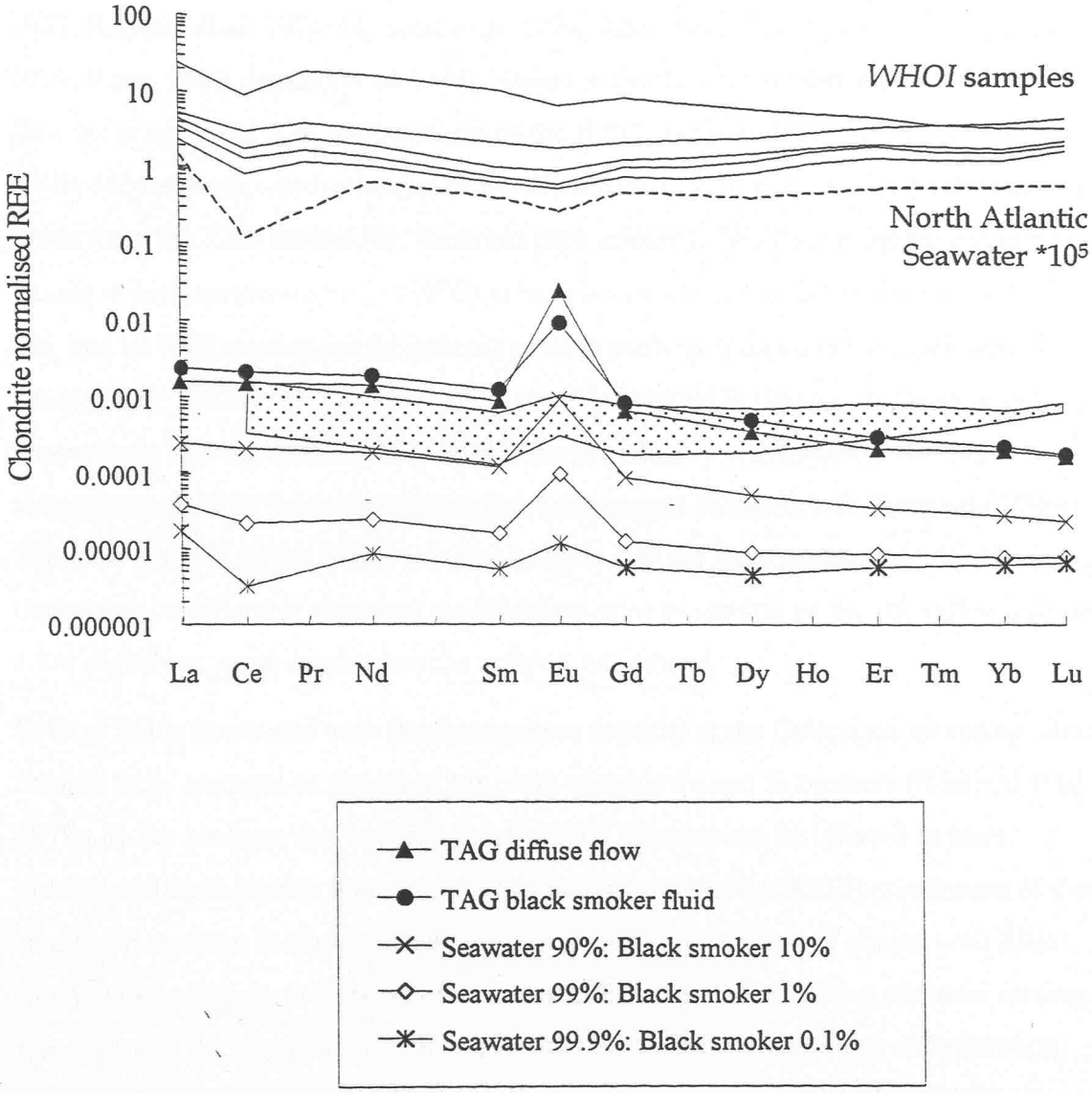

Figure 8.7: Comparison of the chondrite normalised REE patterns for the *WHOI* ferromanganese crusts and various mixtures of TAG black smoker fluid and North Atlantic seawater. Also shown are end-member REE compositions of North Atlantic seawater (concentrations multiplied by 10^5) and a TAG black smoker fluid (data are from Mitra *et al.* [1994]), and diffuse flow sampled at the mound surface [James & Elderfield 1996].The shaded area represents the range in REE compositions of some TAG mound pore fluids [M. Rudnicki pers. comm.]. The REE patterns of the *WHOI* samples cannot be explained as any simple mixture of black smoker fluid and seawater REEs, as mixing alone cannot produce fluids with lower Nd_n/Yb_n ratios than seawater.

Because they cannot be generated by seawater interactions, the REE patterns of four of the *WHOI* samples confirm that diffuse venting is occurring within the low-temperature field, as proposed in previous studies on the basis of other chemical and physical criteria [Rona 1973; R. Scott *et al.* 1974; M. Scott *et al.* 1974; Rona 1975; Thompson *et al.* 1985; Rona 1978; Rona, 1980; Jenkins *et al.* 1980; Nelson & Forde 1991; Elderfield *et al,* 1993; Ravizza *et al.* 1996]. The REE patterns of the *WHOI* samples demonstrate the influence of REEs derived from a hydrothermal fluid with a similar REE composition to diffuse pore fluids from the TAG mound [M. Rudnicki pers. comm.]. This fluid must have reacted with basalts at high temperatures (*c.*350°C) to have become enriched in metals such as Fe and Mn, and its REE content can be inferred to have evolved from an initial black-smoker-like composition. Within the TAG vent field, the TAG mound is the present focus of high-temperature hydrothermal activity. Fluids are presumably channelled to the low-temperature field by faults that dissect the TAG mound [Kleinrock & Humphris 1996]. The REE patterns of the *WHOI* samples indicate that the high-temperature fluid has undergone considerable chemical modification prior to venting on the rift valley wall, in *c.* 1 km shallower water depths than the active TAG mound.

Diffuse fluids associated with ferromanganese deposits at the Galapagos spreading centre contain large amounts of dissolved Mn, with variable Fe and Si contents [Edmond *et al.* 1979*a,b*]. By analogy, the 'hydrothermal' *WHOI* samples can be inferred to have precipitated from similar fluid compositions. The origin of the HREE enrichment of these samples is unclear. It might arise by the precipitation/dissolution of phases with REE-fractionated patterns, or because of a change in REE speciation during seawater mixing. Speciation of the trivalent REEs in seawater is dominated by carbonate complexation [Cantrell & Byrne 1987; Wood 1990*a*]. Seawater is relatively enriched in HREEs because they form more stable carbonate complexes than the LREEs and consequently less prone to particle-reactive uptake from seawater [Cantrell & Byrne 1987]. In acidic hydrothermal solutions the REE are transported as less stable chloride species in the absence of other ligands [Wood 1990*a,b*]. LREEs form more stable Cl complexes than the HREEs in acidic hydrothermal solutions, and Fe-oxides precipitating from such solutions would be HREE enriched. Mixing of hydrothermal fluid with seawater may generate a HREE enrichment in the fluid as REE speciation becomes increasingly dominated by carbonate- rather than chloride complexation at higher dilutions and lower temperatures. However, seawater mixing alone this cannot account for the observed enrichments, because as discussed, these samples are mostly *more* HREE enriched than North Atlantic seawater.

Therefore, fractionation of the REEs to the observed HREE-enriched compositions might have occurred *via* the preferential uptake of LREEs from solution onto particulate phases formed prior to venting, in addition to a change in REE speciation from their transport as chloride- to carbonate dominated REE complexes.

Solution complexation will not affect the Eu and Ce anomaly, which should therefore reflect the redox state of the parental fluid. Europium will be present as Eu^{3+} at temperatures below 250°C and will behave coherently with the other trivalent REEs [Sverjensky 1984]. The 'hydrothermal' *WHOI* samples contain residual Eu enrichments inherited from the high-temperature fluid, that arises from the fractionation of Eu^{2+} from the trivalent REEs at elevated temperatures and pressures (refer to section 2.5) [Sverjensky 1984].

8.7.4 Radiogenic isotope systematics

Because REE residence times are shorter than the oceanic mixing time, Nd-isotopes can used to identify sources of Nd in addition to mixing, transport and depositional processes within the ocean (refer to section 2.10) [Elderfield 1988; Piepgras & Jacobsen 1992]. Seawater below 1000 m depth in the north Atlantic is dominated by North Atlantic Deep Water (NADW), that has low ε_{Nd} (0) values (-13 ± 5) because Nd inputs are dominated by the erosion of continental material [Piepgras *et al.* 1979; Piepgras & Wasserburg 1980; Piepgras & Wasserburg 1987]. Fluids venting from the active TAG mound, 26°N MAR have ε_{Nd} (0) = +11.9 [T. Masuzerawa pers. comm.]. There are no published Nd-isotope data for TAG basalts.

The histogram in Fig. 8.5 shows that Nd isotope data for Atlantic ferromanganese nodules and exhibit distinctive and tightly clustered ε_{Nd} (0) values of –10 to –14 [Piepgras *et al.* 1979]. The Nd-isotopic composition of a hydrothermal oxide-rich crusts from the FAMOUS site on the MAR (ε_{Nd} (0) = -11.5) falls within the range of ε_{Nd} (0) values exhibited by the Atlantic ferromanganese nodules [Piepgras *et al.* 1979; Piepgras & Wasserburg 1980]. The similarity of the Nd isotopic composition of the hydrothermal and hydrogenous deposits is consistent with inferences that mantle-derived hydrothermal Nd is confined to deposits accumulating around hydrothermal vents, and is rapidly overprinted by seawater-scavenged Nd (refer to section 2.10) [e.g. Mills *et al.* 1993; Halliday *et al.* 1992]. Direct seawater measurements indicate that present-day NADW has a well-defined isotopic composition of ε_{Nd} (0) = -13.5 ± 0.5. A recent comparison of the Nd-isotopic

composition and $^{10}Be/^{9}Be$ ages of hydrogenous ferromanganese crusts in the western North Atlantic by Burton *et al.* [1998] suggests that NADW has evolved to its present composition from more radiogenic isotope compositions of ε_{Nd} (0) = -11 over the last *c.*4 Myr, due to an increasing contribution of more negative waters originating in the Labrador Sea (ε_{Nd} (0) = <-18 [Piepgras & Wasserburg 1987]) to NADW formation. This signal is evident in the ε_{Nd} (0) values of slowly accumulating ferromanganese deposits analysed by Piepgras *et al.* [1979]. These integrate the NADW signal over the time-scale of their formation, and have values up to –10 (Fig. 8.5), compared with the present NADW value of –13.5 [Piepgras *et al.* 1987].

Excluding *WHOI* sample 1247-2-2D, the samples analysed in this study have ε_{Nd} (0) values ranging from –10.7 to –12.3, and are within the range of compositions of Atlantic ferromanganese nodules and hydrothermal crust analysed by Piepgras *et al.* [1979], being slightly more radiogenic than the NADW value of ε_{Nd} (0) = -13 ± 0.5. Ce-enriched (hydrogenous) BRAVEX samples from the low-temperature field are inferred to be accumulating outside the influence of a hydrothermal plume, and more slowly than the Ce-depleted *WHOI* samples from the low-temperature field and BRAVEX samples from the relict *Alvin* zone (section 8.7.2). The Ce-enriched BRAVEX samples have more radiogenic ε_{Nd} (0) values (-10 to –12.2) than samples from the relict *Alvin* zone (-12.1 and –12.2). If the Ce-enriched samples are accumulating relatively slowly, then the thin Mn-oxide coatings analysed in this study may be integrating former (i.e. more radiogenic) and present-day NADW compositions, accounting for the compositions that are more radiogenic than present-day NADW. The ε_{Nd} (0) values of the *WHOI* samples are also more radiogenic than modern NADW (-2.13 to –12.3). Previous radiochemical analyses of hydrothermal ferromanganese crusts from the low-temperature zone indicate they are accumulating two orders of magnitude faster (100 to 200 mm Myr^{-1}) than typical hydrogenous deposits [Scott *et al.* 1974], and they have been dated to *c.*4000 to 125 000 years [Lalou *et al.* 1986; Lalou *et al.* 1990; Lalou *et al.* 1993]. The elevated ε_{Nd} (0) values of the WHOI samples is therefore interpreted to reflect the incorporation of a small amount of basaltic, in addition to seawater-derived Nd.

Sample 1247-2-2D has a more radiogenic composition, *c.*8 ε units higher than the other samples (ε_{Nd} (0) = -2.13). This is inferred to reflect the incorporation of some Nd sourced from a hydrothermal fluid, consistent with REE evidence for the formation of the *WHOI* samples from diffuse hydrothermal fluids, as discussed in section 8.7.3.

The $\varepsilon_{Nd}(0)$ values of the BRAVEX and *WHOI* samples have been plotted against their Yb_n/Nd_n ratios in Fig. 8.8. The Nd isotopic composition of a TAG black smoker fluid [T. Masuzerawa pers. comm.] and NADW are shown for reference [Piepgras & Wasserburg 1987]. Also plotted are some data for a metalliferous sediment core sampled 2 km NE of the TAG mound, which comprises layers dominated by either TAG plume particles or eroded sulphide material [Mills *et al.* 1993]. On this graph the plume-derived sediments, the BRAVEX samples and *WHOI* sample 1243-1 plot in a group that is characterised by relatively low Nd_n/Yb_n ratios (*c.* 0.25) and low, seawater-like $\varepsilon_{Nd}(0)$ values (*c.* −12). The other samples display more scatter in $\varepsilon_{Nd}(0)$ values and comprise the 'hydrothermal' *WHOI* samples (Yb_n/Nd_n = *c.* 1.2) and the sulphidic metalliferous sediments of Mills *et al.* [1993] (Yb_n/Nd_n = *c.* 0.3). Mills *et al.* [1993] found that the Nd-isotope compositions and Nd concentrations of the sediments define two mixing lines between seawater ($\varepsilon_{Nd}(0)$ = =13.5, Nd = 19.9 ppm) and two hydrothermal end-members with inferred $\varepsilon_{Nd}(0)$ values of +10 and Nd concentrations of 2.4 ppm and 0.74 ppm respectively [Mills *et al.* 1993]. These two groups of samples are distinguished in Fig.8.10 by the use of solid (2.4 ppm end-member) and open (0.74 ppm end-member) symbols. The plume-derived sediments (circles) have higher Nd concentrations than the sulphidic portions of the core (~ 12 ppm Nd compared with ~3 ppm). Fig. 8.8 suggests that the process responsible for the Nd enrichment of the plume-derived sediments causes fractionation of the REEs away from compositions predicted by the mixing line by reducing the Yb_n/Nd_n ratios. This trend towards generally lower Yb_n/Nd_n ratios with decreasing $\varepsilon_{Nd}(0)$ towards seawater values is delineated in Fig. 8.8 by the curved arrows. It is inferred that the process responsible for lowering the $\varepsilon_{Nd}(0)$ values of the sediment samples and increasing the degree LREE/HREE fractionation is the scavenging uptake of Nd from seawater. Preferential uptake of the less soluble LREEs from seawater onto oxide or oxyhydroxide particulates is characteristic of natural and experimental systems [Cantrell & Byrne 1987; Elderfield *et al.* 1988; Koeppenkastrop & De Carlo 1992].

The plume-derived sediments, BRAVEX ferromanganese deposits and *WHOI* sample 1243-1 have seawater-like $\varepsilon_{Nd}(0)$ values and exhibit a range of Yb_n/Nd_n ratios, that is inferred to reflect the extent of LREE uptake from seawater. *WHOI* sample 1243-1 shows the greatest degree of LREE-enrichment (lowest Yb_n/Nd_n ratio), and therefore might be expected to possess the highest Nd concentrations. However, sample 1243-1 contains much lower levels of REEs than the BRAVEX samples (7.63 ppm cf. >250 ppm). This

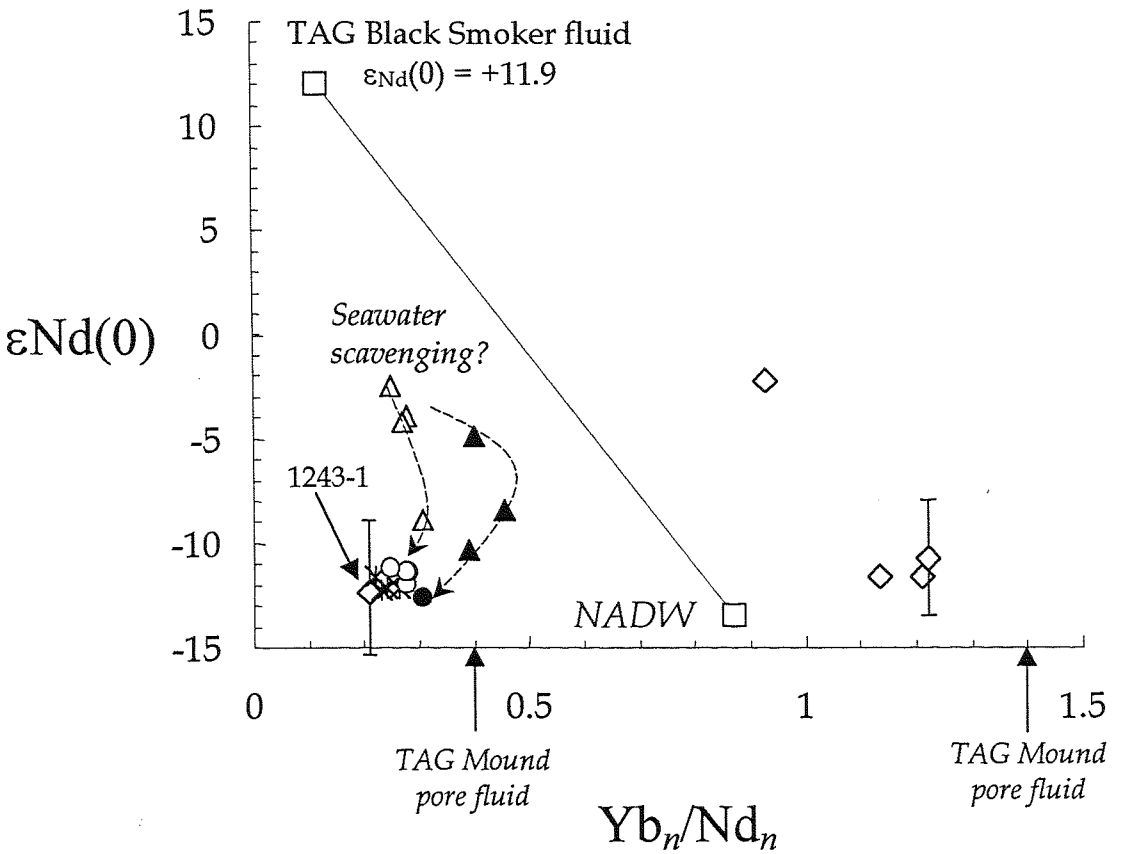

Diamonds are the *WHOI* samples
Crosses are the BRAVEX samples
Circles are TAG plume-derived sediments
Triangles are TAG sulphidic sediments

Figure 8.8: Relationship between $\varepsilon_{Nd}(0)$ value and Yb_n/Nd_n ratio for the *WHOI* and BRAVEX ferromanganese crusts. None of these samples fall on the mixing line defined by NADW [Piepgras & Wasserburg 1987; Mitra *et al.* 1994] and TAG black smoker fluid compositions [Mitra *et al.* 1994; T. Masuzerawa pers. comm.]. The BRAVEX samples, *WHOI* sample 1243-1 and sub-samples of a TAG field core analysed by Mills *et al.* [1993] define a trend towards lower ratios with decreasing $\varepsilon_{Nd}(0)$ value, which is inferred to reflect seawater REE uptake. There are clearly different controls on the Yb_n/Nd_n ratios of the other four *WHOI* samples, which fall within the range exhibited by TAG mound pore fluids. Error bars on the *WHOI* samples are 2σ.

apparent discrepancy may reflect differences in the crystallinity of the BRAVEX samples (amorphous Fe- and Mn-oxides) compared with *WHOI* sample 1243-1 (crystalline Fe-silicates and amorphous Fe-oxides). In experimental studies, scavenging uptake of all REEs from solution onto amorphous FeOOH is greater than onto crystalline goethite, because of the greater effective surface area of the amorphous phases [Koeppenkastrop & De Carlo 1992]. Moreover, while scavenging onto both crystalline and amorphous FeOOH is more efficient for the LREEs than the HREEs, there is a lesser fractionation during scavenging onto the amorphous phase which is more likely to sorb non-selectively both LREEs and HREEs than crystalline FeOOH [Koeppenkastrop & De Carlo 1992]. This observation is consistent with the observations of higher Yb_n/Nd_n ratios for the BRAVEX samples then *WHOI* sample 1243-1, despite their much higher Nd concentrations.

Fig. 8.8 indicates that the 'hydrothermal' *WHOI* samples are incorporating REEs from fluids with highly evolved REE compositions. The Yb_n/Nd_n ratios of the 'hydrothermal' *WHOI* samples fall outside than the range defined by the seawater and hydrothermal end-members but fall within the range of Yb_n/Nd_n ratios of TAG diffuse fluids, as discussed in section 8.7.3.

The osmium isotope composition of four of the *WHOI* samples analysed in this study has been determined by Ravizza *et al.* [1996], and are shown in Table 8.4. Comparison of the REE and osmium isotope geochemistry of these samples can provide further insights into their formation. Over the course of geological time, the decay of ^{187}Re to ^{187}Os has produced large differences in the Os isotopic composition of different geochemical reservoirs within the earth. Os is inferred to be mobilised from the oceanic crust during hydrothermal circulation, and like manganese does not show any preferential partitioning into sulphides [Brügmann *et al.* 1998]. The concentration and isotopic composition of seawater Os of seawater has not been measured directly, but has been inferred from investigations of modern marine sediments [Ravizza & McMurtry 1993]. The inferred $^{187}Os/^{186}Os$ ratios of seawater and basalt are *c.* 8.6 to 8.8 [Ravizza & Turekian 1992] and *c.*1 [Schiano *et al.* 1996] respectively. While this large isotopic contrast gives scope for Os to be used as a sensitive indicator of chemical exchange during hydrothermal processes, measurements are hampered by the low (ppt) Os content of hydrothermal fluids and precipitates [e.g. Brügmann *et al.* 1998]. In spite of these difficulties, studies have found that distal metalliferous sediments on the EPR have values approaching the inferred

seawater value, while hydrothermal sulphides have values $^{187}Os/^{186}Os$ of *c.* 2, indicating that of the majority of the Os has been mobilised from the oceanic crust during hydrothermal circulation [Ravizza & McMurtry 1993].

The *WHOI* samples have $^{187}Os/^{186}Os$ ratios that are less radiogenic (4.24 to 7.14) than the inferred $^{187}Os/^{186}Os$ ratio of seawater (~8.7), indicative of some basaltic Os sourced from a hydrothermal fluid. The Os isotopic ratio of the least radiogenic crust (1244-1C; $^{187}Os/^{186}Os = 4.24$) places an upper limit on the $^{187}Os/^{186}Os$ ratio of the low-temperature fluid, as Os acquired during post-formation uptake from seawater would make the $^{187}Os/^{186}Os$ ratios appear less 'hydrothermal'. Because the $^{187}Os/^{186}Os$ ratio these samples fall approximately mid-way between the isotopic compositions of seawater and oceanic crust, it has been inferred that they contain a roughly 50:50 mixture of seawater and ocean crust-derived (i.e. black smoker) Os [Ravizza *et al.* 1996]. The REE pattern of such a mixture would possess a large positive Eu anomaly and no negative Ce anomaly (refer to Fig. 8.7). However, these four samples have seawater-like Ce anomalies (Fig. 8.7). For these samples it would appear that REEs are scavenged more effectively than Os from seawater by the oxide crusts, implying that the residence time of Os in seawater is less than for the REEs (e.g. 270 yr for Nd [Goldberg *et al.* 1963]). While the inputs and processes controlling the behaviour of the REEs in the marine environment are well-characterised [review by Elderfield *et al.* 1988], the marine geochemical cycle of Os, (including the reactivity of Os in the oceanic environment) is still poorly constrained [e.g. Ravizza & McMurtry 1993]. These observations indicate that a comparison of the Os isotope composition of hydrothermal precipitates with the better-understood REE systematics may prove useful in gaining further insights into the oceanic chemistry of Os.

The $^{187}Os/^{186}Os$ ratios of the *WHOI* samples have been plotted against their εNd(0) values in Fig. 8.9. Approximate NADW and TAG Black Smoker fluid end-member compositions have been plotted using the Nd isotopic data Piepgras & Wasserburg [1987] and T. Masuzerawa [pers. comm], and inferred $^{187}Os/^{186}Os$ ratios of *c.*8.7 and *c.*1 respectively [Ravizza & Turekian 1992; Schiano *et al.* 1996]. The *WHOI* samples display a trend towards less radiogenic $^{187}Os/^{186}Os$ ratios with increasing εNd(0) values, interpreted to reflect the variable incorporation of Nd and Os sourced from a vent fluid. The REE and Os chemistry of *WHOI* sample 1243-1 shows the greatest seawater influence, possessing a seawater-scavenged REE pattern (Fig. 8.4), the lowest εNd(0) value and the most radiogenic $^{187}Os/^{186}Os$ ratio. On the basis of their REE distribution patterns, REEs in the

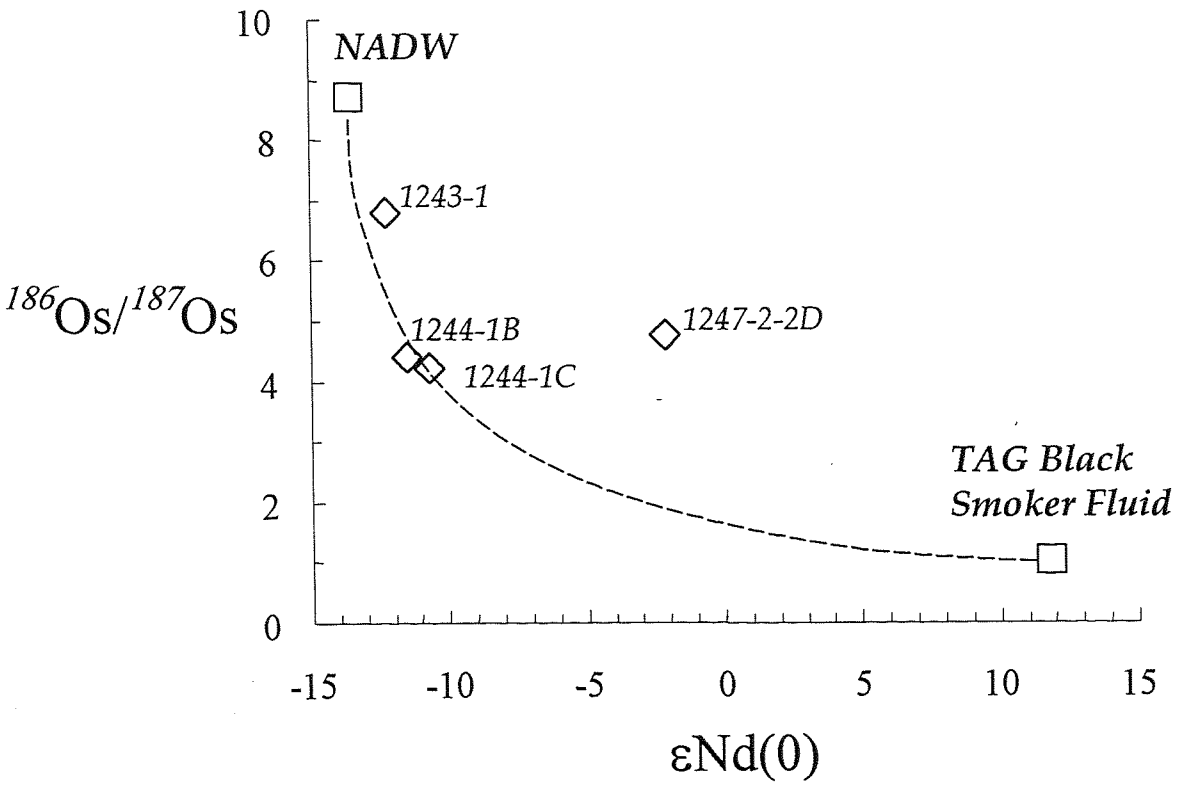

Figure 8.9: Relationship between $^{187}Os/^{186}Os$ ratio and εNd(0) for the *WHOI* samples. Osmium isotope data for the *WHOI* samples are from Ravizza *et al.* [1996]. Approximate NADW and TAG Black Smoker fluid end-member compositions are plotted using inferred $^{187}Os/^{186}Os$ ratios of *c.* 8.7 and *c.* 1 respectively [Ravizza & Turekian 1992; Schiano *et al.* 1996]. Nd isotopic data for NADW and TAG vent fluids are from Piepgras & Wasserburg [1987] and T. Masuzerawa [pers. comm]. The *WHOI* samples display a trend towards less radiogenic $^{187}Os/^{186}Os$ ratios with increasing εNd(0), interpreted to reflect the variable incorporation of Nd and Os sourced from a vent fluid.

other three *WHOI* samples shown in Fig. 8.9 are inferred to be dominantly sourced from an evolved, diffuse fluid (refer to section 8.7.3). This interpretation is reinforced by the less radiogenic Os isotope compositions of these samples, which is interpreted to reflect the incorporation of some hydrothermally-derived Os, in addition to Nd.

While the controls on the behaviour of the REEs in hydrothermal fluids and precipitates are relatively well established, the behaviour of Os in these systems is more poorly understood. Some published Os isotope data for TAG hydrothermal sediments are shown plotted against Eu anomaly in Fig. 8.10. The circles in Fig. 8.10 represent data for sub-samples of a push core (2182-4) collected near the base of the TAG hydrothermal mound [German *et al.* 1993]. This ~13 cm core contains two metalliferous layers derived from mass wasting of sulphidic material from the TAG mound superimposed on a background of Fe-oxyhydroxide sedimentation from the TAG plume.

A negative correlation might be expected between the two parameters in Fig. 8.10 (i.e. high Eu/Eu* corresponding to low $^{187}Os/^{186}Os$ ratios) given that TAG black smoker fluids and NADW are characterised by Eu/Eu* = 9.1 and 0.63, and inferred $^{187}Os/^{186}Os$ ratios of *c.*1 and *c.*8.7 respectively. However, this trend is not apparent in either the *WHOI* samples (diamonds) or the TAG mound sediment core (circles). Sub-samples of the TAG mound sediment core (excluding one sample) exhibit only minor variations in $^{187}Os/^{186}Os$ ratio over a wide range of Eu anomalies (Eu/Eu* = 0.8 to 3.7). The high Eu/Eu* values correspond to core layers containing slumped sulphides. These sulphides have vent fluid-like REE patterns with large positive Eu anomalies, and have been interpreted as having undergone no significant reaction with seawater [German *et al.* 1993]. However, the $^{187}Os/^{186}Os$ ratios of the majority of the sediment core layers are indistinguishable from seawater, in spite of REE patterns that indicate mixing between different proportions of vent fluid- and seawater-derived REEs. Conversely, for the recorded range in $^{187}Os/^{186}Os$ ratios of the *WHOI* samples (4.24 to 6.8), there is very little variation in the Eu anomaly (Eu/Eu* = 0.68 to 0.83). Clearly Os and the REEs are behaving very differently in these samples. This must reflect fundamental differences in the oceanic chemistry of these elements, which may relate to factors such as their hydrothermal geochemistry, complexation in seawater, particle reactivity and redox chemistries.

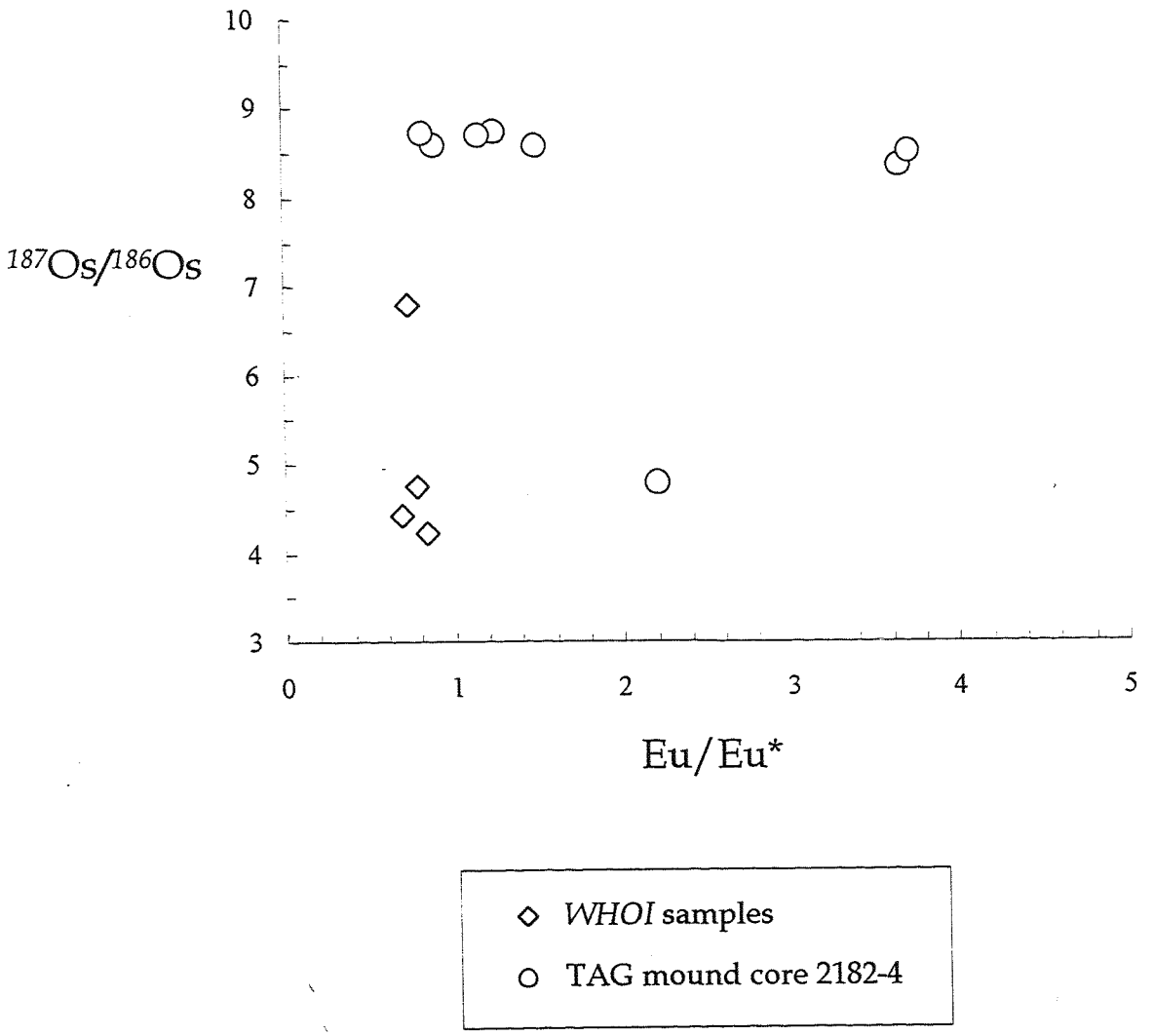

Figure 8.10: Relationship between $^{187}Os/^{186}Os$ ratio and the Eu anomaly for four of the *WHOI* samples and TAG mound sediment core 2182-4. Osmium isotope data for the *WHOI* samples are from Ravizza *et al.* [1996]. Sediment core REE data are from German *et al.* [1993]. There is a decoupling between the Eu anomaly and $^{187}Os/^{186}Os$ ratio as indicators of hydrothermal inputs, which must reflect differences in the marine geochemistry of Os and the REEs.

8.8 Conclusions

Mn- and Fe-rich oxide deposits from the TAG vent field exhibit two types of REE fractionation pattern, that is inferred to reflect their mode of formation rather than their mineralogy, sampling depth or accumulation rate. Samples from the inactive *Alvin* zone located 2 km north-east of the active TAG mound have REE patterns dominated by seawater-scavenged REEs. While BRAVEX samples from the low-temperature field located *c.* 1 km higher on the east rift valley wall have similar REE characteristics, the four *WHOI* samples from the low-temperature field are inferred to have incorporated REEs from diffuse hydrothermal fluids seeping from the valley wall.

The BRAVEX samples and *WHOI* sample 1243-1 have REE patterns dominated by REEs scavenged from seawater, that have a high affinity for both Mn- and Fe oxide surfaces. Experimental studies have shown that enhanced Ce scavenging is a feature of manganese- rather than iron oxyhydroxides, and accounts for the typical Ce-enrichment of hydrogenous ferromanganese deposits [e.g. Koeppenkastrop & De Carlo 1992]. However, BRAVEX samples from the relict *Alvin* zone (that lies between 3550 and 3450 m depth) have negative Ce anomalies, and are inferred to be incorporating a flux of Ce-depleted oxyhydroxide particles from the overlying TAG plume, that achieves neutral buoyancy between 3450 and 3200m above the seafloor. *WHOI* sample 1243-1 from the low-temperature field is similarly Ce-depleted, and shows a greater seawater REE influence than the other *WHOI* samples. However, the Os isotope composition of sample 1243-1 and the other *WHOI* samples suggests the incorporation of some Os sourced from a hydrothermal fluid. Ce-enriched BRAVEX samples from the low-temperature field are inferred to be accumulating outside the influence of a hydrothermal plume. Their formation is dominated by hydrogenous enrichment processes with preferential Ce uptake compared to the trivalent REEs.

Four of the *WHOI* samples have precipitated from and/or been subject to alteration by slightly Eu-enriched, evolved hydrothermal fluids with lower Nd_n/Yb_n ratio than either seawater or end-member black smoker fluid compositions. The REE data confirm that diffuse venting is occurring within the low-temperature field, as proposed in previous studies on the basis of other chemical and physical criteria [Rona 1973; R. Scott *et al.* 1974; M. Scott *et al.* 1974; Rona 1975; Thompson *et al.* 1985; Rona 1978; Rona, 1980; Jenkins *et al.* 1980; Nelson & Forde 1991; Elderfield *et al,* 1993; Ravizza *et al.* 1996]. The Mn-enriched diffuse fluids are inferred to have similar REE compositions to some TAG

mound pore fluids [M. Rudnicki pers. comm.]. Given that some of the Mn-Fe oxides from the low-temperature field have been dated at 125,000 yr, it seems likely that the diffuse fluids and/or plume particulates that contribute to the formation of the TAG low-temperature deposits were sourced from the relict *Alvin* or *Mir* zones when they were hydrothermally active (from 100 kyr and 40 kyr respectively), in addition to the TAG mound. The affinity of REEs for metal oxide surfaces is such that during exposure to seawater, they will acquire a seawater derived REE pattern that will overprint any hydrothermal REE signature. However, the Nd isotope analyses have confirmed hydrothermal inputs of Nd to one sample, as well as Os to these samples [Ravizza *et al.* 1996].

The focus of many studies of hydrothermally active areas has been the sites of high-temperature venting and associated near-field deposits, whereas the far-field deposits have been relatively under-sampled and in general more poorly characterised. Dredging operations during the BRAVEX cruise confirmed that Mn and Fe-oxide precipitates are extensive over the eastern rift valley wall at TAG between depths of ~2400 m and 2800 m. The REE data presented in this study indicate that the separation of Mn from other hydrothermally-derived metals at TAG is due to both plume processes and the spatial distribution of diffuse flow within the vent field. Diffuse fluids venting on the eastern valley wall at TAG have evolved REE distribution patterns. These fluids transport large amounts of Mn and variable amounts of Fe, but have lost other metals from solution prior to venting on the rift valley wall. This fractionation can be largely attributed to changes in solution E_h upon mixing with oxic seawater. Establishing the relative importance of diffuse venting in axial hydrothermal systems is a prerequisite to resolving global hydrothermal flux and chemical budgets, because the lower-temperature fluids are associated with different heat and chemical fluxes than the spectacular ~350°C black smokers [e.g. Wolery & Sleep 1976; Morton & Sleep 1985; Palmer & Edmond 1989; Schultz et al. 1992; Elderfield & Schultz 1996]. This study has shown diffuse hydrothermal venting to be more extensive within the TAG field than has previously been accepted.

Chapter 9

Summary & Conclusions

While submarine hydrothermal activity is recognised to provide a source of many dissolved elements to the oceans at similar rates to river inputs, numerous factors frustrate quantification of the hydrothermal chemical flux. One problem is that the temporal variability and periodicity of high-temperature venting is not well-constrained. Additionally, upon seafloor venting the chemistry of the pristine vent fluid and local seawater is severely modified within the near-field environment. Mixing processes in hydrothermal plumes generate a flux of trace-metal enriched Fe-oxyhydroxide particles to underlying metalliferous sediments, which may undergo further chemical modification on the seafloor. These processes have been characterised more fully at the TAG site than any other modern vent field, aided by the physical containment of the TAG plume by the walls of the MAR rift valley [e.g. German *et al.* 1990; German *et al.* 1991*a,b*; Rudnicki & Elderfield 1993; Mills *et al.* 1994].

The hydrothermal chemical flux is additionally modified by reactions that occur during the formation of on-axis and ridge flank diffuse fluids. Most research efforts at active vents have been towards characterising black smoker chemistries, as these fluids are easier to sample without dilution by local seawater than lower-temperature diffuse flow. Consequently, the geochemical significance of on-axis diffuse fluids, in addition to those formed during the lower-temperature waning phases of high-temperature hydrothermal systems and off-axis crustal ageing processes (which can continue for up to 10's of Myr) is not well understood. These problems have been addressed through a comparison of the REE systematics of hydrothermal materials from the TAG vent field, 26° N Mid-Atlantic Ridge, and the Troodos Ophiolite, Cyprus. These two areas possibly represent the best characterised localities for modern and ancient ore-forming hydrothermal systems. Previous investigations of both areas have been instrumental in the recognition of the significance of hydrothermal circulation at mid-ocean ridges, and in developing models of the mineralising systems.

The relative importance of diffuse flow versus discrete high-temperature venting in the

axial zone is not well known. Experiments to quantify the balance of on-axis diffuse and high-temperature flow suggest that black smoker fluids may account for only 10% of the axial heat loss [Schultz *et al.* 1992; Schultz *et al.* 1996]. Mixing between black smoker fluids and seawater lowers the temperature of the venting fluid, according to the degree of seawater entrainment and any sub-surface conductive cooling. However, the chemical consequences of sub-surface mixing are much less predictable. Establishing the relative importance of diffuse venting in axial hydrothermal systems is a prerequisite to resolving global hydrothermal flux and chemical budgets, because the lower-temperature fluids are associated with different heat and chemical fluxes than the spectacular ~350°C black smokers [e.g. Wolery & Sleep 1976; Morton & Sleep 1985; Palmer & Edmond 1989; Schultz et al. 1992; Elderfield & Schultz 1996].

At TAG, diffuse fluids have been sampled at the surface of the active sulphide mound, but as at other vents, the far-field deposits have been relatively undersampled and the lower-temperature processes occurring in this environment are less-well characterised. In particular, the origin of Mn and Fe-rich oxide deposits forming within the low-temperature field has remained controversial over 25 years of investigations of the TAG vent field. TAG end-member vent fluids are highly enriched in manganese (600 μmol kg^{-1}), and the origin of these low-temperature deposits reflects the behaviour of this element during mixing with seawater both prior to, and following venting at the seafloor. The REE and Nd isotope data presented in this thesis indicate that ferromanganese deposits within the TAG vent field are forming by a combination of sedimentation of Mn-rich particulates from the hydrothermal plume and direct precipitation from diffuse hydrothermal fluids seeping from the rift valley wall. The REE data confirm that diffuse venting is occurring within the low-temperature field, as proposed in previous studies on the basis of other chemical and physical criteria [Rona 1973; R. Scott *et al.* 1974; M. Scott *et al.* 1974; Rona 1975; Rona 1978; Rona 1980; Jenkins *et al.* 1980; Thompson *et al.* 1985; Nelson & Forde 1991; Elderfield *et al.* 1993; Ravizza *et al.* 1996]. The REE data for these deposits indicate that the separation of Mn from other hydrothermally-derived metals at TAG is due to both plume processes and the spatial distribution of diffuse flow within the vent field. The REE compositions of four of the samples analysed indicates that they have precipitated from and/or been alteration by slightly Eu-enriched, evolved hydrothermal fluids with lower Nd_n/Yb_n ratios than either seawater or end-member black smoker fluid compositions. These Mn-enriched diffuse fluids are inferred to have similar REE compositions to some TAG mound pore fluids [M. Rudnicki pers. comm.], but have quite different REE

characteristics to diffuse fluids sampled at the surface of the TAG mound, which are essentially diluted black smoker fluids [James & Elderfield 1996]. Clearly, different processes are involved in the formation of the diffuse fluids which vent within the low-temperature field, and also the TAG mound pore fluids which display similarly HREE-enriched REE patterns. This study has shown diffuse hydrothermal venting to be more extensive within the TAG field than has previously been accepted. The relative abundances of the different types of diffuse flow needs to be established in order to evaluate the consequences of their formation on hydrothermal chemical budgets at TAG.

The TAG sulphide mound has been episodically constructed during high-temperature venting episodes over the last ~50,000 yrs. Drilling and submersible studies of the TAG deposit indicate that subsurface mixing of hydrothermal fluids with seawater plays a crucial role in creating and modifying the ore deposit. Processes of fluid mixing and modification within the TAG mound involving seawater circulation, the precipitation of anhydrite, pyrite and chalcopyrite, and the dissolution of sphalerite within the mound are reflected in the REE systematics of hydrothermal precipitates and fluids sampled at the mound surface [Mills & Elderfield 1995*a*; James & Elderfield 1996; Mills *et al.* 1996; Humphris 1998; Goulding *et al.* 1998]. Seawater circulation within the mound has effectively zone-refined the ore body through the dissolution and re-precipitation of mound sulphides by diffuse hydrothermal fluids [Tivey *et al.* 1995; Edmond *et al.* 1995]. In light of the TAG studies, similar processes have been invoked to account for the observed metal-enrichments in the upper parts of Cyprus-type ore bodies. However, ophiolites integrate a long (c. 20 Myr) history of seafloor alteration, which will reflect both axial and off-axis hydrothermal processes. The REEs have been used to test the applicability of the TAG models of sulphide mound and metalliferous sediment formation to processes of sulphide mound formation operating within the Troodos ophiolite, Cyprus.

The REE patterns of mound sulphides from the Skouriotissa and Kinousa ore bodies are strikingly different from TAG mound and other oceanic sulphides. Despite the many similarities between modern and ancient massive sulphide deposits, the REE data suggest that the Troodos ore bodies are dominated by seawater REE signatures. The REE patterns of umber, ochre and sulphide sampled from a section through the top of the Skouriotissa ore body clearly demonstrates extensive seawater ingress and circulation throughout the upper ore body, which has resulted in the overprinting of any original hydrothermal signatures in both mound sediments and sulphides. Troodos ore bodies exhibit a similar

compositional zonation to that revealed by ODP drilling of the active TAG deposit [Humphris *et al.* 1995; Hannington *et al.* 1998]. At TAG, the seawater ingress and circulation within the sulphide mound which is responsible for this zonation are reflected in the fractionated REE patterns of Fe-oxyhydroxide sediments which precipitate from diffuse fluids at the mound surface [Mills & Elderfield 1995*a*; Mills *et al.* 1996; Goulding *et al.* 1998]. If these processes were important in the formation and evolution of the Skouriotissa sulphide mound, then ochres forming on the mound surface might be expected to show similar REE patterns to TAG ochres. However, the integrated effects of seawater ingress into the Skouriotissa deposit during waning hydrothermalism, and subsequent sustained seawater alteration during cooling of the mound have obscured any such REE signatures in the sulphides and metalliferous sediments of this ophiolitic deposit. This study has demonstrated that the geochemistry of the sulphide mound deposits continues to evolve following the peak of hydrothermal activity, and that the seawater overprinting of the Skouriotissa deposit is the end product of a process which we only see the initiation of on the modern seafloor [e.g. Tivey *et al.* 1995; Edmond *et al.* 1995; Goulding *et al.* 1998].

Compared with active vents, patterns of multi-stage alteration in ophiolites are the product of prolonged ageing of the oceanic basement, in addition to axial hydrothermal circulation at ancient ridge crests [Gillis & Robinson 1988, Gillis & Robinson 1990*a,b*; Staudigel & Gillis 1990; Bednarz & Schmincke 1990]. In order to document the evolution of hydrothermal fluids within ophiolitic ocean crust, it is therefore necessary to identify and geochemically characterise secondary mineral phases that have precipitated within these contrasting alteration regimes. The distribution of REEs between high- and low-temperature secondary minerals in the host volcanic rocks of a stockwork mineralised alteration pipe within the Troodos ophiolite has been investigated by LA ICP-MS. LA ICP-MS REE data for stockwork mineralised lavas, dykes and interstitial sediments from the Pitharokhoma alteration pipe indicate that REE mobility was associated with the development of both high- (~200 to 350° C) and low-temperature (<100° C) alteration phases that precipitated within contrasting alteration regimes (discharge- and recharge-dominated respectively). Lavas and sediments in the centre of the alteration pipe were altered by ancient analogues of black smoker fluids upwelling in a zone of axial hydrothermal alteration [Jensenius 1984; Richards et al. 1989]. The LREE enriched composition of pyrite, chlorite and chlorite-smectite is inferred to reflect the composition of the ~350° C hydrothermal fluid and contrasts with the typically LREE depleted patterns

of lower-temperature amorphous Fe-oxides and smectite. However, most lavas from the Pitharokhoma alteration pipe have REE compositions similar to Troodos volcanic glasses, indicating that on- and off-axis hydrothermal alteration processes have not induced any significant net REE mobilisation. Low-temperature alteration phases are the major repository for the REEs in lavas that show LREE ± Eu depletions relative to pristine volcanic glass compositions. Hence much of the REE signature of the alteration pipe is a post-mineralisation overprint acquired in the waning stages of hydrothermal activity and during the protracted alteration of the oceanic basement, which continued for ~20 million years following crustal accretion [Staudigel *et al.* 1986; Staudigel & Gillis 1990] rather than on-axis greenschist facies hydrothermal alteration.

The studies presented in this dissertation have demonstrated the use of REEs as tracers of chemical processes in ancient and modern hydrothermal systems on a wide range of temporal and spatial scales. While the rocks of ophiolites integrate multiple alteration episodes, new techniques such as LA ICP-MS allow REE analyses of individual alteration phases, and can be used to de-convolve the complex alteration processes associated with crustal generation at oceanic spreading ridges.

Appendix

Glossary of Terms

AMU	Atomic mass unit
BRAVEX	British-Russian Atlantic vents expedition
BSC	Black smoker complex
BSV	Boninite series volcanics
CHUR	Chondritic uniform reservoir
CSA	Cold seawater alteration
DSDP	Deep sea drilling project
DSRV	Deep sea research vessel
EPR	East Pacific Rise
EDS	Energy dispersive system
GSC	Galapagos Spreading Centre
HDEHP	di-2-ethyl-hexyl-ortho-phosphoric acid
HDPE	High density polyethylene
HREE	Heavy rare earth element
HTA	High temperature alteration
ICRDG	International crustal research drilling group
IAT	Island arc tholeiite
ICP-MS	Inductively coupled plasma mass spectrometry
JdFR	Juan de Fuca Ridge
LA ICP-MS	Laser ablation inductively coupled plasma mass spectrometry
LDPE	Low density polyethylene
LOQ	Limit of quantitation
LPA	Lower pillow alteration zone
LREE	Light rare earth element
LTA	Low temperature alteration
LTZ	Low temperature zone
MAR	Mid-Atlantic Ridge
mbsf	Metres below seafloor
MORB	Mid-ocean ridge basalt
NADW	North Atlantic deep water
NIST	National institute of standards and technology
N-MORB	Normal mid-ocean ridge basalt
NOAA	National oceanic and atmospheric administration
ODP	Ocean drilling programme
OIB	Ocean-island basalt
PMP	Polymethylpentene
ppb	parts per billion
ppm	parts per million
REE	Rare earth element
RSD	Relative standard deviation

SEM	Scanning electron microscopy
SOC	Southampton Oceanography Centre
SRM	Standard reference material
SWZ	Seafloor weathering zone
TAG	Trans-Atlantic geotraverse
TEM	Transmitted electron microscopy
TIMS-ID	Thermal ionisation mass spectrometry isotope dilution
TZ	Transition zone
TZD	Transition zone and dyke complex
UDZ	Upper dyke zone
UPA	Upper pillow alteration zone
UPL	Upper pillow lavas
WHOI	Woods Hole Oceanographic Institution
XRD	X-ray diffraction
XRF	X-ray fluorescence

References

ADAMIDES, N. G. 1980. The form and environment of formation of the Kalavasos ore deposits, Cyprus. *In:* PANAYIOTOU, A. (ed) *Ophiolites,* Geological Survey Department, Cyprus, 117-127.

ADAMIDES, N. G. 1990. Hydrothermal circulation and ore deposition in the Troodos ophiolite, Cyprus. *In:* MALPAS, J. MOORES, E. M., PANAYIOTOU, A. & XENOPHONTOS, C. (eds) *Ophiolites - oceanic crustal analogues,* Proceedings of the symposium Troodos 87, Geological Survey Department, Nicosia, Cyprus, 685-703.

ALLEN, C. R. 1975. The petrology of a portion of the Troodos plutonic complex, Cyprus. PhD thesis, University of Cambridge 250 pp.

ALLERTON, S. & VINE, F. G. 1990. Palaeomagnetic and structural studies of the southeastern part of the Troodos complex. *In:* MALPAS, J. MOORES, E. M., PANAYIOTOU, A. & XENOPHONTOS, C. (eds) *Ophiolites - oceanic crustal analogues,* Proceedings of the symposium Troodos 87, Geological Survey Department, Nicosia, Cyprus, 99-111.

ALLERTON, S. & VINE, F. G. 1992. Deformation styles adjacent to transform faults: evidence from the Troodos ophiolite, Cyprus. *In:* PARSON, L. M., MURTON, B. J. & BROWNING, P. (eds), *Ophiolites and their modern oceanic analogues,* Geological Society, London, Special Publication, **60**, 251-261.

ALT, J. C. 1988. The chemistry and sulfur isotope composition of massive sulfide and associated deposits on Green Seamount, Eastern Pacific. *Economic Geology,* **83,** 1026-1033.

ALT, J. C. 1995. Subseafloor processes in mid-ocean ridge hydrothermal systems. *In:* HUMPHRIS, S. E., ZIERENBERG, R. A. MULLINEAUX, L. S. & THOMSON, R. E. (eds) *Seafloor hydrothermal systems: physical, chemical, biological and geological interactions.* Geophysical Monograph 91, American Geophysical Union, 85-114

ALT, J. C. & EMMERMANN, R. 1985. Geochemistry of hydrothermally altered basalts: Deep Sea Drilling Project Hole 504B, Leg 83. *Initial Reports of the Deep Sea Drilling Program,* **83,** 249-262.

ALT, J. C., LAVERNE, C. & MUEHLENBACHS, K. 1985. Alteration of the upper oceanic crust: Mineralogy and processes in Deep Sea Drilling Project Hole 504B, Leg 83. *Initial Reports of the Deep Sea Drilling Program,* **83**, 217-241.

ALT, J. C., HONNOREZ, J., LAVERNE, C., & EMMERMANN, R. 1986. Hydrothermal alteration of a 1 km section through the upper oceanic crust, Deep Sea Drilling Project Hole 504B: Mineralogy, chemistry, and evolution of seawater-basalt interactions. *Journal of Geophysical Research* **91**, 10309-10335.

ALT, J. C., LONSDALE, P., HAYMON, R. & MUEHLENBACHS, K. 1987. Hydrothermal sulfide and oxide deposits on seamounts near 21° N, East Pacific Rise. *Geological Society of America Bulletin,* **98**, 157-168.

ALT, J. C., TEAGLE, D. A. H., BACH, W., HALLIDAY, A. N. & ERZINGER, J. 1996. Stable and strontium isotopic profiles through hydrothermally altered upper oceanic crust, Hole 504B. *Proceedings of the Ocean Drilling Program, Scientific Results,* **148**, 57-69.

ARRHENIUS, G. & BONATTI, E. 1965. Neptunism and vulcanism in the ocean *In:* SEARS, M. (ed) *Progress in Oceanography.* Oxford Permagon Press Ltd., 7-22.

BACH, W., ERZINGER, J., ALT, J. C. & TEAGLE, D. A. H. 1996. Chemistry of the lower sheeted dyke complex, Hole 504B (Leg 148): Influence of magmatic differentiation and hydrothermal alteration. *In:* ALT, J. C. KINOSHITA, H. STOKKING, L. B. & MICHAEL, P. J. (eds) *Proceedings of the Ocean Drilling Program, Scientific Results,* **148**, 39-55.

BÄCKER, H., LANGE, J. & MARCHIG, V. 1985. Hydrothermal activity and sulphide formation in axial valleys of the East Pacific Rise crest between 18 and 22°S. *Earth and Planetary Science Letters*, **72**, 9-22.

BAGNALL, P. S. 1960. *The geology and mineral resources of the Pano Lefkara-Larnaca area.* Memoir No. 5, The Geological Survey Department, Cyprus, Nicosia, 116 pp.

BAGNALL, P. S. 1964. Wrench faulting in Cyprus. *Journal of Geology,* **72,** 327-345.

BAKER, E. T. 1995. Characteristics of hydrothermal discharge following a magmatic intrusion. *In*: PARSON, L. M., WALKER, C. L. & DIXON, D. R. (eds). *Hydrothermal Vents and Processes*. Geological Society, London, Special Publication, **87**, 65-76.

BAKER, E. T., LAVELLE, J. W. & MASSOTH, G. J. 1985. Hydrothermal particle plumes over the southern Juan de Fuca Ridge. *Nature,* **316**, 342-344.

BAKER, E. T., MASSOTH G. J. & FEELY, R. A.1987. Cataclysmic hydrothermal venting on the Juan de Fuca Ridge. *Nature*, **329**, 149-151.

BAKER, E. T., LAVELLE, J. W., FEELY, R. A., MASSOTH G. J. & WALKER, S. L. 1989. Episodic venting of hydrothermal fluids from the Juan de Fuca Ridge. *Journal of Geophysical Research*, **94,** 9237-9250.

BAKER, E. T., GERMAN, C. R. & ELDERFIELD, H. 1995. Hydrothermal plumes over spreading-centre axes: global distributions and geological inferences. *In:* HUMPHRIS, S. E., ZIERENBERG, R. A., MULLINEAUX, L. S. & THOMSON, R. E. (eds) *Seafloor hydrothermal systems: physical, chemical, biological and geological interactions.* Geophysical Monograph 91, American Geophysical Union, 47-71.

BAKER, J. H. & DE GROOT, P. A. 1983. Proterozoic seawater-felsic volcanics interaction, W. Bergslagen, Sweden. Evidence for high REE mobility and implications for 1.8 Ga seawater compositions. *Contributions to Mineralogy and Petrology,* **82,** 119-130.

BALLARD, R. D., VAN ANDEL, T. H. & HOLCOMB, R. T. 1982. The Galapagos rift at 86°W: Variations in volcanism, structure and hydrothermal activity along a 30-kilometer segment of the rift valley. *Journal of Geophysical Research,* **87**, 1149-1161.

BARAGAR, W. R. A., LAMBERT, M. B., BAGLOW, N. & GIBSON, I. L. 1987. Sheeted dykes of the Troodos ophiolite, Cyprus. *In:* HALLS, H. C. & FAHRIG, W. F. (eds) *Mafic Dyke Swarms.* Geological Association of Canada, Special Paper, **34**, 257-272.

BARAGAR, W. R. A., LAMBERT, M. B., BAGLOW, N. & GIBSON, I. L. 1989. Sheeted dykes of the Troodos ophiolite. In: GIBSON, I. L., MALPAS, J., ROBINSON, P. T. & XENOPHONTOS, C. (eds) *Cyprus Crustal Study Project: Initial Report Hole CY-4*, Geological Survey of Canada, **88-9**, 69-106.

BARAGAR, W. R. A., LAMBERT, M. B., BAGLOW, N. & GIBSON, I. L. 1990. The sheeted dyke zone in the Troodos ophiolite. *In:* MALPAS, J. MOORES, E. M., PANAYIOTOU, A. & XENOPHONTOS, C. (eds) *Ophiolites - oceanic crustal analogues,* Proceedings of the symposium Troodos 87, Geological Survey Department, Nicosia, Cyprus, 37-51.

BARRETT T. J. & JARVIS, I. 1988. Rare earth element geochemistry of metalliferous sediments from DSDP Leg 92: The East Pacific Rise transect. *Chemical Geology,* **67,** 243-259.

BARRETT, T. J., TAYLOR, P. N. & LUGOWSKI, J. 1987. Metalliferous sediments from DSDP Leg 92: The East Pacific Rise transect. *Geochimica et Cosmochimica Acta*, **51**, 2241-2253.

BARRETT, T. J., JARVIS, I. & JARVIS, K. E. 1990. Rare earth element geochemistry of massive sulfides-sulfates and gossans on the Southern Explorer Ridge. *Geology,* **18**, 583-586.

BAU, M. 1991. Rare-earth element mobility during hydrothermal and metamorphic fluid-rock interaction and the significance of the oxidation state of europium. *Chemical Geology*, **93**, 219-230.

BAU, M., KOSCHINSKY, A., DULSKI, P. & HEIN, J. R. 1996. Comparison of the partitioning behaviour of yttrium, rare earth elements and titanium between hydrogenetic marine ferromanganese crusts and seawater. *Geochimica et Cosmochimica Acta*, **60**, 1709-1725.

BEAR, L. M. 1960. *The geology and mineral resources of the Akaki-Lythrodondha area.* Memoir No. 3, The Geological Survey Department, Cyprus, Nicosia, 122 pp.

BEAR, L. M. 1963. *The mineral resources and mining industry of Cyprus.* Memoir No. 1, The Geological Survey Department, Cyprus, Nicosia, 122 pp.

BECKER, K., SAKAI, H., ADAMSON, A., ALEXANDROVICH, J., ALT, J. C., ANDERSON, R. N., BIDEAU, D., GABLE, R., HERZIG, P., HOUGHTON, S., ISHIZUKA, H., KAWAHATA, H., KINOSHITA, H., LANGSETH, M. G., LOVELL, M. A., MALPAS, J., MASUDA, H., MERRIL, R. B., MORIN, R. H., MOTTL, M. J., PARISO, J. E., PEZARD, P., PHILLIPS, J., SPARKS, J. & UHLIG, S. 1989. Drilling deep into young oceanic crust, Hole 504B, Costa Rica Rift. *Reviews in Geophysics,* **27**, 79-102.

BEDNARZ, U. & SCHMINCKE, H.-U. 1990. Chemical patterns of seawater and hydrothermal alteration in the northeastern Troodos extrusive series and sheeted dyke complex. *In:* MALPAS, J. MOORES, E. M., PANAYIOTOU, A. & XENOPHONTOS, C. (eds) *Ophiolites - oceanic crustal analogues,* Proceedings of the symposium Troodos 87, Geological Survey Department, Nicosia, Cyprus, 639-653.

BENCE, A. E. 1983. Volcanogenic massive sulfides: rock/water interactions in basaltic systems and their effect on the distribution of rare earth elements and selected first series transition elements. *Proceedings of the 4th International Symposium on water rock interaction,* 48-49.

BENCE, A. E. & TAYLOR, B. E. 1985. Rare earth element systematics of West Shasta metavolcanic rocks: petrogenesis and hydrothermal alteration. *Economic Geology,* **80,** 2164-2176.

BENDER, M., BROECKER, W., GORNITZ, V., MIDDEL, U., KAY, R., SUN, S.-S. & BISCAYE, P. 1971. Geochemistry of three cores form the East Pacific Rise. *Earth and Planetary Science Letters*, **12**, 425-433.

BERNDT, M. E., SEYFRIED, W. E. & BECK, J. W. 1988. Hydrothermal alteration processes at midocean ridges: Experimental and theoretical constraints from Ca and Sr exchange reactions and Sr isotopic ratios. *Journal of Geophysical Research*, **93**, 4573-4583.

BERNDT, M. E., SEYFRIED , W. E. & JANECKY, D. R. 1989. Plagioclase and epidote buffering of cation ratios in mid-ocean ridge hydrothermal fluids: Experimental results in and near the supercritical region. *Geochimica et Cosmochimica Acta*, **53**, 2283-2300.

BERNER, R. A. & LASAGA, A. C. 1989. Modelling the geochemical carbon cycle. *Scientific American*, **260**, 54-62.

BICKLE, M. J. & TEAGLE, D. A. H. 1992. Strontium alteration in the Troodos ophiolite: implications for fluid fluxes and geochemical transport in mid-ocean ridge hydrothermal systems. *Earth and Planetary Science Letters*, **113**, 219-237.

BICKLE, M. J., TEAGLE, D. A. H., BEYNON, J. & CHAPMAN, H. J. 1998. The structure and controls on fluid-rock interactions in ocean ridge hydrothermal systems: Constraints from the Troodos Ophiolite. *In:* MILLS, R. A. & HARRISON, K. (eds) *Modern Ocean Floor Processes and the Geological Record*, Geological Society, London, Special Publication, **148**

BISCHOFF, J. L. & DICKSON, F. W. 1975. Seawater-basalt interaction at 200°C and 500 bars: Implications for the origin of sea-floor heavy-metal deposits and regulation of seawater chemistry. *Earth and Planetary Science Letters*, **25**, 385-397.

BONATTI, E. 1975. Metallogenesis at oceanic spreading centres. *Annual Reviews in Earth and Planetary Science*, **3**, 401-431.

BONATTI, E., GUERSTEIN-HONNOREZ, B.-M. & HONNOREZ, J. 1975. Copper-iron sulfide mineralizations from the equatorial Mid-Atlantic Ridge. *Economic Geology,* **61**, 1258-1265.

BÖSTROM, K. & PETERSON, M. N. A. 1966. Precipitates from the hydrothermal exhalations on the East Pacific Rise. *Economic Geology*, **61**, 1258-1265.

BÖSTROM, K. & PETERSON, M. N. A. 1969. The origin of Aluminium-poor ferromanganoan sediments in areas of high heat flow on the East Pacific Rise. *Marine Geology*, **7**, 427-447.

BOWERS, T. S., VON DAMM, K. L. & EDMOND, J. M. 1985. Chemical evolution of mid-ocean ridge hot springs. *Geochimica et Cosmochimica Acta*, **49**, 2239-2252.

BOWERS, T. S., CAMPBELL, A., MEASURES, C., SPIVAK, A., KHADEM, M. & EDMOND, J. 1988. Chemical controls on the composition of vent fluids at 13°-11° and 21°N, East Pacific Rise. *Journal of Geophysical Research*, **93**, 4522-4536.

BOYLE, J. F. & ROBERTSON, A. H. F. 1984. Evolving metallogenesis at the Troodos spreading axis. *In:* GASS, I. G., LIPPARD, S. J. & SHELTON, A. W. (eds*) Ophiolites and oceanic lithosphere,* Geological Society, London, Special Publication, **13**, 155-167

BOYLE, J. F. 1990. The composition and origin of oxide metalliferous sediments from the Troodos ophiolite, Cyprus. *In:* MALPAS, J. MOORES, E. M., PANAYIOTOU, A. & XENOPHONTOS, C. (eds) *Ophiolites - oceanic crustal analogues,* Proceedings of the symposium Troodos 87, Geological Survey Department, Nicosia, Cyprus, 705-719.

BROWN, D. & MCCLAY, K. R. 1998. Sulfide textures in the active TAG massive sulphide deposit, 26°N, Mid-Atlantic Ridge. *Proceedings of the Ocean Drilling Program, Scientific Results,* **158**, 193-200.

BRÜGMANN, G. E., BIRCK, J. L., HERZIG, P. M. & HOFFMAN, A. W. 1998. Os isotopic

composition and Os and Re distribution in the active mound of the TAG hydrothermal system, Mid-Atlantic Ridge. *Proceedings of the Ocean Drilling Program, Scientific Results,* **158**, 91-100.

BURTON, K. W., CHRISTENSEN, J. N., LEE, D.-C., HALLIDAY, A. N. & HENDERSON, G. M. 1998. The radiogenic isotope geochemistry of North Atlantic Deep Water during the Neogene recorded by hydrogenous ferromanganese crusts. *Mineralogical Magazine,* **62**, 263-264.

CALVERT, S. E., PIPER, D. Z. & BAEDECKER, P. A. 1987. Geochemistry of the rare earth elements in ferromanganese nodules from DOMES Site A, northern equatorial Pacific. *Geochimica et Cosmochimica Acta,* **51,** 2331-2338.

CAMPBELL, A. C., BOWERS, T. S., MEASURES, C. I., FALKNER, K. K., KHADEM, M. & EDMOND, J. M. 1988a. A time series of vent fluid compositions from 21°N, East Pacific Rise (1979, 1981, 1985), and the Guaymas Basin, Gulf of California (1982, 1985). *Journal of Geophysical Research,* **93**, 4537-4549.

CAMPBELL, A. C., PALMER, M. R., KLINKHAMMER, G. P., BOWERS, T. S., EDMOND, J. M., LAWRENCE, J. R., CASEY, J. F., THOMPSON, G., HUMPHRIS, S., RONA, P. & KARSON, J. A. 1988b. Chemistry of hot springs on the Mid-Atlantic Ridge. *Nature*, **335**, 514-519.

CAMPBELL, I. H., LESHER, C. M., COAD, P., FRANKLIN, J. M., GORTON, M. P. & THURSTON, P. C. 1984. Rare-earth element mobility in alteration pipes below massive Cu-Zn-Sulfide deposits. *Chemical Geology*, **45**, 181-202.

CANN, J. R. & STRENS, M. R. 1982. Black smoker fuelled by freezing magma. *Nature,* **298,** 147-149.

CANN, J. R. & STRENS, M. R. 1989. Modelling periodic megaplume emission by black smoker systems. *Journal of Geophysical Research,* **94**, 12227-12237.

CANN, J. R., WINTER, C. K. & PRITCHARD, R. G. 1977. A hydrothermal deposit from the floor of the Gulf of Aden. *Mineralogical Magazine*, **41**, 193-199.

CANN, J. R., STRENS, M. R., & RICE, A. 1985. A simple magma driven thermal balance model for the formation of volcanogenic massive sulphides. *Earth and Planetary Science Letters*, **76**, 123-134.

CANN, J. R., OAKLEY, P. J., RICHARDS, H. G. & RICHARDSON, C. J. 1987. Geochemistry of hydrothermally altered rocks from Cyprus drill holes CY-2 and CY-2A compared with other Cyprus stockworks. *In:* ROBINSON, P. T., GIBSON, I. L. & PANAYIOTOU, A. (eds) *Cyprus crustal study project: Initial report, Holes CY-2 and 2A.* Geological Survey of Canada, 87-102.

CANTRELL, K. J. & BYRNE, R. H. 1987. Rare earth element complexation by carbonate and oxylate ions. *Geochimica et Cosmochimica Acta,* **51,** 597-605.

CARR, J. H & BEAR, L. M. 1960. *The geology and mineral resources of the Peristerona-Lagoudhera area.* Memoir No. 2, Geological Survey Department, Cyprus, Nicosia, 79 pp.

CATHLES, L. M. 1993. A capless 350°C flow zone model to explain megaplumes, salinity variations and high-temperature veins in ridge axis hydrothermal systems, *Economic Geology*, **88**, 1977-1988.

CHAPMAN, H. J. & SPOONER, E. T. C. 1977. ^{87}Sr enrichment of ophiolitic sulphide deposits in Cyprus confirms ore formation by circulating seawater. *Earth and Planetary Science Letters*, **35**, 71-77.

CHESTER, R. 1990. Marine Geochemistry. Chapman & Hall. 698 pp

CHRISTENSEN, N. I. & SALISBURY, M. H. 1975. Structure and composition of the lower oceanic crust. *Reviews of Geophysics and Space Physics,* **13,** 57-86.

CLAUDE-IVANAJ, C., ABOUCHAMI, W., GALER, S. J. G., HOFMANN, A. W. & KOSCHINSKY, A. 1998. High resolution ^{230}Th/^{232}Th and ^{234}U/^{238}U chronology of a hydrogenous Fe-Mn crust from the NE Atlantic. *Mineralogical Magazine,* **62**, 335-336.

COLEMAN, R. G. & PETERMAN, Z. E. 1975. Oceanic plagiogranite. *Journal of Geophysical Research,* **80**, 1099-1108.

CONSTANTINOU, G. 1980. Metallogenesis associated with the Troodos ophiolite. PANAYIOTOU, A. (ed) *Ophiolites,* Geological Survey Department, Nicosia, Cyprus, 663-674.

CONSTANTINOU, G. 1987. Massive sulphide deposits. *In*: XENOPHONTOS, C. & MALPAS, J. G. (eds*) Field excursion guidebook, Symposium Troodos 87: Ophiolites and oceanic*

lithosphere. Nicosia, Geological Survey Department, 92-113.

CONSTANTINOU, G. & GOVETT, G. J. S. 1972. Genesis of sulphide deposits, ochre and umber of Cyprus. *Transactions of the Institution of Mining and Metallurgy*, **B81**, 34-46.

CONSTANTINOU, G. & GOVETT, G. J. S. 1973. Geology, geochemistry and genesis of Cyprus sulfide deposits. *Economic Geology*, **68**, 843-858.

CORLISS, J. B. 1971. The origin of metal-bearing submarine hydrothermal fluids. *Journal of Geophysical Research*, **76**, 8128-8138.

CORLISS, J. B. 1972. Rare earth data for iron- and manganese-rich sediments associated with the sulphide bodies of the Troodos massif, Cyprus, *Prog. Ab. Geol. Soc. Am.*, **4**, 476-477.

CORLISS, J. B., LYLE, M. & DYMOND, J. 1978. The chemistry of hydrothermal mounds near the Galapagos Rift. *Earth and Planetary Science Letters*, **40**, 12-24.

CORLISS, J. B., DYMOND, J., GORDON, L., EDMOND, J., VON HERZON, R., BALLARD, R., GREEN, K., WILLIAMS, D., BAINBRIDGE, A., CRANE, K. & VAN ANDEL, T. 1979. Submarine thermal springs on the Galapagos rift. *Science*, **203**, 1073-1083.

COWAN, J. & CANN, J. 1988. Supercritical two-phase separation of hydrothermal fluids in the Troodos ophiolite. *Nature*, **333**, 259-261.

COWEN, J. P., MASSOTH, G. J. & BAKER, E. T. 1986. Bacterial scavenging of Mn and Fe in mid- to far-field hydrothermal plume particles, *Nature*, **322**, 169-171.

COWEN, J. P., MASSOTH, G. J. & FEELY, R. A. 1990. Scavenging rates of dissolved manganese in a hydrothermal vent plume. *Deep Sea Research*, **37**, 1619-1637.

CROUDACE, I. W. & GILLIGAN, J. M. 1990.Versatile and accurate trace element determinations in iron-rich and other geological samples using X-ray fluorescence analysis. *X-Ray Spectrometry*, **19**, 117-123.

DAVIS, E. E., CHAPMAN, D. S., FORSTER, C. B. & VILLINGER, H. 1989. Heat-flow variations correlated with buried basement topography on the Juan de Fuca Ridge flank. *Nature*, **342**, 533-537.

DE BOER, P. L. 1986. Changes in organic carbon burial during the early Cretaceous. *In:* SUMMERHAYES, C. P. & SHACKLETON, N. J. (eds), *North Atlantic Palaeoceanography*, Geological Society, London, Special Publication, **21**, 321-331.

DE CARLO, E. H. & MCMURTRY, G. M. 1992. Rare-earth element geochemistry of ferromanganese crusts from the Hawaiian Archipelago, Central Pacific. *Chemical Geology* **95**, 235-250.

DELANEY, J. R., MOGK, D. W. & MOTTL, M. J. 1987. Quartz-cemented breccias from the Mid-Atlantic Ridge: Samples of a high salinity hydrothermal upflow zone. *Journal of Geophysical Research*, **92**, 9175-9192.

DELANEY, J. R., ROBIGOU, V., MCDUFF, R. E. & TIVEY, M. K. 1992. Geology of a vigorous hydrothermal system on the Endeavour Segment, Juan de Fuca Ridge. *Journal of Geophysical Research*, **97**, 19663-19682.

DETRICK, R. S., HONNOREZ, J., ADAMSON, A. C., BRASS, G., GILLIS, K. M., HUMPHRIS, S. E., MEVEL, C., MEYER, P., PETERSON, N., RAUTENSCHLEIN, M., SHIBATA, T., STAUDIGEL, H., YAMAMOTO, K. & WOOLRIDGE, A. L. 1986a. Drilling the Snake Pit hydrothermal sulfide deposit on the Mid-Atlantic Ridge, latitude 23°22'N. *Geology*, **14**, 1004-1007.

DETRICK, R. S., HONNOREZ, J., ADAMSON, A. C., BRASS, G., GILLIS, K. M., HUMPHRIS, S. E., MEVEL, C., MEYER, P., PETERSON, N., RAUTENSCHLEIN, M., SHIBATA, T., STAUDIGEL, H., YAMAMOTO, K. & WOOLRIDGE, A. L. 1986b. Mid-Atlantic Bare rock drilling and hydrothermal vents. *Nature*, **321**, 14-15.

DETRICK, R. S. 1991. Ridge crest magma chambers: A review of results from marine seismic experiments at the East Pacific Rise. *In:* PETERS, T. J., NICOLAS, A. & COLEMAN, R. G. (eds) *Ophiolite Genesis and evolution of the oceanic lithosphere*. Ministry of Petroleum and Minerals, Sultanate of Oman, 7-20.

DICKSON, P., SCHULTZ, A. & WOODS, A. 1995. Preliminary modelling of hydrothermal circulation within mid-ocean ridge sulphide structures. *In:* PARSON, L. M., WALKER, C. L. & DIXON, D. R. (eds) *Hydrothermal Vents and Processes*. Geological Society, London, Special Publication, **87**, 77-86.

DIXEY, F. 1975. The geology of the Kyrenia range. Unpublished report, Department of Geology,

University of Leicester, 20 pp.

DUCLOZ, C. 1972. The geology of the Bellapais-Kythrea area of the Central Kyrenia Range. *Cyprus Geological Survey Department Bulletin*, **6**, 75 pp.

DYMOND, J. & VEEH, H. H. 1975. Metal accumulation rates in the southeast Pacific and the origin of metalliferous sediments. *Earth and Planetary Science Letters*, **28**, 13-22.

DYMOND, J. & EKLUND, W. 1978. A microprobe study of metalliferous sediment components. *Earth and Planetary Science Letters*, **40**, 243-251.

DYMOND, J. & ROTH, S. 1988. Plume dispersed hydrothermal particles: a time-series record of settling flux from the Endeavour Ridge using moored sensors. *Geochimica et Cosmochimica Acta*, **52**, 2525-2536.

DYMOND, J., CORLISS, J. B., HEATH, G. R., FIELD, C. W., DASCH, E. J. & VEEH, E. H. 1973. Origin of metalliferous sediments from the Pacific Ocean. *Geological Society of America Bulletin*, **84**, 3355-3372.

EBERHART, G. L., RONA, P. A. & HONNOREZ, J. 1988. Geologic controls of hydrothermal activity in the Mid-Atlantic ridge rift valley: tectonics and volcanics. *Marine Geophysical Researches*, **10**, 233-259.

EDMOND, J. M., MEASURES, C., MCDUFF, R. E., CHAN, L. H., COLLIER, R., GRANT, B., GORDON, L. I. & CORLISS, J. B. 1979a. Ridge crest hydrothermal activity and the balances of the major and minor elements in the ocean: The Galapagos data. *Earth and Planetary Science Letters*, **46**, 1-18.

EDMOND, J. M., MEASURES, C. I., MANGUM, B., GRANT, B., SCLATER, F. R., COLLIER, R., HUDSON, A., GORDON, L. I. & CORLISS, J. B. 1979b. On the formation of metal-rich deposits at ridge crests. *Earth and Planetary Science Letters*, **46**, 19-30.

EDMOND, J. M., VON DAMM, K. L., MCDUFF, R. E. & MEASURES, C. I. 1982. Chemistry of hot springs on the East Pacific Rise and their effluent dispersal. *Nature*, **297**, 187-191 .

EDMOND, J. M., CAMPBELL, A. C., PALMER, M. R., KLINKHAMMER, M. R., GERMAN, C. R., EDMONDS, H. N., ELDERFIELD, H. E., THOMPSON, G. & RONA, P. A. 1995. Time series studies of vent fluids from the TAG and MARK sites (1986, 1990) Mid-Atlantic Ridge: a new solution chemistry model and a mechanism for Cu/Zn zonation in massive sulphide ore bodies. *In:* PARSON, L. M., WALKER, C. L. & DIXON, D. R. (eds) *Hydrothermal Vents and Processes*. Geological Society, London, Special Publication, **87**, 7-86.

EDMONDS, H. N., GERMAN, C. R., GREEN, D. H. R., HUH, Y. GAMO, T. & EDMOND, J. M. 1996. Continuation of the hydrothermal fluid chemistry time series at TAG, and the effects of ODP drilling. *Geophysical Research Letters*, **23**, 3487-3489.

ELDERFIELD, H. 1988. The oceanic chemistry of the rare-earth elements. *Philosophical Transactions of the Royal Society of London*, **325**, 105-126.

ELDERFIELD, H. & GREAVES, M. J. 1981. Negative Ce anomalies in the rare earth element patterns of oceanic ferromanganese nodules. *Earth and Planetary Science Letters*, **55**, 163-170.

ELDERFIELD, H. & SHOLKOVITZ, E. R. 1987. Rare earth elements in the pore waters of reducing nearshore sediments. *Earth and Planetary Science Letters*, **82**, 280-288.

ELDERFIELD, H & RUDNICKI, M. 1992. Iron fountains on the seabed. *New Scientist*, June 1992, 31-35.

ELDERFIELD, H. & SCHULTZ, A. 1996. Mid-ocean ridge hydrothermal fluxes and the chemical composition of the ocean. *Annual Reviews in Earth and Planetary Science*, **24**, 191-224.

ELDERFIELD, H., GASS, I. G., HAMMOND, A. & BEAR, L. M. 1972. The origin of ferromanganese sediments associated with the Troodos massif of Cyprus. *Sedimentology*, **19**, 1-19.

ELDERFIELD, H., HAWKESWORTH, C. J., GREAVES, M. J. AND CALVERT, S. E. 1981a. Rare earth element geochemistry of oceanic ferromanganese nodules and associated sediments. *Geochimica et Cosmochimica Acta*, **45**, 513-528.

ELDERFIELD, H., HAWKESWORTH, C. J., GREAVES, M. J. & CALVERT, S. E. 1981b. Rare earth element zonation in Pacific ferromanganese nodules. *Geochimica et Cosmochimica Acta*, **45**, 1231-1234.

ELDERFIELD, H., MILLS, R. A. & RUDNICKI, M. 1993. Geochemical and thermal fluxes, high-temperature venting and diffuse flow from mid-ocean ridge hydrothermal systems: the TAG hydrothermal field, Mid-Atlantic Ridge 26°N. *In:* PRITCHARD, H. M., ALABASTER, T.,

HARRIS, N. B. W. AND NEARY, C. R. (eds) *Magmatic processes and Plate tectonic.*, Geological Society, London, Special Publication, **76**, 295-307.

EMBLEY, R. W., JONASSON, I. R., PERFIT, M. R., FRANKLIN, J. M., TIVEY, M. A., MALAHOFF, A., SMITH, M. F. & FRANCIS, T. J. G. 1988. Submersible investigations of an extinct hydrothermal system on the Galapagos Ridge: sulfide mounds, stockwork zone, and differentiated lavas. *Canadian Mineralogist*, **26**, 517-540.

EVENSEN, N. M., HAMILTON, P. J. & O'NIONS, R. K. 1978. Rare earth abundances in chondritic meteorites. *Geochimica et Cosmochimica Acta*, **42**, 1199-1212.

FEELY, R. A., LEWISON, M., MASSOTH, G. J., ROBERT-BALDO, G., LAVELLE, J. W., BYRNE, R. H., VON DAMM, K. L. & CURL, H. C. 1987. Composition and dissolution of black smoker particulates from active vents on the Juan de Fuca Ridge. *Journal of Geophysical Research*, **92**, 11347-11363.

FEELY, R. A., MASSOTH, G. J., BAKER, E. T., COWEN, J. P., LAMB, M. F. & KROGSLUND, A. 1990. The effect of hydrothermal processes on midwater phosphorus distributions in the northeast Pacific. *Earth and Planetary Science Letters*, **96**, 305-318.

FEELY, R. A., TREFRY, J. H., MASSOTH, G. J. & METZ, S. 1991. A comparison of the scavenging of phosphorus and arsenic from seawater by hydrothermal iron oxyhydroxides in the Atlantic and Pacific Oceans. *Deep Sea Research*, **38**, 617-623.

FEELY, R. A., MASSOTH, G. J., BAKER, E. T., LEBON, G. T. & GEISELMAN, T. 1992. Tracking the dispersal of hydrothermal plumes from the Juan de Fuca Ridge using suspended matter compositions. *Journal of Geophysical Research*, **9**, 3457-3468.

FEHN, U., GREEN, K. E., VON HERZON, R. P. & CATHLES, L. M. 1983. Numerical models for the hydrothermal field at the Galapagos spreading centre. *Journal of Geophysical Research*, **88**, 1033-1048.

FLEET, A. J. 1983. Hydrothermal and hydrogenous ferro-manganese deposits: do they form a continuum? The rare earth element evidence. *In:* RONA, P. A., BOSTROM, K., LAUBIER, L. & SMITH, K. L. (eds) *Hydrothermal Processes at Seafloor Spreading Centres*, Plenum Press,

FLEET, A. J. & ROBERTSON, A. H. F. 1980. Ocean ridge metalliferous and pelagic sediments of the Semail Nappe, Oman. *Journal of the Geological Society of London*, **137**, 403-422.

FORNARI, D. J. & EMBLEY, R. E. 1995. Tectonic and volcanic controls on hydrothermal processes at the mid-ocean ridge: an overview based on near-bottom and submersible studies. *In:* HUMPHRIS, S. E., ZIERENBERG, R. A., MULLINEAUX, L. S. & THOMSON, R. E. (eds) *Seafloor hydrothermal systems: physical, chemical, biological and geological interactions.* Geophysical Monograph 91, American Geophysical Union, 1-46.

FOUQUET, Y., AUCLAIR, G., CAMBON, P. & ETOUBLEAU, J. 1988. Geological setting and mineralogical and geochemical investigations on sulfide deposits near 13°N on the East Pacific Rise. *Marine Geology*, **84**, 145-178.

FRANCHETEAU, J. & BALLARD, R. D. 1983. The East Pacific Rise near 21°N and 20°S: inferences for along-strike variability of axial processes of the Mid-Ocean Ridge. *Earth and Planetary Science Letters*, **64**, 93-116.

FRANKLIN, J. M., SANGSTER, D. M. & LYDON, J. W. 1981. Volcanic-associated massive sulfide-deposits. *In:* SKINNER, B. J. (ed), *Economic Geology 75th Anniversary Volume*, 77-86.

GALE, N. H., SPOONER, E. T. C. & POTTS, P. J. 1981. The lead and strontium isotope geochemistry of metalliferous sediments associated with Upper Cretaceous ophiolitic rocks in Cyprus, Syria and the Sultanate of Oman. *Canadian Journal of Earth Sciences*, **18**, 1290-1302.

GAMO, T., CHIBA, H., MASUDA, H., EDMONDS, H. N., FUJIOKA, K., KODAMA, Y. NANBA, H. & SANO, Y. 1996. Chemical characteristics of hydrothermal fluids from the TAG mound of the Mid-Atlantic Ridge in August 1994: implications for spatial and temporal variability of hydrothermal activity. *Geophysical Research Letters*, **23**, 3483-3486.

GASS, I. G. 1960. *The geology and mineral resources of the Dhali area.* Memoir No. 4, The Geological Survey Department, Cyprus, Nicosia, 116 pp.

GASS, I. G. 1968. Is the Troodos massif of Cyprus a fragment of Mesozoic ocean floor? *Nature*, **220**, 39-42.

GASS, I. G. 1980. The Troodos massif: Its role in the unravelling of the ophiolite problem and its significance in the understanding of constructive plate margin processes. *In:* PANAYIOTOU, A. (ed) *Ophiolites,* Geological Survey Department, Nicosia, Cyprus, 23-35.

GASS, I. G. & MASSON-SMITH, D. 1963. The geology and gravity anomalies of the Troodos massif, Cyprus. *Philosophical Transactions of the Royal Society of London,* **255 A,** 417-467.

GASS, I. G. & SMEWING, J. D. 1973. Intrusion, extrusion and metamorphism at constructive margins: Evidence from the Troodos Massif, Cyprus. *Nature*, **242**, 26-29.

GEORGE, R. P. J. 1975. The internal structure of the Troodos ultramafic complex, Cyprus. PhD thesis, University of New York (Stonybrook) 196 pp.

GERMAN, C. R. & SPARKS, R. S. J. 1993. Particle recycling in the TAG hydrothermal plume. *Earth and Planetary Science Letters,* **116,** 129-134.

GERMAN, C. R., KLINKHAMMER, G. P., EDMOND, J. M., MITRA, A. & ELDERFIELD, H. 1990. Hydrothermal scavenging of rare-earth elements in the ocean. *Nature*, **345**, 516-518.

GERMAN, C. R., CAMPBELL, A. C. & EDMOND, J. M. 1991a. Hydrothermal scavenging at the Mid-Atlantic Ridge: modification of trace element dissolved fluxes. *Earth and Planetary Science Letters* **107,** 101-114.

GERMAN, C. R., FLEER, A. P., BACON, M. P. & EDMOND, J. M. 1991b. Hydrothermal scavenging at the Mid-Atlantic Ridge: radionuclide distributions. *Earth and Planetary Science Letters,* **105**, 170-181

GERMAN, C. R., HOLLIDAY, B. P. & ELDERFIELD, H. 1991c. Redox cycling of rare earth elements in the suboxic zone of the Black Sea. *Geochimica et Cosmochimica Acta,* **55,** 3553-3558.

GERMAN, C. R., HIGGS, N. C., THOMSON, J., MILLS, R. A., ELDERFIELD, H., BLUSZTAJN, J., FLEER, A. P. & BACON, M. P. 1993. A geochemical study of metalliferous sediment from the TAG hydrothermal mound, 26°08'N, Mid-Atlantic Ridge. *Journal of Geophysical Research*, **98,** 9683-9692.

GERMAN, C. R., BRIEM, J., DANIELSEN, M., HOLLAND, S., JAMES, R., JÓNSDÓTTIR, A., LUDFORD, E., MOSER, C., ÓLAFSSON, J., PALMER, M. R. & RUDNICKI, M. D. 1994. Hydrothermal activity on the Reykjanes Ridge: the Steinahóll vent-field at 63°06'N. *Earth and Planetary Science Letters,* **121,** 647-654.

GERMAN, C. R., BAKER, E. T. & KLINKHAMMER, G. 1995*a*. Regional setting of hydrothermal activity. *In:* PARSON, L. M., WALKER, C. L. & DIXON, D. R. (eds*), Hydrothermal Vents and Processes,* Geological Society, London, Special Publication, **87**, 3-15.

GERMAN, C. R., BARREIRO, B. A., HIGGS, N. C., NELSON, T. A., LUDFORD, E. M. & PALMER, M. R. 1995*b*. Seawater-metasomatism in hydrothermal sediments (Escanaba Trough, northeast Pacific). *Chemical Geology,* **119**, 175-190.

GERMAN, C. R., PARSON, L. M. & HEAT SCIENTIFIC TEAM 1996. Hydrothermal exploration near the Azores Triple Junction: tectonic control of venting at slow-spreading ridges? *Earth and Planetary Science Letters,* **138,** 93-104.

GILLIS, K. M. & ROBINSON, P. T. 1988. Distribution of alteration zones in the upper oceanic crust. *Geology,* **16**, 262-266.

GILLIS, K. M. & ROBINSON, P. T. 1990a. Multistage alteration in the extrusive sequence of the Troodos Ophiolite, Cyprus. *In:* MALPAS, J. MOORES, E. M., PANAYIOTOU, A. & XENOPHONTOS, C. (eds) *Ophiolites - oceanic crustal analogues,* Proceedings of the symposium Troodos 87, Geological Survey Department, Nicosia, Cyprus, 655-664.

GILLIS, K. M. & ROBINSON, P. T. 1990b. Patterns and processes of alteration in the lavas and dykes of the Troodos Ophiolite, Cyprus. *Journal of Geophysical Research,* **95**, 21523-21548.

GILLIS, K. M., SMITH, A. D. & LUDDEN, J. N. 1990. Trace element and Sr-isotopic contents of hydrothermal clays and sulfides from the Snake Pit hydrothermal field: ODP site 649. *Proceedings of the Ocean Drilling Program, Scientific Results,* **106/109**, 315-319.

GILLIS, K. M., LUDDEN, J. N. & SMITH, A. D. 1992. Mobilisation of REE during crustal ageing in the Troodos Ophiolite, Cyprus. *Chemical Geology,* **98**, 71-86.

GOLDBERG, E. D. 1961. Chemistry in the oceans. In: *Oceanography.* Am. Assoc. Adv. Sci. Publ. **67,** 583-597.

GOLDBERG, E. D., KOIDE, M., SCHMITT, R. A. & SMITH, R. H. 1963. Rare-earth distributions in the marine environment. *Journal of Geophysical Research,* **68**, 4209-4217.

GOLDSTEIN, S. L. & JACOBSEN, S. B. 1987. The Nd and Sr isotope systematics of river-water dissolved material; implications for the sources of Nd and Sr in seawater. *Chemical Geology*, **66**, 245-272.

GOULDING, H. C. 1998. Genesis and preservation of metalliferous sediments, Unpublished PhD thesis, University of Southampton, 200 pp.

GOULDING, H. C., MILLS, R. A. & NESBITT, R. W. 1998. Precipitation of hydrothermal sediments on the active TAG mound: implications for ochre formation. *In:* MILLS, R. A. & HARRISON, K. (eds) *Modern Ocean Floor Processes and the Geological Record*, Geological Society, London, Special Publication, **148**, 201-216

GOVINDARAJU, K. 1996. 1996 compilation of working values and sample description for 383 geostandards. *Geostandards Newsletter Special Issue,* **18**, 1-158.

GRAF, J. 1977. Rare earth elements as hydrothermal tracers during the formation of massive sulphide deposits in volcanic rocks. *Economic Geology*, **72**, 527-548.

GREAVES, M. G., ELDERFIELD, H. & KLINKHAMMER, G. P. 1989. Determination of the rare earth elements in natural waters by isotope-dilution mass spectrometry. *Analytica Chemica Acta,* **218**, 265-280.

GREEN, D. H. & RINGWOOD, A. E. 1967. The genesis of basaltic magmas. *Contributions to Mineralogy and Petrology*, **15**, 103-190.

GREENBAUM, D. 1972. Magmatic processes at ocean ridges: evidence from the Troodos Massif, Cyprus. *Nature*, **238**, 18-21.

GREENBAUM, D. 1977. The chromitiferous rocks of the Troodos ophiolite complex, Cyprus. *Economic Geology*, **72**, 1175-1194.

HAAS, J. R., SHOCK, E. L. & SASSANI, D. C. 1995. Rare earth elements in hydrothermal systems: Estimates of standard partial molal thermodynamic properties of aqueous complexes of the rare earth elements at high pressures and temperatures. *Geochimica et Cosmochimica Acta*, **59**, 4329-4350.

HAJASH, A. 1975. Hydrothermal processes along mid-ocean ridges: an experimental investigation. *Contributions to Mineralogy and Petrology*, **53**, 205-226.

HALLIDAY, A. N., DAVIDSON, J. P., HOLDEN, P., OWEN, R. M. & OLIVAREZ, A. M. 1992. Metalliferous sediments and the scavenging residence time of Nd near hydrothermal vents. *Geophysical Research Letters,* **19**, 761-764.

HANNINGTON, THOMPSON, G., RONA, P. & SCOTT, S. 1988. Gold and native copper in supergene sulphides from the Mid-Atlantic Ridge. *Nature,* **333**, 64-66.

HANNINGTON, M., HERZIG, P., SCOTT, S., THOMPSON, G. & RONA, P. 1991. Comparative mineralogy and geochemistry of gold-bearing sulfide deposits on the mid-ocean ridges. *Marine Geology,* **101**, 217-248.

HANNINGTON, M. D., JONASSON, I. R., HERZIG, P. M. & PETERSEN, S. 1995. Physical and chemical processes of seafloor mineralisation at mid-ocean ridges. *In:* HUMPHRIS, S. E., ZIERENBERG, R. A., MULLINEAUX, L. S. & THOMSON, R. E. (eds) *Seafloor hydrothermal systems: physical, chemical, biological and geological interactions.* Geophysical Monograph 91, American Geophysical Union, 115-157.

HANNINGTON, M. D., GALLEY, A. G., HERZIG, P. M. & PETERSEN, S. 1998. Comparison of the TAG mound and stockwork complex with Cyprus-type massive sulphide deposits. *Proceedings of the Ocean Drilling Program, Scientific Results,* **158**, 389-415.

HASKIN, L. A. 1984. Petrogenic modelling – use of rare earth elements. *In:* HENDERSON, P. (ed) *Rare earth element geochemistry.* Advances in Geochemistry 2, Elsevier Press, 153-196.

HAYMON, R. M. 1983. Growth history of hydrothermal black smoker chimneys. *Nature,* **301,** 695-698.

HAYMON, R. M. & KASTNER, M. 1981. Hot spring deposits on the East Pacific Rise at 21°N: preliminary description of mineralogy and genesis. *Earth and Planetary Science Letters,* **53**, 363-381.

HAYS, J. D. & PITMAN, W. C. 1973. Lithospheric plate motion, sea level changes and ecological consequences. *Nature,* **246**, 18-22.

HEIN, J. R., YEH, H.-W., GUNN, S. H., GIBBS, A.-E. & WANG, C.-H. 1994. Composition and origin of hydrothermal ironstones from central Pacific seamounts. *Geochimica et Cosmochimica Acta,* **58,** 179-189.

HELLMAN, P. L. & HENDERSON, P. 1977. Are rare earth elements mobile during spilitisation? *Nature*, **267**, 38-40.

HENDERSON, P. 1982. *Inorganic Geochemistry,* Permagon, Oxford, 353 pp.

HERZIG, P. M., HANNINGTON, M. D., SCOTT, S. D., MALIOTIS, G., RONA, P. A. & THOMPSON, G. 1991. Gold-rich sea-floor gossans in the Troodos ophiolite and on the Mid-Atlantic Ridge. *Economic Geology,* **86,** 1747-1755.

HERZIG, P. M., PETERSEN, S. & HANNINGTON, M. D. 1998. Geochemistry and sulfur-isotope composition of the TAG hydrothermal mound, Mid-Atlantic Ridge, 26°N. *Proceedings of the Ocean Drilling Program, Scientific Results,* **158**, 47-70.

HESS, J., BENDER, M. & SCHILLING, J.-G. 1991. Assessing seawater/basalt exchange of strontium isotopes in hydrothermal processes on the flanks of mid-ocean ridges. *Earth and Planetary Science Letters,* **103**, 133-142.

HONNOREZ, J., ALT, J. C., HONNOREZ-GUERSTEIN, B.-M., LAVERNE, C., MUEHLENBACHS, K., RUIZ, J. & SALTZMAN, E. 1985. Stockwork-like sulfide mineralisation in young oceanic crust: Deep Sea Drilling Project Hole 504B. *Initial Reports of the Deep Sea Drilling Program,* **83**, 263-282.

HONNOREZ, J., ALT, J. C. & HUMPHRIS, S. E. 1998. Vivisection and autopsy of active and fossil hydrothermal alterations of basalts beneath and within the TAG hydrothermal mound. *Proceedings of the Ocean Drilling Program, Scientific Results,* **158**, 231-254.

HUMPHRIS, S. E. 1998. Rare earth element composition of anhydrite: Implications for deposition and mobility within the active TAG hydrothermal mound. *Proceedings of the Ocean Drilling Program, Scientific Results,* **158**, 143-159.

HUMPHRIS, S. E. & THOMPSON, G. 1978. Hydrothermal alteration of oceanic basalts by seawater. *Geochimica et Cosmochimica Acta,* **42,** 107-125.

HUMPHRIS, S. & KLEINROCK, M. 1996. Detailed morphology of the TAG active hydrothermal mound: Insights into its formation and growth. *Geophysical Research Letters,* **23,** 3443-3446.

HUMPHRIS, S., MORRISON, M. & THOMPSON, R. 1978. Influence of rock crystallisation history upon subsequent lanthanide mobility during hydrothermal alteration of basalts. *Marine Geology*, **23**, 125-137.

HUMPHRIS, S. E., HERZIG, P. M., MILLER, D. J., ALT, J. C., BECKER, K., BROWN, D., BRUGMANN, G., CHIBA, H., FOUQUET, Y., GEMMELL, J. B., GUERIN, G., HANNINGTON, M. D., HOLM, N. G., HONNOREZ, J. J., ITURRINO, G. J., KNOTT, R., LUDWIG, R., NAKAMURA, K., PETERSEN, S., REYSENBACH, A-L., RONA, P. A., SMITH, S., STURZ, A. A., TIVEY, M. K. & ZHAO, X. 1995. The internal structure of an active sea-floor massive sulphide deposit. *Nature,* **377**, 713-716.

HUMPHRIS, S. E., ALT, J. C., TEAGLE, D. A. H. & HONNOREZ, J. 1998. Geochemical changes during hydrothermal alteration of basement in the stockwork beneath the active TAG hydrothermal mound. *Proceedings of the Ocean Drilling Program, Scientific Results,* **158**, 255-276.

IRVING, E., PARK, J. K., HAGGERTY, S. E., AUMENTO, F. & LONCAREVIC, B. 1970. Magnetism and opaque mineralogy of basalts from the Mid-Atlantic Ridge at 45° N. *Nature,* **228,** 974-976.

JAMES, R. H. & ELDERFIELD, H. 1996. Chemistry of ore-forming fluids and mineral formation rates in an active hydrothermal sulphide deposit on the Mid-Atlantic Ridge. *Geology,* **24**, 1147-1150.

JAMES, R. H., ELDERFIELD, H. & PALMER, M. R. 1995. The chemistry of hydrothermal fluids from the Broken Spur site, 29° N, Mid-Atlantic Ridge. *Geochimica et Cosmochimica Acta,* **59,** 651-659.

JANECKY, D. R. & SEYFRIED, W. E. 1983. The solubility of magnesium-hydroxide-sulfate-hydrate in seawater at elevated temperatures and pressures. *American Journal of Science,* **283,** 831-860.

JANNASCH, H. W. 1995. Microbial Interactions with hydrothermal fluids. *In:* HUMPHRIS, S. E., ZIERENBERG, R. A., MULLINEAUX, L. S. & THOMSON, R. E. (eds) *Seafloor hydrothermal systems: physical, chemical, biological and geological interactions.* Geophysical Monograph 91, American Geophysical Union, 273-298.

JAQUES, A. L. & GREEN, D. H. 1980. Anhydrous melting of peridotite at 0-15 Kb pressure and the generation of tholeiitic basalts. *Contributions to Mineralogy and Petrology,* **73,** 287-310.

JARVIS, K. E., GRAY, A. L & HOUK, R. S. 1992. Handbook of Inductively Coupled Plasma Mass Spectrometry. Blackie & Son Ltd.

JENKINS, W. J., EDMOND, J. M. & CORLISS, J. B. 1978. Excess ^{3}He and ^{4}He in Galapagos submarine hydrothermal waters. *Nature,* **228,** 974-976.

JENKINS, W. J., RONA, P. A. & EDMOND, J. M. 1980. Excess ^{3}He in the deep water over the Mid-Atlantic Ridge at 26°N: Evidence of hydrothermal activity. *Earth and Planetary Science Letters,* **49,** 39-44.

JENKYNS, H. C. 1980. Cretaceous anoxic events: from continents to oceans. *Journal of the Geological Society of London,* **137,** 171-188.

JENSENIUS, J. 1984. The geology and petrology of the Pitharokhoma massive sulphide deposit, Cyprus. Unpublished M.S. thesis, University of Copenhagen 62 pp.

JENSENIUS, J. & OUDIN, E. 1983. Mineralogy of the Pitharokhoma ore deposit (Cyprus). *Bureau de Recherches Geologiques et Minieres (Paris),* Rept 83 SGN 870 MGA, 46 pp.

JUTEAU, T., NOACK, Y., WHITECHURCH, H., & COURTIS, C. 1979. Mineralogy and geochemistry of alteration products in Holes 417A and 417D basement samples (Deep Sea Drilling Project Leg 51). *Initial Reports of the Deep Sea Drilling Program,* **53,** 1273-1297.

KADKO, D. 1993. An assessment on the effect of chemical scavenging within hydrothermal plumes upon ocean chemistry. *Earth and Planetary Science Letters,* **120,** 361-374.

KADKO, D. & MOORE, W. 1988. Radiochemical constraints on the crustal residence time of submarine hydrothermal fluids: Endeavour Ridge. *Geochimica et Cosmochimica Acta,* **52,** 659-668.

KADKO, D., KOSKI, R., TATSUMOTO, M. & BOUSE, R. 1985. An estimate of hydrothermal fluid residence times and vent chimney growth rates based on ^{210}Pb/Pb ratios and mineralogic studies of sulfides dredged from the Juan de Fuca Ridge. *Earth and Planetary Science Letters,* **76,** 35-44.

KADKO, D. C., ROSENBERG, N. D., LUPTON, J. E., COLLIER, R. W. & LILLEY, M. D. 1990. Chemical reaction rates and entrainment within the Endeavour ridge hydrothermal plume. *Earth and Planetary Science Letters,* **99,** 315-335.

KADKO, D., BAROSS, J. & ALT, J. 1995. The magnitude and global implications of hydrothermal flux. *In:* HUMPHRIS, S. E., ZIERENBERG, R. A., MULLINEAUX, L. S. & THOMSON, R. E. (eds) *Seafloor hydrothermal systems: physical, chemical, biological and geological interactions.* Geophysical Monograph 91, American Geophysical Union, 446-466.

KARPOFF, A. M., WALTER, A.-V. & PFLUMIO, C. 1988. Metalliferous sediments within lava sequences of the Sumail ophiolite (Oman): Mineralogical and geochemical characterization, origin and evolution. *Tectonophysics,* **151,** 223-245.

KARSON, J. A. 1990. Seafloor spreading on the Mid-Atlantic Ridge: implications for the structure of ophiolites and oceanic lithosphere produced in slow-spreading environments. *In:* MALPAS, J. MOORES, E. M., PANAYIOTOU, A. & XENOPHONTOS, C. (eds) *Ophiolites - oceanic crustal analogues,* Proceedings of the symposium Troodos 87, Geological Survey Department, Nicosia, Cyprus, 547-557.

KARSON, J. A. 1991. Accommodation zones and transfer faults: Integral components of Mid-Atlantic Ridge extensional systems. *In:* PETERS, T. J., NICOLAS, A. & COLEMAN, R. G. (eds) *Ophiolite Genesis and evolution of the oceanic lithosphere.* Ministry of Petroleum and Minerals, Sultanate of Oman, 21-37.

KARSON, J. A. & RONA, P. A. 1990. Block-tilting, transfer faults, and structural control of magmatic and hydrothermal processes in the TAG area, Mid-Atlantic Ridge 26°N. *Geological Society of America Bulletin,* **102,** 1635-1645.

KELLEY, D. S. & ROBINSON, P. T. 1990. Development of a brine-dominated hydrothermal system at temperatures of 400-500°C in the upper level plutonic sequence, Troodos ophiolite,

Cyprus. *Geochimica et Cosmochimica Acta,* **54,** 635-661.

KELLEY, D. S., ROBINSON, P. T. & MALPAS, J. G. 1992. Processes of brine generation and circulation in the oceanic crust: fluid inclusion evidence from the Troodos ophiolite, Cyprus. *Journal of Geophysical Research,* **97,** 9307-9322.

KIM, K. H. & MCMURTRY, G. M. 1986. Radial growth rates and ^{210}Pb ages of hydrothermal massive sulfides from the Juan de Fuca Ridge. *Earth and Planetary Science Letters,* **104,** 299-314.

KLEINROCK, M. & HUMPHRIS, S. 1996. Structural control on sea-floor hydrothermal activity at the TAG active mound. *Nature,* **382,** 149-153

KLINKHAMMER, G. 1980. Observations of the distribution of manganese over the East Pacific Rise. *Chemical Geology,* **29,** 211-226.

KLINKHAMMER, G. & HUDSON, A. 1986. Dispersal patterns for hydrothermal plumes in the South Pacific using manganese as a tracer. *Earth and Planetary Science Letters,* **79,** 241-249.

KLINKHAMMER, G., BENDER, M. & WEISS, R. F. 1977. Hydrothermal manganese in the Galapagos Rift. *Nature,* **269,** 319-320.

KLINKHAMMER, G., ELDERFIELD, H. & HUDSON, A. 1983. Rare earth elements in seawater near hydrothermal vents. *Nature,* **305,** 185-188.

KLINKHAMMER, G., RONA. P., GREAVES, M. & ELDERFIELD, H. 1985. Hydrothermal manganese plumes in the Mid-Atlantic rift valley. *Nature,* **314,** 727-731.

KLINKHAMMER, G. P., ELDERFIELD, H., GREAVES, M., RONA, P. & NELSON, T. 1986. Manganese geochemistry near high-temperature vents in the Mid-Atlantic Ridge rift valley. *Earth and Planetary Science Letters,* **80,** 230-240.

KLINKHAMMER, G. P., ELDERFIELD, H., EDMOND, J. M. & MITRA, A. 1994. Geochemical implications of rare earth element patterns in hydrothermal fluids from mid-ocean ridges. *Geochimica et Cosmochimica Acta,* **58,** 5105-5113.

KLINKHAMMER, G., P., CHIN, C. S., WILSON, C. & GERMAN, C. R. 1995. Venting from the Mid-Atlantic Ridge at 37°17'N: the Lucky Strike hydrothermal site. *In:* PARSON, L. M., WALKER, C. L. & DIXON, D. R. *Hydrothermal Vents and Processes.* Geological Society, London, Special Publication, **87,** 87-96.

KNOTT, R., FOUQUET, Y., HONNOREZ, J., PETERSEN, S. & BOHN, M. 1998. Petrology of hydrothermal mineralisation: a vertical section through the TAG mound. *Proceedings of the Ocean Drilling Program, Scientific Results,* **158,** 5-26.

KOEPPENKASTROP, D. & DE CARLO, E. H. 1992. Sorption of rare-earth elements from seawater onto synthetic mineral particles: An experimental approach. *Chemical Geology,* **95,** 261-263.

KONG, L. S. L., SOLOMON, S. C. & PURDY, G. M. 1992. Microearthquake characteristics of a mid-ocean ridge along-axis high. *Journal of Geophysical Research,* **97,** 1659-1685.

KOSTOPOULOS, D. K. & MURTON, B. J. 1992. Origin and significance of components in boninite genesis: significance of the OIB component. *In:* PARSON, L. M., MURTON, B. J. & BROWNING, P. (eds*), Ophiolites and their modern oceanic analogues,* Geological Society, London, Special Publication, **60,** 133-154.

KRAUSKOPF, K. B. 1957. Separation of manganese from iron in sedimentary processes. *Geochimica et Cosmochimica Acta,* **12,** 61-84.

LALOU, C. & BRICHET, E. 1982. Ages and implications of East Pacific Rise sulphide deposits at 21° N. *Nature,* **300,** 169-171.

LALOU, C., BRICHET, E. & HEKINIAN, R. 1985. Age dating of sulfide deposits from axial and off-axial structures on the East Pacific Rise near 12°50'N. *Earth and Planetary Science Letters,* **75,** 59-71.

LALOU, C., THOMPSON, G., RONA, P. A., BRICHET, E. & JEHANNO, C. 1986. Chronology of selected hydrothermal Mn oxide deposits from the transatlantic geotraverse "TAG" area, Mid-Atlantic Ridge 26°N. *Geochimica Cosmochimica Acta,* **50,** 1737-1743.

LALOU, C., BRICHET, E. & THOMPSON, G. 1988. Radionuclide gradients in two Mn oxide deposits from the Mid-Atlantic Ridge: possible influence of a hydrothermal plume. *Canadian Mineralogist,* **26,** 713-720.

LALOU, C., THOMPSON, G., ARNOLD, M., BRICHET, E., DRUFFEL, E. & RONA, P. A. 1990.

Geochronology of TAG and Snakepit hydrothermal fields, Mid-Atlantic Ridge: witness to a long and complex hydrothermal history. *Earth and Planetary Science Letters,* **97,** 113-128.

LALOU, C., REYSS, J., BRICHET, E., ARNOLD, M., THOMPSON, G., FOUQUET, Y. & RONA, P. A. 1993. New age data for Mid-Atlantic Ridge hydrothermal sites: TAG and Snakepit chronology revisited. *Journal of Geophysical Research,* **98,** 9705-9713.

LALOU, C., REYSS, J. L. & BRICHET, E. 1998. Age of sub-bottom sulfide samples at the TAG active mound. *Proceedings of the Ocean Drilling Program, Scientific Results,* **158,** 111-117.

LILLEY, M. D., FEELY, R. A. & TREFRY, J. H. 1995. Chemical and biological transformations in hydrothermal plumes. *In:* HUMPHRIS, S. E., ZIERENBERG, R. A., MULLINEAUX, L. S. & THOMSON, R. E. (eds) *Seafloor hydrothermal systems: physical, chemical, biological and geological interactions.* Geophysical Monograph 91, American Geophysical Union, 369-391.

LISTER, C. R. B. 1972. On the thermal balance of a mid-ocean ridge. *Geophysical Journal of the Royal Astronomical Society,* **84,** 515-535.

LISTER, C. R. B. 1982. "Active" and "passive" hydrothermal systems in the oceanic crust: predicted physical conditions. *In:* FANNING, K. A. & MANHEIM, F. T. (eds) *The dynamic environment of the ocean floor.* D. C. Heath, Lexington, MA, 225-278.

LOWELL, R. P. & GERMANOVICH, L. N. 1994. On the temporal evolution of high temperature hydrothermal systems at ocean ridge crests. *Journal of Geophysical Research,* **99,** 565-576.

LUDDEN, J. N. & THOMPSON, G. 1978. Behaviour of rare earth elements during submarine weathering of tholeiitic basalt. *Nature,* **274,** 147-149.

LUDDEN, J. & THOMPSON, G. 1979. An evaluation of the behaviour of the rare earth elements during the weathering of sea-floor basalt. *Earth and Planetary Science Letters,* **43,** 85-92.

LUPTON, J. E. 1995. Hydrothermal plumes: near and far field. *In:* HUMPHRIS, S. E., ZIERENBERG, R. A., MULLINEAUX, L. S. & THOMSON, R. E. (eds) *Seafloor hydrothermal systems: physical, chemical, biological and geological interactions.* Geophysical Monograph 91, American Geophysical Union, 317-346.

LUPTON, J. E. & CRAIG, H. 1981. A major Helium-3 source at 15°S on the Eat Pacific Rise. *Science,* **214,** 13-18.

LUPTON, J. E., WEISS, R. F. & CRAIG, H. 1977. Mantle helium in hydrothermal plumes in the Galapagos Rift. *Nature,* **267,** 603-604.

LUPTON, J. E., KLINKHAMMER, G. P., NORMARK, W. R., HAYMON, R., MACDONALD, K. C., WEISS, R. F. & CRAIG, H. 1980. Helium-3 and manganese at the 21°N East Pacific Rise hydrothermal site. *Earth and Planetary Science Letters,* **50,** 115-127.

LYDON, J. W. & GALLEY, A. 1986. The chemical and mineralogical zonation of the Mathiati alteration pipe, Cyprus, and its genetic significance. *In:* GALLAGHER, M. J., IXER, R. A., NEARY, C. R. AND PRITCHARD, H. M. (eds) *Metallogeny of basic and ultrabasic rocks.* The Institute of Mining and Metallogeny, 49-68.

MACDONALD, K. C., BECKER, K., SPEISS, F. N. & BALLARD, R. D. 1980. Hydrothermal heat flux of the "black smoker" vents on the East Pacific Rise. *Earth and Planetary Science Letters,* **48,** 1-7.

MACLEAN, W. H. 1988. Rare earth element mobility at constant inter-REE ratios in the alteration zone at the Phelps Dodge massive sulphide deposit, Matagami, Quebec. *Mineralium Deposita,* **23,** 231-238.

MACLEAN, W. H. & HOY, L. D. 1991. Geochemistry of hydrothermally altered rocks at the Horne Mine, Noranda, Quebec. *Economic Geology,* **86,** 506-528.

MACLEOD, C. J 1990. Role of the Southern Troodos Transform Fault in the rotation of the Cyprus microplate: evidence from the Eastern Limassol Forest Complex. *In:* MALPAS, J. MOORES, E. M., PANAYIOTOU, A. & XENOPHONTOS, C. (eds) *Ophiolites - oceanic crustal analogues,* Proceedings of the symposium Troodos 87, Geological Survey Department, Nicosia, Cyprus, 75-85.

MALPAS, J. 1990. Crustal accretionary processes in the Troodos ophiolite, Cyprus: evidence from field mapping and deep crustal drilling. *In:* MALPAS, J. MOORES, E. M., PANAYIOTOU, A. & XENOPHONTOS, C. (eds) *Ophiolites - oceanic crustal analogues,* Proceedings of the symposium Troodos 87, Geological Survey Department, Nicosia, Cyprus, 65-74.

MALPAS, J. & LANGDON, G. 1984. Petrology of the Upper Pillow Lava suite, Troodos ophiolite, Cyprus. *In:* GASS, I. G., LIPPARD, S. J. & SHELTON, A. W. (eds), *Ophiolites and oceanic lithosphere.* Geological Society, London, Special Publication, **13**, 155-167.

MALPAS, J., CASE, G. & MOORE, P. 1989. Geology of the area immediately surrounding the CY-4 borehole, Cyprus Crustal Study Project. *In:* GIBSON, I. L., MALPAS, J., ROBINSON, P. T. & XENOPHONTOS, C. (eds) Cyprus Crustal Study Project Initial Report Hole CY-4, *Geological Survey of Canada,* **88-9**, 31-37.

MANDERNACK, K. W. & TEBO, B. M. 1993. Manganese scavenging and oxidation at hydrothermal vents and in vent plumes. *Geochimica et Cosmochimica Acta,* **57**, 3907-3923.

MARCHIG, V., GUNLACH, H., MÖLLER, P. & SCHLEY, F. 1982. Some geochemical indicators for discrimination between diagenetic and hydrothermal metalliferous sediments. *Marine Geology,* **50**, 241-256.

MARCHIG, V., GUNLACH, H., HOLLER, G. & WILKE, M. 1988. New discoveries of massive sulphides on the East Pacific Rise. *Marine Geology,* **84**, 179-190.

MCCONNELL, R. K., GUPTA, R. N. & WILSON, J. T. 1966. Compilation of deep crustal seismic refraction profiles. *Reviews of Geophysics and Space Physics,* **4**, 41-100.

MCGREGOR, B. A. & RONA, P. A. 1975. Crest of the Mid-Atlantic Ridge at 26°N. *Journal of Geophysical Research,* **80**, 3307-3314.

MCLENNAN, S. M. 1989. Rare earth elements in sedimentary rocks: Influence of provenance and sedimentary processes. *In:* LIPIN, B. R. & MCKAY, G. A. (eds) *Sedimentary rocks: Influence of provenance and sedimentary processes*, Mineralogical Society of America, 169 -200.

MCMURTRY, G. M. & YEH, H.-W. 1981. Hydrothermal clay mineral formation of East Pacific Rise and Bauer Basin sediments. *Chemical Geology,* **32**, 189-205.

MCMURTRY, G. M., WANG, C.-H. & YEH, H.-W. 1983. Chemical and isotopic investigations into the origin of clay minerals from the Galapagos hydrothermal mounds field. *Geochimica et Cosmochimica Acta,* **47**, 475-489.

MENZIES, M. A. & ALLEN, C. R. 1974. Plagioclase lherzolite residual mantle relationships within two eastern Mediterranean ophiolites. *Contributions to Mineralogy and Petrology*, **45**, 197-213.

METZ, S. & TREFRY, J. H. 1985 Geochemistry of Metalliferous sediment from the TAG hydrothermal field, Mid-Atlantic Ridge. *Eos,* **66**, 936.

METZ, S., TREFRY, J. H. & NELSON, T. A. 1988. History and Geochemistry of a metalliferous sediment core from the Mid-Atlantic Ridge at 26° N. *Geochimica et Cosmochimica Acta,* **52**, 2369-2378.

MEVEL, C. 1985. Mineralogy and chemistry of secondary phases in low temperature altered basalts from Deep Sea Drilling Project legs 51, 52 and 53. *Initial Reports of the Deep Sea Drilling Program,* **83**, 1299-1312.

MEVEL, C. & CANNAT, M. 1991. Lithospheric stretching and hydrothermal processes in oceanic gabbros from slow-spreading ridges. *In:* PETERS, T. J., NICOLAS, A. & COLEMAN, R. G. (eds) *Ophiolite Genesis and evolution of the oceanic lithosphere*. Ministry of Petroleum and Minerals, Sultanate of Oman, 293-312.

MEYER, P. S. & BRYAN, W. S. 1996. Petrology of basaltic glasses from the TAG segment: Implications for a deep hydrothermal heat source. *Geophysical Research Letters,* **23**, 3435-3438.

MICHARD, A. 1989. Rare earth element systematics in hydrothermal fluids. *Geochimica et Cosmochimica Acta*, **53**, 745-750.

MICHARD, A. & ALBARÈDE, F. 1986. The REE content of some hydrothermal fluids. *Chemical Geology*, **55**, 51-60.

MICHARD, A., ALBARÈDE, F., MICHARD, G., MINSTER, J.-F. & CHARLOU, J.-L. 1983. Rare earth element systematics and uranium in high-temperature solutions from East Pacific Rise hydrothermal vent field (13° N). *Nature*, **303**, 795-797.

MICHARD, G., ALBARÈDE, F., MICHARD, A., MINSTER, J.-F. & CHARLOU, J.-L. 1984. Chemistry of solutions from the 13°N East Pacific Rise hydrothermal site. *Earth and Planetary Science Letters,* **67**, 297-307.

MILLS, R. A. 1992. A geochemical and isotopic study of hydrothermal sediments from the Mid-Atlantic Ridge, 26° N. PhD thesis, University of Cambridge 214 pp.

MILLS, R. A. 1995. Hydrothermal deposits and metalliferous sediments from TAG, 26°N Mid-Atlantic Ridge. *In:* PARSON, L. M., WALKER, C. L. AND DIXON, D. R. (eds) *Hydrothermal Vents and Processes*. Geological Society, London, Special Publication, **87**, 121-132.

MILLS, R. A. & ELDERFIELD, H. 1995a. Rare earth element geochemistry of hydrothermal deposits from the active TAG Mound, 26°N Mid-Atlantic Ridge. *Geochimica et Cosmochimica Acta,* **59**, 3511-3524.

MILLS, R. A. & ELDERFIELD, H. 1995b. Hydrothermal activity and the geochemistry of metalliferous sediment. *In:* HUMPHRIS, S. E., ZIERENBERG, R. A., MULLINEAUX, L. S. & THOMSON, R. E. (eds) *Seafloor hydrothermal systems: physical, chemical, biological and geological interactions.* Geophysical Monograph 91, American Geophysical Union, 392-407.

MILLS, R. A., ELDERFIELD, H. & THOMSON, J. 1993. A dual origin for the hydrothermal component in a metalliferous sediment core from the Mid-Atlantic Ridge. *Journal of Geophysical Research,* **98,** 9671-9681.

MILLS, R. A., THOMSON, J., ELDERFIELD, H., HINTON, R. W. & HYSLOP, E. 1994. Uranium enrichment in metalliferous sediments from the Mid-Atlantic Ridge. *Earth and Planetary Science Letters*, **124**, 35-47.

MILLS, R. A., CLAYTON, T. & ALT, J. C. 1996. Low-temperature fluid flow through sulfidic sediments from TAG: modification of fluid chemistry and alteration of mineral deposits. *Geophysical Research Letters,* **23,** 3495-3498.

MILLS, R. A., TEAGLE, D. A. H. & TIVEY, M. K. 1998. Fluid mixing and anhydrite precipitation within the TAG mound. *Proceedings of the Ocean Drilling Program, Scientific Results,* **158**, 119-127.

MINAI, Y., ISHII, T., NAKAMURA, Y., WAKITA, H. & TOMINAGA, T. 1990. Neutron activation analysis of altered oceanic tholeiite: Variation of lanthanide concentration with degree of alteration. *Journal of Radioanalytical and Nuclear Chemistry Letters*, **146**, 375-384.

MITRA, A., ELDERFIELD, H. & GREAVES, M. J. 1994. Rare earth elements in submarine hydrothermal fluids and plumes from the Mid-Atlantic Ridge. *Marine Chemistry*, **46**, 217-235.

MIYASHIRO, A. 1973. The Troodos ophiolite complex was probably formed in an island arc. *Earth and Planetary Science Letters*, **19**, 218-229.

MOORE, W. S. & VOGT, P. R. 1976. Hydrothermal manganese crusts from two sites near the Galapagos spreading axis. *Earth and Planetary Science Letters*, **29**, 349-356.

MOORE, W. S. & STAKES, D. 1990. Ages of barite-sulfide chimneys from the Mariana Trough. *Earth and Planetary Science Letters*, **100**, 265-274.

MOORES, E M. & VINE, F. J. 1971. Troodos Massif , Cyprus, and other ophiolites as oceanic crust: evaluation and implications. *Philosophical Transactions of the Royal Society of London,* **268,** 443-466.

MOORES, E M., ROBINSON, P. T., MALPAS, J. & XENOPHONTOS, C. 1984. A model for the origin of the Troodos massif, Cyprus, and other Mideast ophiolites. *Geology,* **12,** 500-503.

MOORES, E M., VARGA, R. J., VEROSUB, K. L. & RAMSDEN, T. 1990. Regional structure of the Troodos dyke complex. *In:* MALPAS, J. MOORES, E. M., PANAYIOTOU, A. & XENOPHONTOS, C. (eds) *Ophiolites - oceanic crustal analogues,* Proceedings of the symposium Troodos 87, Geological Survey Department, Nicosia, Cyprus, 27-35.

MORGAN, J. W. & WANDLESS, G. A. 1980. Rare earth element distribution in some hydrothermal minerals: Evidence for crystallographic control. *Geochimica et Cosmochimica Acta,* **44**, 973-980.

MORTON, J. L. & SLEEP, N. H. 1985. A mid-ocean ridge thermal model: constraints on the volume of axial hydrothermal heat flux. *Journal of Geophysical Research,* **90**, 11345-11353.

MOTTL, M. J. & MCCONACHY, T. F. 1990. Chemical processes in buoyant hydrothermal plumes on the East Pacific Rise near 21°N. *Geochimica et Cosmochimica Acta,* **54,** 1911-1927.

MUEHLENBACHS, K. & CLAYTON, R. N. 1972. Oxygen isotope geochemistry of submarine greenstones. *Canadian Journal of Earth Science,* **9,** 471-478.

NEHLIG, P. & JUTEAU, T. 1988. Deep crustal seawater penetration and circulation at ocean ridges: evidence from the Oman ophiolite. *Marine Geology,* **84**, 209-228.

NELSON, T. A. & FORDE, E. B. 1991. The structure, mass and interactions of the hydrothermal plumes at 26°N on the Mid-Atlantic Ridge. *Earth and Planetary Science Letters,* **106,** 1-16.

NOJIRI, Y., ISHIBASHI, J., KAWAI, T., OTSUKI, A. & SAKAI, H. 1989. Hydrothermal plumes along the North Fiji Basin spreading axis. *Nature,* **342,** 667-670.

NORMAN, M. D., PEARSON, N. J., SHARMA, A. & GRIFFIN, W. L. 1996. Quantitative analysis of trace elements in geological materials by Laser Ablation ICPMS: Instrument operation conditions and calibration values of NIST glasses. *Geostandards Newsletter,* **20**, 247-261.

OLIVAREZ, A. M. & OWEN, R. M. 1989. REE/Fe variations in hydrothermal sediments: Implications for the REE content of seawater. *Geochimica et Cosmochimica Acta,* **53,** 757-762.

OLIVAREZ, A. M. & OWEN, R. M. 1991. The europium anomaly of seawater: Implications for fluvial versus hydrothermal REE inputs to the oceans. *Chemical Geology,* **92,** 317-328.

ONUMA, N., HIGUGHI, H., WAKITA, H. & NAGASAWA, H. 1968. Trace element partition between two pyroxenes and the host lava. *Earth and Planetary Science Letters,* **5,** 47-51.

OUDIN, E. & CONSTANTINOU, G. 1984. Black smoker chimney fragments in Cyprus sulphide deposits. *Nature,* **308,** 349-353.

OUDIN, E. PICOT, P. & POUIT, G. 1981. Comparison of sulphide deposits from the East Pacific Rise and Cyprus. *Nature,* **291,** 404-407.

OWEN, R. M. & OLIVAREZ, A. M. 1988. Geochemistry of rare earth elements in Pacific hydrothermal sediments. *Marine Chemistry,* **25,** 183-196.

PALMER, M. R. 1985. Rare earth elements in foraminifera tests. *Earth and Planetary Science Letters,* **73**, 285-298.

PALMER, M. R. & EDMOND, J. M. 1989a. Cesium and rubidium in submarine hydrothermal fluids: evidence for recycling of alkali elements. *Earth and Planetary Science Letters,* **95**, 8-14.

PALMER, M. R. & EDMOND, J. M. 1989b. The strontium isotope budget of the modern ocean. *Earth and Planetary Science Letters,* **92**, 11-26.

PANAYIOTOU, A. 1987. An overview of the geology of Cyprus. *In:* XENOPHONTOS, C & MALPAS, J. G. (eds) *Field excursion guidebook, Symposium Troodos 87: Ophiolites and oceanic lithosphere*. Nicosia, Geological Survey Department, 7-22.

PANTAZIS, T. M. 1967. *The geology and mineral resources of the Pharmakas-Kalavassos area.* Memoir No. 8, The Geological Survey Department, Cyprus, Nicosia, 120 pp.

PEARCE, J. A. 1975. Basalt geochemistry used to investigate past tectonic environments on Cyprus. *Tectonophysics*, **25**, 41-67.

PEARCE, J. A. 1980. Geochemical evidence for the genesis and eruptive setting of lavas from Tethyan ophiolites. *In:* PANAYIOTOU, A. (ed), *Ophiolites,* Geological Survey Department, Cyprus, 261-272.

PEARCE, J. A. 1982. Trace element characteristics of lavas from destructive plate boundaries. *In:* THORPE, R. S. (ed), *Andesites,* John Wiley & Sons, 525-548.

PEARCE, J. A. & Cann, J. R. 1973. Tectonic setting of basic volcanic rocks determined using trace element analyses. *Earth and Planetary Science Letters,* **19**, 290-300.

PEARCE, J. A., LIPPARD, S. J. & ROBERTS, S. 1984. Characteristics and tectonic significance of supra-subduction zone ophiolites. *In:* MILLS, R. A. & HARRISON, K. (eds) *Marginal basin geology, volcanic and associated sedimentary and tectonic processes in modern and ancient marginal basins*, Geological Society, London, Special Publication, **16**, 77-94.

PETERSEN, S., HERZIG, P. M. & HANNINGTON, M. D. 1998. Fluid inclusion studies as a guide to the temperature regime within the TAG hydrothermal mound, 26°N, Mid-Atlantic Ridge. *Proceedings of the Ocean Drilling Program, Scientific Results,* **158**, 163-178.

PEZARD, P. A. 1990. Electrical properties of mid-ocean ridge basalt and implications for the structure of the upper oceanic crust in Hole 504B. *Journal of Geophysical Research,* **95,** 9237-9266.

PFLUMIO, C. 1991. Evidences for polyphased oceanic alteration of the extrusive sequence of the Semail ophiolite from the Salahi Block (northern Oman). *In:* PETERS, T. J., NICOLAS, A. & COLEMAN, R. G. (eds) *Ophiolite Genesis and evolution of the oceanic lithosphere*. Ministry

of Petroleum and Minerals, Sultanate of Oman, 313-351.

PIEPGRAS, D. J. & WASSERBURG, G. J. 1980. Neodymium isotopic variations in seawater. *Earth and Planetary Science Letters,* **50**, 128-138.

PIEPGRAS, D. J. & WASSERBURG, G. J. 1985. Strontium and neodymium isotopes in hot springs on the East Pacific Rise and Guaymas basin. *Earth and Planetary Science Letters*, **72**, 341-356.

PIEPGRAS, D. J. & WASSERBURG, G. J. 1987. Rare earth element transport in the western North Atlantic inferred from Nd isotopic observations. *Geochimica et Cosmochimica Acta,* **51**, 1257-1271.

PIEPGRAS, D. J. & JACOBSEN, S. B. 1992. The behaviour of rare earth elements in seawater: Precise determination of variations in the North Pacific water column. *Geochimica et Cosmochimica Acta,* **56**, 1851-1862.

PIEPGRAS, D. J., WASSERBURG, G. J. & DASCH, E. J. 1979. The isotopic composition of Nd in different ocean masses. *Earth and Planetary Science Letters*, **45**, 223-236.

PIPER, D. Z. 1973. Origin of metalliferous sediments from the East Pacific Rise. *Earth and Planetary Science Letters*, **19**, 75-82.

PIPER, D. Z. 1974. Rare earth elements in the sedimentary cycle: a summary. *Chemical Geology*, **14**, 285-304.

RAITT, R. W. 1963. The crustal rocks. *In:* HILL, M. N. (ed.) *The Sea,* **3**, Wiley-Interscience, New York, 85-102.

RAUTENSCHLEIN, M., JENNER, G. A., HERTOGEN, J., HOFMANN, A. W., KERRICH, R., SCHMINCKE, H.-U. & WHITE, W. M. 1985. Isotopic and trace element composition of volcanic glasses from the Akaki Canyon, Cyprus: implications for the origin of the Troodos ophiolite. *Earth and Planetary Science Letters,* **75**, 369-383.

RAVIZZA, G. & TUREKIAN, K. K. 1992. The osmium isotopic composition of organic-rich marine sediments. *Earth and Planetary Science Letters,* **110,** 1-6.

RAVIZZA, G. & MCMURTRY, G. M. 1993. Osmium isotopic variations in metalliferous sediments from the East Pacific Rise and Bauer Basin. *Geochimica et Cosmochimica Acta,* **57,** 4301-4310.

RAVIZZA, G., MARTIN, C. E., GERMAN, C. R. & THOMPSON, G. 1996. Os isotopes as tracers in seafloor hydrothermal systems: metalliferous deposits from the TAG hydrothermal area, 26° N Mid-Atlantic Ridge. *Earth and Planetary Science Letters,* **138,** 105-119.

REGBA, M., AGRINIER, P. PFLUMIO, C. & LOUBET, M. 1991. A geochemical study of a fossil oceanic discharge zone in the Oman ophiolite (Zuha sulphide prospect): evidence for a polyphased hydrothermal history. *In:* PETERS, T., NICOLAS, A. & COLEMAN, R. G. (eds) *Ophiolite Genesis and Evolution of the Oceanic Lithosphere.* Ministry of Petroleum and Minerals, Sultanate of Oman, 353-383.

RICHARDS, H. G. 1987. Petrology and geochemistry of hydrothermal alteration pipes in the Troodos ophiolite, Cyprus, Unpublished PhD thesis, University of Newcastle-upon-Tyne, 339 pp.

RICHARDS, H. G. & BOYLE, J. F. 1986. Origin, alteration and mineralisation of the inter-lava metalliferous sediments of the Troodos Ophiolite, Cyprus. *In:* GALLAGHER, M. J., IXER, R. A., NEARY, C. R. AND PRITCHARD, H. M. (eds) *Metallogeny of basic and ultrabasic rocks.* The Institution of Mining and Metallogeny, 21-31.

RICHARDS, H. G., CANN, J. R. & JENSENIUS, J. 1989. Mineralogical zonation and metasomatism of the alteration pipes of Cyprus sulphide deposits. *Economic Geology,* **84**, 91-115.

RICHARDSON, C. J., CANN, J. R., RICHARDS, H. G. & COWAN, J. G. 1987. Metal-depleted root zones of the Troodos ore-forming hydrothermal systems, Cyprus. *Earth and Planetary Science Letters*, **84**, 243-253.

ROBERTSON, A. H. F. 1975. Cyprus umbers: basalt-sediment relationships on a Mesozoic ocean ridge. *Journal of the Geological Society of London,* **131**, 511-531.

ROBERTSON, A. H. F. 1976. Origins of ochres and umbers: evidence from Skouriotissa, Troodos Massif, Cyprus. *Transactions of the Institution of Mining and Metallurgy.*, **85**, 245-251.

ROBERTSON, A. H. F. & HUDSON, J. D. 1973. Cyprus umbers: chemical precipitates on a Tethyan ocean ridge. *Earth and Planetary Science Letters,* **18**, 93-101.

ROBERTSON, A. H. F. & FLEET, A. J. 1976. The origins of rare earths in metalliferous sediments of

the Troodos Massif, Cyprus. *Earth and Planetary Science Letters,* **28**, 385-394.

ROBERTSON, A. H. F. & WOODCOCK, N. H. 1980. Tectonic setting of the Troodos massif in the east Mediterranean. *In:* PANAYIOTOU, A. (ed) *Ophiolites,* Geological Survey Department, Cyprus, 36-49.

ROBERTSON, A. H. F. & BOYLE, J. F. 1993. Tectonic setting and origin of metalliferous sediments in the Mesozoic Tethys ocean. *In:* RONA, P. A., BOSTROM, K., LAUBIER, L & SMITH, K. L. *Hydrothermal Processes at Seafloor Spreading Centres,* Plenum Press, 595-663.

ROBERTSON, A. H. F. & VARNAVAS, S. P. 1993. The origin of hydrothermal metalliferous sediments associated with the Early Mesozoic Othris and Pindos ophiolites, mainland Greece. *Sedimentary Geology,* **83**, 87-113.

ROBINSON, P. T. & MALPAS, J. 1990. The Troodos ophiolite of Cyprus: New perspectives on its origin and emplacement. *In:* MALPAS, J. MOORES, E. M., PANAYIOTOU, A. & XENOPHONTOS, C. (eds) *Ophiolites - oceanic crustal analogues,* Proceedings of the symposium Troodos 87, Geological Survey Department, Nicosia, Cyprus, 13-26.

ROBINSON, P. T., MELSON, W. G., O'HEARN, T. & SCHMINCKE, H.-U. 1983. Volcanic glass compositions of the Troodos ophiolite, Cyprus. *Geology,* **11**, 400-404.

RONA, P. A. 1973. New evidence for seabed resources from global tectonics. *Ocean Management,* **1**, 145-159.

RONA, P. A. 1978. Near bottom water temperature anomalies: Mid-Atlantic Ridge crest at latitude 26°N. *Geophysical Research Letters,* **5**, 993-996.

RONA, P. A. 1980. TAG hydrothermal field: Mid-Atlantic Ridge crest at latitude 26°N. *Journal of the Geological Society of London,* **137**, 385-402.

RONA, P. 1984. Hydrothermal mineralization at seafloor spreading centres. *Earth Science Reviews,* **20**, 1-104.

RONA, P. A., THOMSON, G., MOTTL, M. J., KARSON, J. A., JENKINS, W. J., GRAHAM, D., MALLETTE, M., VON DAMM, K. & EDMOND, J. M. 1984. Hydrothermal activity at the Trans-Atlantic Geotraverse hydrothermal field, Mid-Atlantic Ridge crest at 26°N. *Journal of Geophysical Research,* **89**, 11365-11377.

RONA, P.A., KLINKHAMMER, G., NELSON, T. A., TREFREY, J. H. & ELDERFIELD, H. 1986. Black smokers, massive sulphides and vent biota at the Mid-Atlantic Ridge. *Nature,* **321**, 33-37.

RONA, P. A., BOGDANOV, Y, A., GURVICH, E. G., RIMSKI-KORSAKOV, N. A., SAGALEVITCH, A. M., HANNINGTON, M. D. & THOMPSON, G. 1993a. Relict hydrothermal zones in the TAG hydrothermal field, Mid-Atlantic Ridge 26°N, 45°W. *Journal of Geophysical Research,* **98**, 9715-9730.

RONA, P. A., HANNINGTON, M. D., RAMAN, C. V., THOMSON, G., TIVEY, M. K., HUMPHRIS, S. E., LALOU, C. & PETERSON, S. 1993b. Active and relict sea-floor hydrothermal mineralisation at the TAG hydrothermal field, Mid-Atlantic Ridge. *Economic Geology,* **88**, 1989-2017.

ROTH, P. H. 1986. Palaeoceanography of the North Atlantic and Tethys Oceans. *In:* SUMMERHAYES, C. P. & SHACKLETON, N. J. (eds) *North Atlantic Palaeoceanography,* Geological Society, London, Special Publication, **21**, 299-320.

RUDNICKI, M. D. & ELDERFIELD, H. 1992. Theory applied to the Mid-Atlantic Ridge hydrothermal plumes: the finite difference approach. *Journal of Volcanology and Geothermal Research,* **50**, 161-172.

RUDNICKI, M. D. & ELDERFIELD, H. 1993. A chemical model of the buoyant and neutrally buoyant plume above the TAG vent field, 26 degrees N, Mid-Atlantic Ridge. *Geochimica et Cosmochimica Acta,* **57**, 2939-2957.

RUHLIN, D. E. & OWEN, R. M. 1986. The rare earth element geochemistry of hydrothermal sediments from the East Pacific Rise: Examination of a seawater scavenging mechanism. *Geochimica et Cosmochimica Acta,* **50**, 393-400.

SACCOCIA, P. & GILLIS, K. 1995. Hydrothermal upflow zones in the oceanic crust. *Earth and Planetary Science Letters,* **136**, 1-16.

SAUNDERS, A. D. 1984. The rare earth element characteristics of igneous rocks from the ocean basins. *In:* HENDERSON, P. (ed.) *Rare earth element geochemistry.* Advances in Geochemistry 2, Elsevier Press, 205-236.

SCHADE, J., CORNELL, D. H. & THEART, H. F. 1989. Rare earth element and isotopic evidence for the genesis of the Prieska massive sulphide deposit, South Africa. *Economic Geology,* **84,** 49-63.

SCHANDL, E. S. & GORTON, M. P. 1991. Postore mobilisation of the rare earth elements at Kidd Creek and other Archean massive sulphide deposits. *Economic Geology,* **86,** 1546-1553.

SCHIANO, P., BIRCK, J.-L., & ALLÈGRE, C. J. 1996. Re-Os isotope systematics of mid-ocean ridge basalt glasses. *Journal of Conference Abstracts,* **1,** 539.

SCHIFFMAN, P. & SMITH, B. M. 1988. Petrology and oxygen isotope geochemistry of a fossil seawater hydrothermal system within the Solea graben, northern Troodos ophiolite, Cyprus. *Journal of Geophysical Research,* **93,** 4612-4624.

SCHIFFMAN, P., SMITH, B. M., VARGA, R. J. & MOORES, E. M. 1987. Geometry, conditions and timing of off-axis hydrothermal metamorphism and ore-deposition in the Solea graben. *Nature,* **53,** 423-425.

SCHIFFMAN, P., BETTISON, L. A. & SMITH, B. M. 1990. Mineralogy and geochemistry of epidosites from the Solea graben, Troodos ophiolite, Cyprus. *In:* MALPAS, J. MOORES, E. M., PANAYIOTOU, A. & XENOPHONTOS, C. (eds) *Ophiolites - oceanic crustal analogues,* Proceedings of the symposium Troodos 87, Geological Survey Department, Nicosia, Cyprus, 673-682.

SCHMINCKE, H.-U. & BEDNARZ, U. 1990. Pillow, sheet flow and breccia flow volcanoes and volcano-tectonic hydrothermal cycles in the Extrusive Series of the northeastern Troodos ophiolite (Cyprus). *In:* MALPAS, J. MOORES, E. M., PANAYIOTOU, A. & XENOPHONTOS, C. (eds) *Ophiolites - oceanic crustal analogues,* Proceedings of the symposium Troodos 87, Geological Survey Department, Nicosia, Cyprus, 185-206.

SCHMINCKE, H.-U., RAUTENSCHLEIN, M., ROBINSON, P. T. & MEHEGAN, J. M. 1983. Troodos extrusive series of Cyprus: A comparison with oceanic crust. *Geology,* **11,** 405-409.

SCHULTZ, A., DELANEY, J. R. & MCDUFF, R. E. 1992. On the partitioning of heat flux between diffuse flow and point source seafloor venting. *Journal of Geophysical Research,* **97,** 12299-12314.

SCHULTZ, A., DICKSON, P. & ELDERFIELD, H. 1996. Temporal variations in diffuse hydrothermal flow at TAG. *Geophysical Research Letters,* **23,** 3471-3474.

SCLATER, J. G., JAUPART, C. & GALSON, D. 1980. The heat flow through oceanic and continental crust and the heat loss of the Earth. *Reviews of Geophysics and Space Physics,* **18,** 269-311.

SCOTT, M., SCOTT, R. B., RONA, P. A., BUTLER, L. W. & NALWARK, A. J. 1974. Rapidly accumulating manganese deposits from the median valley of the Mid-Atlantic Ridge. *Geophysical Research Letters,* **1,** 355-358.

SCOTT, M., SCOTT, R. B., MORSE, J. W., BETZER, P. R., BUTLER, L. W. & RONA, P. A. 1978. Metal-enriched sediments from the TAG hydrothermal field. *Nature,* **276,** 811-813.

SCOTT, R. B., RONA, P. A., SCOTT, M. R. & MCGREGOR, B. A. 1974. The TAG hydrothermal field. *Nature,* **251,** 301-302.

SCOTT, S. D., CHASE, R. L., HANNINGTON, M. D., MICHAEL, P. J., MCCONACHY, T. F.& SHEA, G. T. 1990. Sulfide deposits, tectonics and petrogenesis of Southern Explorer Ridge, northeast Pacific Ocean. *In:* MALPAS, J. MOORES, E. M., PANAYIOTOU, A. & XENOPHONTOS, C. (eds) *Ophiolites - oceanic crustal analogues,* Proceedings of the symposium Troodos 87, Geological Survey Department, Nicosia, Cyprus, 719-733.

SEARLE, D. L. & PANAYIOTOU, A. 1980. Structural implications in the evolution of the Troodos massif, Cyprus. *In:* PANAYIOTOU, A. (ed) *Ophiolites,* Geological Survey Department, Cyprus, 50-60.

SEARLE, D. L. 1992. The volcano-tectonic setting of oceanic lithosphere generation. *In:* PARSON, L. M., MURTON, B. J. & BROWNING, P. (eds), *Ophiolites and their modern oceanic analogues,* Geological Society, London, Special Publication, **60,** 65-79.

SEYFRIED, W. E., BERNDT, M. E. & SEEWALD, J. S. 1988. Hydrothermal alteration processes at mid-oceanic ridges: Constraints from diabase alteration experiments, hot spring fluids and composition of the oceanic crust. *Canadian Mineralogist,* **26,** 787-804.

SEYFRIED, W. E., DING, K. & BERNDT, M. E. 1991. Phase equilibria constraints on the chemistry of hot spring fluids at mid-ocean ridges. *Geochimica et Cosmochimica Acta,* **55,** 3559-3580.

SHANNON, R. D. 1976. Revised effective ionic radii and systematic studies of inter-atomic

distances in halides and chalcogenides. *Acta Crystallographica,* **32,** 751-767.

SHEARME, S., CRONAN, D. S. & RONA, P. A. 1983. Geochemistry of sediments from the TAG hydrothermal field, Mid-Atlantic Ridge at latitude 26°N. *Marine Geology,* **51,** 269-291.

SHELTON, A. W. & GASS, I. G. 1980. Rotation of the Cyprus microplate. *In:* PANAYIOTIOU, A. (ed) *Ophiolites,* Geological Survey Department, Cyprus, 61-65.

SKORNYAKOVA, I. S. 1965. Dispersed iron and manganese in Pacific Ocean sediments. *International Geology Review,* 7, 2161-2174.

SLEEP, N. H. 1991. Hydrothermal circulation, anhydrite precipitation and thermal structure at ridge axes. *Journal of Geophysical Research,* **96,** 2375-2387.

SMEWING, J. D., SIMONIAN, K. O. & GASS, I. G. 1975. Metabasalts from the Troodos Massif, Cyprus: genetic implications deduced from petrography and trace element geochemistry. *Contrib. Mineralogy and Petrology,* **51,** 49-64.

SMITH, D. K. & CANN, J. R. 1993. Building the crust at the Mid-Atlantic Ridge. *Nature,* **365,** 707-715.

SMITH, G. C. & VINE, F. J. 1987. Electrical conductivity of basalts from CCSP Drill Holes CY-2 and CY-2a at Agrokipia Mines, Cyprus. *In:* ROBINSON, P. T., GIBSON, I. L. & PANAYIOTOU, A. (eds) *Cyprus Crustal Study Project Initial Report Holes CY-2 and 2a,* Geological Survey of Canada, **85-29,** 339-346.

SMITH, S. E. & HUMPHRIS, S. E. 1998. Geochemistry of basaltic rocks from the TAG hydrothermal mound (26°08'N), Mid-Atlantic Ridge. *Proceedings of the Ocean Drilling Program, Scientific Results,* **158,** 213-229.

SPEER, K. G. & RONA, P. A. 1989. A model of an Atlantic and Pacific hydrothermal plume. *Journal of Geophysical Research,* **94,** 6213-6220.

SPEISS, F. N., MACDONALD, K. C., ATWATER, T., BALLARD, R., CARANZA, A., CORDOBA, D., COX, C., DIAZ GARCIA, V. M., FRANCHETEAU, J., GUERRERO, J., HAWKINS, J., HAYMON, R., HESSLER, R., JUTEAU, T., KASTNER, M., LARSON, R., LUYENDYKE, B., MACDOUGALL, J. D., MILLER, S., NORMARK, W., ORCUTT, J. & RANGIN, C. 1980a. East Pacific Rise: hot springs and geophysical experiments. *Science,* **207,** 1421-1433.

SPIESS, F. N., FEVRIER, M., BISCHOFF, J. L., PICOT, P. & SHANKS, W. C. 1980b. Sulfide deposits from the East Pacific Rise near 21°N. *Science,* **207,** 1433-1444.

SPIVACK, A. J.& EDMOND, J. M. 1987. Boron isotope exchange between seawater and the oceanic crust. *Geochimica et Cosmochimica Acta,* **51,** 1033-1043.

SPOONER, E. T. C. & FYFE, W. S. 1973. Sub-seafloor metamorphism, heat and mass transfer. *Contributions to Mineralogy and Petrology,* **42,** 287-304.

SPOONER, E. T. C. & BRAY, C. J. 1977. Hydrothermal fluids of seawater salinity in ophiolitic sulphide ore deposits in Cyprus. *Nature,* **266,** 808-812.

SPOONER, E. T. C., CHAPMAN, H. J. & SMEWING, J. D. 1977. Strontium isotope contamination and oxidation during ocean floor hydrothermal metamorphism of the ophiolitic rocks of the Troodos massif, Cyprus. *Geochimica et Cosmochimica Acta,* **41,** 873-890.

STAKES, D. & MOORE, W. S. 1991. Evolution of hydrothermal activity on the Juan de Fuca Ridge: observations, mineral ages and Ra isotope ratios. *Journal of Geophysical Research,* **96,** 21739-21752.

STAUDIGEL, H. & HART, S. R. 1983. Alteration of basaltic glass: Mechanisms and significance for the oceanic crust-seawater budget. *Geochimica et Cosmochimica Acta,* **47,** 337-350.

STAUDIGEL, H. & GILLIS, K. 1990. The timing of hydrothermal alteration in the Troodos ophiolite. *In:* MALPAS, J. MOORES, E. M., PANAYIOTOU, A. & XENOPHONTOS, C. (eds) *Ophiolites - oceanic crustal analogues,* Proceedings of the symposium Troodos 87, Geological Survey Department, Nicosia, Cyprus, 665-672.

STAUDIGEL, H., GILLIS, K. & DUNCAN, R. 1986. K/Ar and Rb/Sr ages of celadonites from the Troodos ophiolite, Cyprus. *Geology,* **14,** 72-75.

STEIN, C. A. & STEIN, S. 1994. Constraints on hydrothermal heat flux through the oceanic lithosphere from global heat flow. *Journal of Geophysical Research,* **99,** 3081-3095.

STEIN, C. A., STEIN, S. & PELAYO, A. M. 1995. Heat flow and hydrothermal circulation. *In:* HUMPHRIS, S. E., ZIERENBERG, R. A., MULLINEAUX, L. S. & THOMSON, R. E. (eds) *Seafloor hydrothermal systems: physical, chemical, biological and geological interactions.*

Geophysical Monograph 91, American Geophysical Union, 425-445.

SUDARIKOV, S. M., DAVYDOV, M. P., BAZELYAN, V. L. & TARASOV, V. G. 1995. Distribution and transformation of Fe and Mn in hydrothermal plumes and sediments and the potential function of microbiocoenoses. In: PARSON, L. M., WALKER, C. L. AND DIXON, D. R. (eds) *Hydrothermal Vents and Processes*. Geological Society, London, Special Publication, **87**, 249-255.

SUN, S. S. & MCDONOUGH, W. F. 1989. Chemical and isotopic systematics of ocean basalts: implications for mantle composition and processes. *In:* SAUNDERS, A. D. & NORRY, M. J. (eds) *Magmatism in the Ocean Basins*. Geological Society, London, Special Publication, **42**, 313-345.

SVERJENSKY, D. A. 1984. Europium redox equilibria in aqueous solution. *Earth and Planetary Science Letters*, **67**, 70-78.

SWARBRICK, R. E. 1980. The Mamonia complex of SW Cyprus: a Mesozoic continental margin and its relationship to the Troodos complex. *In:* PANAYIOTOU, A. (ed) *Ophiolites*, Geological Survey Department, Cyprus, 50-60.

TAYLOR, R. N. & NESBITT, R. W. 1988. Light rare-earth enrichment of supra subduction-zone mantle: Evidence from the Troodos ophiolite, Cyprus. *Geology*, **16**, 846-850.

TAYLOR, R. N., MURTON, B. J. & NESBITT, R. W. 1992. Chemical transects across intra-oceanic arcs: implications for the tectonic setting of ophiolites. *In:* PARSON, L. M., MURTON, B. J. & BROWNING, P. (eds) *Ophiolites and their modern oceanic analogues.*, Geological Society, London, Special Publication, **60**, 117-132.

TEAGLE, D. A. H., ALT, J. C., BACH, W., HALLIDAY, A. N. & ERZINGER, J. 1996. Alteration of upper ocean crust in a ridge-flank hydrothermal upflow zone: mineral, chemical and isotopic constraints from hole 896A. *Proceedings of the Ocean Drilling Program, Scientific Results*, **148**, 119-151.

TEAGLE, D. A. H., ALT, J. C., HUMPHRIS, S. E. & HALLIDAY, A. N. 1998. Dissecting an active hydrothermal deposit: the strontium and oxygen isotopic anatomy of the TAG hydrothermal mound – whole rock and silicate minerals. *Proceedings of the Ocean Drilling Program, Scientific Results*, **158**, 297-329.

TEMPLE, D. G., SCOTT, R. B. & RONA, P. A. 1979. Geology of a submarine hydrothermal field, Mid-Atlantic Ridge, 26°N. *Journal of Geophysical Research*, **84**, 7453-7466.

THOMPSON, G. 1983. Basalt-seawater interaction. *In:* RONA, P. A., BOSTROM, K. & SMITH, K. L. (eds) *Hydrothermal Processes at Seafloor Spreading Centres*. Plenum, New York, 225-278.

THOMPSON, G., MOTTL, M. J. & RONA, P. A. 1985. Morphology, mineralogy and chemistry of hydrothermal deposits from the TAG area, 26°N Mid-Atlantic Ridge. *Chemical Geology*, **49**, 243-257.

THOMPSON, G., HUMPHRIS, S. E., SCHROEDER, B, SULANOWSKA, M. & RONA, P. A. 1988. Active vents and massive sulphides at 26°N (TAG) and 23°N (Snakepit) on the Mid-Atlantic Ridge. *Canadian Mineralogist*, **26**, 697-711.

TIVEY, M. K. 1995. Modelling chimney growth and associated fluid flow at seafloor hydrothermal vent sites. *In:* HUMPHRIS, S. E., ZIERENBERG, R. A., MULLINEAUX, L. S. & THOMSON, R. E. (eds) *Seafloor hydrothermal systems: physical, chemical, biological and geological interactions.* Geophysical Monograph 91, American Geophysical Union, 158-177.

TIVEY, M. K. & DELANEY, J. R. 1986. Growth of large sulfide structures on the Endeavour segment of the Juan de Fuca Ridge. *Earth and Planetary Science Letters*, **77**, 330-317.

TIVEY, M. K. & MCDUFF, R. E. 1990. Mineral precipitation in the walls of black smoker chimneys: A quantitative model of transport and chemical reaction. *Journal of Geophysical Research*, **95**, 12617-12637.

TIVEY, M. K., HUMPHRIS, S. E., THOMPSON, G., HANNINGTON, M. D. & RONA, P. A. 1995. Deducing patterns of fluid flow and mixing within the TAG active hydrothermal mound using mineralogical and geochemical data. *Journal of Geophysical Research*, **100**, 12527-12555.

TIVEY, M. K., MILLS R. A. & TEAGLE, D. A. H. 1998. Temperature and salinity of fluid inclusions in anhydrite as indicators of seawater entrainment and heating in the TAG active mound. *Proceedings of the Ocean Drilling Program, Scientific Results*, **158**, 179-191.

TOOMEY, D. R., SOLOMON, S. C., PURDY, G. M. & MURRAY, M. H. 1985. Microearthquakes beneath the median valley of the Mid-Atlantic Ridge near 23°N: Hypocentres and focal mechanisms. *Journal of Geophysical Research,* **90**, 5443-5458.

TOOMEY, D. R., SOLOMON, S. C. & PURDY, G. M. 1988. Microearthquakes beneath the median valley of the Mid-Atlantic Ridge near 23°N: Tomography and tectonics. *Journal of Geophysical Research,* **93**, 9093-9112.

TOTH, J, R. 1980. Deposition of submarine crusts rich in manganese and iron. *Geological Society of America Bulletin,* **91,** 44-54.

TREFRY, J. H. & METZ, S. 1989. Role of hydrothermal precipitates in the geochemical cycling of vanadium. *Nature,* **342**, 531-533.

TROCINE, R. P. & TREFRY, J. H. 1988. Distribution and chemistry of suspended particles from an active hydrothermal vent site on the Mid-Atlantic Ridge at 26° N. *Earth and Planetary Science Letters,* **88**, 1-15.

VALSAMI, E. & CANN, J. R. 1992. Mobility of rare earth elements in zones of intense hydrothermal alteration in the Pindos ophiolite, Greece. *In:* PARSON, L. M., MURTON, B. J. & BROWNING, P. (eds) *Ophiolites and their Modern Oceanic Analogues*. Geological Society, London, Special Publication, **60**, 219-232.

VANKO, D. A., LAVERNE, C., TARTAROTTI, P. & ALT, J. C. 1996. Chemistry and origin of secondary minerals from the deep sheeted dykes cored during Leg 158 (Hole 504B). *Proceedings of the Ocean Drilling Program, Scientific Results,* **148**, 71-83.

VARGA, R. J. & MOORES, E. M. 1985. Spreading structure of the Troodos ophiolite, Cyprus. *Geology*, **13**, 846-850.

VARGA, R. J. & MOORES, E. M. 1990. Intermittent magmatic spreading and tectonic extension in the Troodos Ophiolite: implications for exploration for black smoker-type ore deposits. *In:* MALPAS, J. MOORES, E. M., PANAYIOTOU, A. & XENOPHONTOS, C. (eds) *Ophiolites - oceanic crustal analogues,* Proceedings of the symposium Troodos 87, Geological Survey Department, Nicosia, Cyprus, 53-64.

VINE, F. J. & SMITH, G. C. 1990. Structure and physical properties of the Troodos crustal section at ICRDG drillholes CY1, 1a and 4. *In:* MALPAS, J. MOORES, E. M., PANAYIOTOU, A. & XENOPHONTOS, C. (eds) *Ophiolites - oceanic crustal analogues,* Proceedings of the symposium Troodos 87, Geological Survey Department, Nicosia, Cyprus, 113-124.

VON DAMM, K. L. 1990. Seafloor hydrothermal activity: Black smoker chemistry and chimneys. *Annual Review of Earth and Planetary Science*, **18**, 173-205.

VON DAMM, K. L. 1995. Controls on the chemistry and temporal variability of seafloor hydrothermal fluids. *In:* HUMPHRIS, S. E., ZIERENBERG, R. A., MULLINEAUX, L. S. & THOMSON, R. E. (eds*) Seafloor hydrothermal systems: physical, chemical, biological and geological interactions.* Geophysical Monograph 91, American Geophysical Union, 222-247.

VON DAMM, K. L., EDMOND, J. M., GRANT, B., MEASURES, C. I., WALDEN, B. & WEISS, R. F. 1985a. Chemistry of submarine hydrothermal solutions at 21°N, East Pacific Rise. *Geochimica et Cosmochimica Acta*, **49**, 2197-2220.

VON DAMM, K. L., EDMOND, J. M., GRANT, B., MEASURES, C. I. & GRANT, B. 1985b. Chemistry of hydrothermal solutions at Guaymas Basin, Gulf of California. *Geochimica et Cosmochimica Acta*, **49**, 2221-2237.

VON DAMM K. L., OOSTING, S. E., KOSLOWSKI, R., BUTTERMORE, L. G., COLODNER, D. C., EDMONDS, H. N., EDMOND, J. M. & GREBMEIER, J. M. 1995. Evolution of East Pacific Rise hydrothermal vent fluids following a volcanic eruption. *Nature,* **375,** 47-50.

VON DAMM, K. L., BUTTERMORE, L. G., OOSTING, S. E., BRAY, A. M., FORNARI, D. J., LILLEY, M. D. & SHANKS, W. C. 1997. Direct observation of the evolution of a seafloor 'black smoker' from vapor to brine. *Earth and Planetary Science Letters,* **149**, 101-111.

WEISS, R. F., LONSDALE, P., LUPTON, J. E., BAINBRIDGE, A. E. & CRAIG, H. 1977. Hydrothermal plumes in the Galapagos Rift. *Nature,* **267**, 600-603.

WELLS, D. M., MILLS, R. A. & ROBERTS, S 1998. Rare earth elements mobility in a mineralised alteration pipe within the Troodos ophiolite, Cyprus. *In:* MILLS, R. A & HARRISON, K. (eds) *Modern Ocean Floor Processes and the Geological Record.* Geological Society, London,

Special Publication, **148**, 153-176.

WHITE, R. S. 1984. Atlantic oceanic crust: seismic structure of a slow-spreading ridge. *In:* GASS, I. G., LIPPARD, S. J. & SHELTON, A. W. (eds*), Ophiolites and oceanic lithosphere,* Geological Society, London, Special Publication, **13**, 219-232.

WHITE, W. M. & HOFMANN, A. W. 1982. Sr and Nd isotope geochemistry of oceanic basalts and mantle evolution. *Nature,* **296**, 821-825.

WHITFORD, D. J., KORSCH, M. J., PORRITT, P. M. & CRAVEN, S. J. 1988. Rare-earth element mobility around the volcanogenic polymetallic massive sulfide deposit at Que River, Tasmania, Australia. *Chemical Geology,* **68,** 105-119.

WILSON, C., CHARLOU, J.-L., LUDFORD, E., KLINKHAMMER, G., CHIN, C., BOUGAULT, H., GERMAN., C., SPEER. K. & PALMER, M. 1996. Hydrothermal anomalies in the Lucky Strike segment on the Mid-Atlantic Ridge. *Earth and Planetary Science Letters*, **142**, 467-477.

WILSON, R. A. M. 1959. *The geology of the Xeros-Troodos area with an account of the mineral resources*. Memoir No. 1, The Geological Survey Department, Cyprus, Nicosia, 184 pp.

WOLERY, T. J. & SLEEP, N. H. 1976. Hydrothermal circulation and geochemical flux at mid-ocean ridges. *Journal of Geology,* **84**, 249-275.

WOOD, S. A. & WILLIAMS-JONES, A. E. 1994. The aqueous geochemistry of the rare-earth elements and yttrium 4. Monazite solubility and REE mobility in exhalative massive sulfide-depositing environments. *Chemical Geology,* **115**, 47-60.

WOOD, S. A. 1990a. The aqueous geochemistry of the rare-earth elements and yttrium 1. Review of available low-temperature data for inorganic complexes and the inorganic REE speciation of natural waters. *Chemical Geology,* **82,** 159-186.

WOOD, S. A. 1990b. The aqueous geochemistry of the rare-earth elements and yttrium 2. Theoretical predictions of speciation in hydrothermal solutions to 350°C at saturation water pressure. *Chemical Geology,* **88**, 99-125.

YOU, C.-F. & BICKLE, M. J. 1998. Evolution of an active sea-floor massive sulphide deposit. *Nature,* **394**, 668-671.

ZINDLER, A. & HART, S. 1986. Chemical geodynamics. *Annual Reviews in Earth and Planetary Science*, **14**, 493-571.

SOUTHAMPTON UNIVERSITY LIBRARY

USER'S DECLARATION

AUTHOR: Wells D.M

TITLE: [illegible]

DATE: [illegible]

I undertake not to reproduce this thesis, or any substantial portion of it, or to quote extensively from it without first obtaining the permission, in writing, of the Librarian of the University of Southampton.

To be signed by each user of this thesis

DATE	SIGNATURE	ADDRESS